ENGINEERING EVALUATION OF POST-LIQUEFACTION RESIDUAL STRENGTH

(VOLUME 2, PART 2: APPENDICIES B & C)

by

Joseph P. Weber, Raymond B. Seed, Robb E. S. Moss, Juan M. Pestana,
Chukwuebuka Nweke, Tonguc T. Deger and Khaled Chowdhury

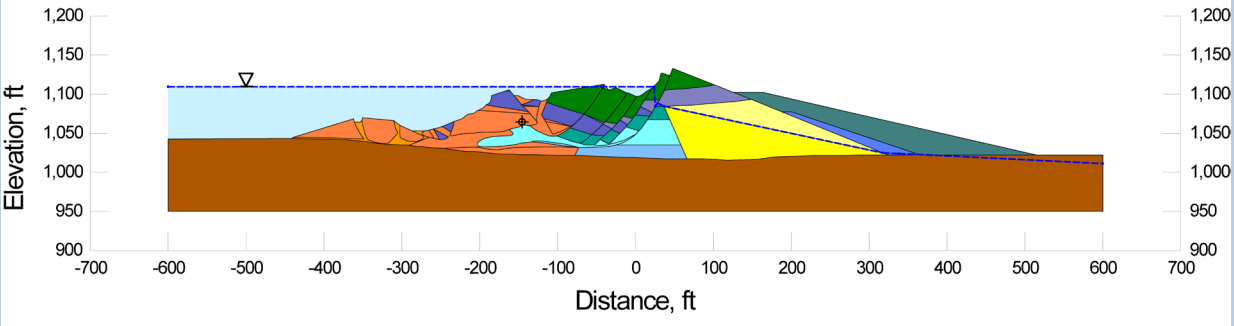

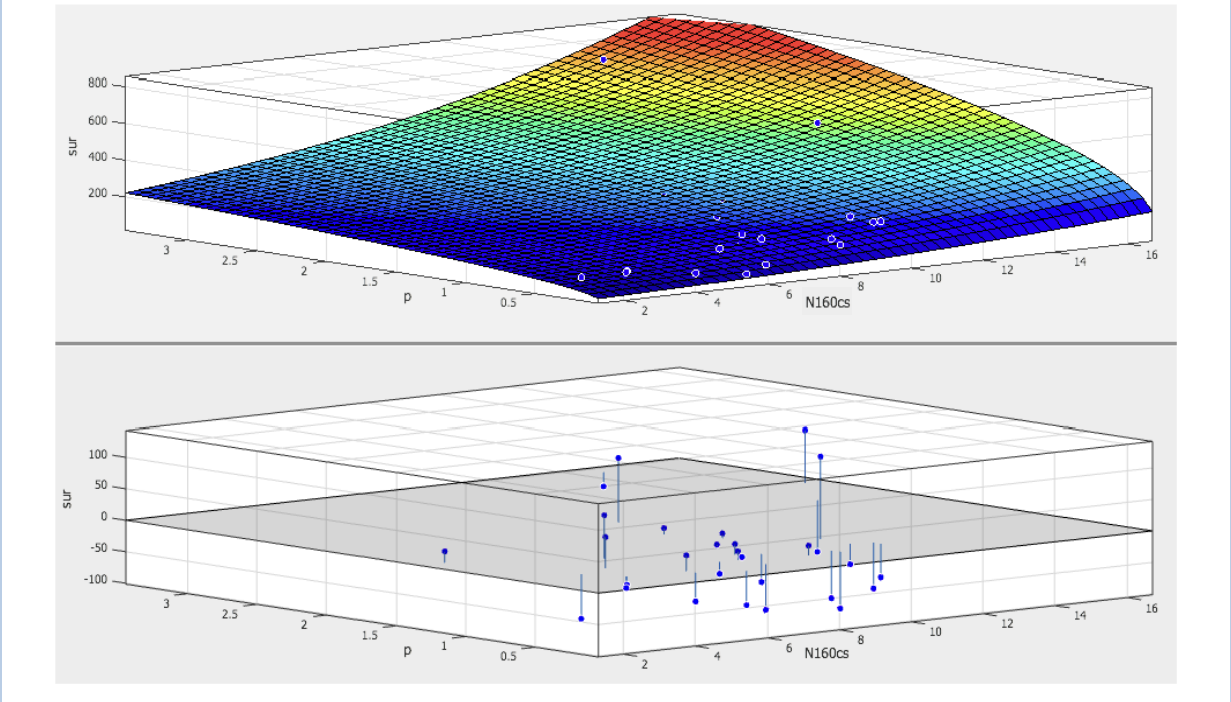

Geotechnical Research Report No. UCB/GT/22-01
Department of Civil and Environmental Engineering
University of California at Berkeley

August 2022

Appendix B:

Back-Analyses of Class B Liquefaction Failure Case Histories

Class B Case Histories:

B.1: Zeeland-Vlieteploder (1889)

B.2: Sheffield Dam (1925)

B.3: Helsinki Harbor (1936)

B.4: Solfatara Canal Dike (1940)

B.5: Lake Merced Bank (1957)

B.6: El Cobre Tailings Dam (1965)

B.7: Metoki Road Embankment (1968)

B.8: Hokkaido Tailings Dam (1968)

B.9: Upper San Fernando Dam – D/S Slope (1971)

B.10: Tar Island Dyke (1974)

B.11: Mochi-Koshi Tailings Dam, Dikes 1 and 2 (1978)

B.12: Nerlerk Embankment, Slides 1, 2 and 3 (1983)

B.13: Asele Roadway Embankment (1983)

B.14: Nalband Railway Embankment (1988)

B.15: Sullivan Tailings (1991)

B.16: Jamuna Bridge (1994)

B.1 Zeeland - Vlietepolder (Netherlands; 1889)

B.1.1 Brief Summary of Case History Characteristics

Name of Structure	Zeeland - Vlietepolder
Location of Structure	Zeeland Province, Netherlands
Type of Structure	Delta Bank
Date of Failure	September 11, 1889
Nature of Failure	Static, During 1889 Low Tide
Approx. Maximum Slope Height	9.5 ft.

B.1.2 Introduction and Description of Failure

The Dutch Province of Zeeland is in the southwest corner of Holland, fronting the North Sea, and immediately north of Belgium, as shown in Figure B.1.1. This is a very active deltaic area, with deposition of sediments from several large rivers (including the Rhine, Meuse and Scheldt rivers). The rapid deltaic deposition produces large numbers of coastal failures, and Silvis and de Groot (1995) state that several hundreds of coastal slope failures have been reported in this region over the past two centuries.

Most of these failures have occurred primarily in relatively uniformly graded, fine deltaic sands and silty sands, and liquefaction is suspected to be the common causative mechanism. Failures appear to be related to localized over-steepening of coastal and offshore slopes, and these failures are routinely also associated with very low tides suggesting that tidal drawdown and resulting reversal of seepage flow back towards the sea may also contribute to the initiation of many of these slides.

Most of these coastal slides occur mainly below the surface of the sea, and so it is often difficult to determine both pre-failure and post-failure cross-section geometries with any confidence. Pre-failure geometries can only reliably be determined if a coastal bathymetric survey was undertaken shortly before the failure, and a concerted effort would be required to ascertain the post-failure geometry at depth of the runout slide mass. As a result, it has not been possible to perform well-constrained back-analyses of most of these failures.

A singular exception was the slide that occurred on September 11, 1889 in a coastal area known as Vlietepolder. Figure B.1.2 shows the pre-failure and post-failure cross-sections for this slide feature (Koppejan et al., 1948). The pre-failure cross section is available because the pre-failure survey was recent enough as to provide a reliable geometry, and the post-failure cross-section was determined shortly after the failure before potentially significant erosion by currents or tides. This slide involved approximately 940,000 m^3 of material, and nearly 60,000 m^3 of land area above the low water mark was lost. Observations made during this failure, and experience with multiple previous failures in this region, suggest that this was a retrogressively progressive failure (Andresen and Bjerrum, 1968, Bjerrum, 1971; Casagrande, 1976), and the analyses performed as part of these current studies suggest this as well.

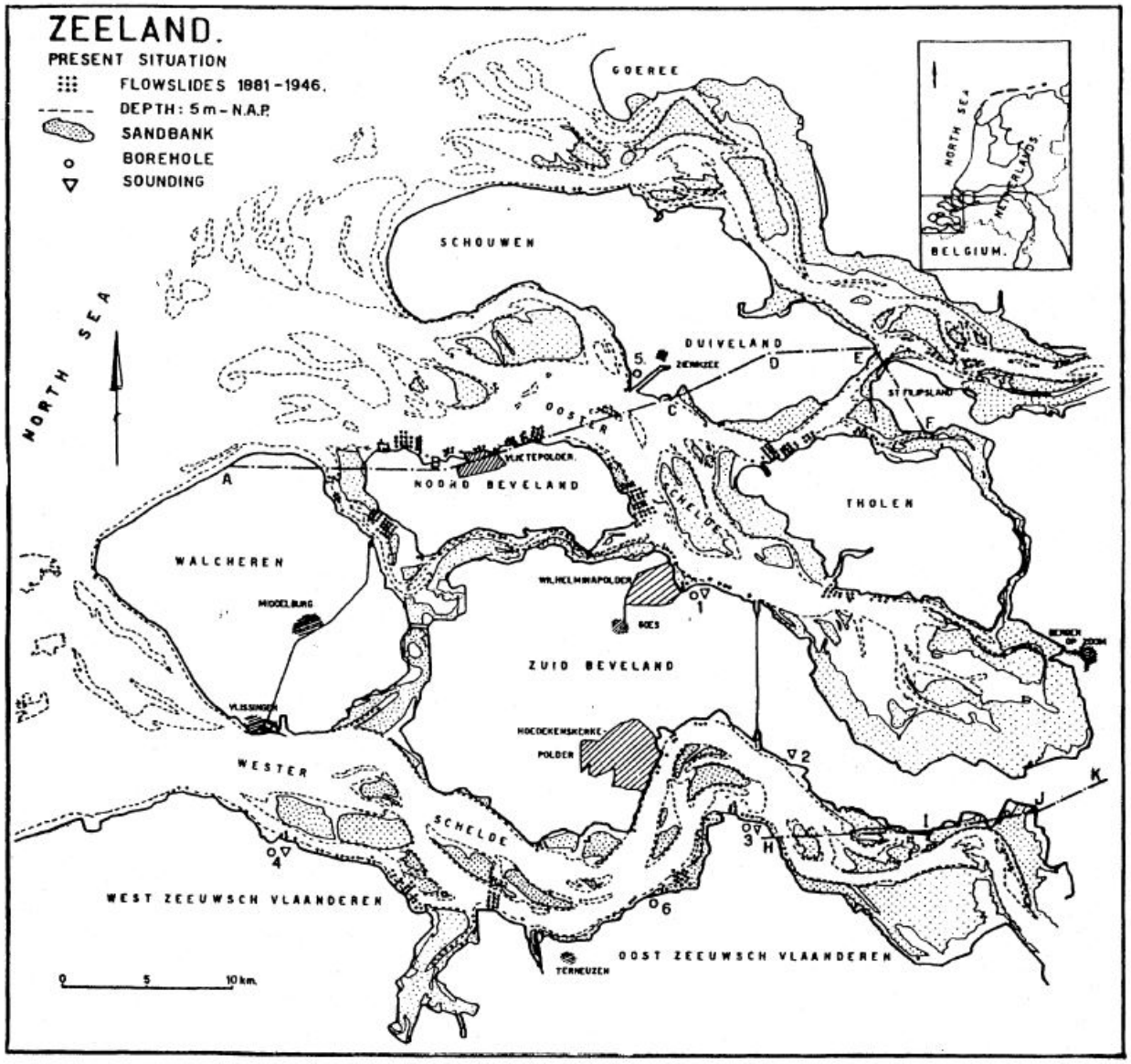

Figure B.1.1: Map of the Zeeland region showing locations of a number of flow slides that occurred between 1881 to 1946 (Koppejan et al., 1948).

B.1.3 Geology and Site Conditions

The coastal and offshore soils of the Zeeland region are comprised primarily of deltaic deposits from Rhine, Meuse and Scheldt rivers. The uppermost (most recent) deposits are the Holocene age Dunkirk and Calais deposits, and it is within these deposits that the failure occurred. Both the Dunkirk and Calais deposits are comprised mainly of uniformly graded fine sands to clayey sands, deposited primarily as sandy tidal channel sediments with a loose structure (Koppejan et al., 1948), though occasional deposits of peats and clays also occur. These loose sandy soils are notoriously susceptible to liquefaction-induced coastal slides. These Holocene deposits are underlain by Pleistocene deposits of the Twente and Tegelen formations.

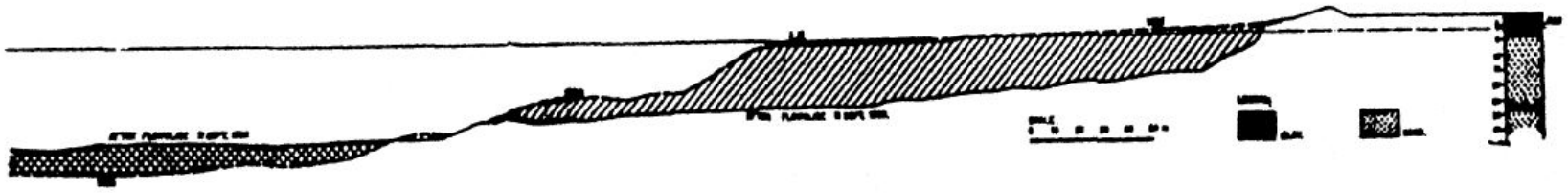

Figure B.1.2: Pre-failure and post-failure cross-sections for the Vlietepolder coastal failure of September 11, 1889 (Koppejan et al., 1948).

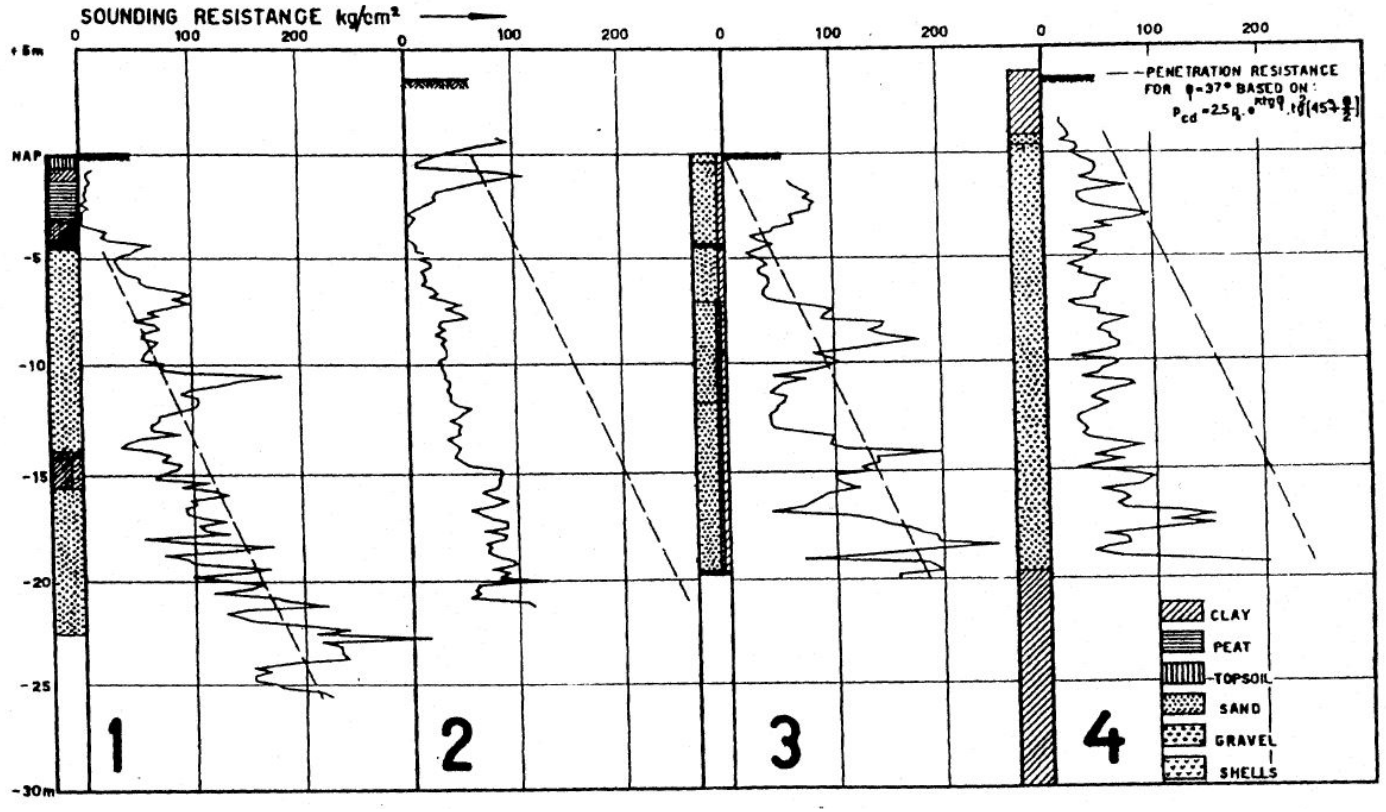

Figure B.1.3: Logs of four mechanical CPT soundings from the Zeeland region (Koppejan et al., 1948).

The Twente formation consists primarily of fine grained aeolian sands and medium grained glaciofluvial sands, and the Tegelen formation consists of generally coarser fluvial sands and gravels, and these older formations are usually denser than the younger Holocene deposits (Silvis and de Groot, 1995). Of the approximately 700 flow slides identified by Ligtenberg-Mak et al. (1990), approximately 75% occurred primarily in Dunkirk channel deposits, 14% in Calais channel deposits, and 1% in older Pleistocene sands.

Figure B.1.3 presents the logs of four mechanical cone penetration soundings from Koppejan et al. (1948). The numbers of the logs correspond to locations shown in Figure B.1.1. None of these soundings were performed at the site of the coastal slope failure of September 11, 1889, but these are considered indicative of the general conditions of the younger Holocene deposits of this region. Conversions to equivalent modern CPT tip resistances are challenging, but Olson (2001) estimated equivalent (and overburden corrected) CPT q_{c1} values for these four soundings, and estimated an average value of $q_{c1} \approx 3.0$ MPa, with lower and upper bounds of approximately 1.7 MPa and 4.4 MPa, respectively. No potentially useful values of SPT blowcounts are known to be available in this region.

B.1.4 Initial Yield Stress Analyses

Figure B.1.4 shows the cross-section used for back-analyses of the post-liquefaction initial yield strength $S_{r,yield}$ that would be required within the liquefied soils to produce a calculated Factor of Safety equal to 1.0. This is not the actual post-liquefaction strength, but it proves to be useful in developing estimates of post-liquefaction strength (S_r) for this case history.

Unit weights of the non-saturated sands and silty sands above the phreatic surface were modeled with a unit weight of $\gamma_m \approx 112$ lbs/ft^3, and this was then varied over a range of 110 to 115 lbs/ft^3 for parameter sensitivity studies. Unit weights of the saturated sands and silty sands below the phreatic surface were modeled with a unit weight of $\gamma_s \approx 117$ lbs/ft^3, and this was then varied over a range of 115 to 120 lbs/ft^3 for parameter sensitivity studies. The friction angle of the non-saturated materials above the phreatic surface was modeled with $Ø' \approx 30°$, and a range of $Ø' \approx 28°$ to 32°.

The available information suggests that this was an incrementally retrogressive failure, and the analyses performed here support this. A number of "initial" potential failure slices were analyzed, and the solid line in Figure B.1.4(a) shows the most critical of these (with the lowest post-liquefaction Factor of Safety). The back-calculated value of $S_{r,yield}$ for this failure surface is $S_{r,yield} = 480$ lbs/ft^2 based on the best estimate soil parameters from above. Additional initial potential failure surfaces were also analyzed, including wedge-like surfaces as well as rotational surfaces, and parameters were varied as described above. Initial failures near the toe of the main slope (as illustrated in Figure B.1.4(a)) dominated the possible initial failure surfaces based on criticality. For these types of initial failure surfaces, the best estimate of the most critical failure surface produced the value of $S_{r,yield} = 430$ lbs/ft^2, and additional analyses of the likely ranges of parameters and potential initial failure surfaces produced a range of approximately $S_{r,yield} = 347$ to 507 lbs/ft^2.

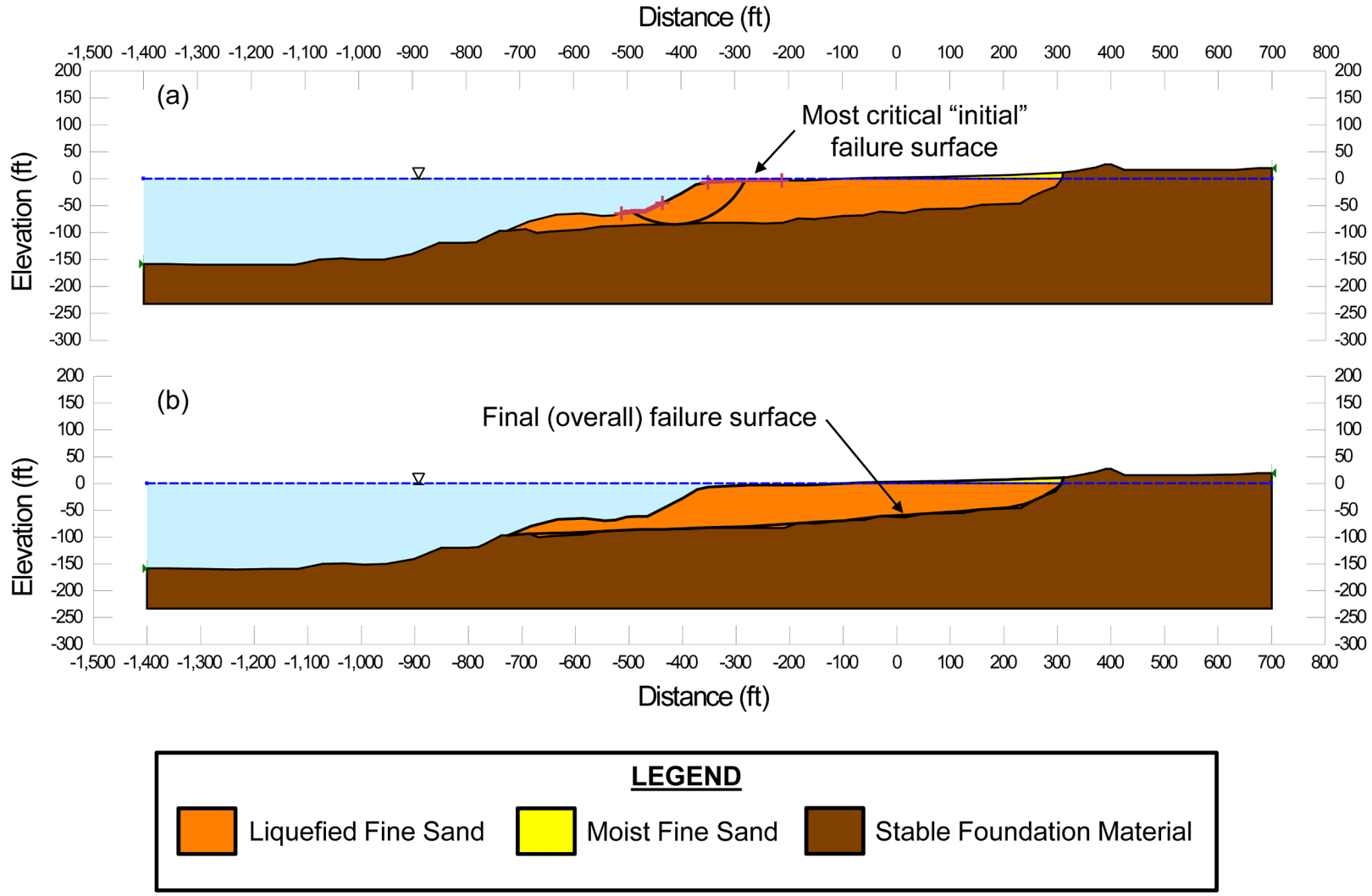

Figure B.1.4: Cross-sections used to perform back-analyses to determine $S_{r,yield}$ for the Zeeland - Vlietepolder slide of September 11, 1889.

Figure B.1.4(b) shows the best estimate of the final (overall) failure surface when retrogressive sliding had progressed fully to the eventual rear-most scarp. For this failure surface, back-analyses produced a best estimate of $S_{r,yield}$ = 248 lbs/ft^2, and a range of approximately $S_{r,yield}$ = 213 to 289 lbs/ft^2. This is not considered likely to represent the actual "yield" value, because it is expected that this was an incrementally progressive retrogressive failure.

The best overall estimate of $S_{r,yield}$ for this case was then developed by averaging the $S_{r,yield}$ values for smaller initial yield slices with the $S_{r,yield}$ values for the overall final) slide scarp. Given the geometry of the cross-section, a 2:1 weighted average was used here where

$$S_{r,yield} = [\ 2 \times S_{r,yield}\ (\text{smaller initial yield surface}) + S_{r,yield}\ (\text{final overall failure scarp})] / 3$$

Based on the range of variations in properties and parameters, and a range of potential failure mechanisms and associated feasible failure surfaces, the resulting best estimate overall of "representative" $S_{r,yield}$ was found to be $S_{r,yield}$ = 369 lbs/ft^2, with a range of $S_{r,yield} \approx$ 302 to 434 lbs/ft^2.

Olson (2001) also performed back-analyses to estimate $S_{r,yield}$. He analyzed a suite of rotational potential failure surfaces generally similar to those shown in Figure B.1.4(a), and his best estimate of $S_{r,yield}$ was 16.1 kPa (336 lbs/ft^2), with a range of 15.0 to 16.8 kPa (313 to 350 lbs/ft^2).

B.1.5 Residual Strength Analyses Based on Residual Geometry

It was not possible to perform rigorous and reliable back-analyses to determine the value of $S_{r,resid/geom}$ required to produce a calculated Factor of Safety equal to 1.0 based on residual geometry. This case is one of six cases (out of the 29 cases back-analyzed as part of these current studies) where the slide mass "went over a lip" and then traveled down a steeper slope, and the ensuing displacements either (1) could not be reliably tracked, or (2) could not be reliably back-analyzed. Both situations apply in th is current case because the post-failure geometry of the failure mass runout is largely undefined. The cross-section provided by Koppejan et al. (1948), as presented in Figure B.1.2, shows only a portion of the failure mass runout. A majority of the displaced failure mass is unaccounted for and will occur to the left of that figure. This is a significant source of uncertainty for this case history.

In these current studies, it was assumed that $S_{r,resid/geom}$ would have at least been higher than zero. Values of $S_{r,resid/geom}$ back-calculated from the reasonably well-documented Class A case histories were next examined, and for the range of effective overburden stress and $N_{1,60,CS}$ values for this current case an approximate range of $S_{r,resid/geom} \approx$ 70 to 170 lbs/ft^2 was conservatively assumed, based on analyses of other Class A and Class B case histories. This range of values was selected to be slightly conservatively biased (a conservative bias of approximately 10% reduction of best estimates of $S_{r,resid/geom}$ was targeted here), so that any resulting error in evaluation of overall S_r would also be slightly conservative (nominally by approximately 5% or so).

It is interesting to note that this range of $S_{r,resid/geom} \approx$ 70 to 170 lbs/ft^2 agrees fairly well with the range developed by Olson (2001), based on alternate approaches, as described below.

Based on what he acknowledged to be the "incomplete" post-failure geometry of Figure B.1.2, Olson assumed an infinite slope with a top and base slope of 4°, and a best estimate thickness of the final runout materials of 8.5 m (and a range of thicknesses of 7 to 10 m), and calculated $S_{r,resid/geom} \approx 5.5$ kPa (115 lbs/ft^2), with a range of $S_{r,resid/geom} \approx 4.5$ to 6.5 kPa (94 to 136 lbs/ft^2). Olson's range is somewhat narrower than the range (70 to 170 lbs/ft^2) used in these current studies, but the two ranges are "centered" at approximately the same values, despite the different approaches and assumptions employed.

B.1.6 Overall Estimates of S_r

Overall estimates of S_r for this Class B case history were made based on the pre-failure geometry, the partial post-failure geometry, the approximate runout features and characteristics, and the values of $S_{r,yield}$ and $S_{r,resid/geom}$ as calculated and/or estimated in the preceding sections.

Runout characteristics for this case cannot be accurately assessed due to the incomplete post-failure cross section as reported. Runout distance, and runout ratio, appear to be "large", but the failure mass travelled out over a "lip" at the toe of the slide scarp, and then down what may at least initially been a steeper slope.

Runout ratio (defined as runout distance traveled by the center of gravity of the overall failure mass divided by the initial slope height from toe to back heel of the failure) was taken to be at least medium to large. This allowed Equation 4-4, and Figures 4.7 and 4.11 to serve as one basis for estimation of post-liquefaction strength S_r. Using the ranges of $S_{r,yield}$ and $S_{r,resid/geom}$ from Sections B.13.4 and B.13.5, and assuming that $\xi \approx 0.4$ to 0.65 for this large runout case, with 0.525 as the best estimate, provided a best estimate value of $S_r \approx 128$ lbs/ft^2 and an estimated range of $S_r \approx 74$ to 196 lbs/ft^2. A second basis for estimation of S_r was the use of the relationship of Figure 4.9, and the range of values of $S_{r,yield}$ from Section B.1.4. Based on the large runout distance, values of initial (pre-failure displacement) Factor of Safety were taken as approximately 0.4 to 0.6, and this produced a best estimate value of $S_r \approx 185$ lbs/ft^2 and an estimated range of $S_r \approx 121$ to 260 lbs/ft^2. No similar use was made of Figure 4.9 in conjunction with the ranges of $S_{r,resid/geom}$ estimated in Section B.4.5 because these estimates of $S_{r,resid/geom}$ were considered to be very approximate.

The estimates by each of the two methods above were then averaged together, and this produced a best estimate value of $S_r \approx 156$ lbs/ft^2 and an estimated range of $S_r \approx 74$ to 260 lbs/ft^2. These estimates of variance are non-symmetric about the best estimated mean value, and the range was judged to represent approximately +/- 2.5 standard deviations, so further adjustments were then necessary.

Overall, based on an assumed normal distribution, it was judged that the (mean and median) best estimate of post-liquefaction strength for this case history is

$$\overline{S_r} = 156 \text{ lbs/ft}^2$$

and that the best estimate of standard deviation of mean overall post-liquefaction strength is

$$\sigma_{\bar{S}} = 37 \text{ lbs/ft}^2$$

Olson (2001) and Olson and Stark (2002) did not apply their "kinetics" method to this case, and so they did not independently develop an estimate of S_r that incorporated momentum effects. Instead they simply used their value of $S_{r,resid/geom}$ as a conservative approximation of S_r for this less well-defined case, and used S_r = 5.5 kPa (115 lbs/ft^2), with a range of 4.5 to 6.5 kPa (105 to 155 lbs/ft^2) in developing their predictive relationship. Because these values are based on residual post-failure geometry with an assumed Factor of Safety equal to 1.0, they do not include momentum effects and so they will be too low.

A better basis for comparison would be to take Olson's back-calculated values of $S_{r,yield}$ and $S_{r,resid/geom}$, and then use Equation 4-1 which estimates S_r as

$$S_r \approx \xi \bullet (S_{r,yield} + S_{r,resid/geom}) / 2 \qquad \text{[Eq. 4-1, repeated]}$$

with $\xi \approx 0.8$ as a first-order approximation. The result would then be an estimated value of $S_r \approx 180$ lbs/ft^2, in reasonably good agreement with these current studies.

Similarly, Wang (2003) and Wang and Kramer (2008) did not employ their zero inertial force (ZIF) method to incorporate inertial effects in back-analyses of this failure. Instead they selected their value of S_r based on selection and then averaging of back-analyses results of several previous investigators. For this case Wang (2003) selected only a "modified" value based on Olson's values of $S_{r,yield}$ and $S_{r,resid/geom}$, but with a value of $\xi = 1.0$ (rather than 0.8). That would generally tend to moderately over-estimate the actual value of S_r for this case. The resulting value would be $S_r \approx 180$ lbs/ft^2, as listed in Tables 4.3 and 4.6.

B.1.7 Evaluation of Initial Effective Vertical Stress

Average initial (pre-failure) effective vertical stress was assessed for the liquefied portion of the overall (final scarp) failure surface in Figure B.13.4. Parameters and sensitivity analyses were as described previously in Section B.13.4. Additional analyses were then performed for alternate potential failure surfaces, including failure surfaces for initial slices of a retrogressive incremental failure eventually extending back to the apparent back heel of the final failure. Depths of failure surfaces were varied, and both rotational and translational (wedge-like) failure surfaces were considered. When an initial (smaller) "toe" slice of a retrogressive failure was analyzed, the resulting average value of σ_{vo}' was then averaged with the value of the overall (Final) slide scarp, and this averaged value of the two failure surfaces was taken as "representative" here. This produced a moderately large, but finite, range of estimated values of average pre-failure effective stress within the liquefied materials controlling the failure.

The resulting best estimate of average pre-failure effective stress within the liquefied materials controlling the failure was then $\sigma_{vo}' \approx 2{,}471$ lbs/ft^2, with a reasonable range of $\sigma_{vo}' \approx 1{,}626$ to 3,350 lbs/ft^2. This range is slightly non-symmetric about the median value, and

this range was judged by the engineering team to represent approximately ± 2 standard deviations. Overall, the best characterization of initial (pre-failure) average effective vertical stress was then taken to be represented by a mean value of

$$\overline{\sigma'_{vo}} \approx 2{,}488 \text{ lbs/ft}^2$$

and with a standard deviation of

$$\sigma_{\overline{\sigma}} \approx 431 \text{ lbs/ft}^2$$

An estimate of σ_{vo}' was also calculated by Olson and Stark (2001, 2002). They reported a weighted average mean value of $\sigma_{vo}' \approx 115$ kPa (2,401 lbs/ft^2), and a range of 57 to 172 kPa (1,190 to3,592 lbs/ft^2), in excellent agreement with these current studies. Average initial vertical effective stresses were not directly reported by Wang (2003) and Kramer (2008), but they were published more recently in the publication by Kramer and Wang (2015). As discussed in Section 2.3.8.1(b)-(iii), Wang (2003) did not perform any independent analyses to assess σ_{vo}' for his 22 "secondary" cases, and this is one of those cases. Instead, he compiled values of S_r from multiple previous investigators, and averaged these for a best estimate. He also compiled multiple values of S_r/σ_{vo}' from previous investigators, and averaged these for a best estimate. He then used these two best-estimate values of S_r and S_r/σ_{vo}' to infer a resulting representative value of σ_{vo}'. As described in Section 2.3.8.1(b)-(iii), the resulting averaged values of S_r and of S_r/σ_{vo}' were incompatible with each other for a number of Wang's "secondary" case histories, and this process produced unreasonable, and in some cases physically infeasible, values of σ_{vo}' for a number of case histories. Wang's value of $\sigma_{vo}' = 4{,}708$ is clearly physically infeasible for this case, based on the cross-section, and so it is not considered a useful check here. Agreement between Olson's value, which is well-documented, and the values developed in these current studies is excellent.

B.1.8 Evaluation of $N_{1,60,CS}$

As explained previously in Section B.1.3, there were no published standard penetration test data for this failure case history, and no site specific penetration data of any kind. As a result, there is considerable uncertainty with regard to selection of representative $N_{1,60,CS}$ values for this case history.

Olson (2001) and Olson and Stark (2002) reprocessed the four logs of mechanical cone soundings from Figure B.1.2, and estimated an average value of $q_{c1} \approx 3.0$ MPa, with lower and upper bounds of approximately 1.7 MPa and 4.4 MPa, respectively. These conversions to equivalent modern CPT values are challenging. They then further converted these estimated CPT tip resistances to estimated SPT $N_{1,60}$ values, producing a best estimate representative value of $N_{1,60} = 7.5$ blows/ft, and a range of 4.2 to 10.9 blows/ft. These are $N_{1,60}$ values, and they include no fines adjustment. Given the low to moderate reported clayey fines content of the sediments, fines adjustment to $N_{1,60,CS}$ values would be expected to increase these values.

Wang (2003) and Kramer (2008) selected a slightly higher fines adjusted value of $\overline{N_{1,60,CS}} \approx 8.5$ blows/ft, and a very high standard deviation of $\sigma_{\overline{N}} \approx 5.5$ blows/ft. Precise details are not presented, but it is noted here that a high standard deviation is potentially justified based on the overall uncertainties involved. This high standard deviation would produce negative values of $N_{1,60,CS}$ at a mean minus 1.55 standard deviations level, and at a mean plus two standard deviations level would produce a value of $N_{1,60,CS} \approx 19.5$ blows/ft, which would appear to be high for the materials as described and as they performed. These upper and lower values (even the low probability negative values) are not mathematically problematic in the framework of the regressions subsequently performed by Kramer (2008) to develop predictive correlations, but this standard deviation is somewhat larger than the one employed in these current studies.

In these current studies, the principal overall uncertainties were considered to be: (1) use of the sparse available mechanical cone penetration logs/data from four sites not located or near to the actual site of the failure, and with four different tip resistance profiles and signatures, (2) conversion of (now historic) mechanical cone data to equivalent modern CPT tip resistances, and (3) conversion of CPT tip resistances to equivalent SPT $N_{1,60,CS}$ values. Overall uncertainties (and variance or standard deviation of the mean value) with regard to resulting values of $N_{1,60,CS}$ will necessarily be high. Advice was sought from Robertson (2014) regarding interpretation of the mechanical cone tip resistances and conversion to equivalent modern CPT tip resistances. Several methods were taken to estimate conversion of the resulting CPT tip resistances to equivalent SPT $N_{1,60,CS}$ values, with adjustments as necessary to the SPT fines corrections being employed in these current studies. Considering the ranges of values produced, and the overall uncertainties, an overall best estimate value of $\overline{N_{1,60,CS}} \approx 8$ blows/ft was selected, with a standard deviation of this mean of $\sigma_{\overline{N}} \approx 2.1$ blows/ft.

Overall agreement with regard to characterization of $N_{1,60,CS}$ (and $N_{1,60}$) among these two previous studies, and the current study, is considered to be very good for this case, with the exception of characterization of variance (or standard deviation) of the mean value of $\overline{N_{1,60,CS}}$.

B.2 Sheffield Dam (California, USA; 1925)

B.2.1 Brief Summary of Case History Characteristics

Name of Structure	Sheffield Dam
Location of Structure	California, USA
Type of Structure	Zoned Embankment Dam
Date of Failure	June 29, 1925
Nature of Failure	Seismic, During 1925 Santa Barbara Earthquake (M_L = 6.3)
Approx. Maximum Slope Height	25 ft.

B.2.2 Introduction and Description of Failure

The Sheffield Dam suffered a catastrophic liquefaction-induced translational failure during the 1925 Santa Barbara earthquake (M_L = 6.3). The epicenter of the earthquake was located approximately seven miles northwest of the dam, and Seed et al. (1969) estimated the peak ground surface acceleration at the dam at approximately 0.15g. There were no local ground motion records obtained. Local witnesses reported that shaking lasted approximately 15 to 18 seconds, but there is no instrumental confirmation of either this estimated level or duration of shaking.

Figure B.2.1 shows the approximate pre-failure cross-section and reservoir water level (Seed et al., 1969). At the time of the failure, the reservoir surface was approximately halfway up the concrete-lined upstream face of the dam.

Figure B.2.2 shows a photograph of the dam shortly after the failure (Engineering News Record, 1925), and Figure B.2.3 shows a plan view of the approximate post-failure configuration (Engineering News Record, 1925).

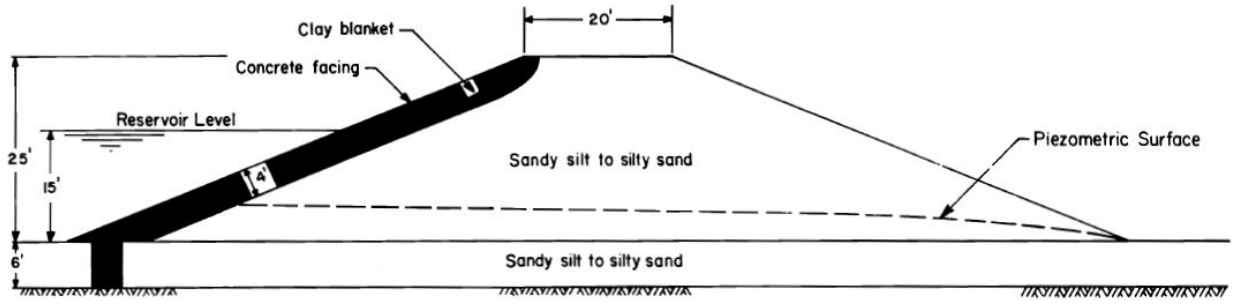

Figure B.2.1: Cross-section through the original embankment of the Sheffield Dam (Seed et al., 1969).

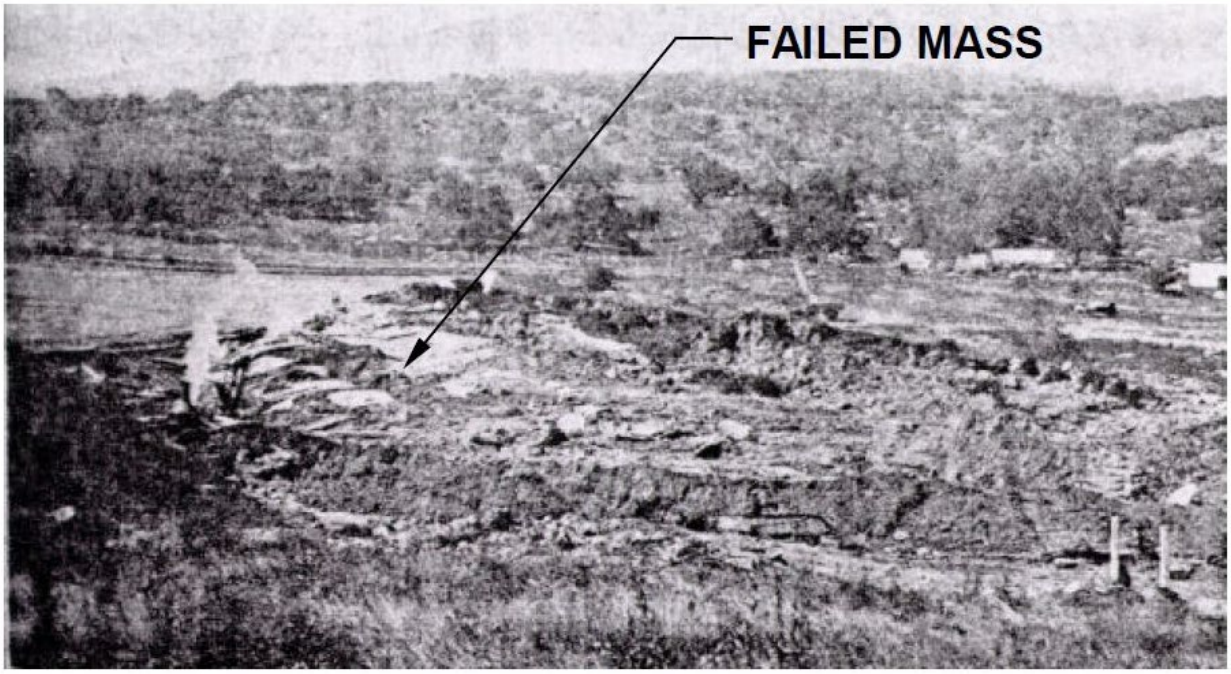

Figure B.2.2: Post-failure photograph of the Sheffield Dam (Photo from Engineering News Record, 1925).

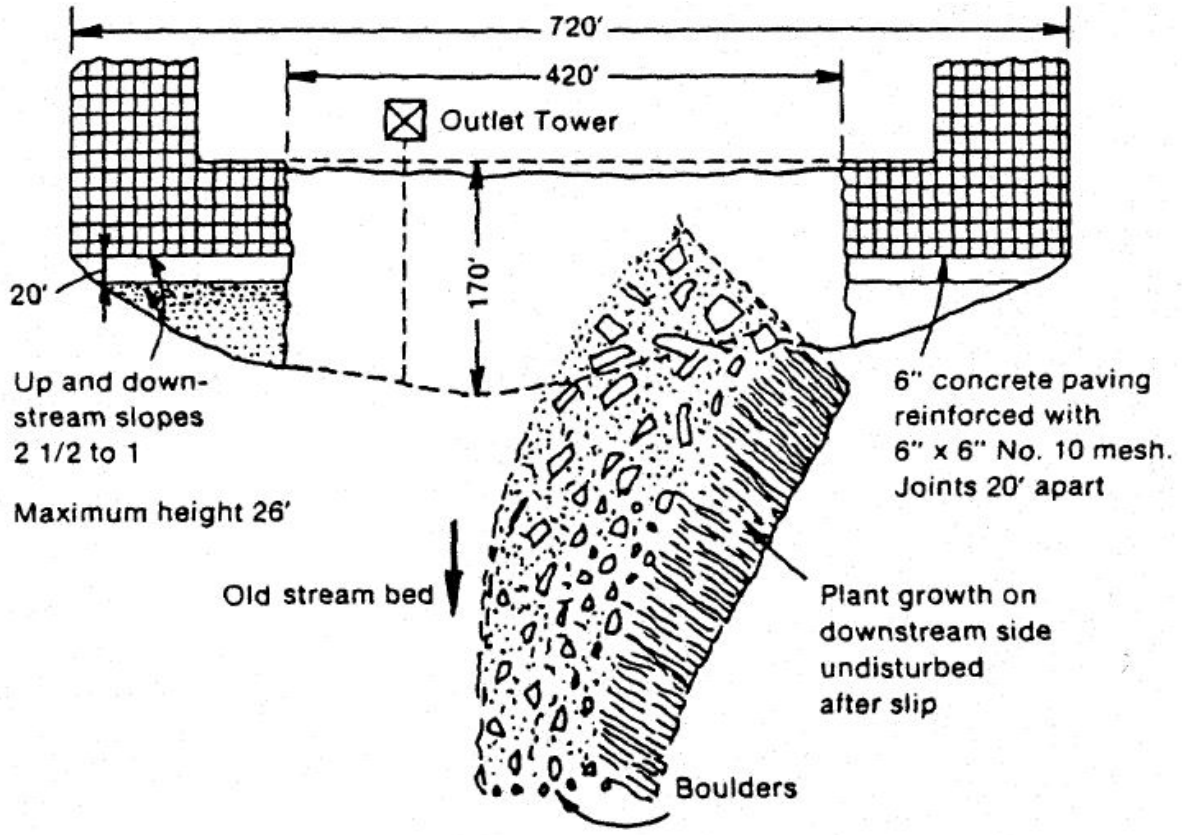

Figure B.2.3: Plan view showing post-failure conditions (Engineering News Record, 1925).

There were no eyewitnesses to the failure, but a number of engineers examined the dam after the failure had occurred. It appeared that the failure had occurred as a largely translational failure, with the failure surface located approximately at the base of the earthen embankment, and with the primary slippage occurring in either the lower embankment soils or the upper foundation soils immediately below. A section of the embankment dam approximately 530 feet in length had traveled a maximum distance of approximately 200 feet, and much of it remained largely intact during these movements. As this failure mass traveled, it rotated in a counter-clockwise direction, reaching the final position shown in Figures B.2.2 and B.2.3.

Although both the Wachusett Dam and Calaveras Dam liquefaction failures had previously occurred, soil liquefaction was still not generally well understood in 1925, so it is interesting to note that Willis (1925) surmised: "The foundations of the dam had become saturated and the rise of water as the ground was shaken formed a liquid layer of sand under the dam, on which it floated out, swinging about as if on a hinge." This was an apt description of the failure.

B.2.3 Geology and Site Conditions

The dam had been constructed in 1917 to serve as a reservoir for the Santa Barbara Municipal Water Department. The earthen dam embankment had a maximum crest height of approximately 25 feet, and a crest length of approximately 220 feet. After the failure, the dam was reconstructed with a more conservative cross-section.

The original (pre-failure) dam embankment was constructed across a ravine in recent alluvial terrace deposits. The U.S. Army Corps of Engineers (1949) studied the dam, and determined that there had been no stripping of these alluvial terrace deposits beneath the footprint of the original dam prior to dam embankment construction. Because the reconstruction of the dam after the failure had included stripping of these upper foundation materials beneath the reconstructed footprint, the USACE performed a suite of five borings closely adjacent to (and downstream) of the reconstructed dam in order to characterize the likely conditions beneath the original dam. The alluvial terrace deposits were found to consist primarily of loose silty sand, with fines contents of approximately 33% to 48%. Atterberg Limits tests subsequently performed by Seed et al. (1969) found the silt fines to be low plasticity silts with PI ≈ 4%, and LL ≈ 24%. In-situ density tests of these silty sands indicated dry unit weights of $\gamma_d \approx 89.7$ lbs/ft^3 in the upper one to three feet or so, and significantly higher unit weights of $\gamma_d \approx 101.1$ lbs/ft^3 at greater depths. Seed et al. (1969) determined the maximum dry density by the Standard Proctor Compaction Test (ASTM D698) for these silty sands to by $\gamma_{d,max} \approx 118.0$ lbs/ft^3, indicating that the very loose upper several feet of foundation material were at an equivalent Relative Compaction of approximately RC = 76% (Std. Proctor). These were very loose silty sands and sandy silts, and it is within this relatively thin veneer of loose, saturated, upper foundation soils that the liquefaction-induced failure and slippage appears to have occurred.

The original dam embankment was constructed of these same silty sands and sandy silts, excavated (borrowed) from within the reservoir footprint. The embankment fill was placed in lifts, but was compacted only by means of routing of light construction vehicles over the evolving fill; there was no formal compaction, and no useful vibratory compaction was employed. As a result,

these embankment materials were also loose, saturated silty sands and sandy silts, and so it is also possible that the failure occurred in part due to liquefaction of the loose, saturated silty sands and sandy silts at the base of the embankment fill. It is unlikely, however, that this lightly rolled fill was actually looser than the top veneer of the underlying foundation soils, and so it has generally been assumed (e.g. Seed et al., 1969; Seed and Harder, 1990; Olson, 2001, etc.) that the failure was due to liquefaction-induced loss of strength of the very loose upper foundation soils immediately beneath the embankment. These current studies will also take this view.

The original embankment had an upstream side facing consisting of a concrete facing 6 inches in thickness, underlain by a clay blanket approximately 3.5 feet in thickness. This served to constrain the flow through the embankment. There were no data upon which to base estimates of the phreatic surface through the dam at the time of the failure. The phreatic surface shown in Figure B.2.1 was based on judgment, and a similar phreatic surface is assumed in these current studies. Back-analyses of this failure case history are not very sensitive to minor changes in this assumed phreatic surface, so long as the upper foundation soils are modeled as saturated.

B.2.4 Initial Yield Stress Analyses

Figure B.2.4 shows the cross-section used for back-analyses of the post-liquefaction initial yield strength $S_{r,yield}$ that would be required within the liquefied upstream shell materials to produce a calculated Factor of Safety equal to 1.0. This is not the actual post-liquefaction strength, but it proves to be useful in developing estimates of post-liquefaction strength (S_r) for this case history.

As explained in the preceding sections, failure is assumed to have occurred primarily due to liquefaction of the very loose silty sands of the upper few feet of the foundation soils immediately underlying the embankment fill.

Unit weights of the non-saturated embankment silty sands above the phreatic surface were modeled with a unit weight of $\gamma_m \approx 115$ lbs/ft^3, and this was then varied over a range of 112 to 118 lbs/ft^3 for parameter sensitivity studies. Unit weights of the saturated silty embankment sands below the phreatic surface were modeled with a unit weight of $\gamma_s \approx 120$ lbs/ft^3, and this was then varied over a range of 117 to 123 lbs/ft^3 for parameter sensitivity studies. The friction angle of the loose silty sands above the phreatic surface was modeled with $Ø' \approx 30°$, and a range of $Ø' \approx 28°$ to 33°.

A number of potential failure surfaces were analyzed, including (1) monolithic sliding along the full base of the entire embankment, and (2) smaller initial failures nearer to the downstream side, followed by (assumed) retrogressive propagation of the failure back towards the upstream side. These back-analyses showed that it was likely that this had been a retrogressive failure, initiating with a failure slice or wedge on the downstream side and then progressing, on a slice by slice basis, eventually back to the reservoir side. The depth that the failure surface penetrates into the foundation soils was also varied during the sensitivity studies.

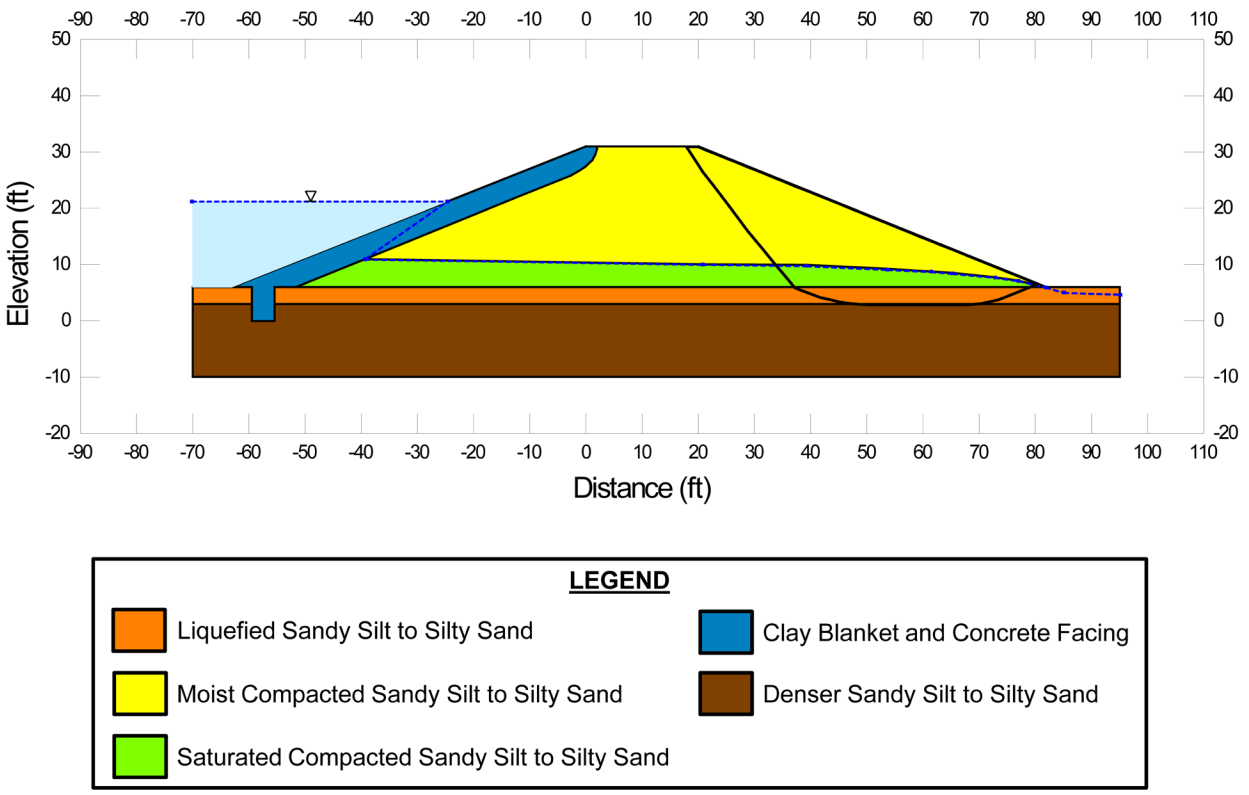

Figure B.2.4: Cross-section of Sheffield Dam used to back-calculate $S_{r,yield}$, showing the most critical initial failure surface.

Seed et al. (1969) had concluded that the entire base of the dam had liquefied, and that the reservoir pressures against the concrete-lined upstream face had then had pushed the dam downstream. These current studies found that to be unlikely, at least in the simplified manner described. Instead this appears likely to have been an incrementally retrogressive slide, initiated by liquefaction along the full base of the embankment, but with the first failure slices initiating nearer the downstream side. The failure then likely progressed incrementally back towards the upstream side, where reservoir pressures against the increasingly unbraced upstream face eventually produced a breach. The photograph and plan view of Figures B.2.2 and 2.2.3 are inconclusive here, suggesting some degree of de-aggregation of the slide mass but shedding no conclusive light on the question as to whether (1) the slide mass de-aggregated (incrementally) before the failure reached the reservoir side, or (2) the slide mass initiated movements monolithically and then de-aggregated as it traveled.

If the slide had initiated monolithically, then the post-liquefaction initial yield strength would have been the lateral force applied by the reservoir to the upstream face divided by the area of the base of the embankment. This would produce a calculated value of $S_{r,yield} \approx 51$ lbs/ft^2.

Initial failure of smaller slide features nearer to the downstream face (as the beginning stage of a retrogressive failure) appears more likely, based on these back-analyses, and the most

critical potential failure surface of this type is shown in Figure B.2.4. Based on the parameters described above, this failure surface results in a best estimate value of $S_{r,yield}$ = 345 lbs/ft^2, with a range of $S_{r,yield} \approx$ 299 to 370 lbs/ft^2.

Olson also performed back-analyses to estimate $S_{r,yield}$. He also assumed that the failure was retrogressive, and that an initial failure slice initiated first near the downstream side. His assumed initial failure surfaces were wedge-like failures similar to the failure shown in Figure B.2.4, except that (1) he assumed that the very loose upper foundation soils extended to slightly greater depths (approximately 7 feet below the base of the embankment), and (2) his toe failures exited farther downstream of the toe of the embankment. Olson's back-calculated best estimate of $S_{r,yield}$ was 15.4 kPa (321 lbs/ft^2), with a range of 12.7 to 18.0 kPa (265 to 376 lbs/ft^2). These appear to be in excellent agreement with the values back-calculated in these current studies.

B.2.5 Residual Strength Analyses Based on Residual Geometry

It was not possible to perform rigorous and reliable back-analyses to determine the value of $S_{r,resid/geom}$ required to produce a calculated Factor of Safety equal to 1.0 based on residual geometry because the post-failure residual geometry could not be suitably reliably determined based on the available information and data. The reported post-failure conditions, and the available photographs (e.g. Figure B.2.1) clearly show that the post-liquefaction strength was greater than zero, but they do not provide a basis for very refined estimates. This is a principal source of uncertainty for this case history.

Olson (2001) attempted to estimate the slopes and thicknesses of the post-failure residual embankment geometry based on available photographs, and then performed a simplified infinite slope analyses (for assumed residual, static conditions). The approximate slope angle used was not stated, nor the soil thicknesses, but the result was a reported best-estimate value of $S_{r,resid/geom}$ = 4.0 kPa (84 lbs/ft^2), with no range given.

In these current studies, it was assumed that $S_{r,resid/geom}$ would have at least been higher than zero. Values of $S_{r,resid/geom}$ back-calculated from the reasonably well-documented Class A case histories were examined for insight as to "expected" ranges of post-liquefaction strengths, and for the range of effective overburden stress and $N_{1,60,CS}$ values for this current case an approximate range of $S_{r,resid/geom} \approx$ 70 to 140 lbs/ft^2 was conservatively assumed, based on analyses of other Class A and B case histories. This range of values was selected to be slightly conservatively biased (a conservative bias of approximately 20% reduction of best estimates of $S_{r,resid/geom}$ was targeted here), so that any resulting error in evaluation of overall S_r would also be slightly conservative (nominally by approximately 10% or so). It is interesting to note that the mid-range value here would be 105 lbs/ft^2, in fairly good agreement of with the value of $S_{r,resid/geom}$ calculated and reported by Olson (2001) as described in the preceding paragraph.

B.2.6 Overall Estimates of S_r

Overall estimates of S_r for this Class B case history were made based on the observed geometry and runout features and characteristics, and the values of $S_{r,yield}$ and $S_{r,resid/geom}$ as calculated or estimated in the two preceding sections.

Runout characteristics for this case include a runout distance travelled by the center of gravity of the overall failure mass of D ≈ 125 feet, and a slope height (from toe to top of the back scarp) of H = 25 feet, producing a runout ratio of D/H ≈ 6. This led to a best estimate of $\xi \approx 0.5$ with a likely range of $\xi \approx 0.4$ to 0.6. Based on the relationship of Equation 4-4 and Figure 4.11, and best estimate values (and ranges) of $S_{r,yield}$ and $S_{r,resid/geom}$ from the preceding Sections B.6.4 and B.6.5, this produces and an overall best estimate of $S_r \approx 112$ lbs/ft^2, and a range of $S_r \approx 74$ to 153 lbs/ft^2. Based on the relationship of Figure 4.9, and the values of $S_{r,yield}$ from Section B.2.4, a second (less precise) estimate of the value of S_r was estimated based on pre-displacement FS ≈ 0.3 to 0.5, which produced estimates of $S_r \approx 105$ to 204 lbs/ft^2. Variance in values of back-calculated $S_{r,yield}$ and $S_{r,resid/geom}$ from these current studies were then also considered, and so were values back-calculated or estimated by previous investigators. Values from previous investigators were given little weight here, however, and these were simply examined largely to ensure that previous studies were understood and that the current engineering team had made suitable accommodation for potential uncertainty or variance.

Overall, based on an assumed normal distribution, it was judged that the (mean and median) best estimate of post-liquefaction strength for this case history is

$$\overline{S_r} = 138 \text{ lbs/ft}^2$$

and that the best estimate of standard deviation of mean overall post-liquefaction strength is

$$\sigma_{\overline{S}} = 23 \text{ lbs/ft}^2$$

Seed (1987) had reported a value of $S_r = 50$ lbs/ft^2 based on a simplified analysis of monolithic sliding along the full base of the dam pushed by lateral forces from the reservoir against the upstream face. That appears to have been an overconservative analysis, and it was adjusted upwards by Seed and Harder (1990) who reported a value of $S_r \approx 75$ lbs/ft^2, with a range of 50 to 100 lbs/ft^2, for this case. But theirs was still a deliberately conservative estimate for a case that they considered to be poorly constrained by the available data and information. Olson (2001) and Olson and Stark (2002) did not apply their "kinetics" method to this case, and so they did not independently develop an estimate of S_r that incorporated momentum effects. Instead, as described previously in Section B.2.5, they attempted to estimate the slopes and thicknesses of the post-failure residual embankment geometry based on available photographs, and then performed a simplified infinite slope analysis (for assumed residual, static conditions). They did not state the approximate slope angle they used, nor the soil thicknesses, but they reported a best-estimate value of $S_{r,resid/geom} = 4.0$ kPa (84 lbs/ft^2), which they judged to support the values of Seed and Harder (1990), and they then adopted the range of Seed and Harder. Similarly, Wang (2003) and Wang and Kramer (2008) did not employ their zero inertial force (ZIF) method to incorporate inertial effects in back-analyses of this failure. Instead they selected their value of S_r based on examination

of values from back-analyses by several previous investigators, and in the end selected $\overline{S_r}$ = 100.0 lbs/ft^2, and a standard deviation of $\sigma_{\overline{S}}$ = 29.8 lbs/ft^2. This may have been influenced significantly by the deliberately conservative (low) estimates of Seed and Harder (1990), which were repeated by Olson and Stark (2001, 2002) and thus entered twice into their suite of previous values considered.

Agreement between the values used in these three previous studies, and the values developed and employed in these current studies, is not very good unless one delves into the background (genesis) of the values used in the three preceding studies cited here. The current engineering team feel that the new values presented herein serve to correct the previous conservatism of Seed (1987) and of Seed and Harder (1990) for this challenging case history, and the (also low) values of Olson and Stark (2001, 2002) and Kramer and Wang (2003, 2008) which had been affected by the initial low estimates of Seed and Harder (1990) and of Seed (1987).

B.2.7 Evaluation of Initial Effective Vertical Stress

Average initial (pre-failure) effective vertical stress was assessed for the liquefied portion of the failure surface shown in Figure B.2.4). Parameters and sensitivity analyses were as described previously in Section B.2.4. Values of initial effective vertical stress were also calculated for assumed liquefaction across the full base of the embankment, but due to approximate symmetry, the resulting average initial vertical stresses did not differ significantly from those calculated for the liquefied portions of the failure plane of Figure B.2.4.

The resulting best estimate of average pre-failure effective stress within the liquefied materials controlling the failure was then $\sigma_{vo}' \approx$ 1,301 lbs/ft^2, with a reasonable range of $\sigma_{vo}' \approx$ 1,166 to 1,450 lbs/ft^2. This range is slightly non-symmetric about the median value, and this range was judged by the engineering team to represent approximately ± 2 standard deviations. Overall, the best characterization of initial (pre-failure) average effective vertical stress was then taken to be represented by a mean value of

$$\overline{\sigma'_{vo}} \approx 1{,}308 \text{ lbs/ft}^2$$

and with a standard deviation of

$$\sigma_{\overline{\sigma}} \approx 71 \text{ lbs/ft}^2$$

An estimate of σ_{vo}' was also calculated by Olson and Stark (2001, 2002). They reported a weighted average mean value of $\sigma_{vo}' \approx$ 68.4 kPa (1,428 lbs/ft^2), in good agreement with these current studies. Average initial vertical effective stresses were not directly reported by Wang (2003) and Kramer (2008), but they were published more recently in the publication by Kramer and Wang (2015). As discussed in Section 2.3.8.1(b)-(iii), Wang (2003) did not perform any independent analyses to assess σ_{vo}' for his 22 "secondary" cases, and this is one of those cases. Instead, he compiled values of S_r from multiple previous investigators, and averaged these for a best estimate. He also compiled multiple values of S_r/σ_{vo}' from previous investigators, and

averaged these for a best estimate. He then used these two best-estimate values of S_r and S_r/σ_{vo}' to infer a resulting representative value of $\sigma_{vo}' = 1{,}389$ lbs/ft^2. This is in good agreement with the values of (1) Olson (2001) and (2) these current studies.

B.2.8 Evaluation of $N_{1,60,CS}$

As described in Section B.2.3, there were no penetration test data available for the silty sands of the upper foundation immediately underlying the dam embankment within which the failure appears to have occurred. In situ density tests, and a Standard Proctor compaction test (ASTM D698) had indicated that the uppermost one to three feet of these soils existed at an equivalent relative compaction of RC = 76%.

Based on this relative compaction of 76% (Standard Proctor), and the correlations of Holtz and Gibbs (1979) and of Robertson and Campanella (1983), Olson (2001) estimated that the corresponding in situ relative density was approximately 20 to 40%. Then, based on this estimated range of relative density, he estimated an approximate value of $N_{1,60}$ on the order of 4 to 6 blows/ft.

Seed (1987) and Seed and Harder (1990) had employed similar processes and chains of logic, and had developed estimates of fines corrected $N_{1,60,CS}$ = 6 to 8 blows/ft, respectively.

In these current studies, this same approach is employed, and the characterization of penetration resistance is represented by a best estimate mean value of $\overline{N_{1,60,CS}} \approx 7$ blows/ft, and an estimated standard deviation of this mean of $\sigma_{\overline{N}} \approx 2.3$ blows/ft.

Wang (2003) and Kramer (2008) jointly developed a representative value of $\overline{N_{1,60,CS}} = 8.2$ blows/ft, and their estimated standard deviation of that overall mean value for this case history was $\sigma_{\overline{N}} = 6.8$ blows/ft. Details of the development of this interpretation by Wang and Kramer are not presented, but the very large variance (or standard deviation) in $\overline{N_{1,60,CS}}$ appears to have been an artifact of the procedures that they used to estimate such variances for poorly defined cases.

Overall agreement between these three independent assessments of representative $\overline{N_{1,60,CS}}$ values is judged to be very good, excepting the very large standard deviation ascribed by Wang and Kramer which reflects what they view to be large uncertainties with respect to the selection of a representative value of $N_{1,60,CS}$ for this case.

B.3 Helsinki Harbor (Finland; 1936)

B.3.1 Brief Summary of Case History Characteristics

Name of Structure	Helsinki Harbor
Location of Structure	Helsinki, Finland
Type of Structure	Harbor
Date of Failure	November 30, 1936
Nature of Failure	Static, During Fill Placement
Approx. Maximum Slope Height	19 ft.

B.3.2 Introduction and Description of Failure

A statically-induced liquefaction flow failure occurred on November 30, 1936 during construction of an engineered fill to serve as an extension of a section of the southern section of Helsinki Harbor. Figure B.3.1 shows both a plan view of this failure, and at the left-hand side of the figure it also shows the pre-failure and post-failure cross-sections through approximately the centerline of the feature.

The harbor extension was being created by placing sandy hydraulic fill into an outer confining berm that had been created by placement of blasted rock. The outer berm was not yet complete when hydraulic fill placement began, with an open "gap" in the rockfill dike, as shown in Figure B.3.1.

Figure B.3.1 shows pre-failure conditions at the time of the failure of November 30. During the night preceding the failure, a small slide (or slump) had occurred in the hydraulic sand fill adjacent to the opening in the rock dike. Filling was re-started the next day, and after only a few loads of additional sand had been placed a large flow failure occurred which carried approximately 6,000 m^3 of the hydraulic sand fill out through the gap in the rock dike and into the harbor (Andresen and Bjerrum, 1968). Detailed investigations after the failure showed that approximately 2 to 3 m of hydraulic sand fill remained in place over the foundation marine clays, and that the foundation clays were not disturbed and had not participated in the failure. This was thus a flow slide in the hydraulic sand fill, likely triggered by local over-steepening, that progressively retrogressed (and spread) until a large portion of the sand fill had become involved and had been carried out into the harbor.

B.3.3 Geology and Site Conditions

The soils of the Helsinki Harbor region are primarily deltaic and estuarine silty sands and clays. Fortunately, the clays that underlay the sandy hydraulic fill were not involved in this failure, so it is only necessary to characterize the silty sands of the hydraulic fill itself.

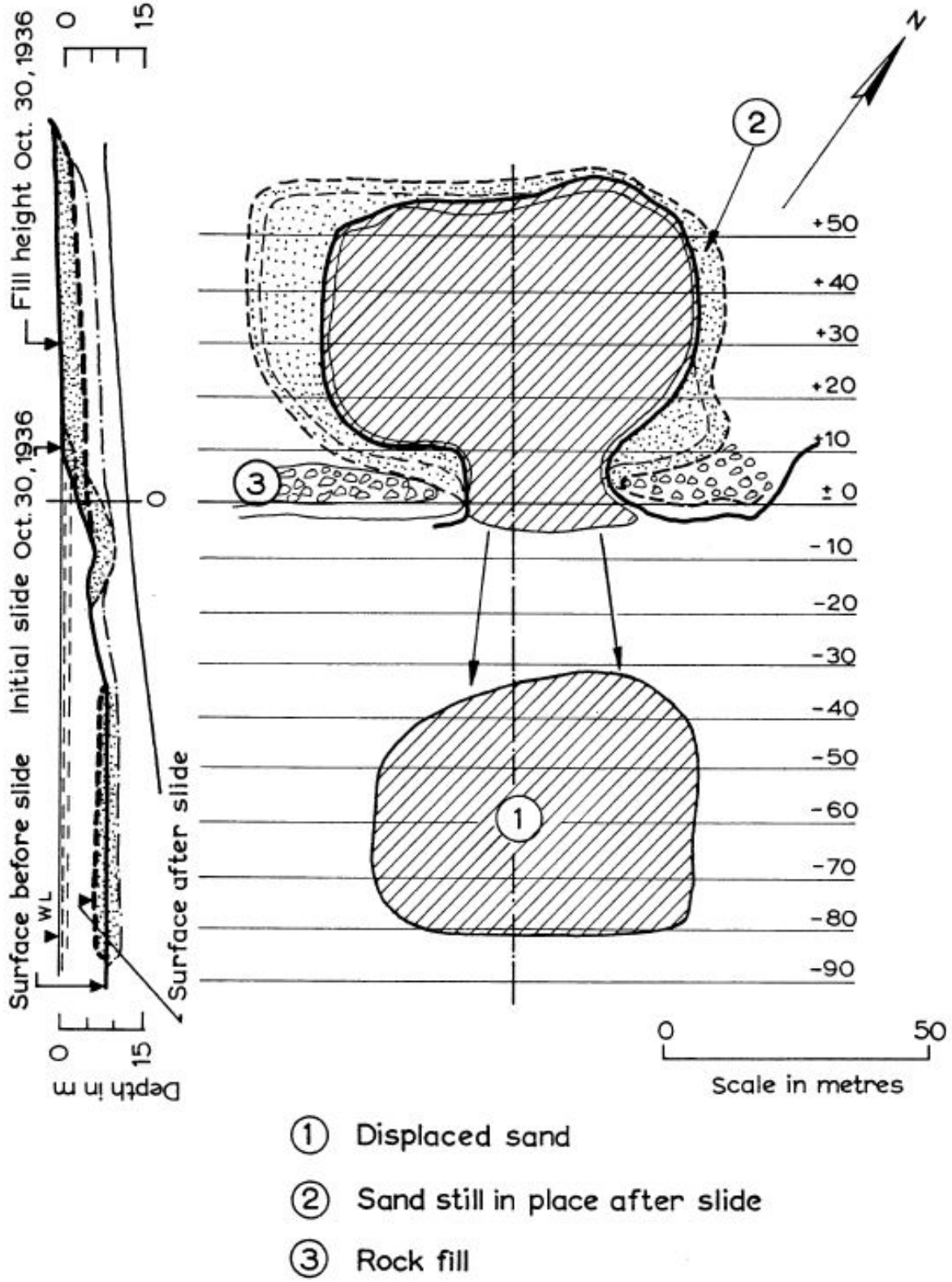

Figure B.3.1: Plan view, and pre-failure and post-failure cross-sections, of the Helsinki Harbor flow slide of November 30, 1936 (Figure from Andresen and Bjerrum, 1968).

The hydraulic fill is known to have been obtained from a nearby borrow source, and so it is generally assumed that the sandy fill was comprised of locally available deltaic deposits, and likely consisted of fine sands with variable fines content. This fill was hydraulically placed, and without compaction. Unfortunately, there is no further information or data available regarding the sandy hydraulic fill, and so gradation, fines contents, etc. are not known. The hydraulic fill would have been a loose, saturated sandy material, but there were no penetration test data or other useful data to provide a useful basis for quantitative assessment of penetration resistances.

B.3.4 Initial Yield Stress Analyses

Figure B.3.2 shows the cross-sections used for back-analyses of the post-liquefaction initial yield strength $S_{r,yield}$ that would be required within the foundation and embankment materials of the north dike section to produce a calculated Factor of Safety equal to 1.0. This is not the actual post-liquefaction strength, but it proves to be useful in developing estimates of post-liquefaction strength (S_r) for this case history.

This failure is known to have been an incrementally progressive retrogressive failure, initiated by a small failure near to the opening in the rock dike, and then retrogressing in a slice by slice progression to the eventual full failure scarp. Accordingly, both smaller (initiating) failures and also the overall (final) failure scarp will be analyzed with regard to values of $S_{r,yield}$.

Unit weights of saturated hydraulic sand fill materials were modeled with a unit weight of $\gamma_m \approx 113$ lbs/ft^3, and this was then varied over a range of 111 to 115 lbs/ft^3 for parameter sensitivity studies. Unit weights of the non-saturated sands and silty sands above the phreatic surface were modeled with a unit weight of $\gamma_s \approx 118$ lbs/ft^3, and this was then varied over a range of 116 to 120 lbs/ft^3 for parameter sensitivity studies. The friction angle of the non-saturated hydraulic fill materials above the phreatic surface was modeled with $Ø' \approx 30°$, and a range of $Ø' \approx 28°$ to 32°.

Both rotational and wedge-like potential initiating failure surfaces were analyzed, and the failure surface shown in Figure B.3.2(a) is the most critical potential "initiating" failure surface found. The value of $S_{r,yield}$ associated with this failure surface, based on best estimate soils parameters, is $S_{r,yield} = 104$ lbs/ft^2. Additional potential failure surfaces were analyzed, and parameters were varied over the ranges described above. The best overall characterization of localized "initiating" likely critical potential failure surfaces produced a best estimate value of $S_{r,yield} = 104$ lbs/ft^2, and a range of $S_{r,yield} = 88$ to 121 lbs/ft^2.

Figure B.3.2(b) illustrates the back-analysis of $S_{r,yield}$ for the overall (final) eventual failure scarp. Failure surface geometry and unit weights were varied, and the overall best estimate was found to be $S_{r,yield} = 60$ lbs/ft^2, with a range of $S_{r,yield} = 51$ to 71 lbs/ft^2.

Olson (2001) also calculated values of $S_{r,yield}$ for this case history. He analyzed rotational potential failure surfaces similar to the one shown in Figure B.3.2, and including failures that transgressed slightly into the underlying harbor clays. His reported best estimate of $S_{r,yield}$ was $S_{r,yield} = 3.8$ kPa (79 lbs/ft^2), with a range of 2.2 to 4.4 kPa (46 to 92 lbs/ft^2). This was in

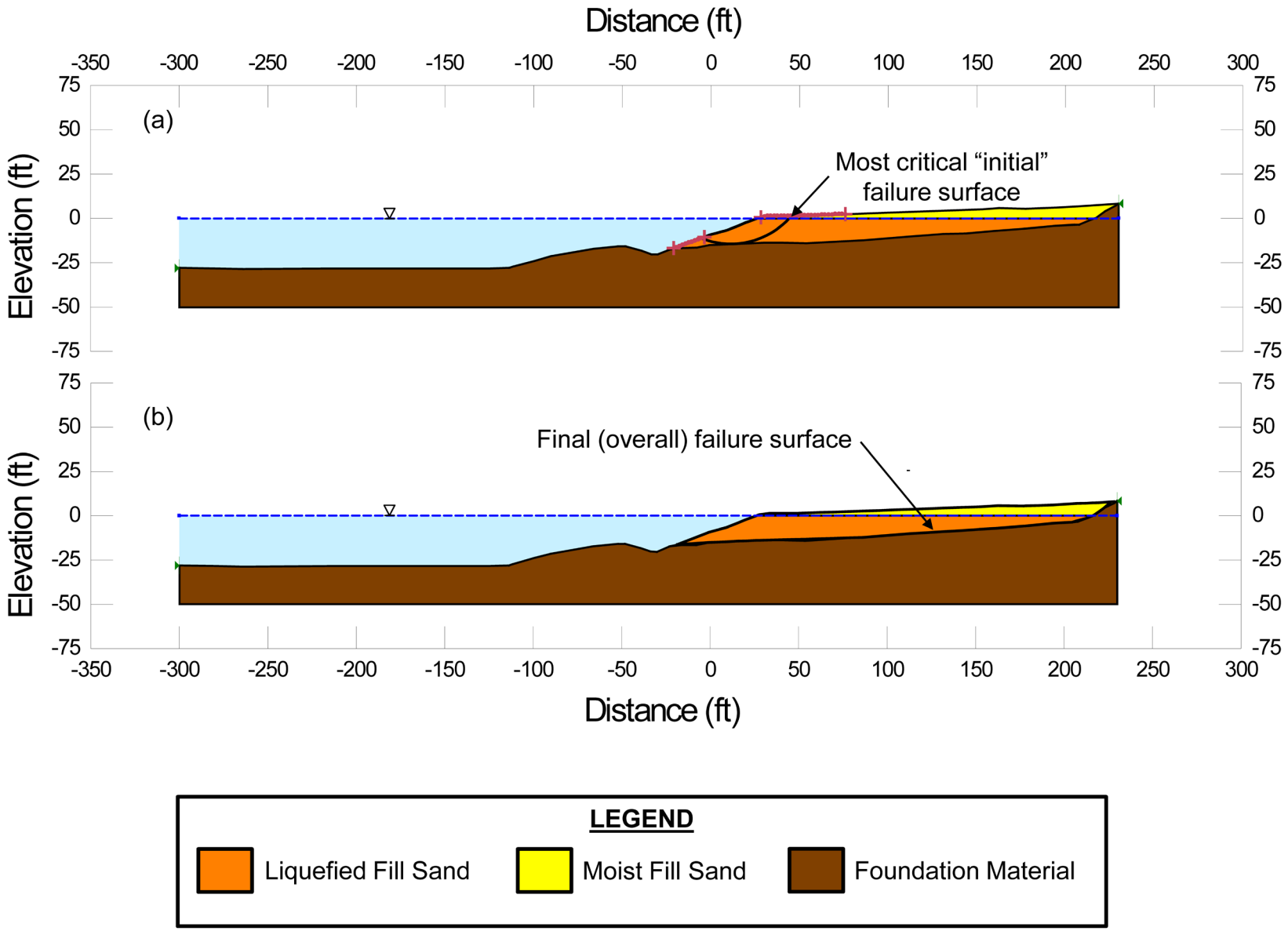

Figure B.3.2: Cross-sections used for back-analyses of $S_{r,yield}$ for the Helsinki Harbor liquefaction flow failure.

reasonably good agreement with the values calculated for the smaller "initiating" failures in these current studies as described above.

Overall estimates of "representative" $S_{r,yield}$ for purposes of evaluation of overall S_r were then developed by weighted averaging, employing a 3:1 weighting factor (for this strongly retrogressive failure) as

$S_{r,yield}$ = [3 x $S_{r,yield}$ (smaller initial yield surface) + $S_{r,yield}$ (final overall failure scarp)] / 4

Based on the range of variations in properties and parameters, and a range of potential failure mechanisms and associated feasible failure surfaces, the resulting best estimate overall of "representative" $S_{r,yield}$ was found to be $S_{r,yield}$ = 93 lbs/ft^2, with a range of $S_{r,yield}$ ≈ 79 to 109 lbs/ft^2.

B.3.5 Residual Strength Analyses Based on Residual Geometry

Back-analyses were also performed to evaluate the "apparent" post-liquefaction strength ($S_{r,resid/geom}$) required to produce a calculated Factor of Safety equal to 1.0 based on residual geometry. This is not a direct measure of post-liquefaction strength (S_r), as it neglects momentum effects and would underestimate S_r, but it is useful for overall evaluation of S_r for this case history.

Figure B.3.1 shows the post-failure cross-section geometry, both for the remaining hydraulic fill that remained in place within the partially confined filling basin, and also the hydraulic fill materials that flowed out through the opening in the rock dike and into the harbor. The average slope of the post-failure top of the hydraulic fill that traveled out into the harbor was reported to be approximately 4° to 5° (Andresen and Bjerrum, 1968). This is not the apparent slope shown in Figure B.3.1, but it is assumed that this slope is largely correct as reported and that the slope shown in the figure may be somewhat approximate in this regard.

Olson took this view, and employed an infinite slope analysis under static conditions, with slopes of 4° to 5° simultaneously modelled at both the top and the base of the failure mass, and with a modeled thickness of failure mass hydraulic fill materials reportedly taken from Figure B.3.1 (but the thickness selected was not stated), and he calculated and reported a best estimate of $S_{r,resid/geom}$ = 1.55 kPa (32 lbs/ft^2), with a range of $S_{r,resid/geom}$ = 1.1 to 2.0 kPa (23 to 42 lbs/ft^2).

In these current studies, a similar approach was taken, producing a best estimate value of $S_{r,resid/geom}$ ≈ 45 lbs/ft^2, and a range of $S_{r,resid/geom}$ ≈ 30 to 60 lbs/ft^2, with top and base slopes of 4° to 5°, and with failure mass thicknesses of 8 to 10 feet.

B.3.6 Overall Estimates of S_r

Overall estimates of S_r for this Class B case history were made based on the pre-failure geometry, the partial post-failure geometry, and the approximate runout features and characteristics, and the values of $S_{r,yield}$ and $S_{r,resid/geom}$ as calculated and/or estimated in the preceding sections.

Runout distance of the center of mass of the overall failure was approximately D ≈ 300 feet, and the initial failure slope height was H = 26 feet. This produces a runout ratio (defined as runout distance traveled by the center of gravity of the overall failure mass divided by the initial slope height from toe to back heel of the failure) of D/H = 11.5. This allows Equation 4-4, and Figures 4.7 and 4.11, to serve as one basis for estimation of post-liquefaction strength S_r. Using the ranges of $S_{r,yield}$ and $S_{r,resid/geom}$ from Sections B.3.4 and B.3.5, and assuming that $\xi \approx 0.45$ to 0.65 for this large runout case, with 0.525 as the best estimate, provided a best estimate value of $S_r \approx 38$ lbs/ft^2 and an estimated range of $S_r \approx 31$ to 55 lbs/ft^2. A second basis for estimation of S_r was the use of the relationship of Figure 4.9, and the range of values of $S_{r,yield}$ from Section B.3.4. Based on the large runout distance, values of initial (pre-failure displacement) Factor of Safety were taken as approximately 0.4 to 0.6, and this produced a best estimate value of $S_r \approx 46$ lbs/ft^2 and an estimated range of $S_r \approx 37$ to 64 lbs/ft^2. No similar use was made of Figure 4.9 in conjunction with the ranges of $S_{r,resid/geom}$ estimated in Section B.4.5 because these estimates of $S_{r,resid/geom}$ were considered to be very approximate.

The estimates by each of the two methods above were then averaged together, and this produced a best estimate value of $S_r \approx 42$ lbs/ft^2 and an estimated range of $S_r \approx 31$ to 64 lbs/ft^2. These estimates of variance are non-symmetric about the best estimated mean value, and the range was judged to represent approximately +/- 1.5 standard deviations, so further adjustments were then necessary.

Overall, based on an assumed normal distribution, it was judged that the (mean and median) best estimate of post-liquefaction strength for this case history is

$$\overline{S_r} = 48 \text{ lbs/ft}^2$$

and that the best estimate of standard deviation of mean overall post-liquefaction strength is

$$\sigma_{\overline{S}} = 14 \text{ lbs/ft}^2$$

Olson (2001) and Olson and Stark (2002) did not apply their "kinetics" method to this case, and so they did not independently develop an estimate of S_r that incorporated momentum effects. Instead they simply used their value of $S_{r,resid/geom}$ as a conservative approximation of S_r for this less well-defined case, and used $S_r = 1.55$ kPa (33 lbs/ft^2), with a range of 1.1 to 2.0 kPa (23 to 42 lbs/ft^2) in developing their predictive relationship. Because these values are based on residual post-failure geometry with an assumed Factor of Safety equal to 1.0, they do not include momentum effects and so they will be too low.

A better estimate can be obtained by using the values of $S_{r,yield}$ and $S_{r,resid/geom}$ back-calculated by Olson (2001), and then combining these using Equation 4-1, and a first-order estimate of $\xi \approx 0.8$. This would produce an estimate of $S_r \approx 44$ lbs/ft^2, as shown in Tables 4.3 and 4.6. This would agree well with the best-estimate value developed in these current studies.

Similarly, Wang (2003) and Wang and Kramer (2008) did not employ their zero inertial force (ZIF) method to incorporate inertial effects in back-analyses of this failure. Instead they selected their value of S_r based on examination of back-analyses of several previous investigators,

and averaged these to develop their selected $\overline{S_r}$ = 53.2 lbs/ft^2, and a (very high) standard deviation of $\sigma_{\overline{S}}$ = 19.0 lbs/ft^2. Their values are also in very good agreement with the values determined in these current studies.

B.3.7 Evaluation of Initial Effective Vertical Stress

This was a somewhat unusual failure case history because the observed failure was so strongly retrogressive; spreading from a small, localized initial failure to eventually encompass a significantly larger overall feature.

Average initial (pre-failure) effective vertical stress was assessed for the liquefied portion of the overall (final scarp) failure surface in Figure B.3.1. Parameters and sensitivity analyses were as described previously in Section B. 3.4. Additional analyses were then performed for alternate potential failure surfaces, including failure surfaces representing initial (smaller) slices of a retrogressive incremental failure eventually extending back to the apparent back heel of the final failure. The values of σ_{vo}' calculated for smaller (initial) failure slices were then averaged together with the values calculated for the overall (final) slide scarp, and these averaged value of the two failure surfaces was taken as "representative" here. This produced a moderately large, but finite, range of estimated values of average pre-failure effective stress within the liquefied materials controlling the failure.

The resulting best estimate of average pre-failure effective stress within the liquefied materials controlling the failure was then $\sigma_{vo}' \approx 842$ lbs/ft^2, with a reasonable range of $\sigma_{vo}' \approx 556$ to 1136 lbs/ft^2. This range is slightly non-symmetric about the median value, and this range was judged by the engineering team to represent approximately ± 2 standard deviations. Overall, the best characterization of initial (pre-failure) average effective vertical stress was then taken to be represented by a mean value of

$$\overline{\sigma'_{vo}} \approx 846 \text{ lbs/ft}^2$$

and a standard deviation of

$$\sigma_{\overline{\sigma}} \approx 105 \text{ lbs/ft}^2$$

The relatively large variance (and standard deviation) here is due in large part to the uncertainties associated with the averaging of smaller initial failure slices with the overall (final) failure scarp.

An estimate of σ_{vo}' was also calculated by Olson and Stark (2001, 2002). They reported a best estimate of $\sigma_{vo}' \approx 25$ kPa (522 lbs/ft^2), with a range of 20.1 to 29.9 kPa (420 to 624 lbs/ft^2). These values are somewhat lower than the values calculated and used in these current studies, and it is not clear why their values are so low. Average initial vertical effective stresses were not directly reported by Wang (2003) and Kramer (2008), but they were published more recently in the publication by Kramer and Wang (2015). As discussed in Section 2.3.8.1(b)-(iii), Wang (2003) did not perform any independent analyses to assess σ_{vo}' for his 22 "secondary" cases, and this is one of those cases. Instead, he compiled values of S_r from multiple previous investigators, and

averaged these for a best estimate. He also compiled multiple values of S_r/σ_{vo}' from previous investigators, and averaged these for a best estimate. He then used these two best-estimate values of S_r and S_r/σ_{vo}' to infer a resulting representative value of σ_{vo}'. As described in Section 2.3.8.1(b)-(iii), the resulting averaged values of S_r and of S_r/σ_{vo}' were incompatible with each other for a number of Wang's "secondary" case histories, and this process produced unreasonable values of σ_{vo}' for a number of case histories. For this case history, however, Wang's resulting value of $\sigma_{vo}' \approx 887$ lbs/ft^2 is in very good agreement with these current studies.

B.3.8 Evaluation of $N_{1,60,CS}$

As discussed previously in Section B.3.3 there were no penetration data of any type available for characterization of the hydraulic fill, and these was also only very limited information available regarding the nature of this sandy fill material.

Olson (2001) cites Sladen and Hewitt (1989) who indicated that hydraulic fills placed using a point source distribution typically have relative densities on the order of 40 to 50%. Based on this estimated range of relative density, and the correlations of Holtz and Gibbs (1979) and of Tokimatsu and Seed (1987), they then estimated an approximate representative value of $N_{1,60} \approx 6$ blows/ft. No range was given.

In this current study, the investigation team largely concurs, but adds a significant standard deviation to account for the multiple uncertainties here. The characterization of penetration resistance for these current studies is $\overline{N_{1,60,CS}} \approx 6$ blows/ft, with a standard deviation of $\sigma_{\overline{N}} \approx 2.0$ blows/ft.

Wang (2003) and Kramer (2008) selected a similar fines adjusted value of $\overline{N_{1,60,CS}} \approx 5.9$ blows/ft, and a very high standard deviation of $\sigma_{\overline{N}} \approx 8.0$ blows/ft. This very high standard deviation produces a value of $N_{1,60,CS}$ equal to zero at just the mean minus 0.73 standard deviations level, and at a mean plus two standard deviations the value would be approximately 21.9 blows/ft, which appears to be unreasonably high for the materials as described (and as they performed). This very high standard deviation in mean $N_{1,60,CS}$ is an artifact of the rigorously defined approach taken to evaluation of $N_{1,60,CS}$ in Dr. Wang's work, and it should be noted that neither the negative $N_{1,60,CS}$ values at mean minus more than 0.73 standard deviations, nor the very high values at mean plus more than about 2 standard deviations, likely had significant adverse impact on their overall predictive correlations. Uncertainty or variance was high, and the impact of this case history on the regressions that produced their predictive relationships was further reduced by their assigning a very low "Weighting Factor" of WF = 0.39 for this case.

Overall agreement with regard to characterization of $N_{1,60,CS}$ among these two previous studies, and the current study, is very good for this case with the exception of characterization of variance (or standard deviation) of the mean value of $N_{1,60,CS}$.

B.4 Solfatara Canal Dike (Mexico; 1940)

B.4.1 Brief Summary of Case History Characteristics

Name of Structure	Solfatara Canal Dike
Location of Structure	Mexico
Type of Structure	Dike
Date of Failure	May 18, 1940
Nature of Failure	Seismic, During 1940 El Centro Earthquake (M_L = 7.1)
Approx. Maximum Slope Height	9.5 ft.

B.4.2 Introduction and Description of Failure

Approximately 60 miles of canal banks were heavily damaged or destroyed in an area extending from the southeastern portion of California's Imperial Valley south across the border into Mexico as a result of earthquake shaking following the El Centro Earthquake of May 18, 1940 (Ross, 1968). Failures along the Solfatara Canal in Mexico accounted for about 12 of the 60 miles that experienced significant damage.

The damage to the dikes on the north and south sides of the Solfatara Canal is described by Ross (1968) as consisting primarily of longitudinal fissures and crest settlement of up to 7 feet into the foundation soils. One section of north dike, approximately 1,000 feet in length, reportedly moved laterally approximately 75 feet according to first hand observations (as subsequently reported in Ross, 1968). An approximate pre-failure and post-failure cross section for this failure section was developed and presented by Ross (1968), based on eyewitness reports and existing photographs, and this is shown in Figure B.4.1. The locations of soil borings S-1 and S-2, which were performed as part of the 1967 investigation by Ross (summarized in Ross, 1968), are also shown in this figure.

B.4.3 Geology and Site Conditions

Figure B.4.2 presents an enlarged view of the boring logs from the 1967 investigation as presented in Ross (1968). The borings were performed using a 5-inch diameter hand auger with no casing or drilling fluid. Borings performed at this site were advanced until the shallower soils sloughed, collapsing the hole. Following collapse of the hole, a probe was pushed with the combined weight of 2 men, estimated at approximately 350 lbs., until refusal in order to provide an indication as to the resistance of the soils beneath the base of the hole.

Boring S.1 was performed in the south dike and is reported to have only encountered levee fill material, consisting of loose clean fine sand. An effort to retrieve samples from the borings using a 2.8-inch diameter piston sampler resulted in the recovery of one sample from Boring S.1 at a depth of 7.4 feet in what is believed to be levee fill material. Results from tests performed on

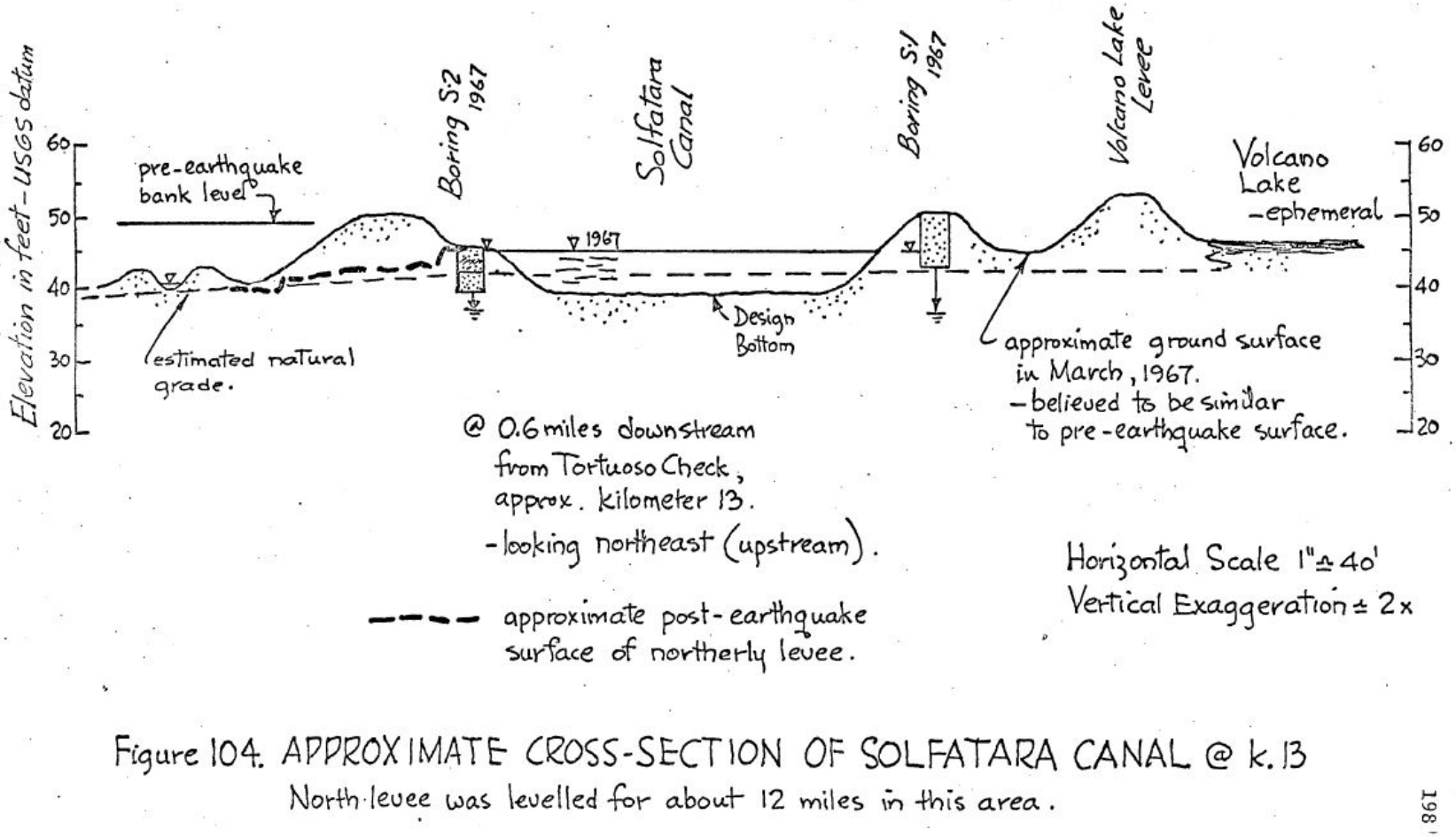

Figure B.4.1: Approximate cross-section showing both pre-failure and post-failure geometry of the Solfatara Canal at the 13 km canal marker (Figure from Ross, 1968)

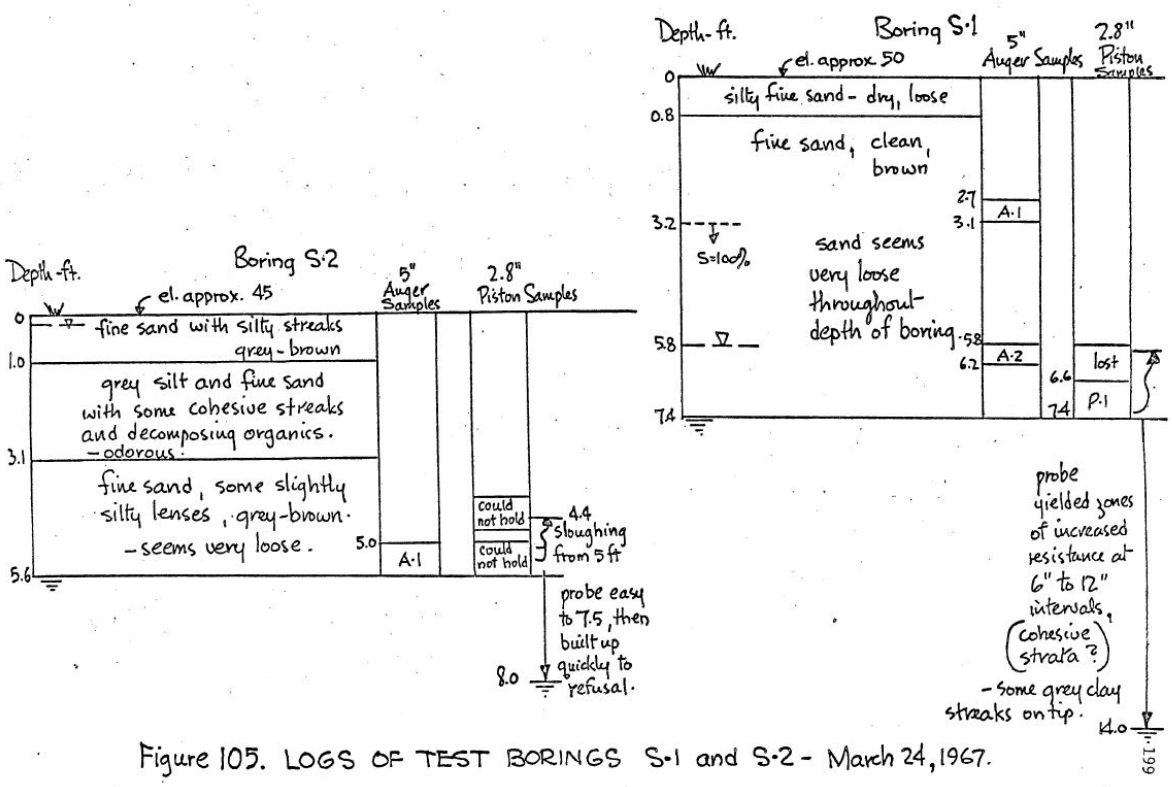

Figure B.4.2: Logs of Borings S-1 and S-2 from the Solfatara Canal at the 13 km canal marker (Figure from Ross, 1968)

the material from this sample P.1 within the levee embankment indicated a relative density of $D_r \approx 32\%$.

Boring S-2 was performed from the top of a bench on the remaining crest of the north dike, which was just above the canal water level at the time of the 1967 investigation. The north levee was found to consist of organic soil in the upper 3 feet, underlain by what is described in Ross (1968) as likely native, very loose fine sand with some slightly silty lenses. The likelihood that these were native soils was based in significant part on the fact that a stratum of decomposing organics, likely from the lakebed of Volcano Lake, was encountered near the top of the boring, underlain by loose sands and silty sands. No sample was able to be recovered from Boring S-2. Three additional borings along this bench, for which logs were not reported, all yielded the same lack of recovery in these loose sands. However, probing beneath the bases of all borings in the north levee did indicate a loose sand layer extending to a depth of about 7.5 feet, below which probing resistance (penetration resistance) reportedly increased rapidly. Ross (1968) considered the sands encountered in these north levee borings to likely represent natural soils. These fine sands and silty sands were very loose, and this along with their saturated condition, was considered to be the reason that samples could not be recovered.

B.4.4 Initial Yield Stress Analyses

Figure B.4.3 shows the cross-section used for back-analyses of the post-liquefaction initial yield strength $S_{r,yield}$ that would be required within the foundation and embankment materials of the north dike section to produce a calculated Factor of Safety equal to 1.0. This is not the actual post-liquefaction strength, but it proves to be useful in developing estimates of post-liquefaction strength (S_r) for this case history.

There were two general sets of potential failure mechanisms that could potentially explain the observed features, and the overall (approximate) observed post-failure geometry of Figure B.4.1. The first involves sliding primarily along liquefied materials at (and within) the upper portions of the loose, saturated native sands and silty sands underlying the embankment fill. The second involves sliding primarily along liquefied materials at (and within) the lower portions of the loose, saturated sands and silty sands of the fill that comprised the levee embankment. Both sets of possibilities were considered in these current studies.

The failure surface shown in Figure B.4.3 is the best estimate of the most critical initial failure surface for this section. This would infer that the failure may have been incrementally progressive, retrogressing in a series of successive slices back towards the eventual back-heel of the overall failure feature. This would also infer that the loose native upper foundation sands and silty sands underlying the levee embankment fill were of critical importance.

Additional failure surfaces, and failure mechanisms, were also back-analyzed. These included failure surfaces encompassing essentially the entire failure mass as initiating monolithically (all at once), and failure surfaces confined to within only the upper (loose, saturated) silty sand levee embankment fill.

There appeared to be little basis for differentiation in basic properties between the embankment fill materials and the underlying native soils. Unit weights of the non-saturated sands and silty sands above the phreatic surface were modeled with a unit weight of $\gamma_m \approx 117$ lbs/ft^3, and this was then varied over a range of 114 to 120 lbs/ft^3 for parameter sensitivity studies. Unit weights of the saturated sands and silty sands below the phreatic surface were modeled with a unit weight of $\gamma_s \approx 122$ lbs/ft^3, and this was then varied over a range of 119 to 125 lbs/ft^3 for parameter sensitivity studies. The friction angle of the loose sands and silty sands above the phreatic surface was modeled with $Ø' \approx 30°$, and a range of $Ø' \approx 28°$ to 33°.

Based on the range of variations in properties and parameters, and a range of potential failure mechanisms and associated feasible failure surfaces, the resulting best estimate value of $S_{r,yield}$ was found to be $S_{r,yield} = 149$ lbs/ft^2, with a range of $S_{r,yield} \approx 119$ to 182 lbs/ft^2.

Olson (2001) also performed back-analyses to estimate $S_{r,yield}$. He stated that his assumed failure mechanism was liquefaction of the loose, saturated levee embankment fill, but his assumed failure surface extended beneath the levee embankment fill and was an initial rotational feature similar to the failure surface shown as the best estimate case in Figure B.4.3 with much of the shear failure occurring within what may have been loose foundation soils. This represents an "initial slice" not encompassing the entire eventual failure mass, and so implies the assumption of a progressively retrogressive failure by slices for this case. Olson then also back-analyzed addi-

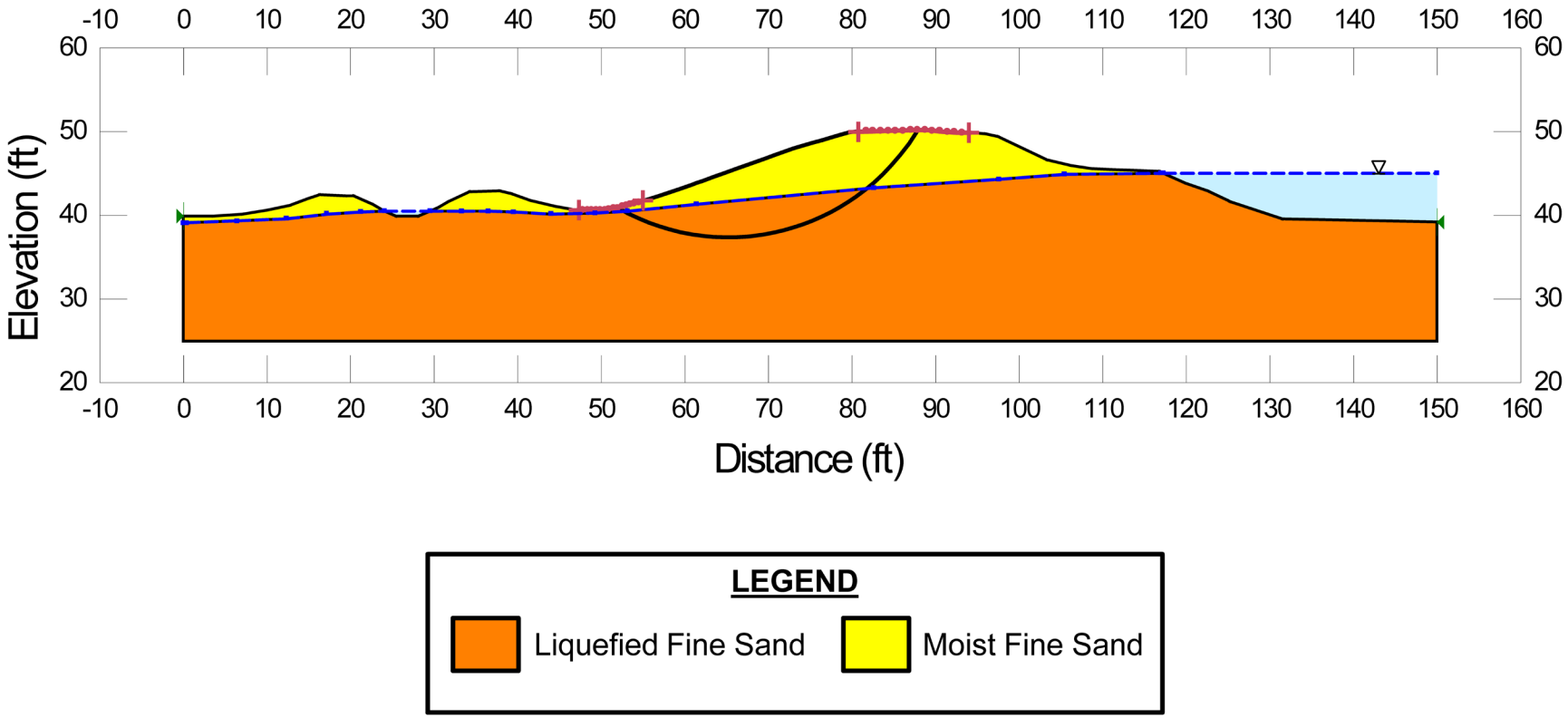

Figure B.4.3: Cross-section showing the pre-failure geometry and conditions for back-analyses of the initial yield strength ($S_{r,yield}$) for the failure section of the north dike of the Solfatara Canal.

tional potential failure surfaces and mechanisms, as with these current studies. Olson's best estimate of $S_{r,yield}$ was 6.0 kPa (125 lbs/ft^2), with a range of 3.9 to 6.75 kPa (81 to 141 lbs/ft^2).

B.4.5 Residual Strength Analyses Based on Residual Geometry

It was not possible to perform rigorous and reliable back-analyses to determine the value of $S_{r,resid/geom}$ required to produce a calculated Factor of Safety equal to 1.0 based on residual geometry because the post-failure residual geometry reported was not fully accurate or reliable. The reported post-failure cross-section shows that the post-liquefaction strength was greater than zero, but does not provide a basis for very refined estimates. This is a principal source of uncertainty for this case history.

The sketch presented in Figure B.5.1 shows the slope of the post-failure embankment to be as steep as 6.5°, but conservation of mass is not achieved with the post-failure cross-section as shown in this figure. The "probing" at the base of the boreholes suggested that the foundation soils became denser (or at least more difficult to penetrate) at a depth of approximately 7.5 feet beneath the bases of the borings, but this provides poor definition of the depth of potentially liquefiable materials. Assuming a range of residual slopes of 4° to 6°, and thicknesses of potentially liquefiable soils that extended up to as much as 0 to 8 feet below the dashed line in Figure B.5.1, infinite slope analyses provide potential estimates of $S_{r,resid/geom} \approx 25$ to 120 lbs/ft^2. Given the overall uncertainties here, the current investigation team selected a best estimate of $S_{r,resid/geom} \approx 70$ lbs/ft^2, with a large range of approximately 25 to 120 lbs/ft^2.

Olson was the other investigator to report a value of $S_{r,resid/geom}$. He assumed that the slope of the failed mass was the same as that of the natural grade, with a slope of approximately 4°. He spread the failure mass (removed from its initial position) over an assumed runout footprint, and estimated the average thickness of the runout failure mass to be approximately 1.8 m. He then performed an infinite slope analysis to estimate $S_{r,resid/geom} = 2.4$ kPa (50 lbs/ft^2). Olson noted that this was essentially the same as the value of post-liquefaction strength reported by Seed and Harder (1990), who reported a value of $S_r \approx 50$ lbs/ft^2 and a range of 25 to 75 lbs/ft^2. The values of Seed and Harder had, however, been targeted at conservative estimation of actual post-liquefaction strength (S_r), rather than $S_{r,resid/geom}$.

B.4.6 Overall Estimates of S_r

Overall estimates of S_r for this Class B case history were made based on the pre-failure geometry and the approximate runout features and characteristics, and the values of $S_{r,yield}$ and $S_{r,resid/geom}$ as calculated in the preceding sections.

Runout characteristics for this case cannot be fully accurately assessed due to the approximate nature of the post-failure cross section as reported. It was noted that runout ratio (runout distance traveled by the center of gravity of the overall failure mass divided by the initial slope height from toe to back heel of the failure) was large to very large. This allowed Equation 4-4, and Figures 4.7 and 4.11 to serve as one basis for estimation of post-liquefaction strength S_r.

Using the ranges of $S_{r,yield}$ and $S_{r,resid/geom}$ from Sections B.4.4 and B.4.5, and assuming that $\xi \approx 0.45$ to 0.65 for this large runout case, with 0.55 as the best estimate, provided a best estimate value of $S_r \approx 60$ lbs/ft^2 and an estimated range of $S_r \approx 32$ to 98 lbs/ft^2. A second basis for estimation of S_r was the use of the relationship of Figure 4.9, and the range of values of $S_{r,yield}$ from Section B.4.4. An additional estimate was made using Figure 4.9 in conjunction with the values of $S_{r,yield}$ from Section B.4.4. Based on the large runout distance, values of initial (pre-failure displacement) Factor of Safety were taken as approximately 0.4 to 0.6, and when combined with the range of $S_{r,yield}$ from Section B.4.4, this produced a best estimate value of $S_r \approx 74$ lbs/ft^2 and an estimated range of $S_r \approx 48$ to 109 lbs/ft^2. No similar use was made of Figure 4.9 in conjunction with the ranges of $S_{r,resid/geom}$ estimated in Section B.4.5 because these estimates of $S_{r,resid/geom}$ were considered to be very approximate. These two sets of estimates of S_r, and of variance or standard deviation, were then averaged. The overall variance was then slightly non-symmetric about the best estimated mean value, so further adjustments were then necessary. Considering these ranges of estimated S_r, and their bases, the best estimate of post-liquefaction strength was then taken as $S_r \approx 64$ lbs/ft^2, with a range of 32 to 109 lbs/ft^2. This was then adjusted to provide a characterization compatible with the assumed normal distribution that would be employed in the regressions that would follow.

Overall, based on an assumed normal distribution, it was judged that the (mean and median) best estimate of post-liquefaction strength for this case history is

$$\overline{S_r} = 64 \text{ lbs/ft}^2$$

and that the best estimate of standard deviation of mean overall post-liquefaction strength is

$$\sigma_{\overline{S}} = 22 \text{ lbs/ft}^2$$

This represents a very large degree of uncertainty, or variance, and it is noted that approximately mean minus three standard deviations produces a value of S_r approximately equal to zero for this case history.

Seed and Harder (1990) reported a value of $S_r \approx 50$ lbs/ft^2 for this case, and a range of 25 to 75 lbs/ft2. Olson (2001) and Olson and Stark (2002) did not apply their "kinetics" method to this case, and so they did not independently develop an estimate of S_r that incorporated momentum effects. Instead they simply used their value of $S_{r,resid/geom}$ as a conservative approximation of S_r for this less well-defined case, and used $S_r = 2.4$ kPa (75lbs/ft^2) in developing their predictive relationship. Similarly, Wang (2003) and Wang and Kramer (2008) did not employ their zero inertial force (ZIF) method to incorporate inertial effects in back-analyses of this failure. Instead they selected their value of S_r based on examination of back-analyses of several previous investigators, and in the end selected $\overline{S_r} = 77.1$ lbs/ft^2, and a standard deviation of $\sigma_{\overline{S}} = 25.6$ lbs/ft^2. Despite these differing approaches taken to evaluation and/or selection of S_r, agreement between the values used in these three previous studies, and the values developed and employed in these current studies, is generally very good for this case history.

B.4.7 Evaluation of Initial Effective Vertical Stress

Average initial (pre-failure) effective vertical stress was assessed for the liquefied portion of the failure surface in Figure B.4.4. Parameters and sensitivity analyses were as described previously in Section B.6.4. Additional analyses were then performed for alternate potential failure surfaces, including failure surfaces representing the end result of retrogressive incremental failures extending back to the apparent back heel of the final failure. Depths of failure surfaces were varied, and both rotational and translational (wedge-like) failure surfaces were considered. This produced a moderately large, but finite, range of estimated values of average pre-failure effective stress within the liquefied materials controlling the failure.

The resulting best estimate of average pre-failure effective stress within the liquefied materials controlling the failure was then $\sigma_{vo}' \approx 669$ lbs/ft^2, with a reasonable range of $\sigma_{vo}' \approx 548$ to 784 lbs/ft^2. This range is slightly non-symmetric about the median value, and this range was judged by the engineering team to represent approximately ± 2 standard deviations. Overall, the best characterization of initial (pre-failure) average effective vertical stress was then taken to be represented by a mean value of

$$\overline{\sigma'_{vo}} \approx 669 \text{ lbs/ft}^2$$

and with a standard deviation of

$$\sigma_{\bar{\sigma}} \approx 59 \text{ lbs/ft}^2$$

An estimate of σ_{vo}' was also calculated by Olson and Stark (2001, 2002). They reported a weighted average mean value of $\sigma_{vo}' \approx 29.9$ kPa (624 lbs/ft^2), in excellent agreement with these current studies. Average initial vertical effective stresses were not directly reported by Wang (2003) and Kramer (2008), but they were published more recently in the publication by Kramer and Wang (2015). As discussed in Section 2.3.8.1(b)-(iii), Wang (2003) did not perform any independent analyses to assess σ_{vo}' for his 22 "secondary" cases, and this is one of those cases. Instead, he compiled values of S_r from multiple previous investigators, and averaged these for a best estimate. He also compiled multiple values of S_r/σ_{vo}' from previous investigators, and averaged these for a best estimate. He then used these two best-estimate values of S_r and S_r/σ_{vo}' to infer a resulting representative value of σ_{vo}'. As described in Section 2.3.8.1(b)-(iii), the resulting averaged values of S_r and S_r/σ_{vo}' were incompatible with each other for a number of Wang's "secondary" case histories, and this process produced unreasonable, and in some cases physically infeasible, values of σ_{vo}' for a number of case histories. Wang's value of $\sigma_{vo}' = 1{,}224$ lbs/ft^2 is clearly physically infeasible for this case, based on the cross-section, and so it is not considered a useful check here. Agreement between Olson's value, which is well-documented, and the value developed in these current studies is very good.

B.4.8 Evaluation of $N_{1,60,CS}$

Section B.5.3 described the geology and materials involved in this case history, and explained that there were no formal penetration data for the materials involved in this failure. This

failure either occurred mainly within the lower portion of the loose sand and silty sand dike embankment fill, or in the upper portion of the immediately underlying loose foundation sands and silty sands.

The single piston sample obtained from Boring S-1 reportedly had a relative density of 32%, but the basis for this D_r is not clearly explained (the full details of evaluation of e_{max} and for e_{min} are not clearly presented). It is also not known with certainty whether this sample represented the embankment fill, or the underlying foundation soils.

Both the embankment sands and silty sands, and the underlying foundation sands and silty sands, were clearly very loose materials, based on the descriptions provided by Ross (1968) and the difficult of retrieving piston samples. Precise estimation of representative penetration resistance for these soils is, however, a significant source of uncertainty for this case history.

Olson (2001) used the reported relative density of $D_r \approx 32\%$, and a suite of relationships between relative density and penetration resistance, to develop an estimate of representative penetration resistance of $N_{1,60} \approx 4$ blows/ft, with a range of approximately 4 to 5 blows/ft. This was an $N_{1,60}$ value, as there was no correction for fines.

In these current studies, a best estimate value of $\overline{N_{1,60,CS}} \approx 4.5$ blows/ft was selected to represent these loose sands and silty sands, and a proportionally large standard deviation of $\sigma_{\overline{N}} \approx 1.5$ blows/ft. was applied to represent the significant uncertainty here. Mean minus three standard deviations produces a value of zero.

Wang (2003) and Kramer (2008) selected a slightly higher value of $\overline{N_{1,60,CS}} \approx 4.9$ blows/ft, and a significantly higher value of $\sigma_{\overline{N}} \approx 6.9$ blows/ft. This very high standard deviation produces a value of $N_{1,60,CS}$ equal to zero at just the mean minus 0.71 standard deviations level, and at a mean plus two standard deviations the value would be approximately 18.7 blows/ft, which appears to be unreasonably high for the materials as described (and as they performed). This very high standard deviation is an artifact of the rigorously defined approach taken to evaluation of $N_{1,60,CS}$ in Wang's work, and it should be noted that neither the negative $N_{1,60,CS}$ values at mean minus more than 0.71 standard deviations, nor the very high values at mean plus more than about 2 standard deviations, likely had significant impact on their overall predictive correlations. The basis for their selection of $\overline{N_{1,60,CS}} \approx 4.9$ blows/ft is not presented.

Seed and Harder (1990) had selected a representative value of $N_{1,60,CS} = 4$ blows/ft.

Overall, the values of representative $N_{1,60}$ and $N_{1,60,CS}$ selected among these three previous studies, and the values selected in this current study, appear to be in generally good agreement, and variance or uncertainty appears to be relatively large.

B.5 Lake Merced Bank (California, USA; 1957)

B.5.1 Brief Summary of Case History Characteristics

Name of Structure	Lake Merced Bank
Location of Structure	California, USA
Type of Structure	Lakeside Bank and Fill
Date of Failure	March 22, 1957
Nature of Failure	Seismic, During 1957 San Francisco Earthquake (M_L = 5.3)
Approx. Maximum Slope Height	32.3 ft.

B.5.2 Introduction and Description of Failure

During the 1957 San Francisco Earthquake (M_L = 5.3), a series of small to moderate slope failures occurred around the edges of the southern end of Lake Merced, near San Francisco. Figure B.5.1 shows the locations of these five features. The largest of these, Slide 1, was investigated by Ross (1968) as part of a study of landslides and sloughs induced both near the Pacific coast as well as around the edges of Lake Merced. The 1957 earthquake was not a large event, but the south end of Lake Merced is located within approximately 3 km of the section of the San Andreas fault which ruptured during this moderate event.

Figure B.5.2 presents a cross-section through the failure (from Ross, 1968), showing the pre-failure and post-failure conditions. The failure appears to have been a liquefaction-induced slope failure, with sliding occurring primarily within loosely placed lake shore fill sands, but also potentially involving some of the underlying natural lakeshore deposits that were also loose and saturated. The post-failure geometry for Slide 2 was not determined in detail, so it is Slide 1 that will be analyzed in these current studies.

The actual shaking level that occurred at Lake Merced during this small magnitude event is unknown, as there were no local strong motion instruments in the area. Based on modern attenuation relationships, and a single instrument recording obtained at Golden Gate Park (approximately 11 km from the fault rupture) which recorded a peak horizontal acceleration of approximately 0.12g, it appears that the peak horizontal acceleration at Lake Merced would have been a bit higher than 0.12g, but with a short duration and a limited number of significant cycles.

B.5.3 Geology and Site Conditions

The lakes occupies a trough that largely parallels the San Andreas fault, which was infilled with marine sediments during the Pleistocene. The uppermost materials in the lake area are primarily fine aeolian sands and silty sands blown across from the coastal sand dunes to the west. These can be very loose. The uppermost lake bed deposits are primarily aeolian and fluvial fine sands and silty sands, with several layers of clays and some peats.

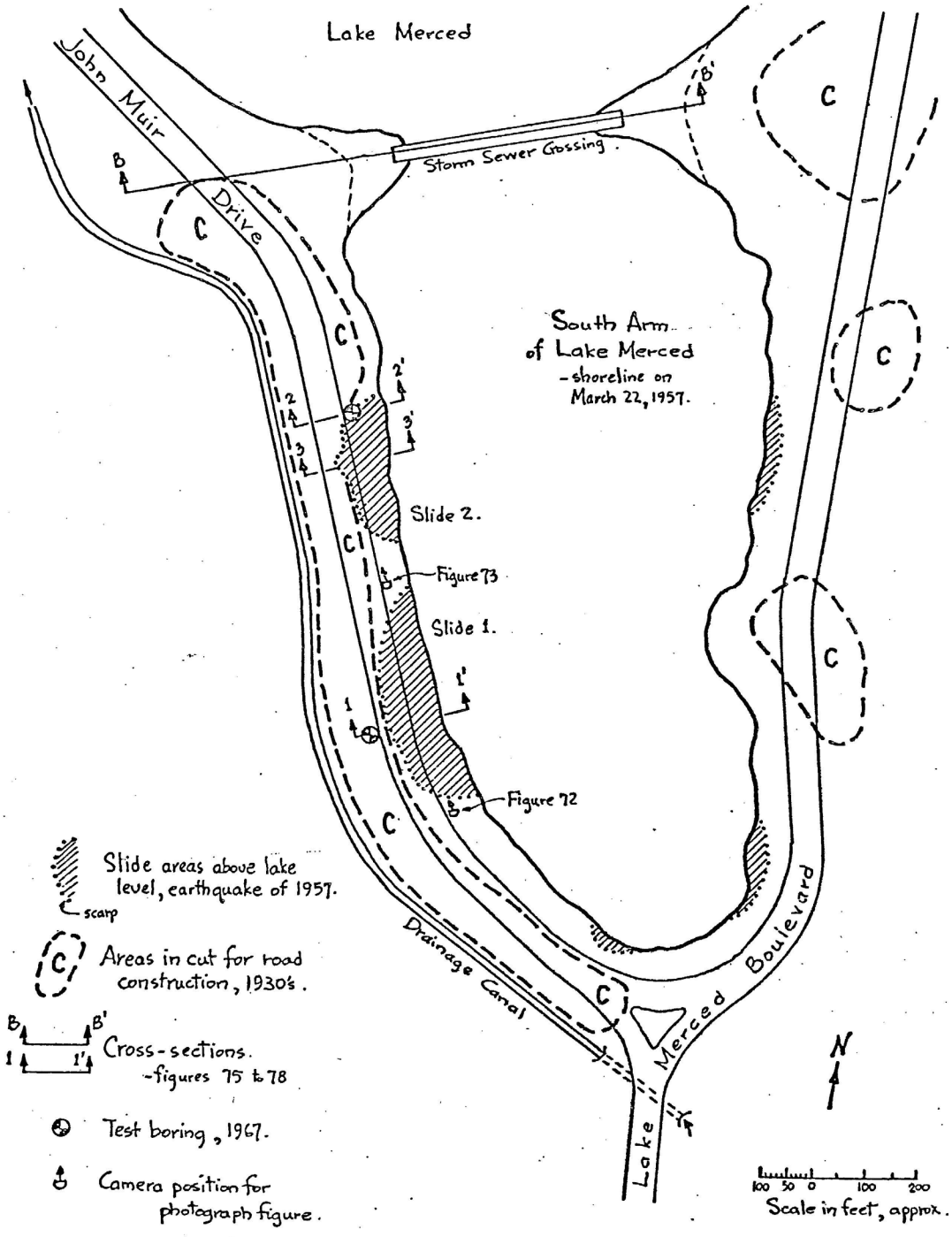

Figure B.5.1: Plan View of the south end of Lake Merced, showing the five edge failures, and the locations of Slides 1 and 2 and of the two borings performed to investigate them (Figure from Ross, 1968).

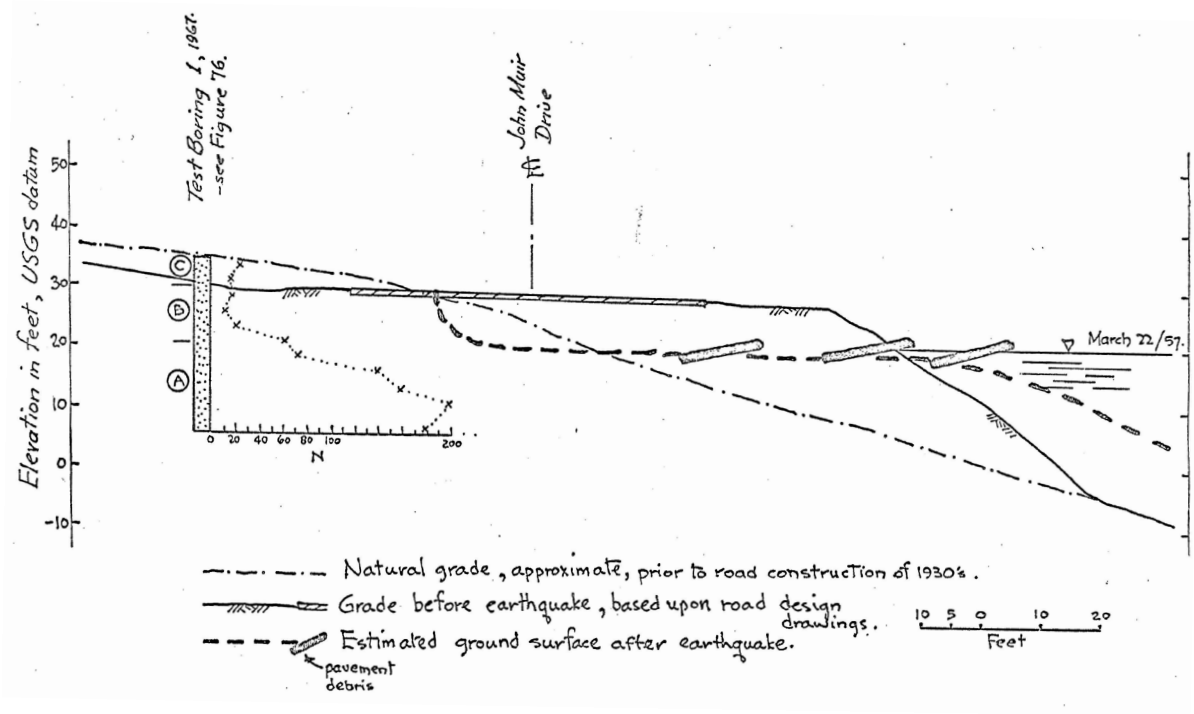

Figure B.5.2: Cross-section through Slide 1 showing the pre-failure and post-failure geometries and the location of Test Boring 1 and the SPT data from this test boring (Figure from Ross, 1968).

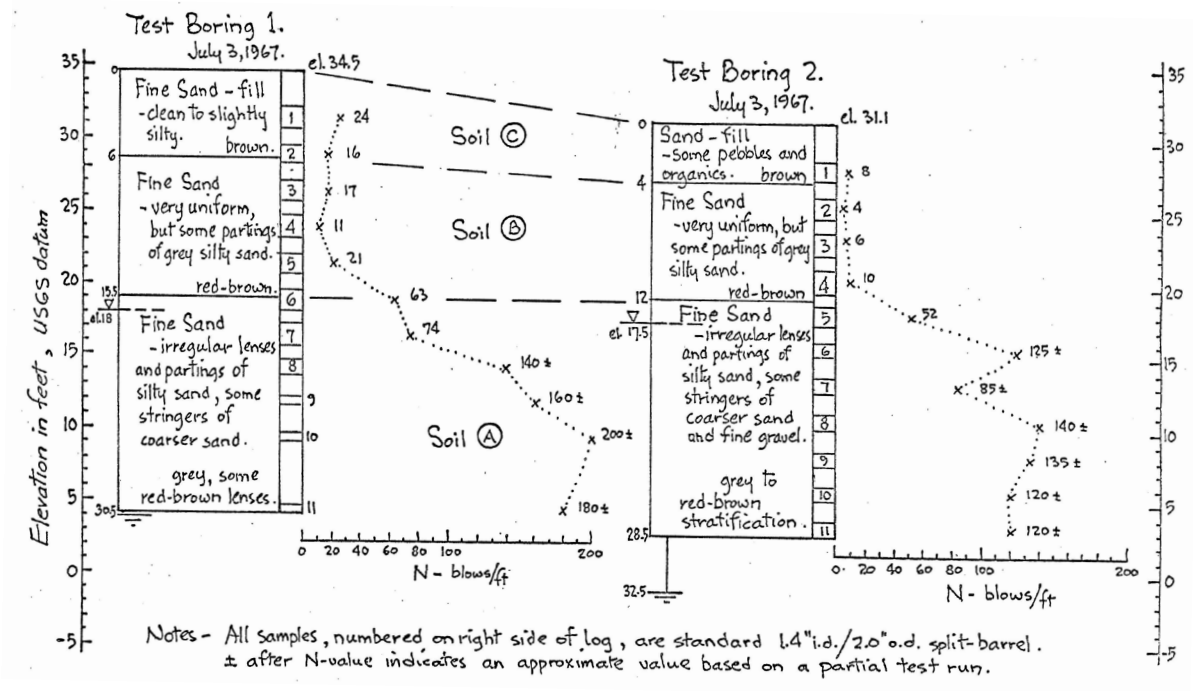

Figure B.5.3: Boring logs from Test Borings 1 and 2 showing soil types and also SPT results (Figure from Ross, 1968).

The current configuration of the west bank of Lake Merced is the result of cut and fill operations performed to create the existing lake shoreline. Figure B.5.1 shows dashed outlines of zones marked "C" indicating areas where borrow materials were excavated for use in road construction. Lakeshore fills were placed to create the necessary right of way for construction of John Muir Drive along the west shoreline. These excavated materials were fine sands and silty sands, and they were placed by end dumping to extend the shoreline into the lake. Compaction details are not known, and previous investigators have assumed that these soils were in a very loose condition. It should be noted, however, that the underlying natural soils were also in a very loose condition, and that liquefaction within only the natural soils underlying the fill would have been sufficient to explain the failure observed.

As shown in Figure B.5.1, two SPT borings were performed to investigate Slide 1 and Slide 2. These two borings were each located behind the rear heel scarps of the slides, and they both appear to have been performed either entirely in native ground, in which case they do not serve to also characterize the fill, or they may have encountered fill in their upper 4 to 6 feet.

Figure B.5.3 presents the logs of these two borings. The uppermost 4 to 6 feet of material encountered in these two borings was logged as "fill" (Soil C), and it was comprised of fine sands with some silt, and in Boring 2 also some pebbles and organics. If this characterization of the upper materials as "fill" is accurate, then as many as 3 SPT blowcounts were obtained in this fill and it was indeed a loosely dumped material.

The next material encountered in both borings is Soil B, and it appears to be very loose fine sand with some occasional silt. This material is logged as natural soil, and it has very low SPT blowcounts as well; characteristic of the local aeolian deposits and dune sands.

The deeper unit encountered (Soil C) was also primarily fine sand with some silt, but it was notably denser, with significantly higher SPT blowcounts.

Various investigators who have back-analyzed this case history have had differing views as to whether or not the uppermost material encountered in Test Borings 1 and 2 was actually fill, or whether there is no SPT data for the fill material so that approximate blowcounts have to be inferred based on assumptions regarding this loosely end dumped material. In either case, most previous investigators have assumed that a majority of the failure occurred due to liquefaction-induced sliding in the lower portion of the fill, and that the native materials played a lesser role.

In these current studies, it is recognized that both the end dumped fill, and the underlying native soils, are fine sands with some silt, and that both are likely to be very loose. Accordingly, a suite of potential failure surfaces, and mechanisms, were analyzed.

Characterization of the fill material can be based either simply on the assumption that it was loosely end dumped, or it can be based on the 3 SPT N-values logged by Ross (1968) as occurring in fill in the upper 4 to 6 feet of Test Borings 1 and 2. Characterization of the underlying uppermost native soil (Soil B) is more straightforward as multiple SPT N-values are available in Test Borings 1 and 2 within this material.

B.5.4 Initial Yield Stress Analyses

Figure B.5.4(a) shows the cross-section used for back-analyses of the post-liquefaction initial yield strength $S_{r,yield}$ that would be required within the liquefied upstream shell materials to produce a calculated Factor of Safety equal to 1.0. This is not the actual post-liquefaction strength, but it proves to be useful in developing estimates of post-liquefaction strength (S_r) for this case history.

There were two general sets of potential failure mechanisms that could potentially explain the observed features, and the overall observed post-failure geometry of Figure B.5.3. The first involves sliding primarily along liquefied materials at (and within) the upper portions of the loose, saturated natural aeolian sands underlying the fill. The second involves sliding along a slightly shallower failure surface within the lower portion of the loose, saturated sand fill. In either case, the failure surface appears to occur roughly sub-parallel to the existing slope face downslope of the toe of the fill. Failure surfaces were varied over a finite range, above and below the failure surface shown in Figure B.5.4(a), and a range of resulting values of $S_{r,yield}$ were back-calculated based on these failure surfaces.

Unit weights of the non-saturated sands above the phreatic surface were modeled with a unit weight of $\gamma_m \approx 105$ lbs/ft^3, and this was then varied over a range of 100 to 110 lbs/ft^3 for parameter sensitivity studies. Unit weights of the saturated sands below the phreatic surface were modeled with a unit weight of $\gamma_s \approx 110$ lbs/ft^3, and this was then varied over a range of 105 to 115 lbs/ft^3 for parameter sensitivity studies. The friction angle of the loose sands above the phreatic surface was modeled with $Ø' \approx 35°$, and a range of $Ø' \approx 32°$ to 38°.

The resulting best estimate value of $S_{r,yield}$ was found to be $S_{r,yield} = 190$ lbs/ft^2, with a range of $S_{r,yield} \approx 153$ to 236 lbs/ft^2.

Olson also performed back-analyses to estimate $S_{r,yield}$. His assumed failure surface was exactly parallel to the apparent slope face downstream of the toe of the fill, and he assumed that the failure occurred within the loose fill material (and not the underlying aeolian sands). He assumed that the drainage length at the toe was "very small", and assigned a drained frictional strength of $Ø' = 35°$ at the toe, but the length of the failure surface over which this was applied is not clearly explained. His most critical failure is a wedge-like failure with an initial back heel steeper than that shown in Figure B.5.4(a). This represents an "initial slice" not encompassing the entire eventual failure mass, and so implies the assumption of a progressively retrogressive "failure by slices" for this case. Olson's back-calculated best estimate of $S_{r,yield}$ was 17.7 kPa (369 lbs/ft^2), with a range of 15.7 to 18.1 kPa (328 to 380 lbs/ft^2).

B.5.5 Residual Strength Analyses Based on Residual Geometry

The calculation of the "apparent" post-liquefaction strength ($S_{r,resid/geom}$) required to produce a calculated Factor of Safety equal to 1.0 based on residual geometry is illustrated in Figure B.5.4(b). Modeling parameters and details are as described in the preceding section.

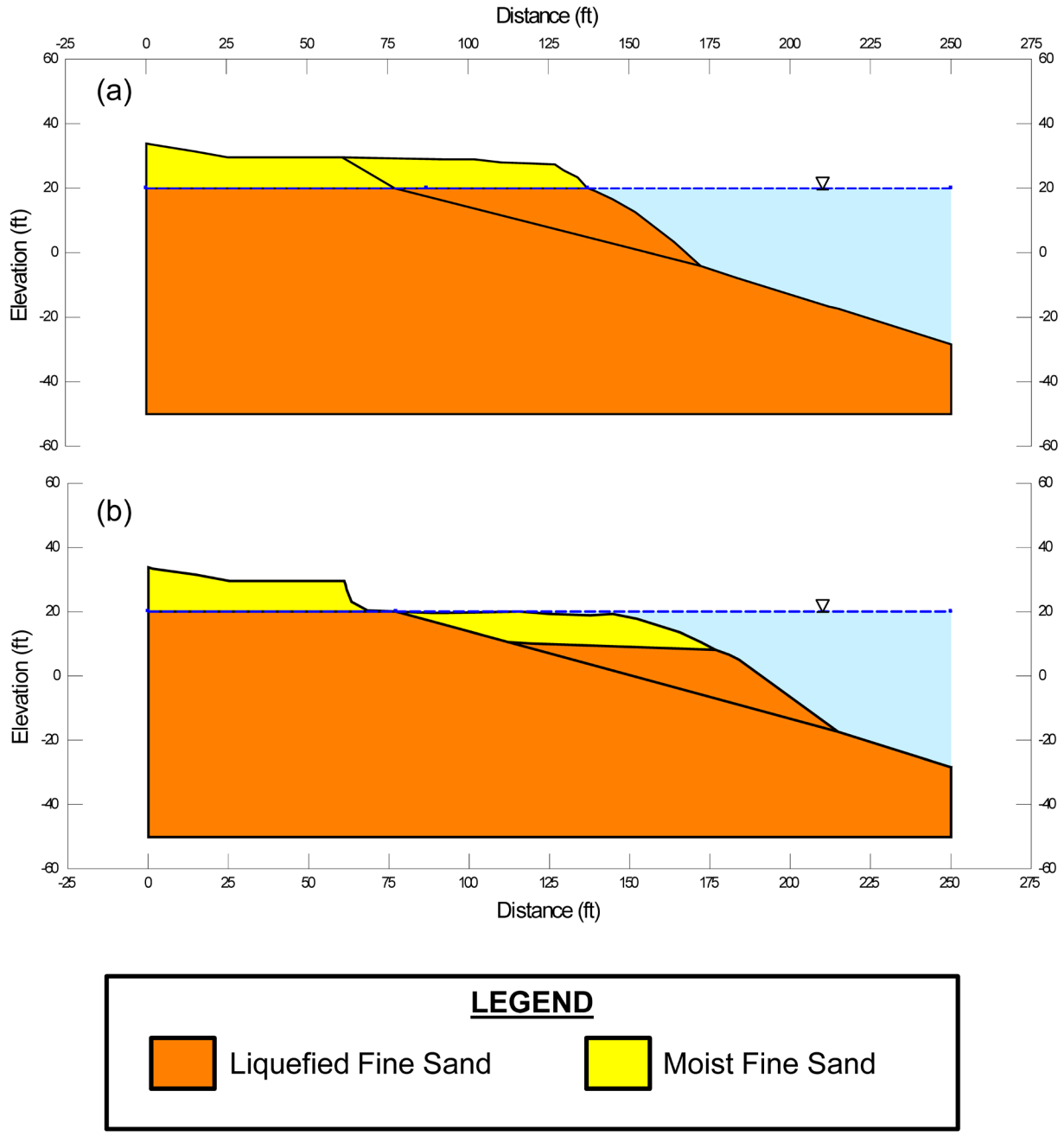

Figure B.5.4: Lake Merced Bank: (a) pre-failure geometry and best estimate failure surface for initial yield stress analyses, and (b) post-failure geometry and the best estimate failure surface for post-failure residual geometry analyses.

Based on the cross-sections shown in Figure B.5.4(b), and the properties and parameters described above, the best-estimate value of $S_{r,resid/geom}$ was $S_{r,resid/geom}$ = 122 lbs/ft^2. Parameters were next varied, as described previously, including analyses of alternate potential failure surfaces slightly above and below the failure surface shown in Figure B.5.4(b). Based on these analyses, it was judged that a reasonable range was $S_{r,resid/geom} \approx$ 101 to 147 lbs/ft^2.

Olson (2001) also back-calculated values of $S_{r,resid/geom}$. His best estimate failure surface was laid back slightly into the apparent underlying natural aeolian sand deposits, and is similar to the failure surface shown in Figure B.5.4 but is laid back even a bit farther into the natural soils near the back heel. He again reportedly assumed, however, that the fill materials largely controlled the failure. Olson's back-calculated best estimate of $S_{r,resid/geom}$ was 6.9 kPa (145 lbs/ft^2), with a range of 4.8 to 7.4 kPa (100 to 155 lbs/ft^2). He attributed the lower end of this range (4.8 kPa) to Seed (1987).

B.5.6 Overall Estimates of S_r

Overall estimates of S_r for this Class B case history were made based on the observed geometry and runout features and characteristics, and the values of $S_{r,yield}$ and $S_{r,resid/geom}$ as calculated in the preceding sections.

Runout characteristics for this case include a runout distance travelled by the center of gravity of the overall failure mass of D = 31.6 feet, and a slope height (from toe to top of the back scarp) of H = 32.3 feet, producing a runout ratio of D/H = 0.98. One set of estimates of S_r was made using the relationship of Equation 4-4 and Figure 4.11, and the resulting best estimate ranges of values of $S_{r,yield}$ and $S_{r,resid/geom}$ from the preceding Sections B.6.4 and B.6.5. Based on apparent runout characteristics, a range of $\xi \approx 0.65$ to 0.95 was employed here, and this this led to best estimate of $S_r \approx$ 125 lbs/ft^2 and a range of $S_r \approx$ 83 to 182 lbs/ft^2. A second estimate was then made based on the relationship shown in Figure 4.9, and the range of values of $S_{r,yield}$ from Section B.5.4. Pre-failure Factors of Safety were estimated, based on runout, to be on the order of 0.55 to 0.8. This produced a resulting likely best estimate of $S_r \approx$ 128 lbs/ft^2, with a likely range of $S_r \approx$ 84 to 189 lbs/ft^2. Values estimated based on Equation 4-4 and Figure 4.11 were given some precedence over the estimates based on Figure 4.9. Variance in values of back-calculated $S_{r,yield}$ and $S_{r,resid/geom}$ from these current studies were then also considered, and so were values back-calculated or estimated by previous investigators. Values from previous investigators were given little weight here, however, and these were simply examined largely to ensure that previous studies were understood and that the current engineering team had made suitable accommodation for potential variability or variance.

Overall, based on an assumed normal distribution, it was judged that the (mean and median) best estimate of post-liquefaction strength for this case history is

$$\overline{S_r} = 136 \text{ lbs/ft}^2$$

and that the best estimate of standard deviation of mean overall post-liquefaction strength is

$$\sigma_{\bar{S}} = 21 \text{ lbs/ft}^2$$

Seed and Harder (1990) reported a value of $S_r \approx 100$ lbs/ft^2 for this case. Olson (2001) and Olson and Stark (2002) did not apply their "kinetics" method to this case, and so they did not independently develop an estimate of S_r that incorporated momentum effects. Instead they simply used their value of $S_{r,resid/geom}$ as a conservative approximation of S_r for this less well-defined case, and used $S_r = 144$ lbs/ft^2 in developing their predictive relationship. Similarly, Wang (2003) and Wang and Kramer (2008) did not employ their zero inertial force (ZIF) method to incorporate inertial effects in back-analyses of this failure. Instead they selected their value of S_r based on examination of back-analyses of several previous investigators, and in the end selected $\overline{S_r} = 139.5$ lbs/ft^2, and a standard deviation of $\sigma_{\bar{S}} = 41.4$ lbs/ft^2. Despite these differing approaches taken to evaluation and/or selection of S_r, agreement between the values used in these three previous studies, and the values developed and employed in these current studies, is very good for this case history.

B.5.7 Evaluation of Initial Effective Vertical Stress

Average initial (pre-failure) effective vertical stress was assessed for the liquefied portion of the failure surface described in Section B.6.4 (and illustrated in Figure B.4.4). Parameters and sensitivity analyses were as described previously in Section B.6.4.

The resulting best estimate of average pre-failure effective stress within the liquefied materials controlling the failure was then $\sigma_{vo}' \approx 834$ lbs/ft^2, with a reasonable range of $\sigma_{vo}' \approx 630$ to 1,038 lbs/ft^2. This range is slightly non-symmetric about the median value, and this range was judged by the engineering team to represent approximately ± 2 standard deviations. Overall, the best characterization of initial (pre-failure) average effective vertical stress was then taken to be represented by a mean value of

$$\overline{\sigma'_{vo}} \approx 834 \text{ lbs/ft}^2$$

and with a standard deviation of

$$\sigma_{\bar{\sigma}} \approx 102 \text{ lbs/ft}^2$$

An estimate of σ_{vo}' was also calculated by Olson and Stark (2001, 2002). They reported a weighted average mean value of $\sigma_{vo}' \approx 1{,}157$ lbs/ft^2. This is larger than the value developed in these current studies, and the difference is largely due to the different failure surfaces assumed by the two investigation teams. Average initial vertical effective stresses were not directly reported by Wang (2003) and Kramer (2008), but they were published more recently in the publication by Kramer and Wang (2015). As discussed in Section 2.3.8.1(b)-(iii), Wang (2003) did not perform any independent analyses to assess σ_{vo}' for his 22 "secondary" cases, and this is one of those cases. Instead, he compiled values of S_r from multiple previous investigators, and averaged these for a best estimate. He also compiled multiple values of S_r/σ_{vo}' from previous investigators, and

averaged these for a best estimate. He then used these two best-estimate values of S_r and S_r/σ_{vo}' to infer a resulting representative value of σ_{vo}'. As described in Section 2.3.8.1(b)-(iii), the resulting averaged values of S_r and S_r/σ_{vo}' were incompatible with each other for a number of Wang's "secondary" case histories, and this process produced unreasonable, and in some cases physically infeasible, values of σ_{vo}' for a number of case histories. Wang's value of σ_{vo}' = 1,316 lbs/ft^2 is in relatively good agreement with that of Olson. But because of differences in assumed failure planes, neither value is directly comparable to the values of σ_{vo}' developed in these current studies.

B.5.8 Evaluation of $N_{1,60,CS}$

Section B.5.3 described the geology and materials involved in this case history, and also presented the available SPT data. This failure either occurred mainly within the lower portion of the loosely end dumped sandy fill, or in the upper portion of the immediately underlying loose aeolian sands.

If the loose fill controlled the failure, then estimation of suitable $N_{1,60,CS}$ values can be developed by either of two approaches. Olson (2001) assumed that the failure was within this fill, and that Test Borings 1 and 2 had occurred behind the rear extent of the fill (as potentially suggested in Figure B.5.5) and so did not serve to characterize this loose fill material. Accordingly, he estimated equivalent approximate $N_{1,60,CS}$ values based on assumed loose conditions associated with end dumping and an absence of useful compaction. An alternate approach would be to assume that the two Test Borings are correctly logged as having penetrated into this loosely end dumped fill, and that the top several SPT values occur within this material as shown in Figures B.5.2 and B.5.3. As the SPT equipment and procedures were not well defined, this still leaves significant uncertainties as to the appropriate characterization of $N_{1,60,CS}$ for this loosely dumped fill.

If the underlying loose aeolian sands (and silty sands) controlled the failure, then the SPT data from Test Borings 1 and 2 are useful here, but there are again significant uncertainties due to the lack of well-defined SPT equipment and procedures.

In these current studies, all of these sets of possibilities were considered. In the end, it did not make a great deal of difference with regard to estimation of representative $N_{1,60,CS}$ values, as the values that the current engineering team would "infer" for the loosely end dumped fill would be very similar to the values apparently measured in the upper "fill" of Test Borings 1 and 2, and the $N_{1,60,CS}$ values of the (also loose) aeolian natural sands underlying the fill are also very similar.

The overall best estimate mean value of $N_{1,60,CS}$ for either the loosely dumped fill sands, or the underlying loose aeolian sands, or a combination of the two, was judged to be $\overline{N_{1,60,CS}} \approx 8.5$ blows/ft. Variance of $\overline{N_{1,60,CS}}$ was estimated primarily on the basis of the perceived uncertainties described previously, including uncertainties as to which of the two materials mainly controlled the failure, whether the Test Borings characterized the loose fill, and the details

regarding the SPT equipment and procedures employed. Considering these, the representation of uncertainty in the representative median value of $\overline{N_{1,60,CS}}$ was taken as $\sigma_{\overline{N}} \approx 2.2$ blows/ft.

Olson and Stark (2001, 2002) developed an estimated representative value of $N_{1,60} = 7.5$ blows/ft for this case history, and they presented no range. Wang (2003) and Kramer (2008) jointly developed a representative value of $\overline{N_{1,60,CS}} = 5.9$ blows/ft, and their estimated standard deviation of that overall mean value for this case history was $\sigma_{\overline{N}} = 8.0$ blows/ft. Details of the development of this interpretation by Wang and Kramer are not presented, but the apparently excessively large variance (or standard deviation) in $\overline{N_{1,60,CS}}$ appears to have been an artifact of the procedures used to estimate such variances for poorly defined cases.

Overall agreement between these three independent assessments of representative $\overline{N_{1,60,CS}}$ values is judged to be generally good, excepting the very large standard deviation ascribed by Wang and Kramer which would lead to negative values of $N_{1,60,CS}$ at a mean minus less than one standard deviation level. That does not necessarily adversely affect the mathematics of their regressions, however, and it is a useful representation of what they view to be large uncertainties with respect to a selection of a representative value of $N_{1,60,CS}$ for this case.

B.6 El Cobre Tailings Dam (Chile; 1965)

B.6.1 Brief Summary of Case History Characteristics

Name of Structure	El Cobre Tailings Dam
Location of Structure	El Cobre, Chile
Type of Structure	Tailings Dam
Date of Failure	March 28, 1965
Nature of Failure	Seismic, During 1965 Chile Earthquake (M_L = 7.4)
Approx. Maximum Slope Height	103 ft.

B.6.2 Introduction and Description of Failure

The Chile earthquake of March 28, 1965 (M_L = 7.4) produced catastrophic failures of multiple mine tailings dams and impoundments in central Chile (Dobry and Alvarez, 1967). Prominent among these failures were the failures of the El Cobre tailings dams, which released more than 2 x 10^6 tons of tailings into the valley downstream, destroying part of the town of El Cobre and resulting in more than 200 deaths.

The El Cobre tailings dams had begun impounding tailings in 1930, and the overall facility consisted of three dams: the Old Dam, the Small Dam, and the New Dam. When the 1965 earthquake occurred, the Old Dam was partially out of service and functioned only as an emergency dam, and the Small Dam was also out of service. The New Dam had recently begun operations in 1963, and was actively accepting tailings.

Both the Old Dam and the New Dam suffered liquefaction-induced failures. There was insufficient documentation of the failure of the New Dam as to represent a suitable basis for forensic back-analyses, and so it is the failure of the Old Dam that has been investigated and back-analyzed by multiple investigation teams, including these current studies.

Figure B.6.1 shows the pre-failure and post-failure cross-sections of the Old Dam, at exaggerated vertical scale (Dobry and Alvarez, 1967). There were no eyewitnesses to the failure of the Old Dam. The failure appears to have occurred almost entirely within the impounded tailings, and did not involve the underlying foundation materials.

Dobry and Alvarez (1967) reported: "The front slope of the southern corner of the Old Dam receded 65m, making the adjacent intermediate terrace disappear completely; the scarp produced was almost vertical…. All the fine and unconsolidated tailings flowed out, and from the upper part only a horseshoe-shaped shell was left, which bound(ed) the back and sides of the large central depression left by the material which had flowed out. The bottom of this central depression was formed by several almost horizontal terraces (2% slope toward the valley)….."

Figure B.6.3(a) shows the rim of horseshoe shaped top deck remaining after the failure, and the depressed central zone from which the liquefied tailings departed, and Figure B.6.3(b) shows the runout materials that flowed out from the impoundment. Runout of the liquefied

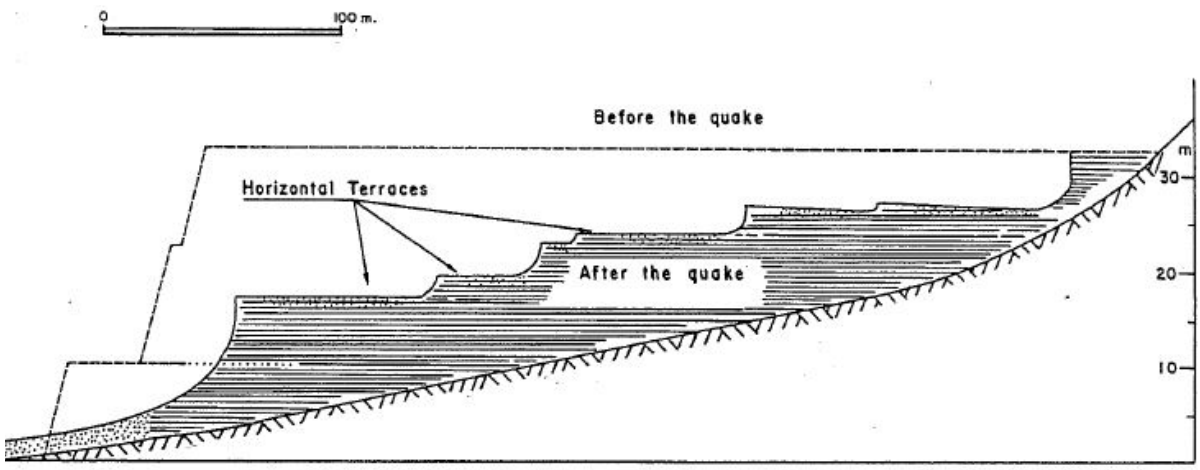

Figure B.6.1: Pre-failure and post-failure cross-sections (at 5:1 exaggerated vertical scale) of the El Cobre Tailings Dam "Old Dam" (Dobry and Alvarez, 1967).

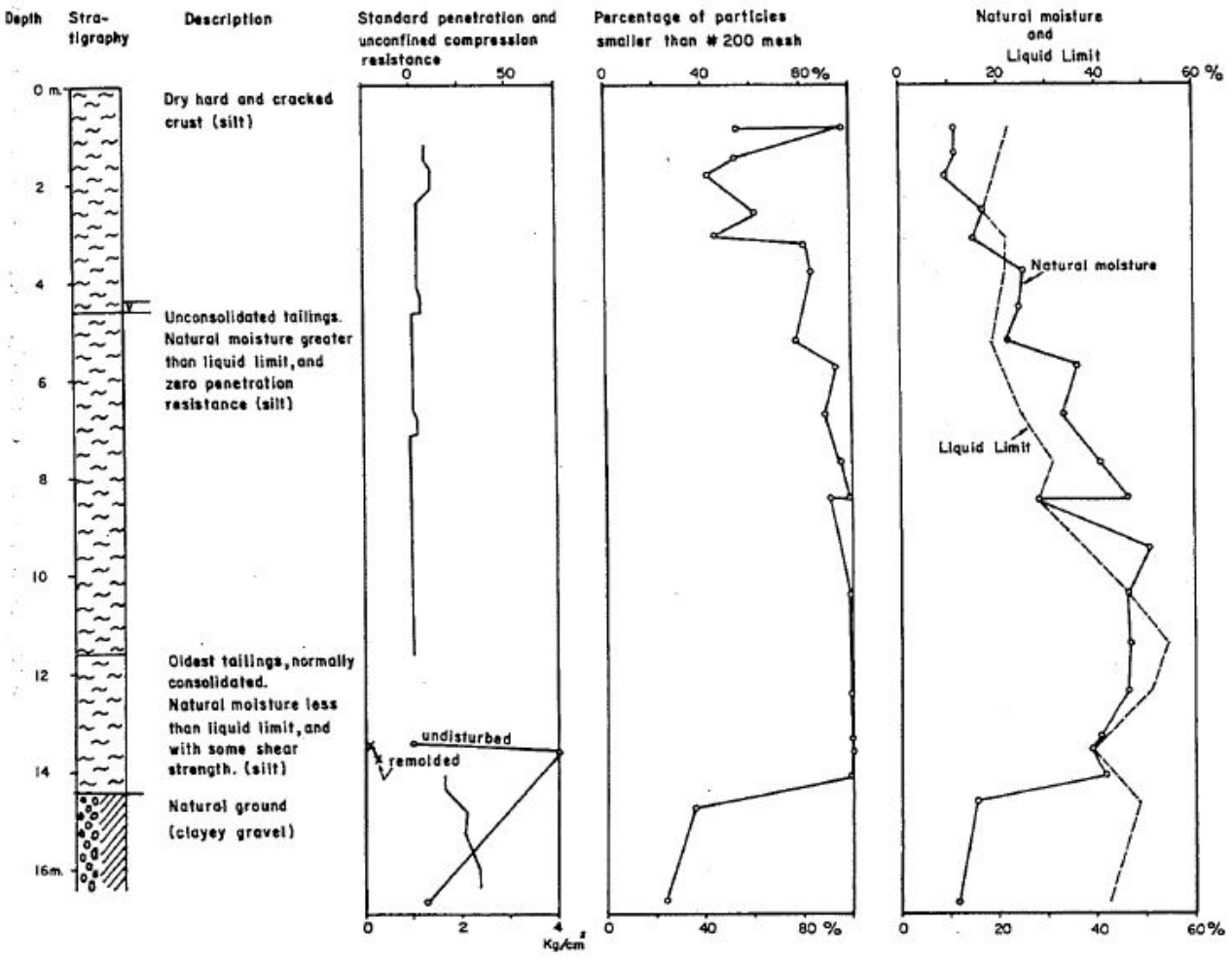

Figure B.6.2: Boring log, SPT results, fines contents, natural water contents and liquid limits in the tailings of the El Cobre "Small Dam" (Dobry and Alvarez, 1967).

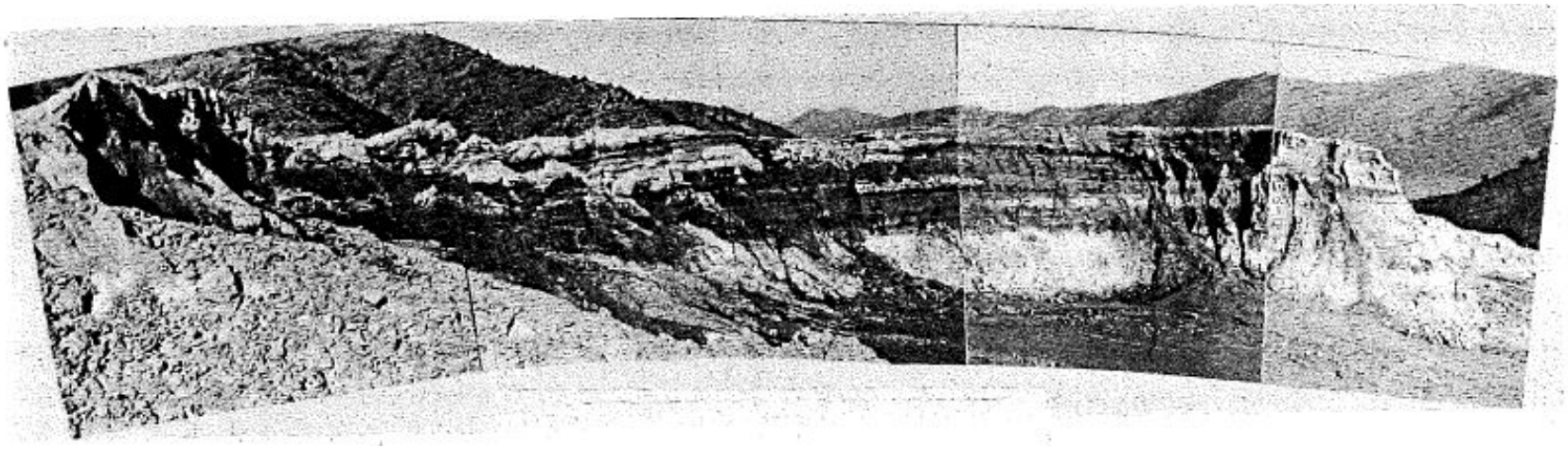

Figure B.6.3(a): Photograph showing post-failure conditions at the Old Dam; photo taken looking upstream towards the back edge and the “horseshoe shaped” scarp (Dobry and Alvarez, 1967).

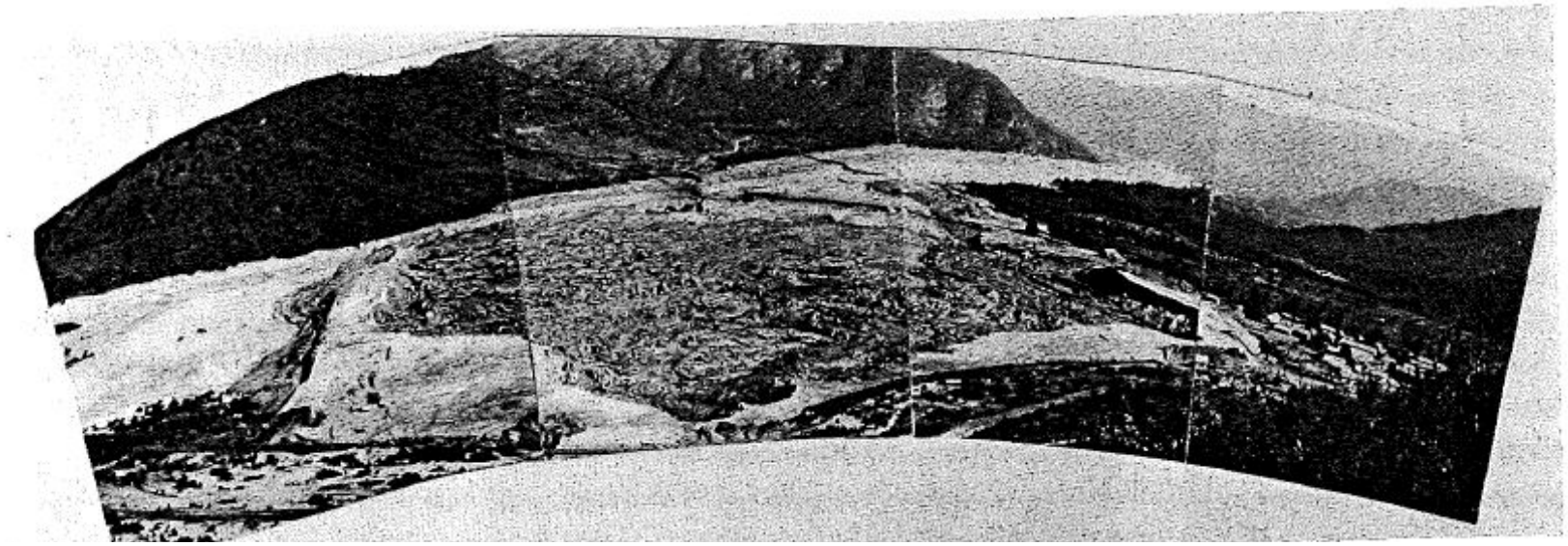

Figure B.6.3(b): Photograph of post-failure conditions at the Old Dam showing the liquefied tailings outflow mass (Dobry and Alvarez, 1967).

tailings traveled significant distances, and the runout materials immediately downstream of the toe of the failure were relatively thinly spread and had relatively low (nearly horizontal) post-failure surface slopes.

B.6.3 Geology and Site Conditions

Figure B.6.2 shows the log of an exploratory SPT boring performed in the Small Dam. The Small Dam and the Old Dam had been filled during the same general period, and with similar materials and similar placement methods, and so it is assumed that the results of this boring log are also generally representative of conditions in the Old Dam.

As shown in the boring log of Figure B.6.2, a relatively dry, desiccated crust was present at the top of the Small Dam, and it is assumed that a similar crust with a thickness of about 4 to 5 meters was also present at the top of the Old Dam. Beneath this desiccated upper crust, the next 7 meters were comprised of underconsolidated tailings, as evidenced by in situ water contents that were higher than the liquid limits of these materials, as shown in Figure B.6.2. Dobry and Alvarez (1967) suggest that a similar layer of underconsolidated tailings, approximately 10 m in thickness, underlay the desiccated upper crust in the Old Dam. The underlying deeper tailings were then more normally consolidated (or nearly normally consolidated), as evidenced by in situ water contents slightly lower than their liquid limits.

These normally consolidated tailings at the base of the impoundment were underlain by the natural foundation soils. These were comprised mainly of clayey gravels, likely of colluvial origin. These were firmer materials than the overlying tailings deposits, and were not involved in the failures that occurred. The phreatic surface within the impoundment was assumed to have been located at or near to the boundary between the desiccated upper crust and the underlying underconsolidated tailings.

Similar stratigraphy and conditions, including the location of the phreatic surface at or near to the boundary between the desiccated upper crust and the underlying underconsolidated tailings, were inferred by Alvarez and Dobry to have been likely present at the Old Dam as well.

The tailings impounded were comprised mainly of fine sandy silts, with fines contents generally of 90% or greater. Liquid limits varied with depth, and were generally between about 10% to 50%. A single boring with multiple SPT tests was performed in the tailings of the Small Dam, and the results are shown in Figure B.6.2.

B.6.4 Initial Yield Stress Analyses

Back-analyses for assessment of both $S_{r,yield}$ and $S_{r,resid/geom}$ were exceptionally difficult for this case history, due to the poorly defined post-failure geometry (especially downstream of the original toe of the Old Dam), and the nature of the apparent failure mechanism(s) involved.

Figures B.6.4(a) and (b), and Figure B.6.5, show examples of some of the analyses performed to attempt to obtain some understanding of the ranges of types of potential failure

mechanisms involved, and the associated values of initial yield strength ($S_{r,yield}$) for each mechanism that would be required within the foundation and embankment materials of the north dike section to produce a calculated Factor of Safety equal to 1.0. $S_{r,yield}$ is not the actual post-liquefaction strength, but it proves to be useful in developing estimates of post-liquefaction strength (S_r) for most of the failure case histories back-analyzed in these current studies.

Figure B.6.4(a) shows the most critical potential failure surface for the types of rotational failures, or semi-rotational and translational failures, that could have removed the buttressing provided at the downstream toe of the overall failure; requiring shearing through some portion of the initial starter dike.

Unit weights of the non-saturated tailings above the phreatic surface were modeled with a unit weight of $\gamma_m \approx 80$ lbs/ft^3, and this was then varied over a range of 76 to 84 lbs/ft^3 for parameter sensitivity studies. Unit weights of the saturated tailings below the phreatic surface were modeled with a unit weight of $\gamma_s \approx 85$ lbs/ft^3, and this was then varied over a range of 81 to 89 lbs/ft^3 for parameter sensitivity studies. The friction angle of the tailings above the phreatic surface was modeled with $Ø' \approx 29°$, and a range of $Ø' \approx 27°$ to 32°. The shell material of the starter dikes was assumed not to liquefy, and was modeled with a friction angle of $Ø' \approx 35°$, and a range of $Ø' \approx 32°$ to 38°. These types of moderate parameter variations proved to be of little significance, however, as the overall uncertainties were dominated by uncertainties as to mechanisms and sequence of failures, rather than variations in parameters of the non-liquefied soils for this case history.

For the failure surface shown in Figure B.6.4(a), the back-calculated value of $S_{r,yield}$ within the liquefied tailings was $S_{r,yield} = 643$ lbs/ft^2. This would not prove to be very useful, however, because (1) post-failure displacements were very large after this initial toe failure, (2) it is likely that some erosion occurred as liquefied materials poured through the opening in the starter dike probably eroded and enlarged the hole and altered the eventual post-failure geometry, and (3) both higher and lower values of $S_{r,yield}$ were subsequently back-calculated for other elements of this likely retrogressive failure.

Figure B.6.4(b) shows an example back-analysis of the failure of the next section (the "first deck" behind the initial toe dike), with the entire deck modeled as failing monolithically. The back-calculated value for this is $S_{r,yield} = 331$ lbs/ft^2.

It is judged by the current engineering team to be unlikely that this entire "first deck" section moved out monolithically. Figure B.6.5 shows an example set of back-analyses of incrementally retrogressive failures sequentially initiating and eventually removing the materials of this "first deck" in a series of sequential (retrogressive) sub-failures. These are a more critical set of failure mechanisms, and they produce significantly higher values of $S_{r,yield}$. The values of $S_{r,yield}$ decrease towards the rear heel, partly due to slight thinning of the materials above the failure surface (which inclines at approximately 2° towards the valley), but the selected lateral thickness of each incremental slice has a significant effect on back-calculated values of $S_{r,yield}$, so the values shown should be considered to be only "illustrative" here. Eventually, the failure surface selected a new (and slightly higher elevation) preferred failure surface, and it "stepped up" to start a second deck section.

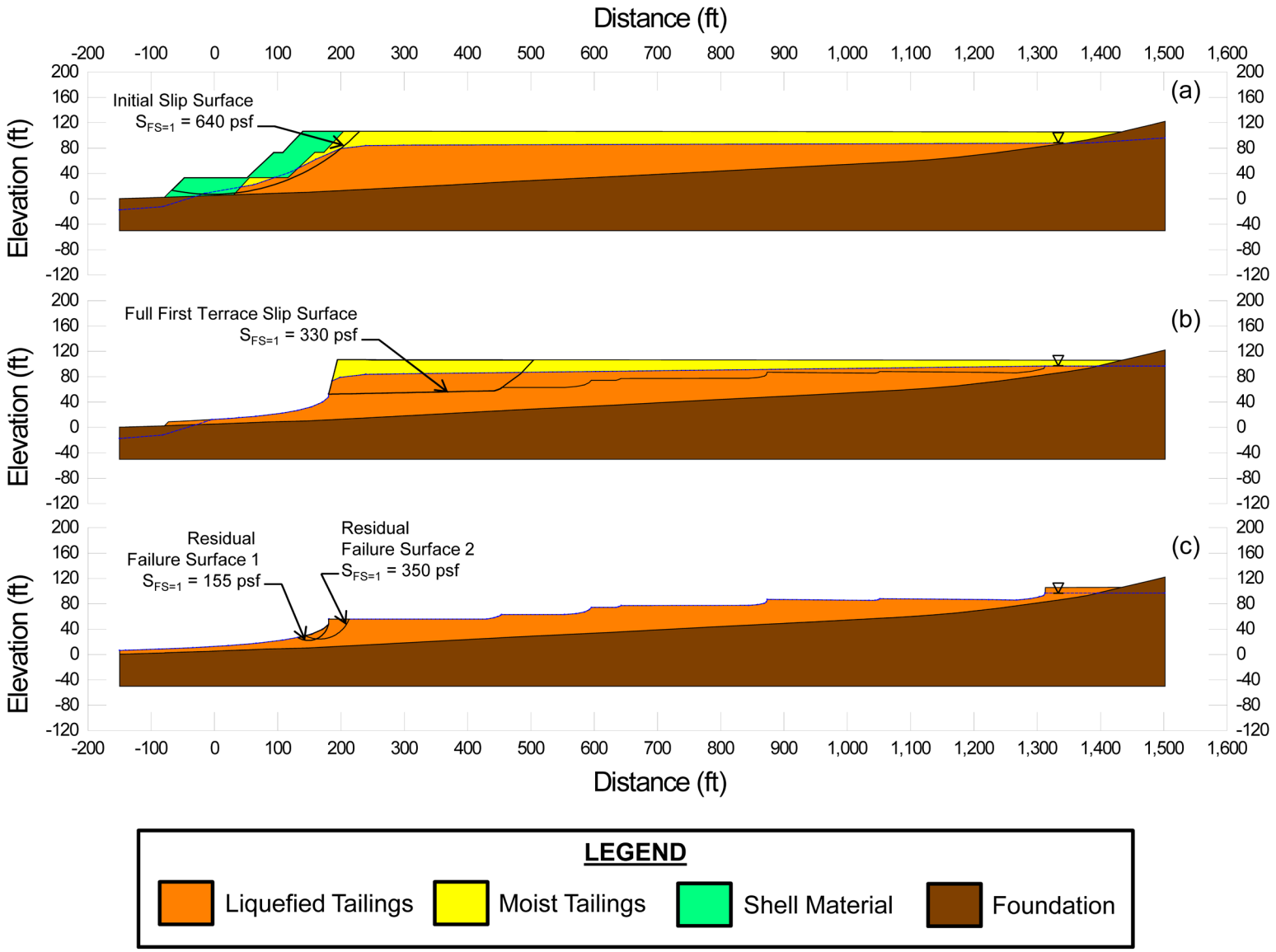

Figure B.6.4: Examples of some of the trial analyses performed to garner an understanding of the potential mechanics and potential strength characteristics of the Old Dam and its potential failure mechanisms.

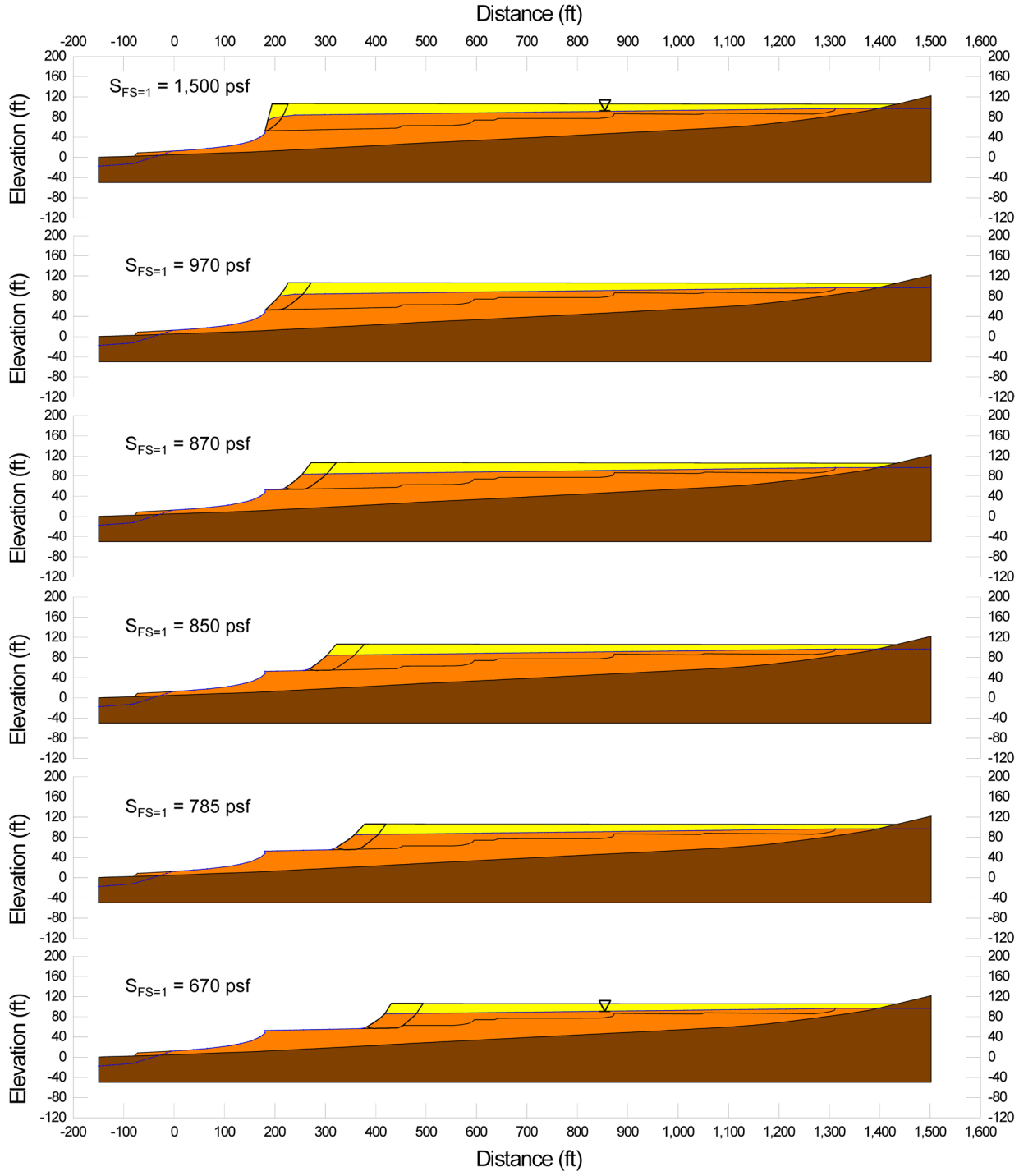

Figure B.6.5: Examples of some of the trial analyses of retrogressive failures of the "first deck" of the Old Dam, and associated values of $S_{r,yield}$.

This process appears to have been repeated, until the eventual final back-heel of the overall feature remained stable. Back-analysis of that eventual back-heel was not fruitful, because it appears likely that the failure "stepped up" into non-saturated materials that did not liquefy at this eventual back heel.

Other sets of similar analyses were performed, and these showed that values of $S_{r,yield}$ of on the order of $S_{r,yield} \approx 250$ to 950 lbs/ft^2 could be back-calculated for these types of retrogressive failures, with values generally decreasing towards the upper (back heel) region as failure progressed.

Due to the very large runout distance, and the large runout ratio, as well as the apparently relatively "clean" deck surfaces shown in Figure B.6.1, it is difficult to make a well-constrained quantitative assessment of a "representative" value of $S_{r,yield}$ for this complicated retrogressive failure. It is also difficult to develop consensus on how to "weight" the various potential values of $S_{r,yield}$ for the different mechanisms and different potential individual failure surfaces. Overall, the current investigation team developed a consensus view that representative values of $S_{r,yield}$ would be on the order of approximately 300 to 600 lbs/ft^2.

Olson (2001) did not develop a back-calculated value of $S_{r,yield}$ for this challenging case history, and so there are no values of $S_{r,yield}$ from previous investigations against which to compare this current range of estimated $S_{r,yield}$ values. This was the only one of his 33 back-analyzed case histories for which Olson did not develop an estimated value (or range of estimated values) of $S_{r,yield}$.

B.6.5 Residual Strength Analyses Based on Residual Geometry

It was not possible to perform rigorous and fully reliable back-analyses to determine the value of $S_{r,resid/geom}$ required to produce a calculated Factor of Safety equal to 1.0 based on residual geometry, because the post-failure residual geometry was insufficiently well defined. This is a significant source of uncertainty for this case history.

Olson (2001) assumed that the thickness of tailings runout shown at the left side of Figure B.6.1 was representative of the thickness of the entire failure mass in order to make what he termed a "crude estimate" of $S_{r,resid/geom}$. He assumed a thickness of 2 m., and an underlying slope of approximately 4° and a top slope of approximately 4°, and with assumed unit weights of 12.6 to 14.1 kNn/m^3. He then used a simplified infinite slope analysis to calculate $S_{r,resid/geom} \approx 1.8$ to 2.0 kPa, (38 to 42 lbs/ft^2) with a best estimate of $S_{r,resid/geom} = 1.9$ kPa (40 lbs/ft^2).

In these current studies, several additional analyses were performed to attempt to further explore potential ranges of values of $S_{r,resid/geom}$.

Figure B.6.4(c) shows two potentially critical rotational failures at the toe of the final overall geometry, and the associated values of $S_{r,resid/geom}$. The overall tailings facility was strongly shaken, and it would seem likely that it liquefied at these locations, in which case these back-calculated values of $S_{r,resid/geom}$ would be valid. But it is also possible that liquefaction of

surrounding and overlying materials "shielded" the tailings at these toe locations, by preventing full cyclic shear stress transfer from overlying materials through softened (liquefied) materials, and that the materials associated with the potential failure surfaces of Figure B.6.4(b) therefore did not "trigger" or liquefy, and so did not achieve a post-liquefaction strength condition. The depths modeled for the two potentially critical failure surfaces shown in Figure B.6.4(b) are limited by the observation that the liquidity index, and thus the likely post-liquefaction strengths, of the materials at the very base of the tailings impoundment are more favorable (see Sections B.6.3 and B.6.8), so that the base of the tailings would have been somewhat stronger than the materials above them.

Additional efforts to evaluate potential values of $S_{r,resid/geom}$ were frustrated by lack of documentation. Conditions further downstream of the toe section shown in Figure B.6.1 are not quantifiably well documented. Aerial photos, and oblique photos, show that tailings flowed out to considerable distances, and they also show an irregular top surface of the flowed tailings that is not reflected in the cross-section of Figure B.6.1. This may reflect the "Several chunks of the upper dry crust were left on these terraces" reported by Dobry and Alvarez (1967).

It cannot be determined whether or not the materials controlling stability of the residual geometry of the "upper decks" liquefied (or "triggered"), and so it cannot be determined with certainty whether post-failure back-analyses of these would provide representative values of $S_{r,resid/geom}$ for this case.

Aerial photo evidence shows considerable flow of tailings extending far downstream of the original dam toe, but lack of quantified characterization of (1) the topography (top slopes) of this failure mass, and (2) the underlying basal contact slopes at the base of this flowed mass precludes reliable back-analyses of $S_{r,resid/geom}$ for these sections, and it is not known with certainty whether or not post-failure erosion carried some materials farther downstream.

The back-calculated (approximate) value of $S_{r/resid/geom} \approx 40$ lbs/ft^2 proposed by Olson appears to be a likely lower bound estimate of $S_{r,resid/geom}$, but there appears to be no fully reliable basis for quantification of useful higher values.

The current investigation team concluded that a slightly higher representative range of values of $S_{r,resid/geom}$ for this case would be estimated as $S_{r,resid/geom} \approx$ 40 to 60 lbs/ft^2, with the expectation that this would likely be somewhat conservatively biased.

B.6.6 Overall Estimates of S_r

Overall estimates of S_r for this Class B case history were very challenging, due to the very large runout and the poorly defined post-failure conditions downstream of the original toe of the dam. Estimates were made by a number of approaches, and then the current engineering team discussed and debated until a consensus was reached with regard to characterization of both the best estimate mean value of post liquefaction strength ($\overline{S_r}$) and also the best estimate standard deviation of this mean ($\sigma_{\overline{S}}$).

The toe of the runout mass extended more than 900 feet beyond the pre-failure toe of the embankment, and the center of gravity of the failure mass appears to have traveled more than 500 to 800 feet. The height of the failure can measured as approximately 105 feet from the original base of the failure at the original toe of the starter dike to the top of the eventual (final) heel scarp, or it can be measured as approximately 95 feet from the toe of the liquefied tailings behind the starter dike to the top of the eventual (final) heel scarp. In either case, the runout ratio is approximately 500/100 to 800/100 ≈ 5 to 8. Based on Figure 4.7, this would suggest a likely value of that $\xi \approx 0.4$ to 0.5 for this relatively large runout case. Based on the ranges of values of $S_{r,yield} \approx 300$ to 600 lbs/ft^2 and $S_{r,resid/geom} \approx$ 40 to 60 lbs/ft^2 from Section B.6.4 and B.6.5, respectively, and Equation 4-4, this would produce an estimated range of values of $S_r \approx 68$ to 165 lbs/ft^2.

The current investigation team then further adjusted this approximate range based on their individual judgments of the available information, with each member weighing their own perceptions as to the apparent characteristics of the failure (including photographs, published descriptions, etc.), and the relative merits of the apparent ranges of values of $S_{r,yield}$ and $S_{r,resid/geom}$ as reported above and the basis upon which they were each developed. The analysis team then developed a consensus overall characterization. It was generally agreed that the value of S_r was likely higher than the lower bound value of $S_{r,yield} \approx 40$ lbs/ft^2 conservatively estimated by Olson (2001), but it was noted that the value may not have been much higher than this.

The result was a likely best estimate range of $S_r \approx 40$ to 150 lbs/ft^2. This range was judged to represent approximately +/- 2 standard deviations, and the overall characterization of S_r for this case was then a best estimate of median post-liquefaction strength for this case history of

$$\overline{S_r} = 95 \text{ lbs/ft}^2$$

and a standard deviation of mean overall post-liquefaction strength is

$$\sigma_{\overline{S}} = 27 \text{ lbs/ft}^2$$

Olson (2001) and Olson and Stark (2002) did not apply their "kinetics" method to this case, and so they did not independently develop an estimate of S_r that incorporated momentum effects. Instead they simply used their value of $S_{r,resid/geom}$ (as described previously in Section B.6.5) as a conservative approximation of S_r, and used $S_r = 1.8$ to 2.0 kPa, (38 to 42 lbs/ft^2) with a best estimate of $S_r = 1.9$ kPa (40 lbs/ft^2).

Similarly, Wang (2003) and Wang and Kramer (2008) did not employ their zero inertial force (ZIF) method to incorporate inertial effects in back-analyses of this failure. Instead Wang's (2003) dissertation states that they selected their value of S_r based on examination of back-analyses of previous investigators, and in the end selected $\overline{S_r} = 195.2$ lbs/ft^2, and a standard deviation of $\sigma_{\overline{S}} = 64.8$ lbs/ft^2. Wang's approach to these "lesser" (or Class B) case histories was to obtain values from multiple previous investigations, and then to simply average them. For this case (El Cobre Tailings Dam), in Table 6-8 of his dissertation, he lists only one source and that is Olson (2001), and he lists Olson's value of S_r as 195 lbs/ft^2. That appears to be an error, as Olson's value was 40 lbs/ft^2. This may be a simple/straightforward error, but it appears more likely that Wang recognized that Olson's value of $S_{r,resid/geom}$ would underestimate the actual value of S_r for this case,

and that he performed his own assessment of either S_r or at least of $S_{r,yield}$, and then developed an independent estimate of overall S_r (but failed to document this work). Wang was regularly taking values of $S_{r,yield}$ and $S_{r,resid/geom}$ for other cases, and then averaging them to estimate S_r, and he may have done that here as well. In any case, his best estimate value of value of $\overline{S_r}$ = 195.2 lbs/ft^2 is significantly higher than those of either Olson (2001) or these current studies.

Wang's approach to estimation of standard deviation of the mean value of S_r for the "Secondary" case histories was to place each case history into one of five categories based on the quality and reliability of the data available, and then to assign coefficients of variation of between 5% to 25% based on these assessments of data quality, quantity and reliability. An equational relationship was then applied to provide scaling of these assessments in a manner that provided approximate consistency with estimates of variance (and standard deviations) for the 10 "Primary" case histories that had been back-analyzed by the ZIF method.

B.6.7 Evaluation of Initial Effective Vertical Stress

Average initial (pre-failure) effective vertical stress was assessed for the liquefied portion of the overall (final scarp) failure surface in Figure B.6.5. Parameters and sensitivity analyses were as described previously in Section B.6.4.

The resulting best estimate of average pre-failure effective stress within the liquefied materials controlling the failure was then $\sigma_{vo}' \approx$ 2,061 lbs/ft^2, with a reasonable range of $\sigma_{vo}' \approx$ 1,709 to 2,441 lbs/ft^2. This range is slightly non-symmetric about the median value, and this range was judged by the engineering team to represent approximately ± 2 standard deviations. Overall, the best characterization of initial (pre-failure) average effective vertical stress was then taken to be represented by a mean value of

$$\overline{\sigma'_{vo}} \approx 2{,}075 \text{ lbs/ft}^2$$

and with a standard deviation of

$$\sigma_{\overline{\sigma}} \approx 183 \text{ lbs/ft}^2$$

An estimate of σ_{vo}' was also calculated by Olson and Stark (2001, 2002). They reported a representative value of $\sigma_{vo}' \approx$ 82.6 to 103.9 kPa (1,725 to 2,169 lbs/ft^2), in very good agreement with these current studies. Average initial vertical effective stresses were not directly reported by Wang (2003) and Kramer (2008), but they were published more recently in the publication by Kramer and Wang (2015). As discussed in Section 2.3.8.1(b)-(iii), Wang (2003) did not perform any independent analyses to assess σ_{vo}' for his 22 "secondary" cases, and this is one of those cases. Instead, he compiled values of S_r from multiple previous investigators, and averaged these for a best estimate. He also compiled multiple values of S_r/σ_{vo}' from previous investigators, and averaged these for a best estimate. He then used these two best-estimate values of S_r and S_r/σ_{vo}' to infer a resulting representative value of σ_{vo}'. As described in Section 2.3.8.1(b)-(iii), the resulting

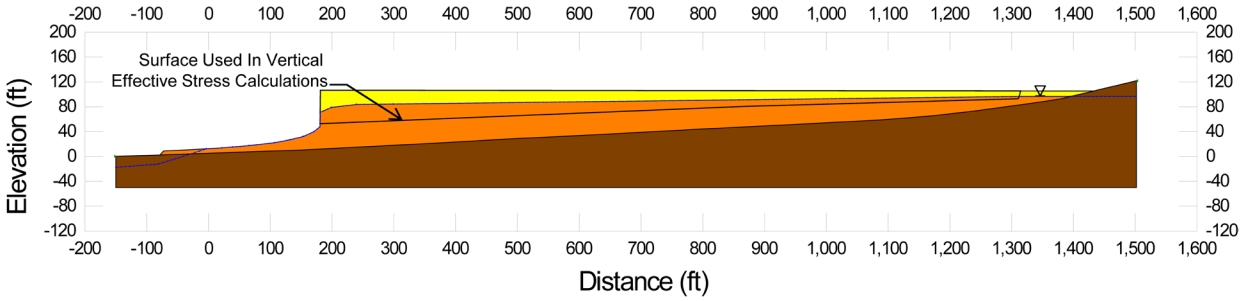

Figure B.6.6: Failure surface used for initial (pre-failure) vertical effective stress calculations.

averaged values of S_r and S_r/σ_{vo}' were incompatible with each other for a number of Wang's "secondary" case histories, and this process produced unreasonable, and in some cases physically infeasible, values of σ_{vo}' for a number of case histories. Wang's value of σ_{vo}' = 9,760 lbs/ft^2 is clearly physically infeasible for this case, based on the cross-section, and so it is not considered a useful check here. Agreement between Olson's value, which is well-documented, and the values developed in these current studies is excellent.

B.6.8 Evaluation of $N_{1,60,CS}$

No SPT data are available from the tailings impounded in the Old Dam, but SPT data are available from a boring performed in the Small Dam, as shown in Figure B.6.2. Equipment and procedure details for these SPT are not known, which is a source of uncertainty here. An additional source of uncertainty here is the need to extrapolate SPT data from the tailings of the Small Dam to represent the tailings of the Old Dam. In addition, Olson (2001) speculated that large pore pressures generated by the SPT in these fines-dominated and very loose soils might have led to underestimation of penetration resistances, as Ishihara (1984) and Ishihara et al. (1990) had suggested for SPT performed in the tailings of the Moshi-Koshi Tailings Dam failure (see Appendix B, Section B.11).

As shown in Figure B.6.2, uncorrected SPT blowcounts in the upper 4 meters of the tailings in the Small Dam were in the range of N = 3 to 12 blows/ft. Below this upper (desiccated) crust the underlying underconsolidated tailings had uncorrected blowcounts of either zero or one (most were reported as zero, only two were reported as one). It is difficult to know exactly what these values mean. A blowcount of zero can mean that the rod weight alone caused bearing failure of the sampler, or it can mean that the sampler was struck once and liquefaction occurred and the sampler sank with no second blow required. Usually that second situation is reported as a blowcount of "one", and the first situation as "zero". Application of fines corrections, to transform $N_{1,60}$ values to $N_{1,60,CS}$ values is also not fully straightforward here.

The tailings at the base of the deposit appear to be less under-consolidated, and it appears that post-liquefaction strengths would be more favorable over the lowest portion of the tailings deposit (see Section B.6.3 and Figure B.6.2). Accordingly, failures were generally assumed not to penetrate into the lowest 1.5 meters of the tailings pile.

In either case, penetration resistance within the portions of the tailings deposit that were under-consolidated was clearly very low.

In these current studies, the representative penetration resistance for these very loose, silty tailings was taken as $\overline{N_{1,60,CS}}$ = 2 blows/ft, with a standard deviation of the value of this mean of $\sigma_{\overline{N}}$ = 1.0 blows/ft.

Olson (2001) and Olson and Stark (2002) did not make a fines adjustment, and so selected a value of $N_{1,60}$ (rather than $N_{1,60,CS}$) for this case history. Their selected value of representative penetration resistance was $N_{1,60}$ = 0 blows/ft.

Wang (2003) and Kramer (2008) made a fines adjustment based on the fines adjustment of Seed and Harder (1990), and selected a somewhat higher value of $\overline{N_{1,60,CS}}$ = 6.8 blows/ft, and a standard deviation of $\sigma_{\overline{N}}$ = 0.9 blows/foot. The full details of the basis for this selection are not reported. It appears likely that an uncorrected blowcount was selected as representative, and that effective overburden corrections then led to a value of $N_{1,60} \approx$ 1.8 blows/ft. Based on the very high fines contents, they appear to then have added 5 blows per foot to develop a best estimate value of $\overline{N_{1,60,CS}}$ = 6.8 blows/ft.

B.7 Metoki Road Embankment (Japan; 1968)

B.7.1 Brief Summary of Case History Characteristics

Name of Structure	Metoki Road Embankment
Location of Structure	Metoki, Japan
Type of Structure	Roadway Embankment
Date of Failure	March 28, 1965
Nature of Failure	Seismic, During 1968 Tokachi-Oki Earthquake (M_w = 8.3)
Approx. Maximum Slope Height	16.4 ft.

B.7.2 Introduction and Description of Failure

A section of the roadway embankment near Metoki, Japan suffered a liquefaction-induced flow failure during the 1968 Tokoachi-Oki earthquake (M_w = 8.3), as reported by Ishihara et al. (1990). Figure B.7.1 shows a plan view of the post-failure conditions, with a temporary detour road in place to the rear of the slide scarp. Figure B.7.2 shows a cross-section of the embankment (at exaggerated vertical scale) along Section f-f', with the temporary detour road in place, and Figure B.7.3 shows an interpreted pre-failure cross-section (at true vertical scale) which will be discussed further.

The phreatic surface was at or near the ground surface at the toe of the embankment, and it is assumed that failure occurred due to seismically induced liquefaction of the loose silty sands of the upper foundation soils underlying the embankment. Maximum lateral displacements of the liquefied materials were on the order of approximately 35 to 40 m.

B.7.3 Geology and Site Conditions

Ishihara et al. (1990) stated that the roadway embankment was founded atop a layer of what they termed "soft" silty sand, and that this upper stratum of soft silty sand was underlain at depth by a "medium soft soil". No further descriptions of these two foundation units are given, so gradations, fines contents, etc. are not known. It is assumed (based on common local practice) that the roadway embankment was also comprised of these locally available silty sands, but there is no information available regarding compaction procedures, etc.

B.7.4 Initial Yield Stress Analyses

Figure B.7.3 shows the cross-section used for back-analyses of the post-liquefaction initial yield strength $S_{r,yield}$ that would be required within the foundation and embankment materials of the north dike section to produce a calculated Factor of Safety equal to 1.0. This is not the actual

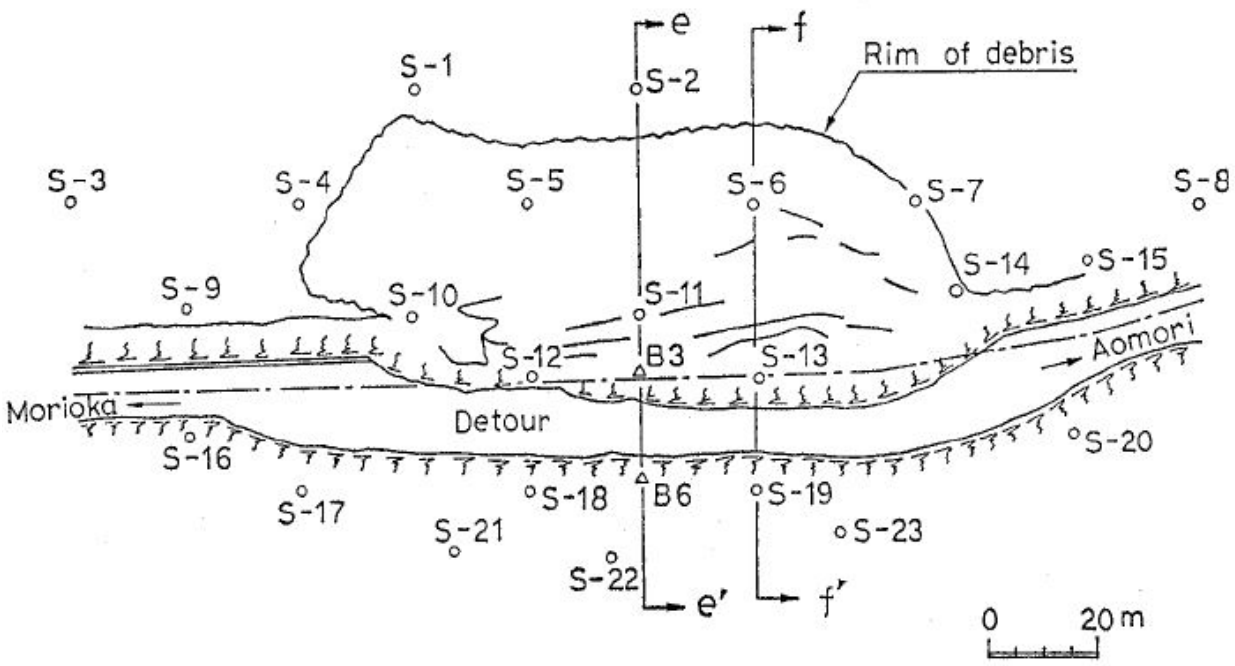

Figure B.7.1: Plan view of the failure of the roadway embankment near Metoki (from Ishihara et al., 1990)

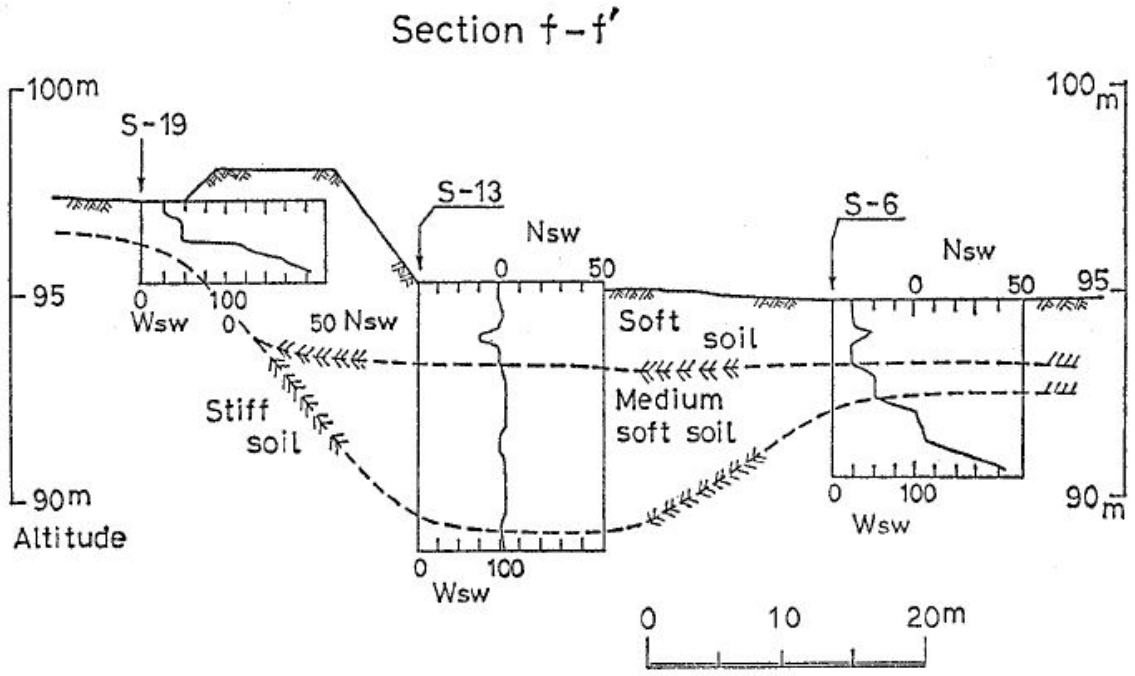

Figure B.7.2: Cross-section f-f' through the repaired Metoki roadway embankment (shown at exaggerated vertical scale), showing also three of the Swedish Cone soundings (Figure from Ishihara et al., 1990).

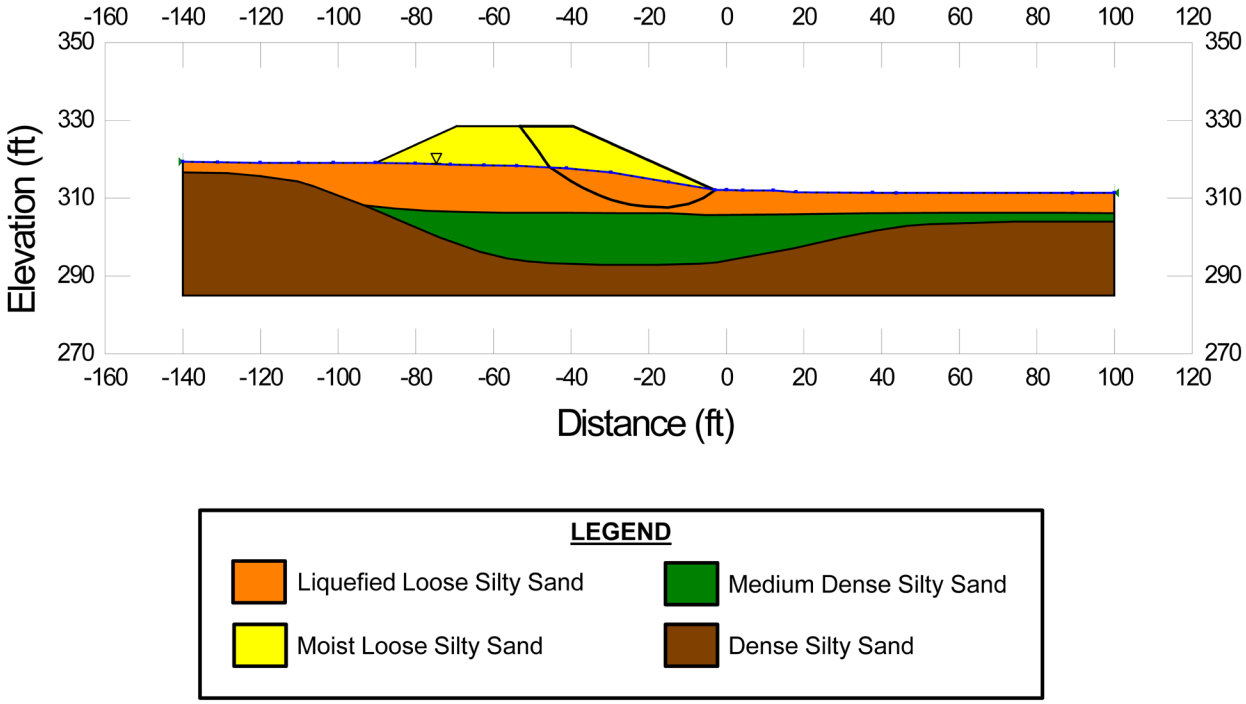

Figure B.7.3: Pre-failure cross-section of the Metoki roadway embankment used for back-analyses of $S_{r,yield}$.

post-liquefaction strength, but it proves to be useful in developing estimates of post-liquefaction strength (S_r) for this case history.

There were two general sets of potential failure mechanisms that could potentially explain the observed features: (1) the failure may have been incrementally retrogressive, initiating with a "slice" near to the front of the feature, and then retrogressing on a slice by slice basis back towards the eventual back heel, or (2) the entire slide may have initiated monolithically (all at once). Both sets of possibilities were analyzed, and multiple potential "initial" failure surfaces were analyzed for the incrementally retrogressive scenario. In all cases, failure was modeled as occurring within the loose, saturated silty sands immediately underlying the embankment fill.

Unit weights of the non-saturated sands and silty sands of the embankment fill above the phreatic surface were modeled with a unit weight of $\gamma_m \approx 110$ lbs/ft^3, and this was then varied over a range of $\gamma_m \approx 107$ to 113 lbs/ft^3 for parameter sensitivity studies. Unit weights of the saturated upper ("soft") foundation silty sands below the phreatic surface were modeled with a unit weight of $\gamma_s \approx 115$ lbs/ft^3, and this was then varied over a range of 112 to 118 lbs/ft^3 for parameter sensitivity studies. The friction angle of the embankment fill materials above the phreatic surface was modeled with $Ø' \approx 30°$, and a range of $Ø' \approx 28°$ to 32°.

Potential initial failure surfaces were modeled as either (1) wedge-like semi-translational features, or (2) rotational features. The rotational failure surface shown in Figure B.7.3 was the most critical post-liquefaction potential failure surface found, though wedge-like failure surfaces

in this same general vicinity were found to produce similar values of $S_{r,yield}$. Because this failure surface conforms only somewhat with the observed final rear slide scarp, it was judged likely that the failure had been essentially monolithically initiated with a failure surface similar to the one shown, or that it had initiated on a failure surface extending slightly farther back towards the rear heel (as the observed field rear slide scarp occurred farther to the left, nearer to the rear edge of the roadway platform of the embankment), or that it had retrogressed in two or more slices.

Based on a range of potential failure surfaces encompassing these possibilities, and the parameters (and parameter variations) described above, it was judged that the resulting best estimate value was $S_{r,yield}$ = 236 lbs/ft^2, with a range of $S_{r,yield} \approx$ 221 to 263 lbs/ft^2.

Olson (2001) also performed back-analyses to evaluate $S_{r,yield}$. He also analyzed both rotational and wedge-like failure surfaces, mainly exiting at approximately the middle third of the roadway platform atop the embankment. His best estimate value was $S_{r,yield}$ = 9.0 kPa (188 lbs/ft^2), with a range of $S_{r,yield} \approx$ 8.5 to 11.1 kPa (176 to 232 lbs/ft^2).

B.7.5 Residual Strength Analyses Based on Residual Geometry

It was not possible to perform rigorous and reliable back-analyses to determine the value of $S_{r,resid/geom}$ required to produce a calculated Factor of Safety equal to 1.0 based on residual geometry. This is a significant source of uncertainty for this case history.

Olson (2001) noted that Ishihara had reported that the original embankment flowed approximately 50 meters, as shown in Figure B.7.1. Based on conservation of mass, he estimated the average or representative thickness of the failed (flow) mass to be approximately 2.3 m. Taking the representative slope of the flow mass at residual geometry as being approximately 2° to 3°, and with a unit weight of 18.1 kN/m^3, he employed an infinite slope analysis to develop a simplified best estimate of $S_{r,resid/geom}$ = 1.8 kPa (38 lbs/ft^2) with a range of 1.4 to 2.2 kPa (29 to 46 lbs/ft^2).

In these current studies, it was assumed that $S_{r,resid/geom}$ would have at least been higher than zero, and likely higher than this simplified estimate of Olson based on approximate geometry and an infinite slope analysis. Values of $S_{r,resid/geom}$ back-calculated from the reasonably well-documented Class A case histories were next examined, and for the range of effective overburden stress and $N_{1,60,CS}$ values for this current case an approximate range of $S_{r,resid/geom} \approx$ 30 to 90 lbs/ft^2 was conservatively assumed, based on analyses of other Class A and B case histories. This range is slightly higher than Olson's simplified estimate, and so was not adjusted further. This range of values was selected to be slightly conservatively biased (a conservative bias of approximately 10% reduction of best estimates of $S_{r,resid/geom}$ was targeted here), so that any resulting error in evaluation of overall S_r would also be slightly conservative (nominally by approximately 5% or so).

B.7.6 Overall Estimates of S_r

Overall estimates of S_r for this Class B case history were made based on the pre-failure geometry and the approximate runout features and characteristics, and the values of $S_{r,yield}$ and $S_{r,resid/geom}$ as calculated and/or estimated in the preceding sections.

Runout characteristics for this case cannot be fully accurately assessed due to the approximate nature of the post-failure geometry as reported. Runout distance, and runout ratio, appear to be "large", and the runout ratio (defined as the distance travelled by the center of gravity of the failure mass divided by the initial slope height measured from the toe to the top back edge of the rear heel scarp) was estimated as approximately 70 feet / 16.4 feet ≈ 4.2.

This allowed Equation 4-4, and Figures 4.7 and 4.11 to serve as one basis for estimation of post-liquefaction strength S_r. Using the ranges of $S_{r,yield}$ and $S_{r,resid/geom}$ from Sections B.7.4 and B.7.5, respectively, and assuming that $\xi \approx 0.4$ to 0.6 for this large runout case (based on a runout ratio of approximately 4.2), Equation 4-4 provided a best estimate value of $S_r \approx 76$ lbs/ft^2 and an estimated range of $S_r \approx 50$ to 106 lbs/ft^2. A second basis for estimation of S_r was the use of the relationship of Figure 4.9, and the range of values of $S_{r,yield}$ from Section B.7.4. Based on the runout ratio of approximately 4.2, values of initial (pre-failure displacement) Factor of Safety were taken as approximately 0.35 to 0. 5, and multiplying these by the range of $S_{r,yield}$ values produced a best estimate value of $S_r \approx 101$ lbs/ft^2 and an estimated range of $S_r \approx 78$ to 132 lbs/ft^2. No similar use was made of Figure 4.9 in conjunction with the ranges of $S_{r,resid/geom}$ estimated in Section B.4.5 because these estimates of $S_{r,resid/geom}$ were considered to be very approximate.

The estimates by each of the two methods above were then averaged together, and this produced a best estimate value of $S_r \approx 89$ lbs/ft^2 and an estimated range of $S_r \approx 50$ to 132 lbs/ft^2. These estimates of variance are non-symmetric about the best estimated mean value, and the range was judged to represent approximately +/- 2 standard deviations, so further adjustments were then necessary.

Overall, based on an assumed normal distribution, it was judged that the (mean and median) best estimate of post-liquefaction strength for this case history is

$$\overline{S_r} = 92 \text{ lbs/ft}^2$$

and that the best estimate of standard deviation of mean overall post-liquefaction strength is

$$\sigma_{\overline{S}} = 20 \text{ lbs/ft}^2$$

Olson (2001) and Olson and Stark (2002) did not apply their "kinetics" method to this case, and so they did not independently develop an estimate of S_r that incorporated momentum effects. Instead they simply used their value of $S_{r,resid/geom}$ as a conservative approximation of S_r for this less well-defined case, and used $S_r = 1.8$ to 2.0 kPa (38 to 42 lbs/ft^2) in developing their predictive relationship. This was a conservative assessment, because these are $S_{r,resid/geom}$ values and they neglect momentum effects.

A better estimate of S_r that approximately incorporates momentum effects, and a better basis for comparison with these current studies, can be obtained by employing their best estimate values of $S_{r,yield}$ = 188 lbs/ft^2 and $S_{r,resid/geom}$ = 38 lbs/ft^2, and an assumed average value of $\xi \approx 0.8$ in Equation 4-4 as

$$S_r \approx 0.5 \times [188 \text{ lbs/ft}^2 + 38 \text{ lbs/ft}^2] \times 0.8 = 90 \text{ lbs/ft}^2$$

This value ($S_r \approx 90$ lbs/ft^2) agrees very closely with the best estimate value of $S_r \approx 92$ lbs/ft^2 developed in these current studies.

Wang (2003) developed his characterization of post-liquefaction strength for the "Secondary" case histories based on averaging of values from multiple previous investigators. For this particular case (Metoki Road) he lists only one previous back-calculated value of S_r = 113 lbs/ft^2, and attributes this to Olson (2001). As discussed in Section 2.3.8 and Chapter 4, this represents the use of Equation 4-4, and Olson's best estimate values of $S_{r,yield}$ = 188 lbs/ft^2 and $S_{r,resid/geom}$ = 38 lbs/ft^2, and an assumed average value of $\xi \approx 1.0$. Because ξ is assumed to be 1.0, this value is about 25% higher than the value calculated above using ξ = 0.8.

Overall, agreement between the three sets of values calculated by (1) Olson (2001) [after combining their best estimate values of $S_{r,yield}$ and $S_{r,resid/geom}$ using Equation 4-4 and ξ = 0.8], (2) Wang (2003) and Kramer (2008) [after combining their best estimate values of $S_{r,yield}$ and $S_{r,resid/geom}$ using Equation 4-4 and ξ = 1.0] and (3) these current studies, is generally very good to excellent.

An interesting additional value of S_r was back-estimated by Ishihara et al. (1990). This was reportedly a simplified estimate, but the basis for this value (details of the back-analysis and/or judgments made) were not documented, and so Wang (2003) did not include this estimate in his averaging of prior results for this case. Ishihara's value was S_r = 6.2 kPa (129 lbs/ft^2), and this is also in generally good agreement with the S_r values of the three other investigation teams discussed above.

B.7.7 Evaluation of Initial Effective Vertical Stress

Average initial (pre-failure) effective vertical stress was assessed for the liquefied portions of the failure surfaces for both rotational and wedge-like failures similar to the one shown in Figure B.7.3. Parameters and sensitivity analyses were as described previously in Section B.7.4. Additional analyses were then performed for alternate potential failure surfaces, including failure surfaces initial (smaller) slices of a retrogressive incremental failure eventually extending back to the apparent back heel of the final failure. Depths of failure surfaces were varied, and both rotational and translational (wedge-like) failure surfaces were considered.

The resulting best estimate of average pre-failure effective stress within the liquefied materials controlling the failure was then $\sigma_{vo}' \approx 868$ lbs/ft^2, with a reasonable range of $\sigma_{vo}' \approx 701$ to 1041 lbs/ft^2. This range is slightly non-symmetric about the median value, and this range was judged by the engineering team to represent approximately ± 2 standard deviations. Overall, the

best characterization of initial (pre-failure) average effective vertical stress was then taken to be represented by a mean value of

$$\overline{\sigma'_{vo}} \approx 871 \text{ lbs/ft}^2$$

and with a standard deviation of

$$\sigma_{\bar{\sigma}} \approx 85 \text{ lbs/ft}^2$$

An estimate of σ_{vo}' was also calculated by Olson and Stark (2001, 2002). They reported a weighted average mean value of $\sigma_{vo}' \approx 41.9$ kPa (875 lbs/ft^2), in excellent agreement with these current studies. Average initial vertical effective stresses were not directly reported by Wang (2003) and Kramer (2008), but they were published more recently in the publication by Kramer and Wang (2015). As discussed in Section 2.3.8.1(b)-(iii), Wang (2003) did not perform any independent analyses to assess σ_{vo}' for his 22 "secondary" cases, and this is one of those cases. Instead, he compiled values of S_r from multiple previous investigators, and averaged these for a best estimate. He also compiled multiple values of S_r/σ_{vo}' from previous investigators, and averaged these for a best estimate. He then used these two best-estimate values of S_r and S_r/σ_{vo}' to infer a resulting representative value of σ_{vo}'. As described in Section 2.3.8.1(b)-(iii), the resulting averaged values of S_r and S_r/σ_{vo}' were incompatible with each other for a number of Wang's "secondary" case histories, and this process produced unreasonable, and in some cases physically infeasible, values of σ_{vo}' for a number of case histories. Wang's value of $\sigma_{vo}' = 2{,}655$ lbs/ft^2 is clearly physically infeasible for this case, based on the cross-section, and so it is not considered a useful check here. Agreement between Olson's value, which is well-documented, and the values developed in these current studies is excellent.

B.7.8 Evaluation of $N_{1,60,CS}$

Twenty three Swedish cone penetration tests were conducted following the failure, but only three of these Swedish cone penetration tests were reported in Ishihara et al. (1990). These are superimposed on section f-f′ in Figure B.7.2. Based on the results of those three cone soundings, and using the correlation of Inada (1982) to convert from Swedish cone tip resistances to equivalent SPT penetration resistances, $N_{1,60}$ is estimated to be approximately 1.5 to 2.5 blows/ft. Ishihara reported the material to be silty sand, but there is no further information as to the likely range of fines contents. Based on the description provided, a representative clean sand corrected blowcount of $N_{1,60,CS} = 3$ blows/ft was chosen for these current studies.

Olson (2001) and Olson and Stark (2002) made no correction for fines, and selected a "representative" uncorrected $N_{1,60}$ value of 2.6 blows/ft for this case. Wang (2003) and Kramer (2008) selected a fines adjusted value of $\overline{N_{1,60,CS}} \approx 2.0$ blows/ft, and a proportionally high standard deviation of $\sigma_{\overline{N}} \approx 1.5$ blows/ft.

Overall agreement with regard to characterization of $N_{1,60}$ or $N_{1,60,CS}$ among these two previous studies, and the current study, is considered to be good for this case with the exception of characterization of variance (or standard deviation) of the mean value of $N_{1,60,CS}$.

B.8 Hokkaido Tailings Dam (Japan; 1968)

B.8.1 Brief Summary of Case History Characteristics

Name of Structure	Hokkaido Tailings Dam
Location of Structure	Hokkaido, Japan
Type of Structure	Tailings Dam
Date of Failure	March 28, 1968
Nature of Failure	Seismic, During 1968 Tokachi-Oki Earthquake (M_w = 8.3)
Approx. Maximum Slope Height	24 ft.

B.8.2 Introduction and Description of Failure

A tailings dam near Hokkaido suffered a liquefaction-induced failure during the 1968 Tokachi-Oki Earthquake (M_w = 8.3), as reported by Ishihara et al. (1990). There are no local instrumental recordings, and shaking levels are not known.

Figure B.8.1 shows a plan view of the failure, and Figure B.8.2 presents pre-failure and post-failure cross-sections (Ishihara et al., 1990). As shown in Figure B.8.2, the failure involved a slope stability failure entirely within the impounded tailings, which flowed out over the top of the starter dike. Neither the confining starter dike nor the underlying foundation soils were involved. As shown in Figure B.8.1, the tailings flowed out to a distance extending approximately 170 meters downstream of the toe of the starter dike.

Tailings were being actively deposited at the time of the failure, and the phreatic surface shown in Figure B.8.2 was inferred by Ishihara et al. (1990).

B.8.3 Geology and Site Conditions

There is no information available regarding foundation conditions, or the nature and condition of materials comprising the starter dike. This is not problematic, because the failure was judged to have occurred entirely within the impounded tailings.

Ishihara et al. (1990) describe the tailings as silty sand, but no further information regarding gradation or fines content is provided. Ishihara et al. estimated the unit weight of the tailings to be on the order of 19.6 kN/m^3. Dutch cone penetration test soundings were performed after the failure, and the results of two of these soundings are presented in Figure B.8.3. With the exception of what may be a stiffer interim deck at a depth of approximately 1.6 meters, the tailings show very low (and relatively consistent) tip resistances over the upper 6 meters at the sites of these two soundings.

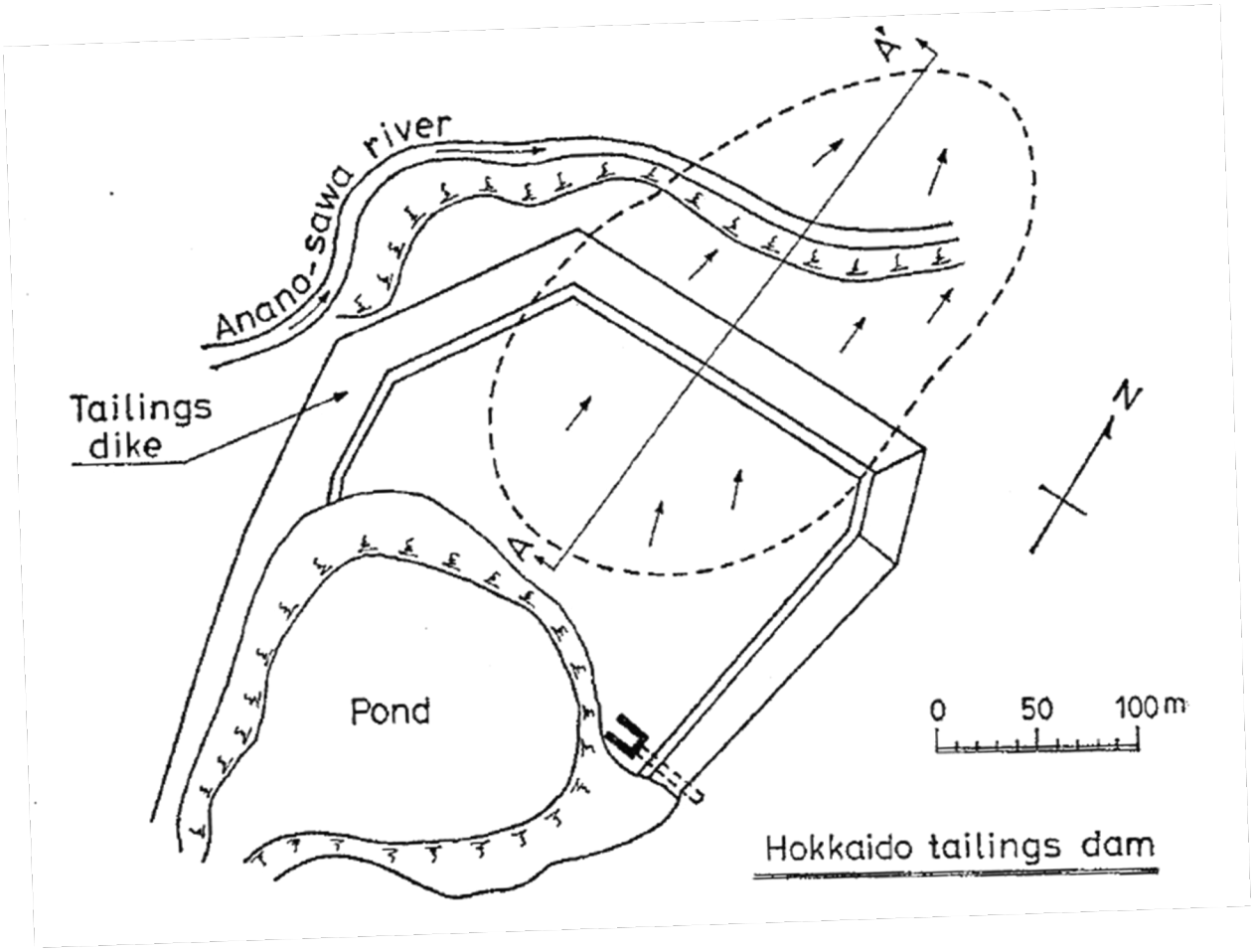

Figure B.8.1: Plan view of the Hokkaido tailings dam showing the approximate extent of the flow failure (figure from Ishihara et al., 1990).

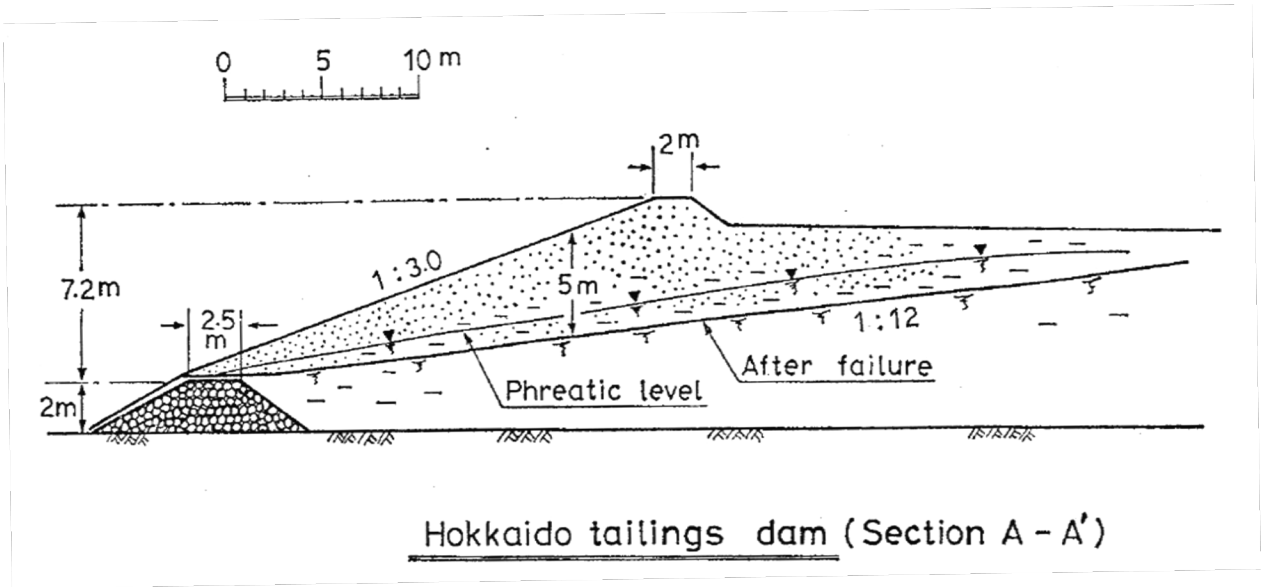

Figure B.8.2: Pre-failure and post-failure cross-sections at Section A-A' from Figure B.8.1 (figure from Ishihara et al., 1990).

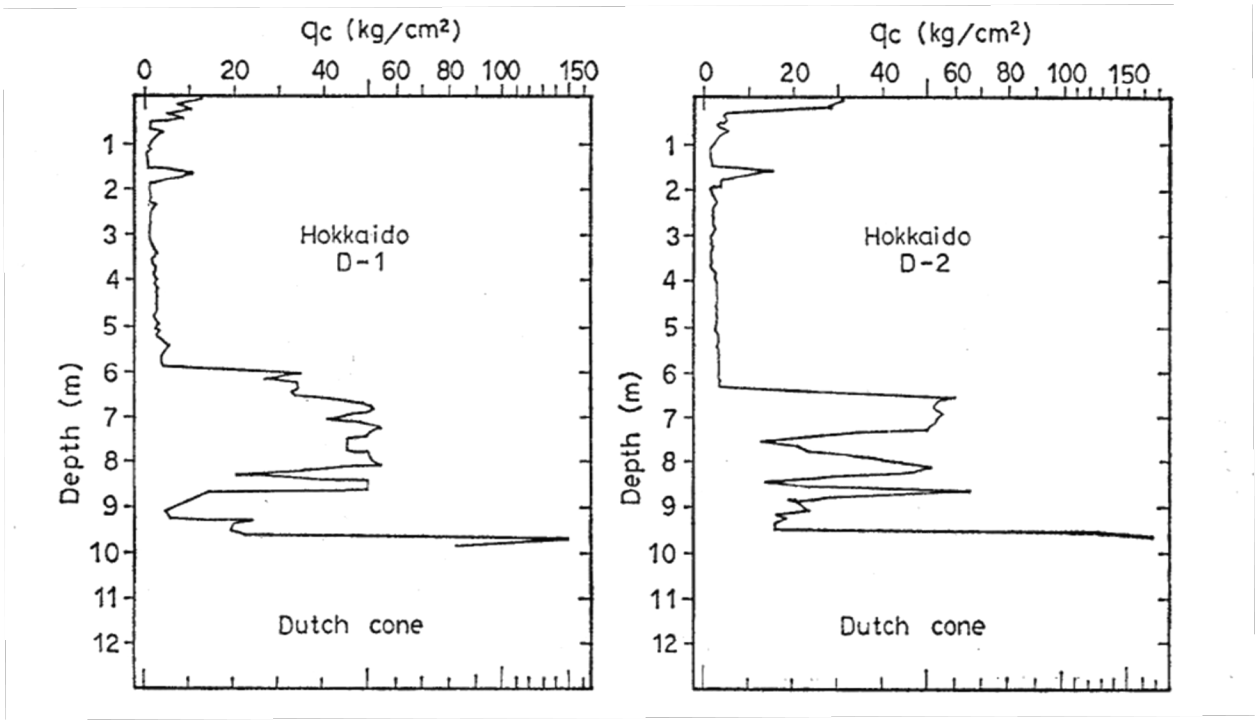

Figure B.8.3: Results of two Dutch cone penetration test soundings performed after the failure (figure from Ishihara et al., 1990).

B.8.4 Initial Yield Stress Analyses

Figure B.8.4(a) shows the cross-section used for back-analyses of the post-liquefaction initial yield strength $S_{r,yield}$ that would be required within the liquefied upstream shell materials to produce a calculated Factor of Safety equal to 1.0. This is not the actual post-liquefaction strength, but it proves to be useful in developing estimates of post-liquefaction strength (S_r) for this case history.

Unit weights of the non-saturated tailings above the phreatic surface were modeled with a unit weight of $\gamma_m \approx 118$ lbs/ft^3, and this was then varied over a range of 114 to 122 lbs/ft^3 for parameter sensitivity studies. Unit weights of the saturated tailings below the phreatic surface were modeled with a unit weight of $\gamma_s \approx 123$ lbs/ft^3, and this was then varied over a range of 119 to 127 lbs/ft^3 for parameter sensitivity studies. The friction angle of the tailings above the phreatic surface was modeled with $Ø' \approx 30°$, and a range of $Ø' \approx 28°$ to 33°.

There were no eyewitness reports, so it is not known with certainty whether this was an incrementally retrogressive failure, or a more monolithic failure in which most or all of the failure mass initiated its movements all at once.

A number of different potential failure surfaces were analyzed. These back-analyses showed that it was likely that this had been a retrogressive failure, initiating with a large initial failure slice or wedge that encompassed the interim crest lip section, and then retrogressing eventually back to the final back heel.

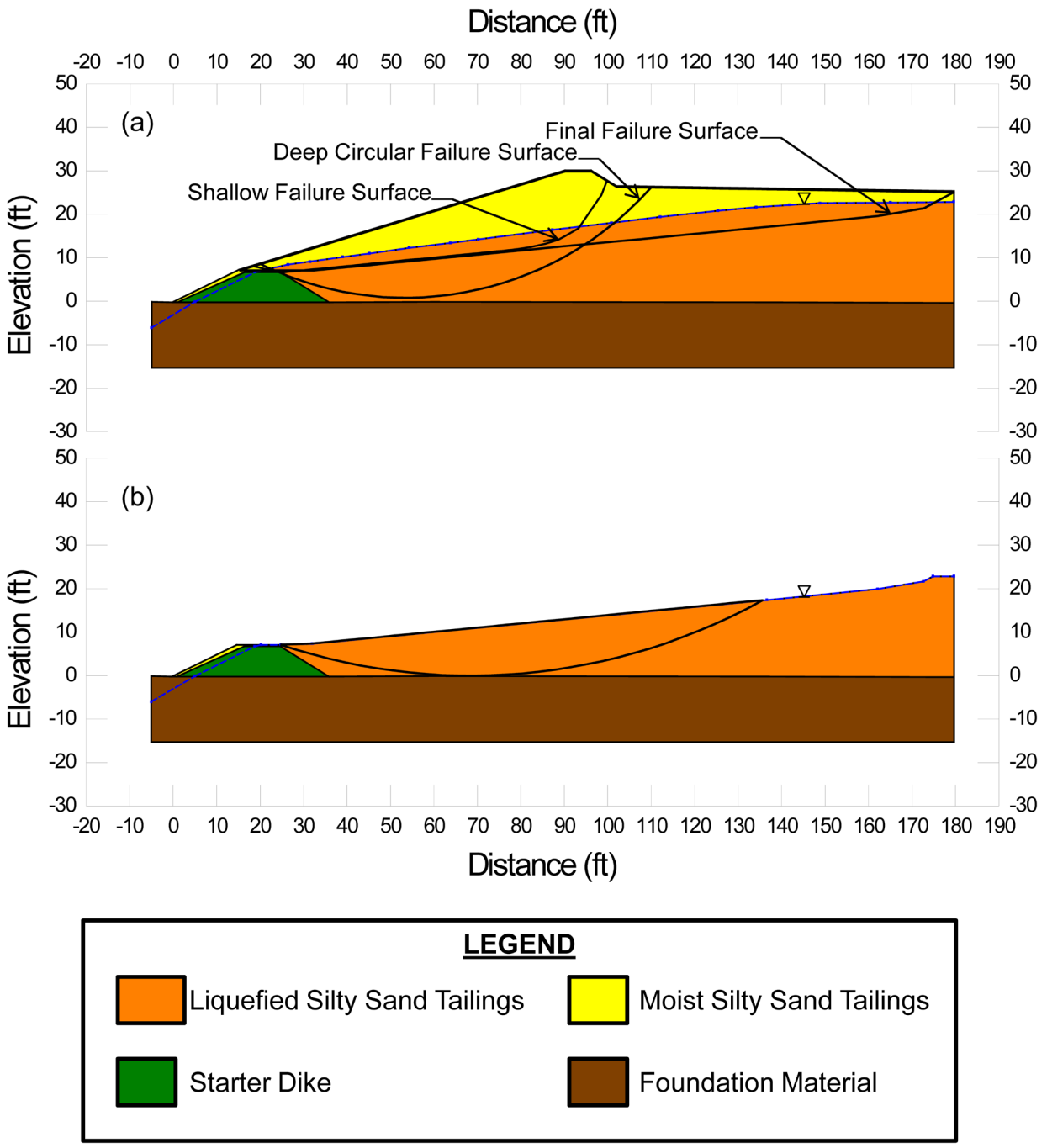

Figure B.8.4: Selected potential failure surfaces analyzed for evaluation of (a) $S_{r,yield}$ and (b) $S_{r,resid/geom}$ for the Hokkaido Tailings Dam

Figure B.8.4(a) shows a select subset of the potential failure surfaces analyzed for back-analyses of $S_{r,yield}$. Based on all of the analyses performed, the most likely failure mechanism was judged to be an initial failure surface similar to the "shallow" failure surface shown in Figure B.8.4(a), as the first stage of an incrementally retrogressive overall failure sequence. The shallow

failure surface shown in this figure is the most critical failure surface of this type, and the calculated best estimate for this surface is $S_{r,yield}$ = 351 lbs/ft^2. Based on parameter variations (parameter sensitivity studies), and moderate variations of failure surface geometries, the likely range is estimated as $S_{r,yield}$ = 306 to 409 lbs/ft^2 for this type of initial failure surface.

The "deep circular failure surface" shown in Figure B.8.4(a) is the most critical of a second set of potential initial failure surfaces passing beneath the final observed post-failure ground surface, and again representing the first stage of an incrementally retrogressive overall failure sequence. For this surface, the best estimate was $S_{r,yield}$ = 242 lbs/ft^2, with a range of $S_{r,yield}$ = 215 to 274 lbs/ft^2.

The third type of potential failure surface analyzed was a failure surface approximating the overall post-failure ground surface, and would reflect either the assumption that this defined the basal overall failure surface, or that it closely approximated at least the latest stages of an incrementally retrogressive failure. The back-calculated initial yield stress for this overall failure surface, and for a monolithically initiated overall failure along this surface, is $S_{r,yield}$ = 109 lbs/ft^2, with a range of $S_{r,yield}$ = 75 to 134 lbs/ft^2, but it was considered unlikely that the failure was monolithically initiated.

Overall assessment of $S_{r,yield}$ for this case was based on weighted averages of the values of $S_{r,yield}$ back calculated for these three types of potential failure surfaces. The shallower initial failure surface near the downstream toe was considered the most likely, and was assigned a weighting factor of 2. The deeper rotational failure surface was assigned a weighting factor of 1. The failure surface representing an overall monolithically initiated failure along the observed post-failure ground surface was assigned a weighting factor of 0.5. Based on these estimates and associated weighting factors, and the back-calculated values from above, the overall best estimate was $S_{r,yield}$ = 254 lbs/ft^2, with a range of $S_{r,yield}$ = 221 to 293 lbs/ft^2.

Olson (2001) also performed back-analyses to estimate $S_{r,yield}$. He also assumed that the failure was retrogressive, and that an initial failure slice initiated first near the downstream side. His assumed initial failure surfaces were rotational failures similar to the "deep rotational" failure shown in Figure B.8.4(a), except that he constrained the base of these rotational failures over a range of elevations that did not pass more than about 0.5 meters below the elevation of the crest of the starter dike. These rotational failure surfaces did extend below the final post-failure surface of the tailings. A range of potential initial rotational failure surfaces were analyzed. Olson's back-calculated best estimate was $S_{r,yield} \approx$ 11.7 kPa (245 lbs/ft^2), with a range of 10.3 to 12.7 kPa (215 to 265 lbs/ft^2). These values were developed by a different set of procedures and judgments, but they are in very good agreement with the values back-calculated in these current studies.

B.8.5 Residual Strength Analyses Based on Residual Geometry

It was not possible to perform rigorous and reliable back-analyses to determine the value of $S_{r,resid/geom}$ required to produce a calculated Factor of Safety equal to 1.0 based on residual geometry. This case is one of six cases (out of the 29 cases back-analyzed as part of these current studies) where the slide mass "went over a lip" and then traveled down a steeper slope, and the

ensuing displacements either (1) could not be reliably tracked, or (2) could not be fully reliably back-analyzed. Both situations apply in this current case because the post-failure geometry of the failure mass runout is not well characterized.

Olson (2001) examined the plan view presented in Figure B.8.1, and assumed conservation of mass, concluding that the average thickness of the failed material downstream of the original dike was probably on the order of 2.5 to 3 meters. He then appears to have performed his simplified (infinite slope) analysis to determine his estimated values of $S_{r,resid/geom}$, but for this case history he does not indicate what slope angle(s) he assumed here either for the top slope or basal slope of the flowed tailings. He reports a best estimate value of $S_{r,resid/geom} \approx 4.8$ kPa (100 lbs/ft^2) for a thickness of 3 meters and a unit weight of 19.6 kN/m^3. His estimated range was $S_{r,resid/geom} \approx 4.1$ kPa (86 lbs/ft^2), which was based on a thickness of 2.5 m, to $S_{r,resid/geom} \approx 6.6$ kPa (125 lbs/ft^2), which was based on an assumed thickness of 4 meters as was used by Ishihara et al. (1990). These calculations would correspond to an assumed infinite slope angle of approximately 4.8° for the runout tailings downstream of the original dam toe, or it would represent the assumption that the observed post-failure slope of 1:12 ≈ 4.8° within the tailings impoundment represented a residual condition.

In these current studies, it was assumed that $S_{r,resid/geom}$ would have at least been higher than zero. Values of $S_{r,resid/geom}$ back-calculated from the reasonably well-documented Class A case histories were next examined, and for the range of effective overburden stress and $N_{1,60,CS}$ values for this current case an approximate range of $S_{r,resid/geom} \approx 30$ to 100 lbs/ft^2 was conservatively assumed, based on analyses of several of the Class A case histories. This range of values was selected to be slightly conservatively biased (a conservative bias of approximately 10% reduction of best estimates of $S_{r,resid/geom}$ was targeted here), so that any resulting error in evaluation of overall S_r would also be slightly conservative (nominally by approximately 5% or so).

Analyses were also performed of the residual slope left in place after the failure, as shown in Figure B.8.4(b). There is no certainty that the tailings below this residual top surface liquefied (or "triggered"), but there is no reason to expect that the relatively steep (1:12) post-failure slope surface shown in Figure B.8.2 would represent bedding planes arising from the hydraulic placement of tailings, and both the initial yield stress analyses performed by Olson (2001) and in these current studies showed that deeper rotational potential failure surfaces may have been the initial most critical failure surfaces for this case. If the deeper tailings did liquefy, then for the rotational failure surface illustrated in Figure B.8.2 the back-calculated value would be $S_{r,resid/geom} \approx 83$ lbs/ft^2. Similarly, if the deeper tailings did liquefy, then an infinite slope analysis of this post-failure slope surface can be performed as an approximation, with a tailings thickness of approximately 2 to 4 m. (6.6 to 13.1 ft.), a unit weight of approximately 19.6 kN/m3 (125 lbs/ft^3), and a slope angle of approximately 4.8° (1:12, H:V), producing values of $S_{r,resid/geom} \approx 69$ to 138 lbs/ft^2.

Overall, considering the estimates (1) made based on infinite slope analyses of assumed downstream (runout) geometry by Olson (2001), (2) similar infinite slope analyses made by Olson using the assumed representative post-failure tailings runout thickness of 6 m as proposed by Ishihara et al. (1990), (3) the rotational failure surface shown in Figure B.8.4(b), (4) approximate infinite slope analyses of the post-failure slope remaining within the tailings impoundment after

the event, and (5) values of $S_{r,resid/geom}$ back-calculated for better-defined post failure conditions from the Class A case histories, it was concluded that a best estimate value would be taken as $S_{r,resid/geom} \approx 70$ lbs/ft^2, with a range of $S_{r,resid/geom} \approx 30$ to 110 lbs/ft^2. It is interesting to note that these values are in good agreement with the values of $S_{r,resid/geom}$ developed by Olson (2001) despite the very different approaches and judgments made in develop the two sets of values.

B.8.6 Overall Estimates of S_r

Overall estimates of post-liquefaction strength S_r were made by two approaches. The first approach was to employ Equation 4-4, and Figure 4.11 as

$$S_r \approx \xi \bullet (S_{r,yield} + S_{r,resid/geom}) / 2$$

where ξ is a function of runout distance and overall failure mechanism characteristics.

Unfortunately, runout characteristics cannot be reliably characterized for this case history, because it is one of the six case histories back-analyzed in which the failure mass "went over a lip" and then down a steeper slope rather than coming to rest on a gentler basal slope as with most of the cases plotted in Figure 4.11. It is clear that runout distance is not small, but runout distance (and runout ratio) cannot be fully reliably quantified. The current engineering team therefore developed a consensus estimate that an appropriate range of values of ξ for this case would be on the order of $\xi \approx 0.45$ to 0.55. Using these values, and the values of $S_{r,yield}$ and $S_{r,resid/geom}$ presented previously in Sections B.8.4 and B.8.5, and the associated ranges of both $S_{r,yield}$ and $S_{r,resid/geom}$, this produced a best estimate of $S_r \approx 81$ lbs/ft^2, with a range of $S_r = 56$ to 111 lbs/ft^2.

The second approach was to employ the relationship presented in Figure 4.9, wherein pre-failure Factor of Safety can be approximately evaluated as a function of runout characteristics. Here again the difficulty was that the post-failure runout characteristics were not fully quantifiable because the failure mass went over a lip and then down a steeper slope. The engineering team developed a consensus estimate that the pre-failure range of Factor of Safety for this case would have been on the order of FS = 0.3 to 0.55. Multiplying these values by the values of $S_{r,yield}$ from Section B.8.4, produces a best estimate of $S_r \approx 95$ lbs/ft^2, with a range of $S_r = 66$ to 132lbs/ft^2.

Averaging the two sets of values developed by these two approaches then produced a best estimate of $S_r \approx 88$ lbs/ft^2, with a range of $S_r = 56$ to 111 lbs/ft^2. The variance was slightly non-symmetric about the best estimate, so this was slightly further adjusted to produce a characterization that could be modeled with a Normal distribution. The range was estimated to represent approximately +/- 1.5 standard deviations.

Overall, based on an assumed normal distribution, it was judged that the (mean and median) best estimate of post-liquefaction strength for this case history is

$$\overline{S_r} = 98 \text{ lbs/ft}^2$$

and that the best estimate of standard deviation of mean overall post-liquefaction strength is

$$\sigma_{\bar{S}} = 25 \text{ lbs/ft}^2$$

Olson (2001) and Olson and Stark (2002) did not apply their "kinetics" method to this case, and so they did not independently develop an estimate of S_r that incorporated momentum effects. Instead, they took their value of $S_{r,resid/geom}$ as representing S_r. Their best estimate value was therefore $S_r = S_{r,resid/geom} = 100$ lbs/ft^2, with a range of 86 to 125 lbs/ft^2, as described previously in Section B.8.5.

A better estimate can be obtained by taking their back-calculated best estimate values of $S_{r,yield}$ and $S_{r,resid/geom}$ are using the simplified Equation 4.1 with a fixed $\xi = 0.8$, in which case the resulting estimate would be

$$S_r \approx \xi \bullet (S_{r,yield} + S_{r,resid/geom}) / 2 \approx (0.8) \bullet (245 \text{ lbs/ft}^2 + 100 \text{ lbs/ft}^2) / 2 \approx 138 \text{ lbs/ft}^2$$

Wang (2003) and Wang and Kramer (2008) did not employ their zero inertial force (ZIF) method to incorporate inertial effects in back-analyses of this failure. Instead they selected their value of S_r based on examination of values from back-analyses by several previous investigators. Wang (2003) selected two values for this case history as:

$S_r = 408$ lbs/ft^2 (Ishihara et al., 1990)

$S_r = 172$ lbs/ft^2 (Olson, 2001)

where Wang's value for "Olson, 2001" was taken as $S_r \approx (S_{r,yield} + S_{r,resid/geom}) / 2$, representing an implied value of $\xi = 1.0$, which would clearly over-estimate S_r for this case. The value of 408 lbs/ft^2 attributed to Ishihara et al. (1990) is mysterious, as the paper by Ishihara actually presents a value of $S_r = 0.67$ t/m^2 (137lbs/ft^2). So both of Wang's selected values appear to be in error, and they are unconservatively high. Averaging these together therefore produced a value that was also unconservatively too high.

B.8.7 Evaluation of Initial Effective Vertical Stress

The representative vertical effective stress for the Hokkaido Tailings Dam was determined by averaging the calculated vertical effective stress on the failure plane in the liquefied zone from the deep and final failure surfaces shown in Figure B.8.4(a). Parameter variations (unit weights) were then varied, and so to some extent were the depths of the potential failure surfaces of each type.

The resulting best estimate of average pre-failure effective stress within the liquefied materials controlling the failure was then $\sigma_{vo}' \approx 1{,}198$ lbs/ft^2, with a reasonable range of $\sigma_{vo}' \approx 916$ to 1,489 lbs/ft^2. This range was judged by the engineering team to represent approximately ± 1.5 standard deviations. Overall, the best characterization of initial (pre-failure) average effective vertical stress was then taken to be represented by a mean value of

$$\overline{\sigma'_{vo}} \approx 1{,}203 \text{ lbs/ft}^2$$

and with a standard deviation of

$$\sigma_{\bar{\sigma}} \approx 191 \text{ lbs/ft}^2$$

An estimate of σ_{vo}' was also calculated by Olson and Stark (2001, 2002). They reported a weighted average mean value of $\sigma_{vo}' \approx 65.9$ kPa (1,376 lbs/ft^2), in very good agreement with these current studies. Average initial vertical effective stresses were not directly reported by Wang (2003) and Kramer (2008), but they were published more recently in the publication by Kramer and Wang (2015). As discussed in Section 2.3.8.1(b)-(iii), Wang (2003) did not perform any independent analyses to assess σ_{vo}' for his 22 "secondary" cases, and this is one of those cases. Instead, he compiled values of S_r from multiple previous investigators, and averaged these for a best estimate. He also compiled multiple values of S_r/σ_{vo}' from previous investigators, and averaged these for a best estimate. He then used these two best-estimate values of S_r and S_r/σ_{vo}' to infer a resulting representative value of σ_{vo}'. As described in Section 2.3.8.1(b)-(iii), the resulting averaged values of S_r and S_r/σ_{vo}' were incompatible with each other for a number of Wang's "secondary" case histories, and this process produced unreasonable, and in some cases physically infeasible, values of σ_{vo}' for a number of case histories. Wang's value of $\sigma_{vo}' = 3{,}336$ lbs/ft^2 is clearly physically infeasible for this case, based on the cross-section, and so it is not considered a useful check here. Agreement between Olson's value, which is well-documented, and the values developed in these current studies is very good.

B.8.8 Evaluation of $N_{1,60,CS}$

Dutch cone soundings were performed after the failure (Ishihara et al, 1990). Only two soundings are published, and these are presented in Figure B.8.3. No standard penetrations tests were performed at this site.

Conversion of the Dutch cone tip resistances to equivalent SPT $N_{1,60,CS}$ values was an approximate exercise, but as the measured penetration resistances were very low the degree of uncertainty was acceptable here. In these current studies, the characterization of penetration resistance is represented by a best estimate mean value of $\overline{N_{1,60,CS}} \approx 4$ blows/ft, and an estimated standard deviation of this mean of $\sigma_{\bar{N}} \approx 1.1$ blows/ft.

Olson employed no fines adjustment, and developed a best estimate of $N_{1,60} = 1.1$ blows/ft, with a range of 1.0 to 1.2 blows/ft.

Wang (2003) and Kramer (2008) jointly developed a representative value of $\overline{N_{1,60,CS}} = 5.1$ blows/ft, and their estimated standard deviation of that overall mean value for this case history was $\sigma_{\bar{N}} = 1.4$ blows/ft. Details of the development of this interpretation by Wang and Kramer are not presented. Kramer and Wang (2105) subsequently converted to a non-fines-corrected representative value of $N_{1,60} = 1.1$ blows/ft, and they do not present their associated variance or standard deviation.

Overall agreement between these three independent assessments of representative $N_{1,60}$ and $N_{1,60,CS}$ values is judged to be very good, allowing for the differences between fines-corrected and non-fines corrected penetration resistance measures.

B.9 Upper San Fernando Dam (California, USA; 1971)

B.9.1 Brief Summary of Case History Characteristics

Name of Structure	Upper San Fernando Dam
Location of Structure	California, USA
Type of Structure	Hydraulic fill dam
Date of Failure	February 9, 1971
Nature of Failure	Seismic, During 1971 San Fernando Earthquake (M_W = 6.7)
Approx. Maximum Slope Height	67 ft.

B.9.2 Introduction and Description of Failure

The Lower San Fernando Dam (also known as the Lower Van Norman Dam, as it was part of the Van Norman Dam complex) suffered a liquefaction-induced landside on its upstream side as a result of the San Fernando Earthquake of February 9, 1971. The back-analysis of that slope failure case history was presented and discussed in Appendix B.4.

The Upper San Fernando Dam (or the Upper Van Norman Dam) also suffered liquefaction-induced damage, and displacements, during the 1971 San Fernando Earthquake. It is the Upper Dam that will be the subject of this Appendix section. The performance of the Upper Dam during the 1971 earthquake was well studied, though it has not received nearly as much attention from researchers as the Lower Dam. Seed et al. (1973, 1975) and Lee et al. (1975) documented immediate post-earthquake investigations and studies, and a number of researchers have studied and/or back-analyzed this dam since. It has not, however, been back-analyzed by many investigation teams for purposes of studying post-liquefaction strengths. Seed and Harder (1990) back-analyzed this dam performance case history for purposes of evaluation of post-liquefaction strengths, but Olson and Stark (2001, 2002) and Wang and Kramer (2003, 2008, 2015) did not. The informal panel of experts advising these current studies agreed unanimously that displacements for this case history were sufficient as to warrant inclusion of this case in these current studies, as fully developed post-liquefaction strength (S_r) would have been produced by the levels of shearing evidenced.

Figure B.9.1 presents a cross-section through the Upper San Fernando Dam after the 1971 earthquake, showing both the pre-earthquake and post-earthquake sections. The Upper dam, like the Lower dam, was also primarily constructed by means of hydraulic fill methods, with some rolled earth sections. Liquefaction occurred within at least some portions of the hydraulic fill on the downstream side of the dam. This loss of strength, likely coupled with cyclic inertial forces from the earthquake, produced moderate but not insignificant displacements of a large "slip mass" towards the downstream side. As shown in Figure B.9.1, the dam crest displaced approximately 5 feet toward the downstream direction, and settled approximately 3 feet. A complementary toe slippage feature was also observed, also shown in Figure B.9.1, with an associated lateral displacement of approximately 7 to 9 feet towards the downstream direction.

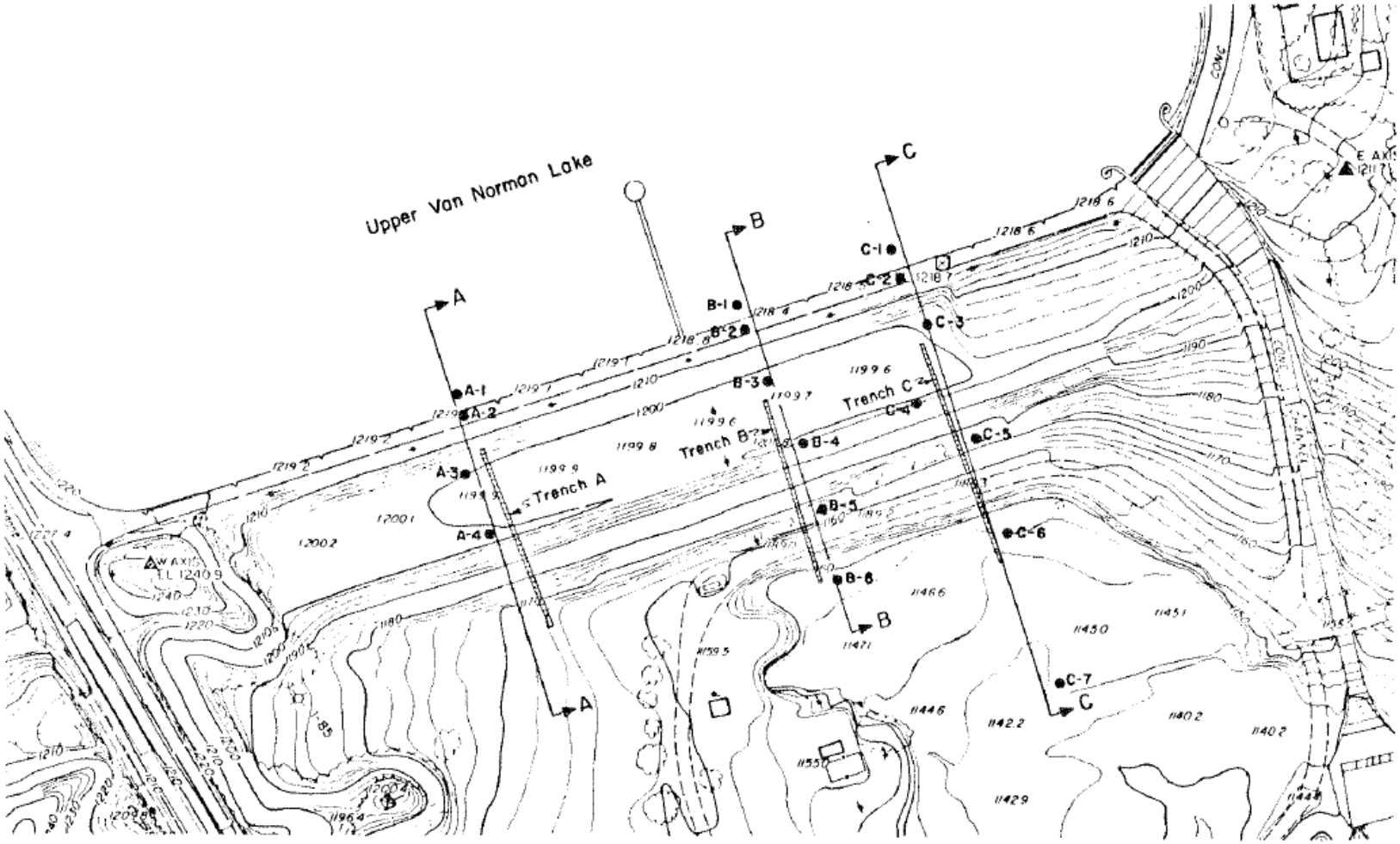

Figure B.9.1: Plan view of the Upper San Fernando Dam showing the locations of post-failure SPT borings performed for the 1971 investigation (Seed et al., 1973).

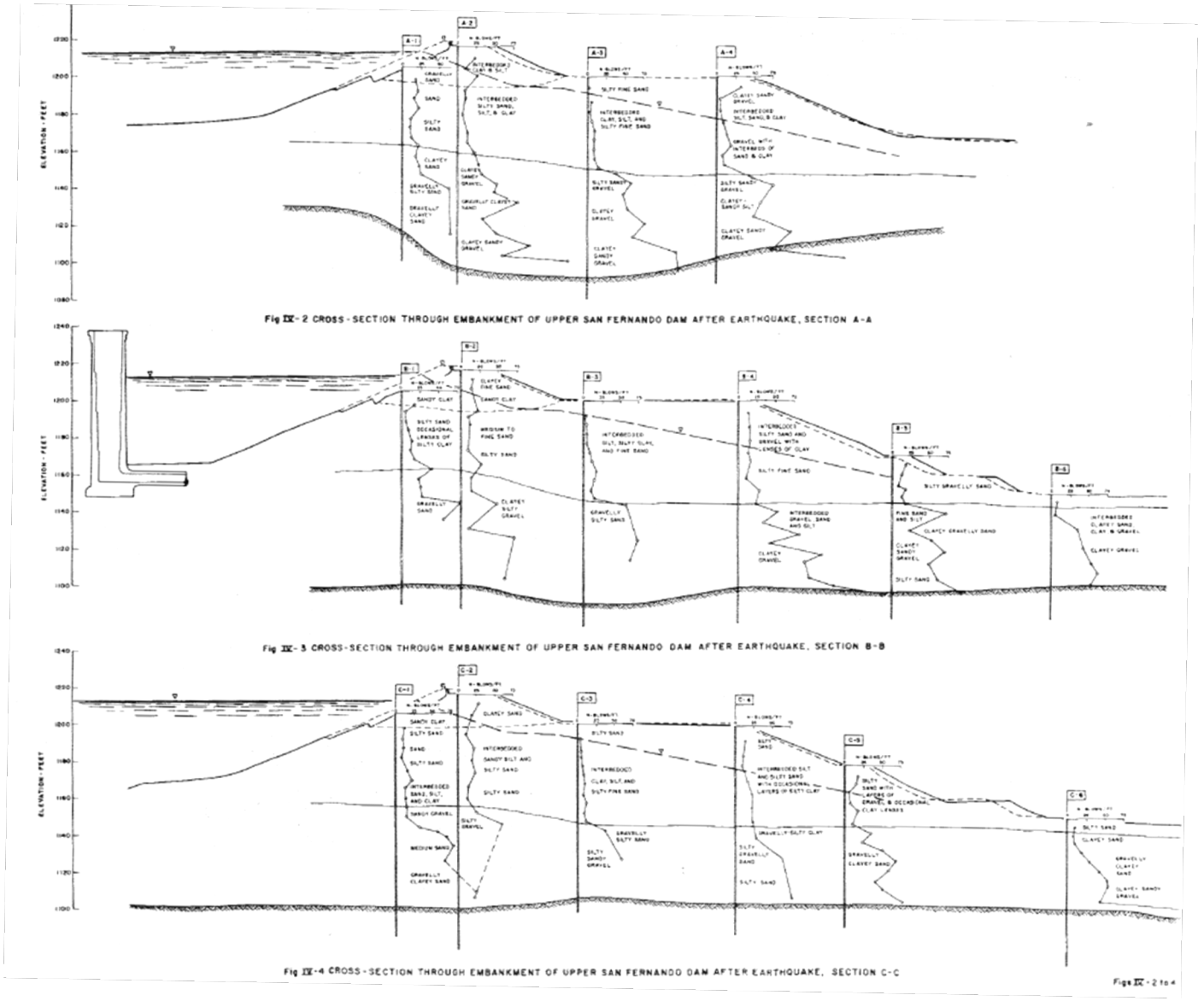

Figure B.9.2: Pre-failure and post-failure cross-sections of the Upper Fernando Dam from the 1971 investigation (Seed et al., 1973).

The downstream movements of the Upper Dam led to some cracking of the embankment, opening up some joints in the outlet conduit which passes through the embankment and leading to formation of a sinkhole along the line of the conduit. The deformations did not, however, result in a breach and release of the reservoir.

There were two seismoscopes at the Lower dam; one on the right abutment and one on the crest. These were not very modern instruments, and interpretation of the recordings was challenging. The crest instrument was carried into the reservoir by the upstream slope failure, but it was recovered and processed. It appeared to indicate that strong shaking had ceased before the upstream slide in the Lower dam was initiated. Morrill (1972) computed maximum spectral displacement for these two strong motion records, and also lists instrument characteristics including the natural period. Duke et al. (1972) computed the spectral accelerations of the two records, and assigned the following values of peak horizontal acceleration: Crest $a_{max} \approx 0.48g$ and abutment $a_{max} \approx 0.55g$. This suggests little amplification from abutment to crest for this event. Scott (1972) performed an additional interpretation of the crest record. Some uncertainties developed where the instrument reached its maximum travel and bumped against its support, and also where the pen ran briefly scale. Scott also concluded that the peak horizontal acceleration at the crest was likely on the order of $a_{max} \approx 0.55$ to $0.6g$, in good agreement with Duke et al.

B.9.3 Geology and Site Conditions

The Lower dam was constructed first, beginning in 1912, and construction of the Upper Dam began in 1921.

Both the Upper and Lower Dams were constructed primarily by means of hydraulic fill placement, and with similar materials and similar procedures. Hydraulic fill was placed simultaneously in a central puddled pool from starter dikes on both the upstream and downstream edges, producing “shells: on both the upstream and downstream sides comprised mainly of silty sands and sandy silts, and also a “puddled clay core”. Another construction method sometimes used when water was scarce was the “semi-hydraulic” procedure, in which the fill would be excavated from the borrow area by teams and Fresno scrapers or steam shovels, and then hauled to the dam, dumped into the pool, and then dispersed by hydraulic monitors operating from barges floating in the pool. Significant portions of the Upper Dam are believed to have been constructed by this semi-hydraulic method, although no detailed records or photographs appear to be available.

Seed et al. (1973) concluded that “Although standard hydraulic fill construction was used for the lower part of the Lower San Fernando Dam and the semi-hydraulic fill process was used for most of the fill at the Upper Dam, the results of drilling, sampling and trenching at both dams indicate no major difference in the type or quality of finished product obtained by either of the two methods.”

As with the Lower dam, additional rolled fill was placed atop the hydraulic fill of the Upper dam to further raise the crest section. The rolled fill was placed as “dry fill” (not hydraulic fill), and the materials were excavated by side hill borrow, spread in thin lifts, sprinkled and wagon-rolled. These materials were not well characterized in the post-failure investigations, but that has

little impact on the back-analyses performed as the strengths of these upper rolled fill materials are not significant because the apparent partially developed failure surface passes beneath these materials and does not shear them (see Figures B.9.2 through B.9.4).

The embankment of the Upper Dam is founded on deposits of "recent" alluvium, consisting of stiff clays and clayey gravels about 50 to 60 feet in thickness. These foundation deposits are not considered to be potentially liquefiable. Underlying the alluvium, and forming the abutments, are poorly cemented conglomeritic sandstone and coarse-grained sandstone of the Saugus Formation (Lower Pleistocene)-[Seed et al., 1973].

B.9.4 Initial Yield Stress Analyses

Back-analyses of the strength required for a static factor of safety equal to 1.0 were performed using the failure surface shown in Figure B.9.4. This is the best-estimate failure surface based on Figure B.9.3 (which is an enlarged view of Cross-Section B-B' from Figure B.9.2. This cross-section is slightly displaced, so the failure surface from Figure B.9.4 was imposed on the pre-earthquake cross-section geometry for this cross-section.

Shear strengths of the liquefied hydraulic fill along the failure surface were modeled as $S_{r,yield}$. Shear strengths of the clayey puddled core zone were modeled as increasing with increased effective overburden stress, based on laboratory testing of these soils as presented in Figure B.9.5.

Unit weights of the upper rolled fill above the phreatic surface were modeled as $\gamma_m = 126$ lbs/ft^3. For parametric sensitivity studies this was then varied over a range of $\gamma_m = 122$ to 130 lbs/ft^3. Unit weights of the upper rolled fill below the phreatic surface were modeled as $\gamma_s = 132$ lbs/ft^3. For parametric sensitivity studies this was then varied over a range of $\gamma_s = 128$ to 136 lbs/ft^3.

Unit weights of the sandy silt and silty sand hydraulic fill above the phreatic surface were modeled as $\gamma_m = 117$ lbs/ft^3. For parametric sensitivity studies this was then varied over a range of $\gamma_m = 112$ to 122 lbs/ft^3. Unit weights of the sandy silt and silty sand hydraulic fill below the phreatic surface were modeled as $\gamma_s = 123$ lbs/ft^3. For parametric sensitivity studies this was then varied over a range of $\gamma_s = 118$ to 128 lbs/ft^3.

Unit weights of the clayey puddled core both above and below the phreatic surface were modeled as $\gamma_m \approx \gamma_s \approx 116$ lbs/ft^3. For parametric sensitivity studies this was then varied over a range of $\gamma_m \approx \gamma_s \approx 112$ to 120 lbs/ft^3.

For these ranges of parameters, and for moderate variations in the vertical location of the failure plane (away from the upstream and downstream faces), the resulting best estimate value was $S_{r,yield} = 744$ lbs/ft^2, with a range of $S_{r,yield} = 602$ to 885 lbs/ft^2.

These back-analyses to evaluate $S_{r,yield}$ were performed only as an approximate check of the back-analyses described below in Section B.9.5. The differences between the two cross-

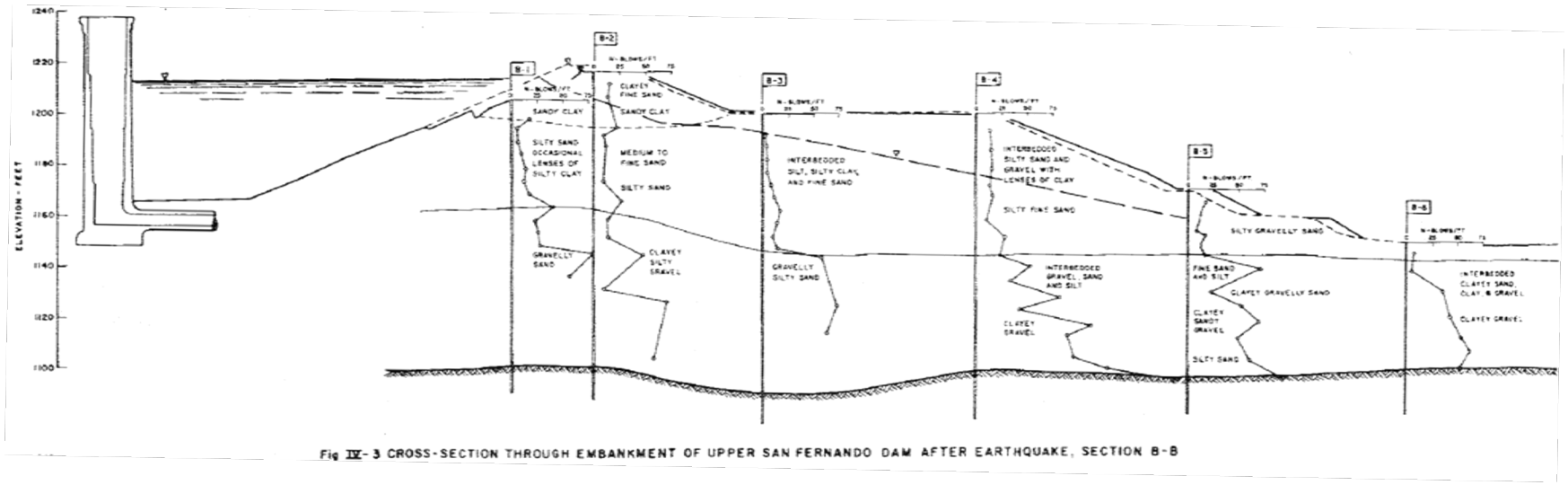

Fig IV-3 CROSS-SECTION THROUGH EMBANKMENT OF UPPER SAN FERNANDO DAM AFTER EARTHQUAKE, SECTION B-B

Figure B.9.3: Pre-failure and post-failure cross-sections of the Upper San Fernando Dam for Section B-B the 1971 investigation (Seed et al., 1973).

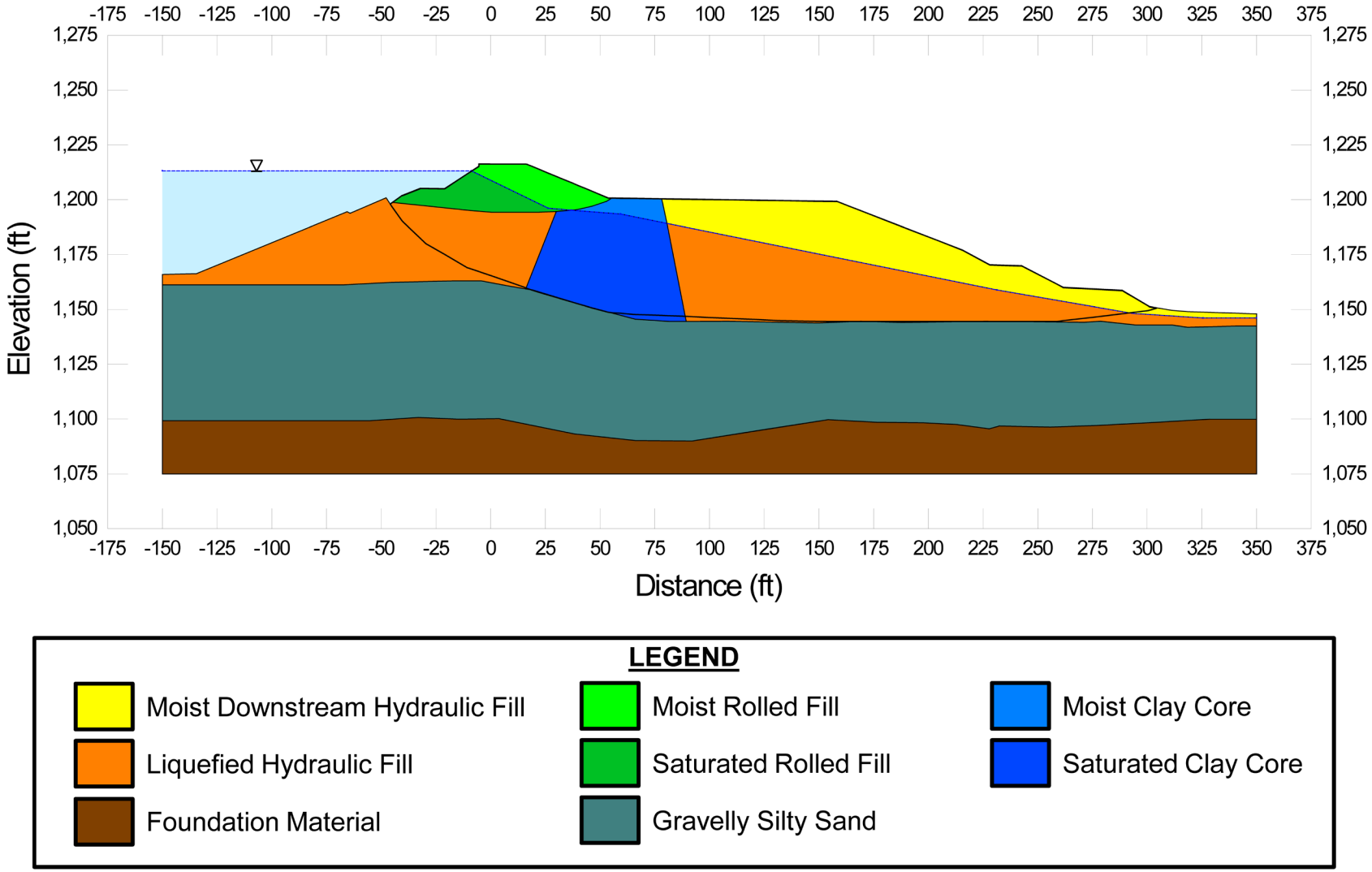

Figure B.9.4: Post-earthquake cross-section through the Upper San Fernando Dam showing potential failure surface analyzed.

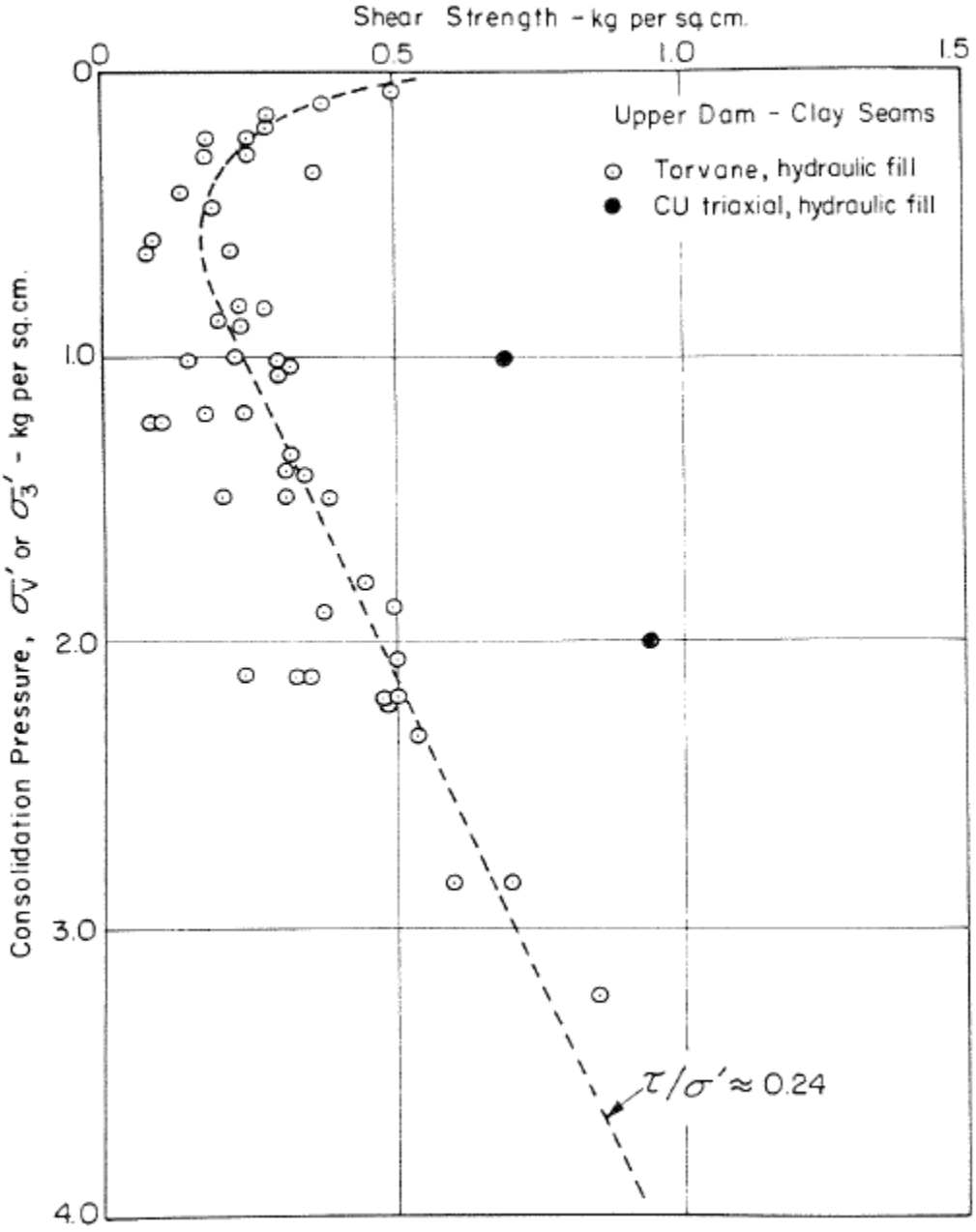

Figure B.9.5: In situ shear strengths of clayey central "puddle core" materials from the Upper San Fernando Dam based on torvane data. (Seed et al. 1973)

sections (pre-earthquake and post-earthquake) are relatively minor, and so these two sets of analyses are nearly redundant.

B.9.5 Residual Strength Analyses Based on Residual Geometry

Back-analyses were also performed to evaluate the value of $S_{r,resid/geom}$ required to provide a static factor of safety equal to 1.0 for post-failure (residual) geometry. The cross-section of Figure B.9.4 was employed here, and the failure surface shown in this figure was taken as the best estimate case. Model parameters were as described in the previous Section B.9.4.

For these ranges of parameters, and for moderate variations in the vertical location of the failure plane (away from the upstream and downstream faces), the resulting best estimate value was $S_{r,resid/geom}$ = 711 lbs/ft^2, with a range of $S_{r,resid/geom}$ = 577 to 848 lbs/ft^2.

B.9.6 Overall Estimates of S_r

A number of approaches were considered for evaluation of S_r. In all of the other liquefaction failure case histories back-analyzed as part of these studies, the failures experienced large displacements after initial liquefaction. This case history is different, because the total shear displacement offsets along the apparent failure surface were only on the order of approximately 5 to 9 feet. These were large enough to reliably reach a value of S_r, but the modest amount of displacement that occurred suggests that the post-liquefaction static Factor of Safety was equal to 1.0 or greater, and that the observed displacements were largely the result of additional cyclic lurching forces during the later stages of the earthquake (after significant liquefaction occurred along at least most or all of the apparent main failure surface).

There are a range of approaches available for calculating and/or estimating these types of displacements induced by cyclic (seismic) lurching. But none of these are of high precision, and it is difficult to make accurate and reliable predictions of cyclic displacements for this type of case wherein (1) liquefaction likely required some time to occur, so that some unknown portion of the seismic motions were expended before significant displacements began to occur, and (2) where overall cyclically-induced displacements are “moderate” (neither “small” nor “large” relative to the scale of the overall slope and the scale of the seismic motions applied.

Various types of simplified Newmark-type analyses are available (e.g. Seed and Martin, 1966; Makdisi and Seed, 1978; Hynes-Griffin and Franklin, 1984; etc.). Some of these can be enhanced by performing seismic response analyses of the overall Embankment, and then extracting from these the Mean Horizontal Equivalent Acceleration (MHEA) time history over the region of the eventual failure mass. This MHEA time history, coupled with pseudo-static stability analyses, can be used to directly integrate the exceedances of average driving shear stresses to develop estimates of overall resulting displacements (e.g. Jibson et al., 1998, Bray and Rathje, 1998; Bray and Travasarou, 2007; etc.).

All of these analytical approaches are sensitive to details of either (a) simplified estimation of MHEA, or (b) site response analyses for evaluation of MHEA time histories. As a result, estimates of displacements for a given set of strengths is relatively imprecise. As demonstrated by Olson and Johnson (2008), when these types of procedures are inverted, and used instead to estimate S_r, the results are highly imprecise as well.

These types of analytical methods are also sensitive to details of the input ground motion parameters (for the most simplified methods), or to actual input ground motion histories (for the more detailed analyses involving full site response analyses). Because the two seismometers at the Lower San Fernando Dam were very old instruments and did not produce good and reliable records of strong shaking, this adds significant further uncertainty.

And finally, a significant additional amount of uncertainty was associated with lack of knowledge as to how much of the input earthquake excitation for this relatively short Mw = 6.6 event was expended in "triggering" liquefaction before significant displacements began to occur. It would be only the remaining incoming strong pulses after significant triggering of liquefaction that would "drive" cyclic displacements for this marginal (moderate displacement) case.

A number of approaches were attempted, and a number of parametrizations of likely input motions, and it was found that for reasonable ranges of modeling details, and for reasonable approaches, a very wide range of uncertainty resulted.

It was also observed, however, that the embankment was certainly stable at the end of the earthquake. This meant that the problem was "bounded"; the static Factor of Safety for the post-earthquake geometry was certainly greater than or equal to 1.0.

It was then possible to make reasonably bounded estimates of S_r, noting that the displacements that accrued were "moderate" and that the levels of shaking and duration of shaking were likely sufficient to trigger liquefaction over much of the hydraulic fill on the downstream side, especially as cyclically-induced downstream shear displacements began to occur, but not with a great deal of energy to spare.

In order that any errors in estimation of S_r would be conservative, it was decided to deliberately target a slightly conservatively range of estimates of S_r here. In Section B.9.5, the best-estimate value of $S_{r,resid/geom}$ was $S_{r,resid/geom} = 711$ lbs/ft^2, with a range of $S_{r,resid/geom} = 577$ to 848 lbs/ft^2. It was decided by consensus that the best estimate of S_r would then be conservatively taken as 0.90 to 1.10 times $S_{r,resid/geom}$. This produced a resulting best estimate of $S_r \approx 711$ lbs/ft^2, with a range of $S_r \approx 519$ to 933 lbs/ft^2. These estimates of variance are non-symmetric about the best estimated mean value, and the range was conservatively judged to represent approximately +/- 1.5 standard deviations, so further adjustments were then necessary.

Overall, based on an assumed normal distribution, it was judged that the (mean and median) best estimate of post-liquefaction strength for this case history is

$$\overline{S_r} = 726 \text{ lbs/ft}^2$$

and that the best estimate of standard deviation of mean overall post-liquefaction strength is

$$\sigma_{\bar{S}} = 138 \text{ lbs/ft}^2$$

Only one previous investigation team had developed an independent estimate of S_r for this case history, and that was Seed and Harder (1990) who estimated $S_r \approx 500$ to 700 lbs/ft^2. This was a bit lower than these current studies, but Seed and Harder had also deliberately cast this value in a conservative range given the uncertainties involved.

B.9.7 Evaluation of Initial Effective Vertical Stress

Average initial (pre-failure) effective vertical stress was assessed for the liquefied portion of the failure surface in Figure B.9.4. Parameters and sensitivity analyses were as described previously in Section B.9.4. Additional analyses were then performed for alternate potential failure surfaces, including failure surfaces representing the end result of retrogressive incremental failures extending back to the apparent back heel of the final failure. Depths of failure surfaces were varied, and both rotational and translational (wedge-like) failure surfaces were considered. This produced a moderately large, but finite, range of estimated values of average pre-failure effective stress within the liquefied materials controlling the failure.

The resulting best estimate of average pre-failure effective stress within the liquefied materials controlling the failure was then $\sigma_{vo}' \approx 3{,}129$ lbs/ft^2, with a reasonable range of $\sigma_{vo}' \approx 2{,}582$ to 3,694 lbs/ft^2. This range is slightly non-symmetric about the median value, and this range was judged by the engineering team to represent approximately ± 2 standard deviations. Overall, the best characterization of initial (pre-failure) average effective vertical stress was then taken to be represented by a mean value of

$$\overline{\sigma'_{vo}} \approx 3{,}138 \text{ lbs/ft}^2$$

and with a standard deviation of

$$\sigma_{\bar{\sigma}} \approx 278 \text{ lbs/ft}^2$$

Olson (2001) and Olson and Stark (2002), in addition to Wang (2003) and Kramer (2008), did not consider this case history, therefore no comparison can be made to those studies. An estimate of vertical effective stress for the case was reported by Stark and Mesri (1992). They reported value of $\sigma_{vo}' \approx 2{,}975$ lbs/ft^2, in very good agreement with these current studies.

B.9.8 Evaluation of $N_{1,60,CS}$

As described in Section A.4.7, following the 1971 San Fernando Earthquake, and extensive investigation was performed on both the Lower and Upper San Fernando Dams. Figures B.9.1 and B.9.2 show a summary of boring locations and results of Standard Penetration Tests for the

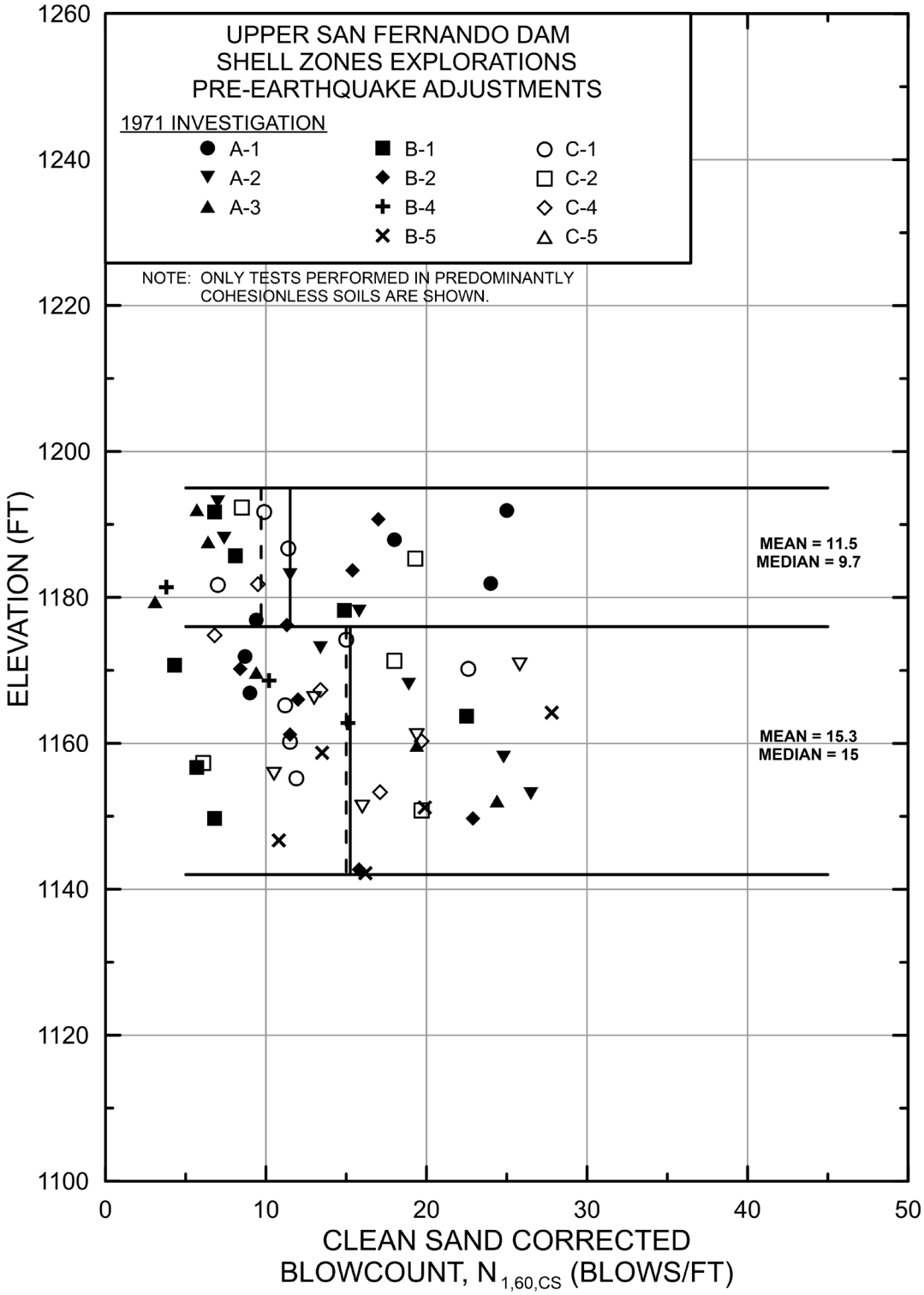

Figure B.9.6: Summary of available SPT data borings that penetrated through the downstream hydraulic fill zones showing corrected $N_{1,60,CS}$ values as adjusted to represent best-estimate values for the upstream side hydraulic fill pre-earthquake conditions.

1971 investigation. The blowcounts were corrected following the same procedures for of the 1971 borings, as were described previously in Section A.4.7 for the Lower San Fernando Dam. Figure B.9.6 shows a summary of the clean sand corrected 1971 SPTs performed in the silty sand and sandy silt hydraulic fill materials. The results were separated into elevation ranges of similar penetration resistances. From Elev. 1195 ft to Elev. 1176 ft the mean and median $N_{1,60,CS}$ values were calculated to be 11.5 and 9.7 blows/ft, respectively. From Elev. 1176 ft to Elev. 1142 ft the mean and median $N_{1,60,CS}$ values were calculated to be 15.3 and 15.0 blows/ft, respectively. While, the upper hydraulic fill material appears to have had a lower clean sand corrected representative blowcount than the lower material, the lower hydraulic fill material was judged to be the material of interest due to the deeper failure surface inferred form the observed displacements. Overall, the characterization of penetration resistance for these current studies was then taken as $\overline{N}_{1,60,CS} \approx$ 15 blows/ft, with a standard deviation of $\sigma_{\overline{N}} \approx 1.8$ blows/ft.

Seed and Harder (1990) were the other investigation team to develop an estimate of representative $N_{1,60,CS}$ for this case. Their fines adjustments differed, and so did some of the other details of the processing and corrections of SPT N-values to develop values of $N_{1,60,CS}$. It appears that these factors largely balanced out, as their final representative value was also $N_{1,60,CS} \approx 15$ blows/ft.

B.10 Tar Island Dyke (Alberta, Canada; 1974)

B.10.1 Brief Summary of Case History Characteristics

Name of Structure	Tar Island Dyke
Location of Structure	Alberta, Canada
Type of Structure	Tailings Dyke
Date of Failure	August 23, 1974
Nature of Failure	Static liquefaction flow failure
Approx. Maximum Slope Height	46.2 ft.

B.10.2 Introduction and Description of Failure

The Tar Island Dyke is located in northern Alberta, Canada. The dyke serves to confine a tailings pond into which waste tailings consisting primarily of fine sands are place after bitumen has been removed from the locally mined tar sands deposits.

Four static liquefaction failures occurred between 1972 and 1974. All four failures occurred at the upstream side of the dyke, and there was no threat of potential tailings release. One of these four failures occurred on August 23, 1974, and it is this failure that had sufficient information available for back-analysis. Descriptions of the failure, and information on geometry, properties, and construction are provided by Mittal and Hardy (1977), Plewes et al. (1989) and Konrad and Watts (1995).

The dyke was constructed by modified upstream construction, with successive raises of the dyke embankment being placed partially atop recently deposited pond tailings, as shown in Figure B.10.1. The failure of August 23, 1974 produced only modest displacements, and resulted in a settlement of approximately 16 ft. of the upstream edge of the crest section of the recently raised dyke embankment. This settlement was nearly level, with just a slight slant downwards towards the upstream edge, and there was little or no lateral separation from the rest of the embankment section. There were a series of vertical cracks through the step over mat parallel to the crest of the dyke, but these did not open significantly. Figure B.10.1 shows an apparent rise in the elevation of the tailings at the left edge of the figure. This does not appear to be the result of "toe bulging" as the mass balance does not work out; the small settlement at the back heel cannot explain the apparent raise at this location.

The embankment section placed atop the recent tailings was called the step over mat. At the time of the failure, the step over mat was approximately 42 feet in height, and the width of the cell of the mat being placed was approximately 120 feet. Mittal and Hardy (1977) attributed the failure to three factors: (1) the adjacent tailings beach upon which the step over section was being placed had been raised by discharging tailings sand into approximately 20 feet of water, resulting in tailings placed below water with very low relative densities, (2) the average rate of raising the dyke during the three month period preceding the failure had been approximately three times faster than had previously been achieved at this site, and (3) the total height (42 feet) of the step-over mat was significantly more than had previously been achieved in a similar period.

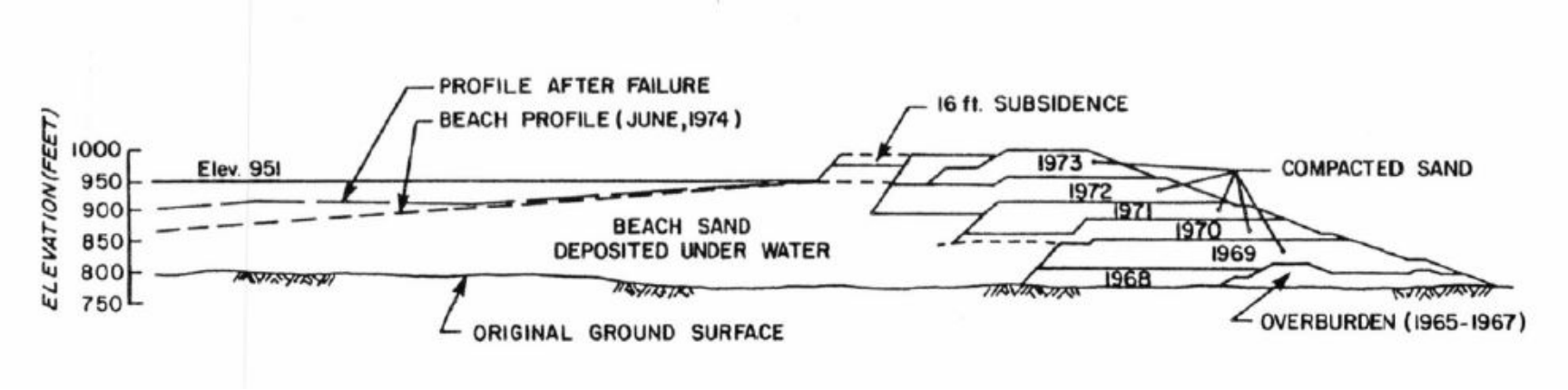

Figure B.10.1: Cross-section of Tar island Dyke showing the subsidence (failure) of August 23, 1974 (from Plewes et al., 1989)

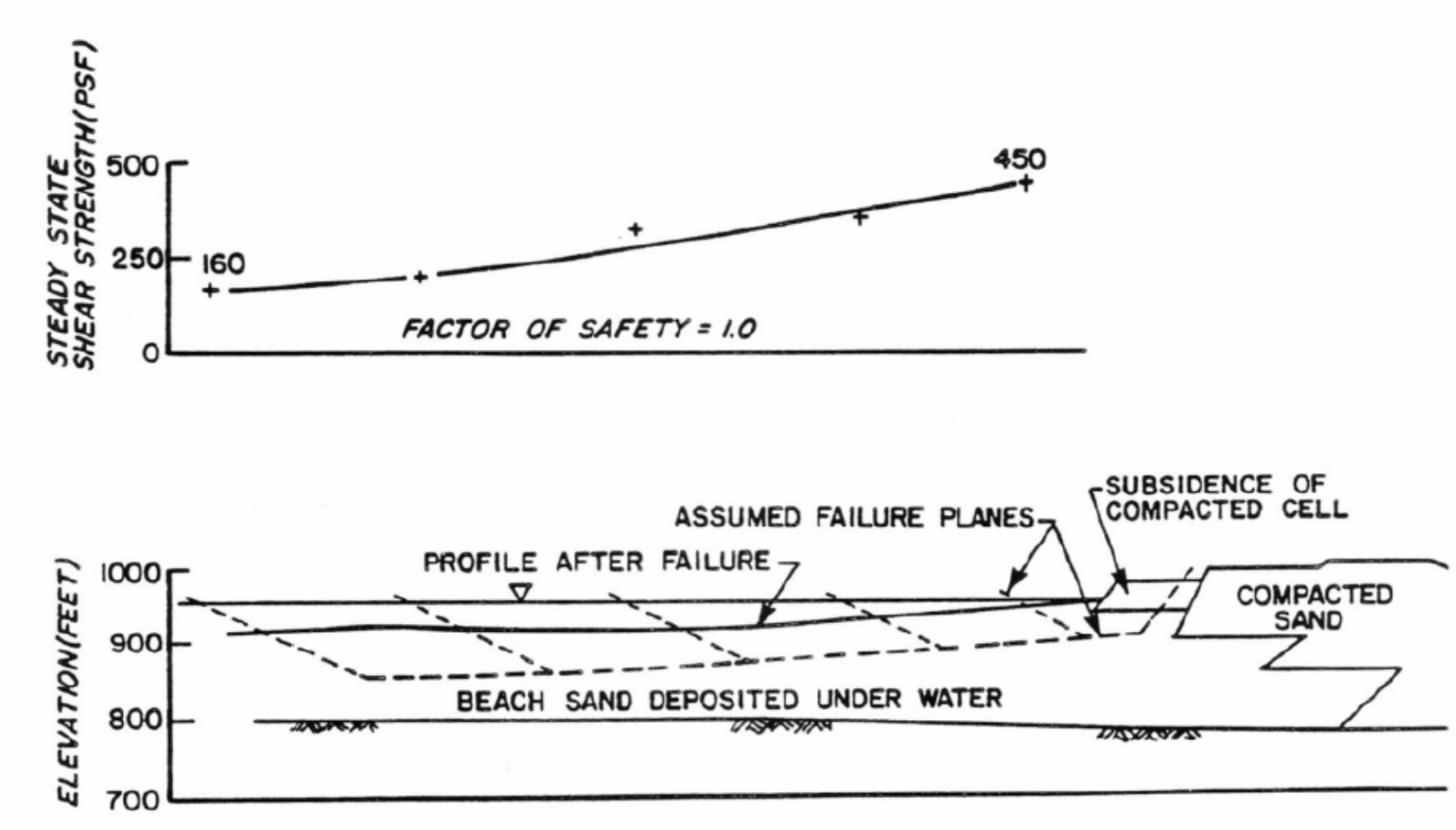

Figure B.10.2: Figure 8 from Plewes et al. (1989) showing potential failure surfaces considered and analyzed in their studies.

B.10.3 Geology and Site Conditions

The Tar Island Dyke was constructed by a "modified" upstream method. The initial starter dyke was placed and compacted as a normal embankment, using excavated "overburden" soils rather than tailings.

Subsequent raises of the dyke were then accomplished by placing sluiced tailings in cells, and compacting them with bulldozers. New tailings were then emplaced behind each successive embankment raise. The next embankment raise was then placed partially atop the underlying compacted embankment section, and partially atop the recently placed tailings. The materials used for these subsequent embankment raises were relatively clean sandy tailings, and these were sluiced into place in large cells and then compacted. It was recognized that this posed some risk of upstream side liquefaction failures, but it was concluded that the downstream side would be suitably stable as to prevent risk of tailings release so long as the overlap of compacted new embankment with the previous compacted embankment section was adequate. Early studies showed that this sluicing and compaction of the embankment fills achieved relative densities of approximately 70 to 75% in the compacted embankment materials (Mittal and Hardy, 1977).

Tailings were placed into the pond by overboarding from the upstream edge of the current embankment. Overboarded tailings deposited above the pond surface (beach deposits) achieved relative densities of on the order of approximately 40%, and overboarded tailings deposited below pond level (underwater deposits) achieved even lower relative densities on the order of approximately 30% (Mittal and Hardy, 1977). The tailings materials were fine, subangular quartz sands with fines contents typically on the order of about 10 to 15%, but this varied somewhat depending on material selection, transport and placement procedures (Mittal and Hardy, 1977; Plewes et al., 1989). These loose, fine tailings were potentially subject to liquefaction.

B.10.4 Initial Yield Stress Analyses

This has been a difficult case history for back-analyses, and it has not been tackled by many investigation teams. There have been a number of different positions taken with regard to likely failure mechanisms and details, and the field evidence is arguably inconclusive.

Mittal and Hardy (1977) stated "It appeared that a layer of beach sand about 15 feet (4.5m) thick below the mat liquefied and flowed out into the pond." That appears unlikely, as it would probably have produced a large lateral translation of the overlying step over mat.

Plewes et al. (1989) considered a number of potential failure surfaces passing through the beach sands (tailings) beneath and outboard of the step over mat, as shown in Figure B.10.2. They calculated values of $S_{r,yield}$ of between 8 kPa (160 lbs/ft^2) to 23 kPa (450 lbs/ft^2) for these trial surfaces. They also felt that because the overall displacements had been relatively small, these values of $S_{r,yield}$ would also represent reasonable estimates of S_r for this case.

Olson (2001) assumed that liquefaction was more likely in the most recently deposited layer of tailings (which were below water deposited beach sands), and that the previous layer of

tailings sands would have consolidated and aged a bit and so would be less susceptible. The upper (potential liquefaction) zone tailings had been placed recently (between April 1 to May 14, 1974). The resulting zone of tailings that they hypothesized to have potentially liquefied is shown by the shaded zone in Figure B.10.3. Olson did not show the actual full failure surfaces that he then analyzed. His verbal description is "Several failure surfaces passing through approximately the center of the zone of liquefaction were analyzed, as shown in Figure A.82 [Figure B.10.3], and values of yield shear strength were varied until a factor of safety was achieved." It is assumed that he meant until a factor of safety of 1.0 was achieved. The resulting best estimate value was $S_{r,yield}$ = 35.9 kPa (750 lbs/ft^2), with a range of $S_{r,yield}$ = 32.3 kPa (675 lbs/ft^2) to 38.6 kPa (806 lbs/ft^2). Lack of detail regarding the actual full failure surfaces analyzed makes this somewhat difficult to interpret.

Figure B.10.4(a) shows the cross-section used for back-analyses of the post-liquefaction initial yield strength $S_{r,yield}$ that would be required within the tailings materials of the typical section of the Tar Island Dyke tailings to produce a calculated Factor of Safety equal to 1.0 for static, pre-failure conditions. This is not the actual post-liquefaction strength, but it proves to be useful in developing estimates of post-liquefaction strength (S_r) for this case history.

In these current studies, a range of potential failure surfaces were considered. One mechanism considered involves smaller rotational or block-like failures that act more like punching/bearing failures of the underlying tailings. The other mechanism considered, is similar to the range of failure surfaces evaluated by Plewes et al. (1989). All of the failure surfaces evaluated were assumed, as Olson assumed, to penetrate into the tailings to a maximum depth approximately equal to the older deposits of tailings. Example failure surfaces for each of these types of mechanism are shown in Figure B.10.4(a)

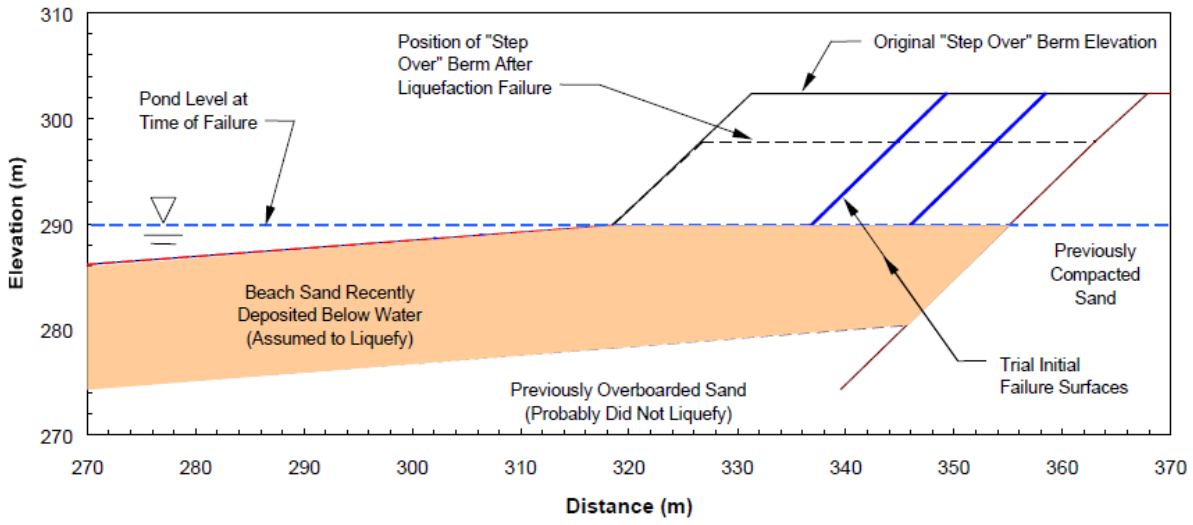

Figure B.10.3: Figure A.82 from Olson (2001) showing the assumed zone of potential liquefaction and the upper portions of example potential failure surfaces analyzed.

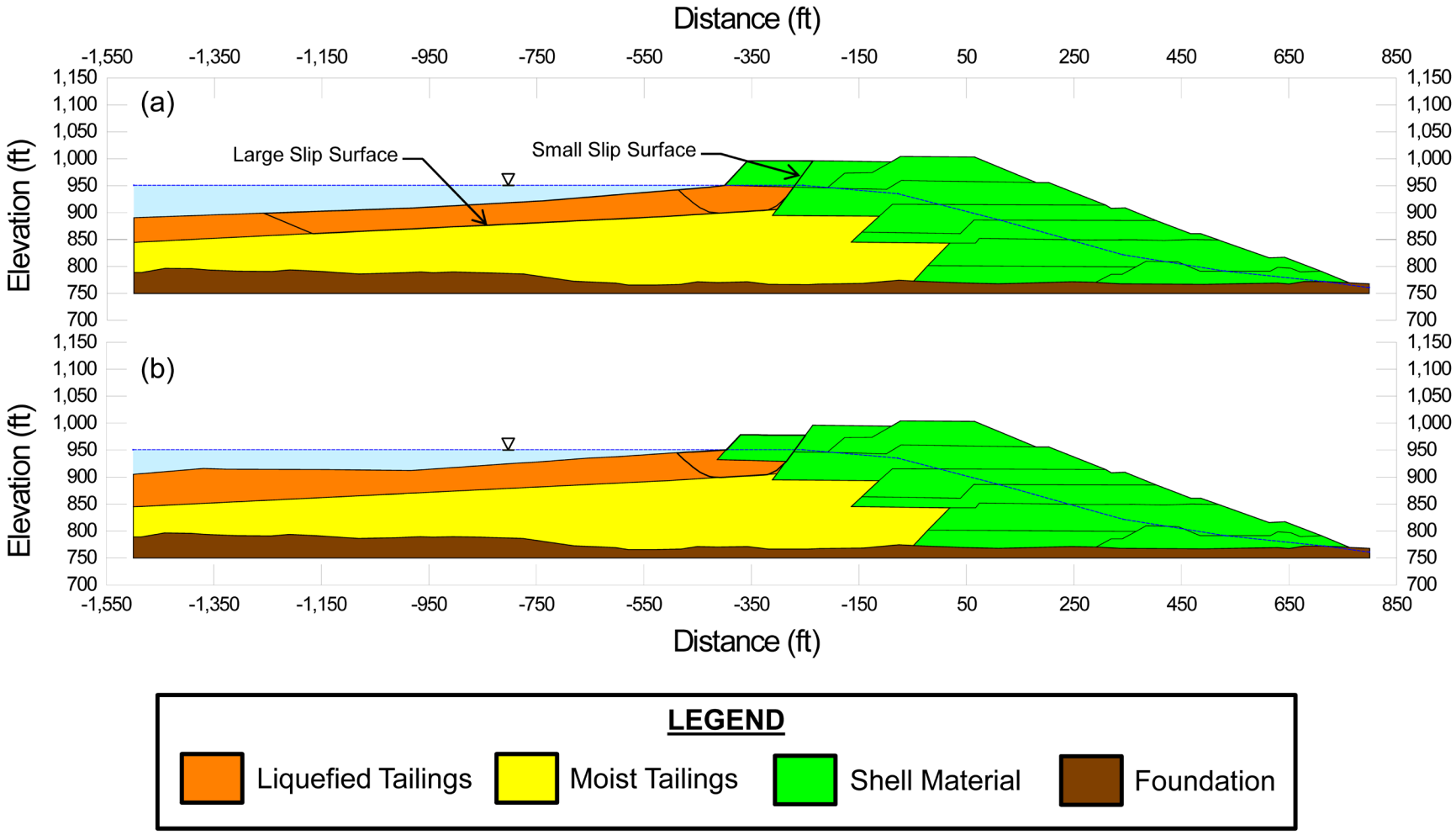

Figure B.10.4: Tar Island Dyke: (a) pre-failure geometry and trail failure surfaces for initial yield stress analyses, and (b) post-failure geometry and failure surface for post-failure residual geometry analyses.

Unit weights of the non-saturated compacted sand dyke fill above the phreatic surface were modeled with a unit weight of $\gamma_m \approx 120$ lbs/ft^3, and this was then varied over a range of $\gamma_m \approx 115$ to 125 lbs/ft^3 for parameter sensitivity studies. Unit weights of the saturated compacted sand dyke fill below the phreatic surface were modeled with a unit weight of $\gamma_s \approx 125$ lbs/ft^3, and this was then varied over a range of 120 to 130 lbs/ft^3 for parameter sensitivity studies. Unit weights of the saturated tailings below the phreatic surface were modeled with a unit weight of $\gamma_s \approx 115$ lbs/ft^3, and this was then varied over a range of 110 to 120 lbs/ft^3 for parameter sensitivity studies. The friction angle of the compacted sand dyke fill materials above the phreatic surface was modeled with $Ø' \approx 32°$, and a range of $Ø' \approx 29°$ to 35°.

Potential initial failure surfaces were modeled as either (1) wedge-like semi-translational features, or (2) semi-rotational/translational features, or (3) the potential monolithically initiated largely translational scenario with a failure mass extending far downslope.

A significant number of smaller punching failure surfaces were analyzed, corresponding to a scenario in which the dyke block punches nearly vertically into the recently placed tailings materials. Figure B.10.4(a) shows an initial failure surface that was the most critical potential initiating failure surface found (lowest post-liquefaction, pre-displacement Factor of Safety) but additional potential failure surfaces were also analyzed, including failure surfaces with more translational features. The resulting best estimate value of $S_{r,yield}$ for the smaller initial yield surface was found to be $S_{r,yield} = 911$ lbs/ft^2, with a likely range of $S_{r,yield} \approx 757$ to 1,067 lbs/ft^2.

For the case of the larger, more translational scenario similar to some of the larger Plewes et al. (1989) surfaces the best estimate value of $S_{r,yield}$ was found to be $S_{r,yield} = 336$ lbs/ft^2, with a range of $S_{r,yield} \approx 272$ to 403 lbs/ft^2.

Based on these analyses, it was judged that the punching mechanism corresponding to the smaller failure surfaces was a more likely failure mechanism. As such, the results from that analysis were weighted more heavily than the results from the larger, more translational, failure surfaces. The weighting factors utilized, expressed in terms of smaller surface to larger surface, were developed by consensus among the current analysis team and the weighting ratio was 7 to 3. Based on that weighting scheme, the range of variations in properties and parameters, and a range of potential failure mechanisms and feasible failure surfaces, the resulting best estimate of "representative" overall $S_{r,yield}$ was found to be $S_{r,yield} = 739$ lbs/ft^2, with a range of $S_{r,yield} \approx 612$ to 868 lbs/ft^2.

These resulting best estimate values and range of $S_{r,yield}$ are in reasonably good agreement with those values developed by Olson (2001), as presented earlier in this section.

B.10.5 Residual Strength Analyses Based on Residual Geometry

Back-analyses were also performed to evaluate the "apparent" post-liquefaction strength ($S_{r,resid/geom}$) required to produce a calculated static Factor of Safety equal to 1.0 based on residual geometry. This is not a direct measure of post-liquefaction strength (S_r), as it neglects momentum effects and would underestimate S_r, but it is useful for overall evaluation of S_r for this case history.

Figure B.10.4(b) shows the post-failure cross-section geometry and an example assumed slip surface utilized in the residual geometry analyses. The slip surface shown is the most critical one (highest resulting value of $S_{r,resid/geom}$). Based on the post-failure cross-section, with additional potential failure surfaces examined in addition to the potential failure surface shown in Figure B.10.4(b), and the properties and parameters described above, a number of alternate potential failure surfaces were analyzed. Material parameters were also varied. Based on these analyses, it was judged that a best estimate value was $S_{r,resid/geom}$ = 452 lbs/ft^2, and a reasonable range was $S_{r,resid/geom} \approx$ 354 to 553 lbs/ft^2.

Olson (2001) performed a simplified infinite slope analysis to evaluate $S_{r,resid/geom}$. He analyzed a tailings slope with top and base slopes of approximately 4°, and an average thickness of approximately 9.1 m. The resulting best estimate value was then $S_{r,resid/geom}$ = 12 kPa (250 lbs/ft^2). Olson adopted the estimated range of Plewes et al. (1989) of $S_{r,resid/geom}$ = 7.7 to 21.6 kPa (160 to 450 lbs/ft^2) as his likely range.

B.10.6 Overall Estimates of S_r

Overall estimates of S_r for this Class B case history were made based on the pre-failure geometry, the partial post-failure geometry, the approximate runout features and characteristics, and the values of $S_{r,yield}$ and $S_{r,resid/geom}$ as calculated and/or estimated in the preceding sections.

Runout distance of the center of mass of the overall failure was approximately D = 18.2 feet, and the initial failure slope height was H = 46.2 feet. This produces a runout ratio (defined as runout distance traveled by the center of gravity of the overall failure mass divided by the initial slope height from toe to back heel of the failure) of D/H = 0.39. This allows Equation 4-4, and Figures 4.7 and 4.11, to serve as one basis for estimation of post-liquefaction strength S_r. Using the ranges of $S_{r,yield}$ and $S_{r,resid/geom}$ from Sections B.15.4 and B.15.5, and assuming that $\xi \approx 0.70$ to 0.95 for this runout ratio, with 0.825 as the best estimate, provided a best estimate value of $S_r \approx$ 492 lbs/ft^2 and an estimated range of $S_r \approx$ 338 to 675 lbs/ft^2. A second basis for estimation of S_r was the use of the relationship of Figure 4.9, and the range of values of $S_{r,yield}$ from Section B.10.4. Based on the runout ratio, values of initial (pre-failure displacement) Factor of Safety were taken as approximately 0.60 to 0.80, and this produced a best estimate value of $S_r \approx$ 517 lbs/ft^2 and an estimated range of $S_r \approx$ 367 to 694 lbs/ft^2. No similar use was made of Figure 4.9 in conjunction with the ranges of $S_{r,resid/geom}$ estimated in Section B.10.5.

The estimates by each of the two methods above were then averaged together, and this produced a best estimate value of $S_r \approx$ 505 lbs/ft^2 and an estimated range of $S_r \approx$ 338 to 694 lbs/ft^2. These estimates of variance are non-symmetric about the best estimated mean value, and the range was judged to represent approximately +/- 1.5 standard deviations, so further adjustments were then necessary.

Overall, taking into consideration the slightly asymmetric range of these results for S_r, it was judged that the (median) best estimate of post-liquefaction strength for this case history is

$$\overline{S_r} = 516 \text{ lbs/ft}^2$$

and that the best estimate of standard deviation of mean overall post-liquefaction strength is

$$\sigma_{\bar{S}} = 119 \text{ lbs/ft}^2$$

Olson (2001) and Olson and Stark (2002) did not apply their "kinetics" method to this case, and so they did not independently develop an estimate of S_r that incorporated momentum effects. Instead, they took their value of $S_{r,resid/geom}$ as representing S_r. Their best estimate value was therefore $S_r = S_{r,resid/geom} = 12$ kPa (250 lbs/ft^2), with a range of $S_r = S_{r,resid/geom} = 7.7$ to 21.6 kPa (160 to 450 lbs/ft^2), as described previously in Section B.8.5.

A better estimate can be obtained by taking their back-calculated best estimate values of $S_{r,yield}$ and $S_{r,resid/geom}$ are using the simplified Equation 4.1 with a fixed value of $\xi = 0.8$, in which case the resulting estimate would be

$$S_r \approx \xi \bullet (S_{r,yield} + S_{r,resid/geom}) / 2 \approx (0.8) \bullet (750 \text{ lbs/ft}^2 + 250 \text{ lbs/ft}^2) / 2 \approx 400 \text{ lbs/ft}^2$$

This is about 20% lower than the values developed in these current studies.

Wang (2003) and Wang and Kramer (2008) did not employ their zero inertial force (ZIF) method to incorporate inertial effects in back-analyses of this failure. Instead they selected their value of S_r based on examination of values from back-analyses by several previous investigators. Wang (2003) selected three values for this case history as:

$S_r = 305$ lbs/ft^2 (Plewes et al. (1989)

$S_r = 80$ lbs/ft^2 (Konrad and Watts, 1995)

$S_r = 400$ lbs/ft^2 (Olson, 2001)

where Wang's value for "Olson, 2001" was taken as $S_r \approx (S_{r,yield} + S_{r,resid/geom}) / 2$, representing an implied value of $\xi = 1.0$, which would clearly over-estimate S_r for this case. Averaging these three values from previous investigations together produced a value of $S_r \approx 346$ lbs/ft^2. The value of $S_r = 80$ lbs/ft^2 proposed by Konrad and Watts appears to be unreasonably low relative to the other two sets of values, and these current studies, so this overall average of Wang (2003) is likely somewhat low as well.

B.10.7 Evaluation of Initial Effective Vertical Stress

Average initial (pre-failure) effective vertical stress was assessed for the liquefied portions of the failure surfaces for both the smaller and larger rotational and wedge-like failures similar to both failure surfaces shown in Figure B.10.4(a). Failure surfaces, parameters and sensitivity analyses were as described previously in Section B.10.4. Depths of failure surfaces were varied slightly, and both rotational and translational (wedge-like) failure surfaces were considered. The same weighting factors utilized in the strength determination for each surface were also implemented for the evaluation of initial effective vertical stress.

The resulting best estimate of average pre-failure effective stress within the liquefied materials controlling the failure was then $\sigma_{vo}' \approx 4{,}180$ lbs/ft^2, with a reasonable range of

$\sigma_{vo}' \approx 3{,}299$ to $5{,}164$ lbs/ft^2. This range is slightly non-symmetric about the median value, and this range was judged by the engineering team to represent approximately ± 2 standard deviations. Overall, the best characterization of initial (pre-failure) average effective vertical stress was then taken to be represented by a mean value of

$$\overline{\sigma'_{vo}} \approx 4{,}197 \text{ lbs/ft}^2$$

and with a standard deviation of

$$\sigma_{\bar{\sigma}} \approx 484 \text{ lbs/ft}^2$$

An estimate of σ_{vo}' was also calculated by Olson and Stark (2001, 2002). They reported a weighted average mean value of $\sigma_{vo}' \approx 205.9$ kPa (4,300 lbs/ft^2), in very good agreement with these current studies. Average initial vertical effective stresses were not directly reported by Wang (2003) and Kramer (2008), but they were published more recently in the publication by Kramer and Wang (2015). As discussed in Section 2.3.8.1(b)-(iii), Wang (2003) did not perform any independent analyses to assess σ_{vo}' for his 22 "secondary" cases, and this is one of those cases. Instead, he compiled values of S_r from multiple previous investigators, and averaged these for a best estimate. He also compiled multiple values of S_r/σ_{vo}' from previous investigators, and averaged these for a best estimate. He then used these two best-estimate values of S_r and S_r/σ_{vo}' to infer a resulting representative value of σ_{vo}'. As described in Section 2.3.8.1(b)-(iii), the resulting averaged values of S_r and S_r/σ_{vo}' were incompatible with each other for a number of Wang's "secondary" case histories, and this process produced unreasonable values for a number of case histories. Wang's value of $\sigma_{vo}' = 6{,}279$ lbs/ft^2 for this case is very high, and it is not considered a useful check here.

B.10.8 Evaluation of $N_{1,60,CS}$

Figure B.10.5 presents CPT and SPT data from the Tar Island site tailings reported by Mittal and Hardy (1977). Konrad and Watts (1995) reported an average $N_{1,60}$ value, conveyed to them through personal communications with H. Plewes, of $N_{1,60} = 7$ blows/ft with an average fines content of approximately 10 to 15%.

Boring 75-ND-4, which was drilled from the beach and appears to have encountered the more recently places tailings sands provides SPT data local to the failure. The precise drilling procedures, equipment and conditions are unknown. Assuming no energy correction (ER = 60%), and applying corrections for effective overburden stress, the approximate representative value of the upper sands of $N_{1,60} \approx 12$ blows/ft. The CPT, 74-DC-4, advanced in the same material, has a representative tip resistance of approximately 2 4 MPa, and this would produce equivalent $N_{1,60,CS}$ values in this same general range.

Incorporating all corrections and considering the sparseness and large degree of uncertainty of the data for this case history, characterization of penetration resistance for these current studies was then taken as $\overline{N_{1,60,CS}} \approx 11$ blows/ft, with a standard deviation of $\sigma_{\bar{N}} \approx 2.3$ blows/ft.

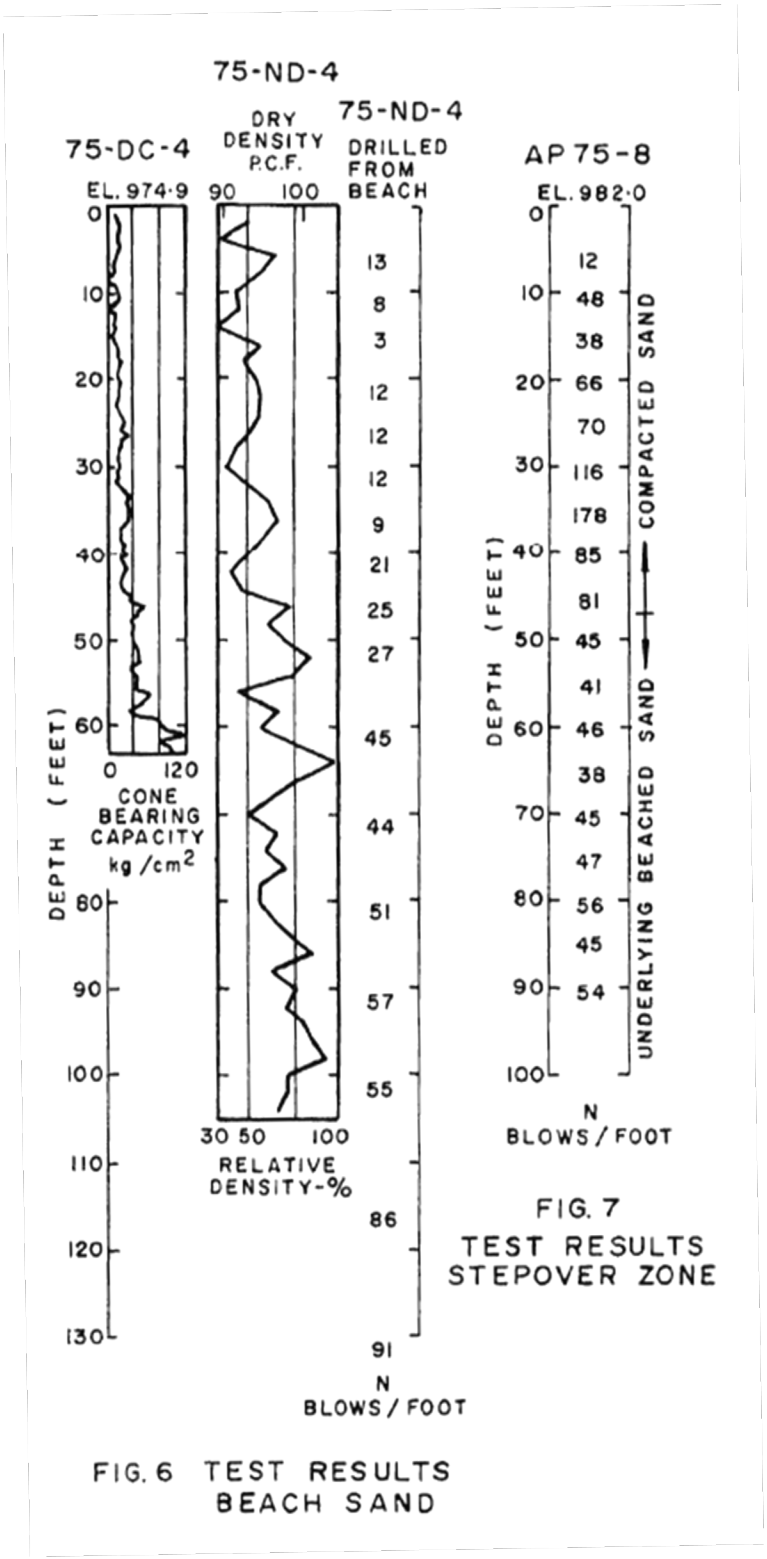

Figure B.10.5: Figures 6 and 7 from Mittal and Hardy (1977) showing the results of field explorations performed at the Tar Island site.

B.11 Mochi-Koshi Tailings Dam (Japan; 1978)

B.11.1 Brief Summary of Case History Characteristics

Name of Structure	Mochi-Koshi Tailings Dam, Dikes 1 and 2
Location of Structure	Izu Peninsula, Japan
Type of Structure	Mine Tailings Dams
Date of Failure	January 14 and 15, 1978
Nature of Failure	Seismic: Dike 1 failed immediately following the 1978 Izu-Ohshima-Kinkai Earthquake (M_L = 7.0), and Dike 2 after large aftershock (M_L = 5.8)
Approx. Maximum Slope Height	Dam 1 = 46.9 ft., Dam 2 = 33.2 ft

B.11.2 Introduction and Description of Failure

A tailings impoundment consisting of three dams on the Izu Peninsula suffered a pair of liquefaction-induced failures during the 1978 Izu-Ohshima-Kinkai Earthquake (M_L = 7.0). Based on surveys of damage, a distribution of shaking density was created and an acceleration of approximately 250 gal. (0.25 g) was estimated at the Mochi-Koshi site (Ishihara, 1984).

The impoundment for gold mine tailings was created with the construction of three dams surrounding a natural bowl-like depression on a mountain top. To construct the impoundment, strongly weathered surface material was first stripped, and an underlying tuff formation was "exposed in a saw-teeth shape" providing a rough contact for the starter dam. Construction of the starter dikes occurred in 1964 by placement of local volcanic soils by means of bulldozers. The tailings, from gold mining operations along the Mochi-Koshi River, were pumped up to the impoundment, raising them 600 m (1,970 ft) through a series of pipes. The tailings material was placed at the site of either Dike 1 or Dike 2 by discharging toward the pond. The dikes were raised at a rate of approximately 2 m (6.6 ft) per year by placing local volcanic soils using the upstream method (Ishihara, 1984).

Dike 1, the largest of the three dikes with a height of 28 m (92 ft) and a width of 73 m (240 ft.), failed immediately following the main earthquake. Ishihara recounted an observer's testimony stating that the dam failed about 10 seconds following the shaking of the main earthquake. The observer recounted seeing the face of the dam swell, and the breach occurred in the upper part of the dam near the left abutment. A huge mass of slime is said to have followed the breach rushing down the valley to the Mochi-Koshi River. In total, approximately 80,000 m^3 (approximately 105,000 yd^3) of tailings were released from the dam. A bed of sediment and tailings, approximately 1.0 to 1.9 m (3.3 to 6.2 ft) thick, remained in the Mochi-Koshi River (Ishihara, 1984).

Dike 2 failed approximately 5 hours and 20 minutes after a M_L = 5.8 aftershock on the day following the main earthquake. That main aftershock occurred at 7:31 am, with an additional

aftershock at 7:36 am. Five to six cracks were observed in the face of Dike 2 parallel to the axis of the dam about an hour after the first large aftershock. The cracks were initially approximately 1 to 3 m (3.3 to 9.8 ft) long and 5 mm (0.2 in) in width. After about an additional hour these cracks had grown to about 5 m (16.4 ft) long and 5 cm (2 in) in width. Another observer onsite observed the central part of Dike 2 gradually sinking at about 1:00 pm that same day, eventually leading to a sudden release of tailings. The initial release of material coincided with a breach of about 20 m (66 ft) of crest width. The breach of the crest was later enlarged to a width of about 65 m (213 ft). In total, approximately 3,000 m^3 (approximately 4,000 yd^3) of material flowed down the valley reaching a maximum distance of 240 m (790 ft); (Ishihara, 1984).

Figure B.11.1 presents a plan view of the Mochi-Koshi tailings impoundment, showing the approximate extent of the two failures. Pre and post-failure cross sections for each dike were also reported, and are presented as Figure B.11.2.

Figures B.11.2(a) and (ba) show pre-failure and post-failure cross-sections through the two dike failures. The post-failure slope of Dike No. 1 was between 4° to 8°, and the failure appears to have passed mainly above the crest of the embankment dam comprised of volcanic soil. The

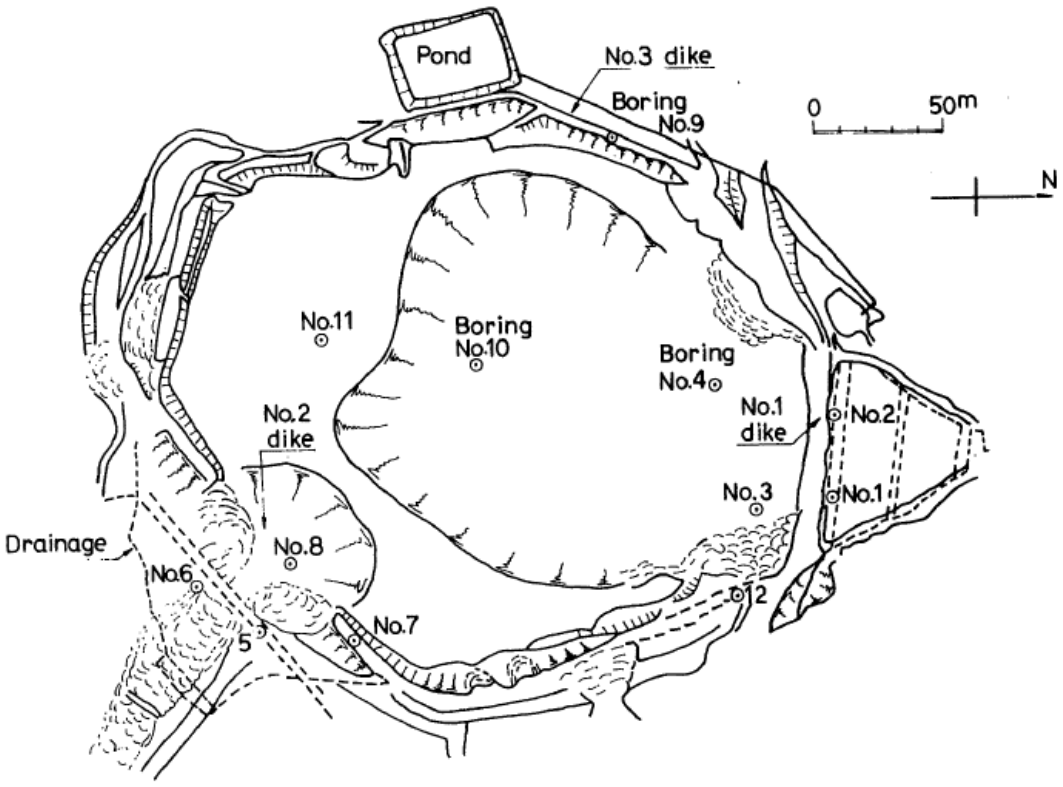

Figure B.11.1: Plan view of the Mochi-Koshi tailings dam showing the approximate extent of the flow failures and the locations of borings performed following the failure (figure from Ishihara, 1984).

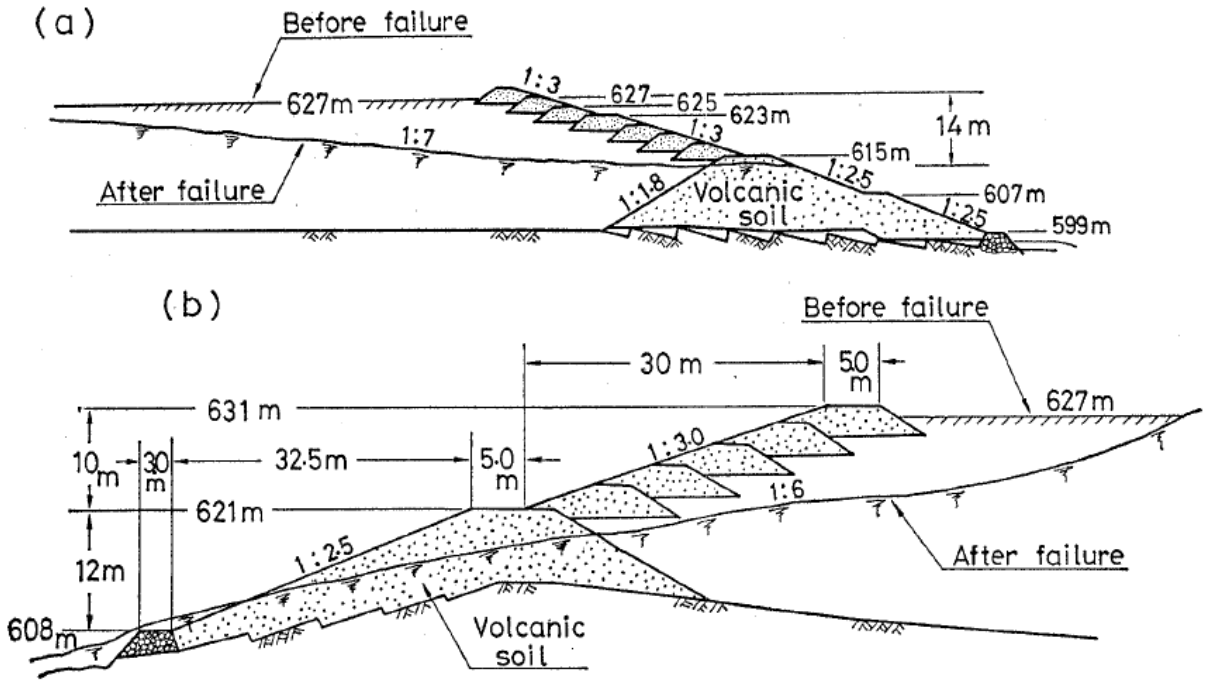

Figure B.11.2: Pre-failure and post-failure cross-sections of (a) Dike 1 and (b) Dike 2 at Mochi-Koshi. (figure from Ishihara et al., 1990)

post-failure slope of tailings at Dike No.2 was a bit steeper, averaging approximately 9° to 10°, and it varied somewhat from the toe to the back heel. The top of the initial retaining dam comprised of volcanic soil was lowered, but this may have been due to erosion by the tailings flowing out through the breach.

B.11.3 Geology and Site Conditions

As described in Section B.11.2, the tailings impoundment was constructed in a bowl-shaped mountain top. The weathered surface material was stripped to the underlying competent tuff formation. The three dams were constructed of local volcanic soils. Placement of the dam materials was first done using bulldozers for the starter dikes, with the subsequent raising of the dikes accomplished using the upstream method of placement (Ishihara, 1984).

Following the failures of the two dams, explorations were performed at the site to assist in the characterization of the material at the site. Based on Figure B.11.1, eleven borings appear to have been performed at the site, however only six boring logs were presented in Ishihara (1984). Those six boring logs will be discussed further in Section B.11.8, and they are reproduced here as Figures B.11.6 through B.11.8. A portable double tube cone penetrometer was also utilized to characterize the site.

These borings, as summarized by Ishihara, indicated that the tailings were comprised of fine silty sands and sandy silts. The silty sands were largely non-plastic, while the siltier materials had reported plasticity indices on the order of PI ≈ 10%. Penetration resistances in the tailings

corresponded to N-values on the order of zero to 7 blows/ft. The uppermost tailings were very loose, having a penetration resistance of nearly zero blows/ft. Ishihara (1984) suggested that some of the very low N-values were the result of liquefaction and disturbance from the earthquake. Penetration resistances were a bit higher in the deeper, consolidated tailings.

The containment dikes, placed using the upstream method, and assumed to have been tracked by bulldozers, had a penetration resistance of about 5 blows/ft. The bulldozer-placed starter dams were found to have a similar penetration resistance as the containment dikes (Ishihara, 1984).

The tailings were comprised of fine layers of sandy stilt and silty sand. The plasticity index, as reported in Ishihara (1984), for the silty sand was found to be approximately 10 and the sandy silt was found to be non-plastic. The sandy silt to silty sand tailings material was estimated by Ishihara et al. (1990) as having approximately 50% average fines content, though this varied considerably in sub-layers as depositional conditions varied.

The locations of the borings are shown in Figures 11.1. The logs of the six borings presented by Ishihara (1984) are reproduced in Figures B.11.6 through B.11.8.

.

B.11.4 Initial Yield Stress Analyses

Figures B.11.3(a) and Figure B.11.4(a) show the cross-sections of Dike 1 and Dike 2, respectively, used for back-analyses of the post-liquefaction initial yield strength $S_{r,yield}$ that would be required within the liquefied upstream shell materials to produce a calculated static Factor of Safety equal to 1.0. This is not the actual post-liquefaction strength, but it proves to be useful in developing estimates of post-liquefaction strength (S_r) for this case history.

Unit weights of the saturated tailings were modeled with a unit weight of $\gamma_s \approx 110$ lbs/ft^3, and this was then varied over a range of 105 to 115 lbs/ft^3 for parameter sensitivity studies. Unit weights of the non-saturated dike material above the phreatic surface were modeled with a unit weight of $\gamma_m \approx 118$ lbs/ft^3, and this was then varied over a range of 113 to 123 lbs/ft^3 for parameter sensitivity studies. Unit weights of the saturated tailings below the phreatic surface were modeled with a unit weight of $\gamma_s \approx 125$ lbs/ft^3, and this was then varied over a range of 120 to 130 lbs/ft^3 for parameter sensitivity studies. The friction angle of the dike material was modeled with $Ø' \approx 35°$, and a range of $Ø' \approx 33°$ to 37°.

The release of tailings from Dike 1 is described by Ishihara (1984) to have occurred very quickly. The failure at Dike 2 is described by Ishihara to have had an initial release with a subsequent breach widening and sloughing some time later. With the very loose nature of the tailings, once the containment dikes failed a retrogressive failure could progress very quickly. It is not known with certainty whether these were incrementally retrogressive failures, or a more monolithic failures in which most or all of the failure masses initiated their movements all at once. Therefore, both mechanisms were considered in the initial yield analyses.

Figure B.11.4(a) shows a select subset of the potential failure surfaces analyzed for back-analyses of $S_{r,yield}$ for Dike 1. Based on all of the analyses performed, the most likely failure

mechanism was judged to be an initial failure surface similar to the smaller circular failure surface shown in Figure B.11.4(a), as the first stage of an incrementally retrogressive overall failure sequence. The calculated best estimate for this surface is $S_{r,yield}$ = 617 lbs/ft^2. Based on parameter variations (parameter sensitivity studies), and moderate variations of failure surface geometries, the likely range is estimated as $S_{r,yield}$ = 489 to 742 lbs/ft^2 for this type of initial failure surface. The other mechanism for Dike 1 considered was a failure surface similar to the final failure surface shown in Figure B.11.4(a). For this monolithically initiated failure, the calculated best estimate for this surface is $S_{r,yield}$ = 158 lbs/ft^2, with a range of $S_{r,yield}$ = 131 to 189 lbs/ft^2 for this type of initial failure surface considering parameter and failure surface sensitivities described above.

Figure B.11.5(a) shows a select subset of the potential failure surfaces analyzed for back-analyses of $S_{r,yield}$ for Dike 2. Based on all of the analyses performed, the most likely failure mechanism was judged to be an initial failure surface similar to the smaller circular failure surface shown in Figure B.11.5(a), as the first stage of an incrementally retrogressive overall failure sequence. The calculated best estimate for this surface is $S_{r,yield}$ = 438 lbs/ft^2, with a range of $S_{r,yield}$ = 353 to 528 lbs/ft^2 for this type of initial failure surface, considering parameter and failure surface

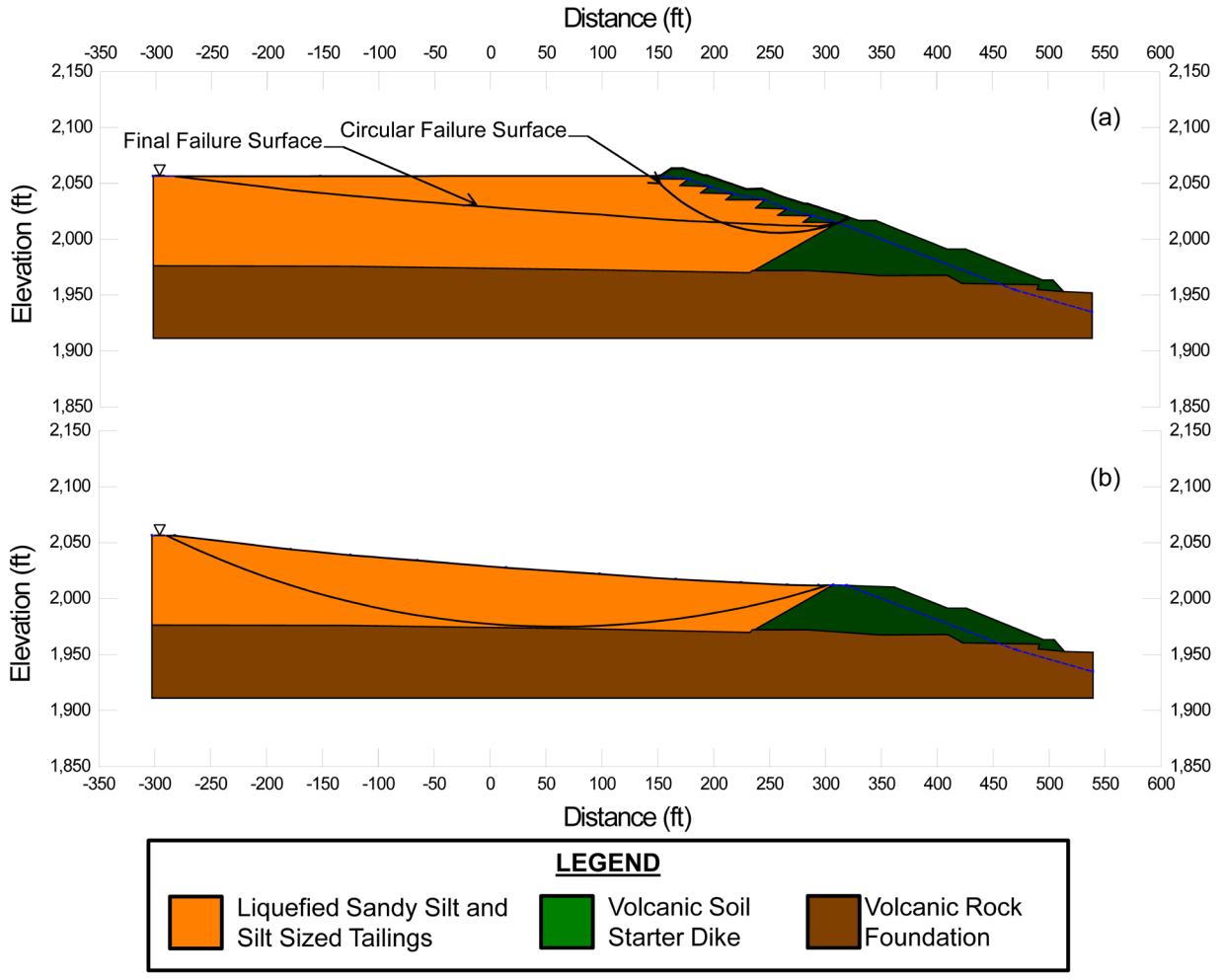

Figure B.11.4: Selected potential failure surfaces analyzed for evaluation of (a) $S_{r,yield}$ and (b) $S_{r,resid/geom}$ for the Mochi-Koshi Tailings Dam 1

variations as described above. The other mechanism for Dike 2 considered was a failure surface similar to the final failure surface shown in Figure B.11.5(a). For this monolithically initiated failure, the calculated best estimate for this surface is $S_{r,yield}$ = 219 lbs/ft^2, with a range of $S_{r,yield}$ = 172 to 269 lbs/ft^2 for this type of initial failure surface considering parameter and failure surface sensitivities described above. .

Overall assessment of $S_{r,yield}$ for this case was based on weighted averages of the two sets of values of $S_{r,yield}$ back-calculated for these two types of potential failure surfaces. The smaller initial failure surfaces near the dam faces were considered the most likely mechanisms for both dams, and were assigned a weighting factor of 4. The failure surfaces representing an overall monolithically initiated failure along the observed post-failure ground surface were assigned a weighting factor of 1. Based on these estimates and associated weighting factors, and the back-calculated values from above, the best estimate for Dike No. 1 was $S_{r,yield}$ = 548 lbs/ft^2, with a range of $S_{r,yield}$ = 443 to 659 lbs/ft^2. Similarly, the best estimate for Dike No. 2 was $S_{r,yield}$ = 394 lbs/ft^2, with a range of $S_{r,yield}$ = 317 to 476 lbs/ft^2.

The best estimates for both Dike 1 and Dike 2 were then averaged to determine an overall best estimate for this case history. The resulting overall best estimate was $S_{r,yield} \approx$ 477 lbs/ft^2, with a range of $S_{r,yield} \approx$ 385 to 574 lbs/ft^2.

Olson (2001) also performed back-analyses to estimate $S_{r,yield}$. He also assumed that the failures were retrogressive. His assumed initial failure surfaces were rotational failures similar to the "circular" failures shown in Figures B.11.4(a) and B.11.5(a). These rotational failure surfaces did extend below the final post-failure surface of the tailings. A range of potential initial rotational failure surfaces were analyzed. Olson's back-calculated best estimate for Dike 1 was $S_{r,yield} \approx$ 21.1 kPa (441 lbs/ft^2), with a range of 18.0 to 23.9 kPa (376 to 499 lbs/ft^2). His back-calculated best estimate for Dike 2 was $S_{r,yield} \approx$ 16.0 kPa (334 lbs/ft^2), with a range of 10.5 to 18.7 kPa (219 to 390 lbs/ft^2). Olson did not combine these; instead he elected to treat these as two separate case histories.

B.11.5 Residual Strength Analyses Based on Residual Geometry

It was not possible to perform rigorous and reliable back-analyses to determine the value of $S_{r,resid/geom}$ required to produce a calculated Factor of Safety equal to 1.0 based on residual geometry. This case is one of six cases (out of the 29 cases back-analyzed as part of these current studies) where the slide mass "went over a lip" and then traveled down a steeper slope, and the ensuing displacements either (1) could not be reliably tracked, or (2) could not be fully reliably back-analyzed. Both situations apply in this current case because the post-failure geometry of the failure mass runout is not well characterized.

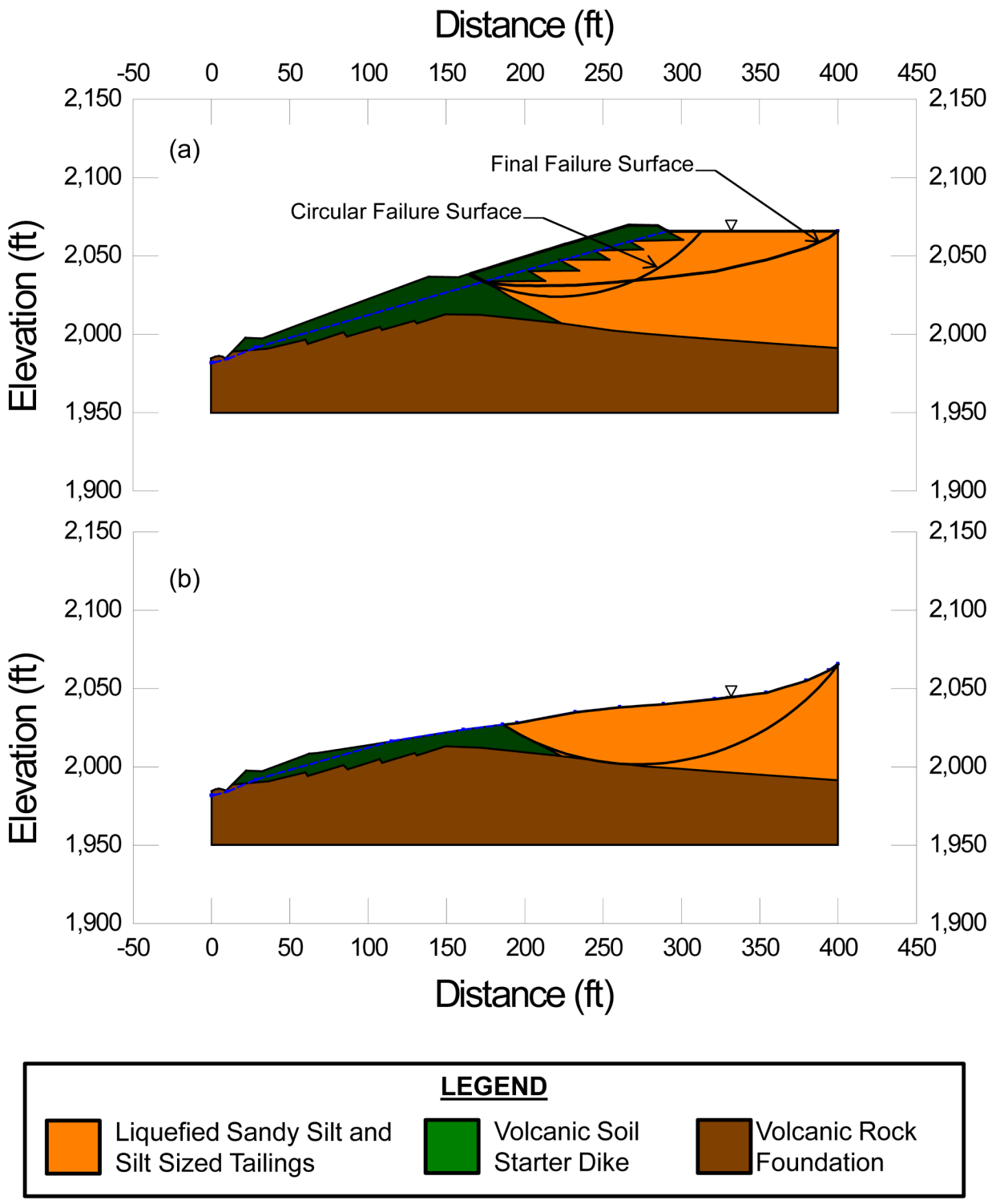

Figure B.11.5: Selected potential failure surfaces analyzed for evaluation of (a) $S_{r,yield}$ and (b) $S_{r,resid/geom}$ for the Mochi-Koshi Tailings Dam 2

Olson (2001) performed infinite slope analyses based on reported thicknesses of residual material that came to rest downslope. For Dike 1, Olson estimated a thickness of about 1.5 m (5 ft) coming to rest at a slope of about 8 deg. Based on those parameters, Olson estimated a value of $S_{r,resid/geom} \approx 3.6$ kPa (75 lbs/ft^2). His estimated range was $S_{r,resid/geom} \approx 2.4$ kPa (50 lbs/ft^2), which was based on a thickness of 1.0 m (3.3 ft.), to $S_{r,resid/geom} \approx 7.2$ kPa (150 lbs/ft^2), based on a thickness of 1.9 m (6.2 ft). For Dike 2, performing a similar set of analyses, Olson estimated a thickness of about 1.8 m (5.9 ft) coming to arrest at a slope of about 10 deg. Based on those parameters, Olson estimated a $S_{r,resid/geom} \approx 5.8$ kPa (121 lbs/ft^2). His estimated range was $S_{r,resid/geom} \approx 4.8$ kPa (100 lbs/ft^2), which was based on a thickness of 1.6 m (5.2 ft), to $S_{r,resid/geom} \approx 6.0$ kPa (125 lbs/ft^2), based on a thickness of 2.0 m (6.6 ft).

Ishihara et al. (1990) performed similar infinite slope analyses, but instead considered a nominal thickness of about 6 m (20 ft) and residual slope of the tailings material remaining in the tailings impoundment. From these analyses, Ishihara et al. estimated a $S_{r,resid/geom} \approx 1.5$ t/m^2 (206 lbs/ft^2) for Dike 1 and $S_{r,resid/geom} \approx 1.75$ t/m^2 (357 lbs/ft^2) for Dike 2.

In these current studies, it was assumed that $S_{r,resid/geom}$ would have at least been higher than zero, and likely higher than the simplified estimate of Olson based on approximate geometry and an infinite slope analysis. Considering how uniform and low the penetration resistance was in the tailings material that remained in the impoundment following the failures, it was judged to be unlikely that the material that remained did not also liquefy. Analyses were also performed of the residual slopes left in place after the failure, as shown in Figure B.11.4(b) and Figure B.11.5(b). If the deeper tailings did liquefy, then for the rotational failure surface for Dike 1 illustrated in Figure B.11.4(b), the back-calculated value would be $S_{r,resid/geom} \approx 270$ lbs/ft^2, with a range of $S_{r,resid/geom} = 209$ to 334 lbs/ft^2., considering similar parameter and failure surface sensitivities as described in Section B.11.4. Performing similar analyses for Dike 2 resulted in a best estimated back-calculated value would be $S_{r,resid/geom} \approx 280$ lbs/ft^2, with a range of $S_{r,resid/geom} = 217$ to 344 lbs/ft^2.

In addition to the previously described analyses, comparisons were also made to similar Class A and B case histories where values of $S_{r,resid/geom}$ back-calculated from the reasonably well-documented. Considering the range of effective overburden stress and $N_{1,60,CS}$ values for this current case, an approximate range of $S_{r,resid/geom} \approx 90$ to 200 lbs/ft^2 was conservatively assumed, based on analyses of other Class A and B case histories.

Overall, considering the estimates (1) made based on infinite slope analyses of assumed downstream (runout) geometry by Olson (2001), (2) similar infinite slope analyses made by Olson using the assumed representative post-failure tailings runout thickness of 6 m as proposed by Ishihara et al. (1990), (3) the rotational failure surface shown in Figure B.8.4(b), (4) approximate infinite slope analyses of the post-failure slope remaining within the tailings impoundment after the event, and (5) values of $S_{r,resid/geom}$ back-calculated for better-defined post failure conditions from the Class A case histories, it was concluded that a best estimate value would be taken as $S_{r,resid/geom} \approx 225$ lbs/ft^2, with a range of $S_{r,resid/geom} \approx 150$ to 300 lbs/ft^2.

B.11.6 Overall Evaluation of S_r

Overall estimates of post-liquefaction strength S_r were made by two approaches. The first approach was to employ Equation 4-4, and Figure 4.11 as

$$S_r \approx \xi \bullet (S_{r,yield} + S_{r,resid/geom}) / 2$$

where ξ is a function of runout distance and overall failure mechanism characteristics.

Unfortunately, runout characteristics cannot be reliably characterized for this case history, because it is one of the six case histories back-analyzed in which the failure mass "went over a lip" and then down a steeper slope rather than coming to rest on a gentler basal slope as with most of the cases plotted in Figure 4.11. It is clear that runout distance is not small, but runout distance (and runout ratio) cannot be fully reliably quantified. The current engineering team therefore developed a consensus estimate that an appropriate range of values of ξ for this case would be on the order of $\xi \approx 0.45$ to 0.60. Using these values, and the values of $S_{r,yield}$ and $S_{r,resid/geom}$ presented previously in Sections B.11.4 and B.11.5, and the associated ranges of both $S_{r,yield}$ and $S_{r,resid/geom}$, this produced a best estimate of $S_r \approx 180$ lbs/ft^2, with a range of $S_r = 117$ to 256 lbs/ft^2.

The second approach was to employ the relationship presented in Figure 4.9, wherein pre-failure Factor of Safety can be approximately evaluated as a function of runout characteristics. Here again the difficulty was that the post-failure runout characteristics were not fully quantifiable because the failure mass went over a lip and then down a steeper slope. The engineering team developed a consensus estimate that the pre-failure range of Factor of Safety for this case would likely have been on the order of FS = 0.35 to 0.55. Multiplying these values by the values of $S_{r,yield}$ from Section B.8.4 produces a best estimate of $S_r \approx 207$ lbs/ft^2, with a range of $S_r = 130$ to 305 lbs/ft^2.

Averaging the two sets of values developed by these two approaches then produced a best estimate of $S_r \approx 194$ lbs/ft^2, with a range of $S_r = 117$ to 305 lbs/ft^2. The variance was slightly non-symmetric about the best estimate, so this was slightly further adjusted to produce a characterization that could be modeled with a Normal distribution. The range was estimated to represent approximately +/- 2.5 standard deviations.

Overall, based on an assumed normal distribution, it was judged that the (mean and median) best estimate of post-liquefaction strength for this case history is

$$\overline{S_r} = 211 \text{ lbs/ft}^2$$

and that the best estimate of standard deviation of mean overall post-liquefaction strength is

$$\sigma_{\overline{S}} = 38 \text{ lbs/ft}^2$$

Olson (2001) and Olson and Stark (2002) did not apply their "kinetics" method to this case, and so they did not independently develop an estimate of S_r that incorporated momentum effects. Instead, they took their value of $S_{r,resid/geom}$ as representing S_r. Their best estimate value for Dike 1 was $S_r = S_{r,resid/geom} = 75$ lbs/ft^2, with a range of 50 to 150 lbs/ft^2, as described previously in

Section B.11.5. For Dike 2 their best estimate was $S_{r,resid/geom}$ = 121 lbs/ft^2, with a range of 100 to 125 lbs/ft^2, also described previously in Section B.11.5. Considering the values estimated by Olson for $S_{r,yield}$ for Dike 1 and Dike 2 ($S_{r,yield}$ = 441 and 334 lbs/ft^2, respectively),and the values of $S_{r,resid/geom}$ for Dike 1 and Dike 2 ($S_{r,resid/geom}$ = 441 and 334 lbs/ft^2, respectively), and using the procedure outlined in Chapter 4, Equation 4-4 of this study would result in more reasonable estimates for residual strength. Using a value of ξ = 0.8, which is roughly an average value for this overall data set, the best estimate value of S_r for Dike 1 would be S_r = 206 lbs/ft^2 and the best estimate value of S_r for Dike 2 would be S_r = 182 lbs/ft^2. The average of these two values would then be $S_r \approx$ 194 lbs/ft^2, in excellent agreement with these current studies.

Wang (2003) and Wang and Kramer (2008) did not employ their zero inertial force (ZIF) method to incorporate inertial effects in back-analyses of this failure. Instead they selected their value of S_r based on examination of values from back-analyses by several previous investigators. The resulting estimates for Dike 1 and Dike 2 were S_r = 159 lbs/ft^2 and S_r = 234 lbs/ft^2, respectively. Averaging these two values produces $S_r \approx$ 197 lbs/ft^2, again in excellent agreement with these current studies. The standard deviations of S_r were also estimated by Kramer and Wang. For Dike 1 the estimated value was σ_s = 47.7 lbs/ft^2, and for Dike 2 σ_s = 78.0 lbs/ft^2.

Despite these differing approaches taken to evaluation and/or selection of S_r, agreement between the values developed in these previous studies, and the values developed and employed in these current studies, is very good for this case history.

B.11.7 Evaluation of Initial Effective Vertical Stress

The representative vertical effective stress for the Mochi-Koshi Tailings Dam dike failures was determined by averaging the calculated vertical effective stress on the failure plane in the liquefied zone from the smaller circular and final failure surfaces shown in Figures B.11.4(a) and B.11.5(a), using the same weighting factors employed for the evaluation of $S_{r,yield}$. Parameter variations (unit weights) were then varied, and so to some extent were variations of the depths of the potential failure surfaces of each type.

The resulting best estimate of average pre-failure effective stress within the liquefied materials controlling the failure of Dike 1 was then $\sigma_{vo}' \approx$ 1,599 lbs/ft^2, with a reasonable range of $\sigma_{vo}' \approx$ 1,249 to 1,961 lbs/ft^2. Similarly, for Dike 2, the best estimate of average pre-failure effective stress was then estimated to be $\sigma_{vo}' \approx$ 1,443 lbs/ft^2, with a reasonable range of $\sigma_{vo}' \approx$ 1,155 to 1,763 lbs/ft^2. Averaging the results from both dams, the overall best estimate was estimated to be $\sigma_{vo}' \approx$ 1,521 lbs/ft^2, with a reasonable range of $\sigma_{vo}' \approx$ 1,202 to 1,862 lbs/ft^2. This non-symmetric range was judged by the engineering team to represent approximately ± 2 standard deviations. Overall, assuming a normal distribution, the best characterization of initial (pre-failure) average effective vertical stress was then taken to be represented by a mean value of

$$\overline{\sigma'_{vo}} \approx 1{,}532 \text{ lbs/ft}^2$$

with a standard deviation of

$$\sigma_{\bar{\sigma}} \approx 165 \text{ lbs/ft}^2$$

An estimate of σ_{vo}' was also calculated by Olson and Stark (2001, 2002). They reported a weighted average mean value of $\sigma_{vo}' \approx 59.9$ kPa (1,251 lbs/ft^2) for Dike 1 and $\sigma_{vo}' \approx 52.2$ kPa (1,090 lbs/ft^2) for Dike 2. These values are slightly lower than the values estimated from these studies, likely due to a slight difference in failure surfaces and assumed unit weights. Average initial vertical effective stresses were not directly reported by Wang (2003) and Kramer (2008), but they were published more recently in the publication by Kramer and Wang (2015). As discussed in Section 2.3.8.1(b)-(iii), Wang (2003) did not perform any independent analyses to assess σ_{vo}' for his 22 "secondary" cases, and this is one of those cases. Instead, he compiled values of S_r from multiple previous investigators, and averaged these for a best estimate. He also compiled multiple values of S_r/σ_{vo}' from previous investigators, and averaged these for a best estimate. He then used these two best-estimate values of S_r and S_r/σ_{vo}' to infer a resulting representative value of σ_{vo}'. As described in Section 2.3.8.1(b)-(iii), the resulting averaged values of S_r and S_r/σ_{vo}' were incompatible with each other for a number of Wang's "secondary" case histories, and this process produced unreasonable, and in some cases physically infeasible, values of σ_{vo}' for a number of case histories. Wang's values of $\sigma_{vo}' = 1{,}746$ lbs/ft^2 (Dike 1) and $\sigma_{vo}' = 2884$ lbs/ft^2 (Dike 2) appear physically unlikely, based on the cross-sections, and so they are not considered a useful check here.

B.11.8 Evaluation of $N_{1,60,CS}$

Following the failure of the two dams, explorations were performed at the site to assist in the characterization of the material at the site. Based on Figure B.11.1, 11 borings appear to have been performed at the site, however only six boring logs were shown in Ishihara (1984). Those six boring logs are reproduced here as Figures B.11.6 though B.11.8. A portable double tube cone penetrometer was also utilized to characterize the site. The results from two tests in the tailings material, as reported by Ishihara et al. (1990), are reproduced here as Figure B.11.9. While these test do show low penetration resistances in the tailings material, since there were a reasonable number of borings with measured blowcounts, they were not heavily relied upon for this study.

The results from the standard penetration tests performed at the site were evaluated. No energy correction (ER = 60%) was applied, and the other necessary corrections for fines and effective overburden stress were applied. After applying corrections, the representative median penetration resistance was determined to be $N_{1,60} \approx 3.7$ blows/ft. Assuming an average fines content of about 50%, a clean sand correction was also applied. In these current studies, the characterization of penetration resistance is represented by a best estimate mean value of $\overline{N_{1,60,CS}} \approx 6$ blows/ft, and an estimated standard deviation of this mean of $\sigma_{\bar{N}} \approx 1.7$ blows/ft.

Olson employed no fines adjustment, and developed a best estimate of $N_{1,60} = 2.7$ blows/ft, with a range of 0.0 to 6 blows/ft.

Wang (2003) and Kramer (2008) jointly developed a representative values of $\overline{N_{1,60,CS}}$ = 8.9 blows/ft for Dam 1 and $\overline{N_{1,60,CS}}$ = 10.0 blows/ft for Dam 2. Their estimated standard deviations of that overall mean values for Dam 1 and Dam 2 were $\sigma_{\overline{N}}$ = 0.6 blows/ft and 1.3 blows/ft., respectively. Full details of the development of this interpretation by Wang and Kramer are not presented. Kramer and Wang (2015) subsequently converted to non-fines-corrected representative values of mean estimates of $N_{1,60}$ = 4 blows/ft and 5.2 blows/ft for Dam No. 1 and Dam No. 2, respectively.

Overall agreement between these three independent assessments of representative $N_{1,60}$ and $N_{1,60,CS}$ values is judged to be good, allowing for the differences between fines-corrected and non-fines corrected penetration resistance measures. The values developed in these current studies are in the mid-range of he values developed by these other investigation teams.

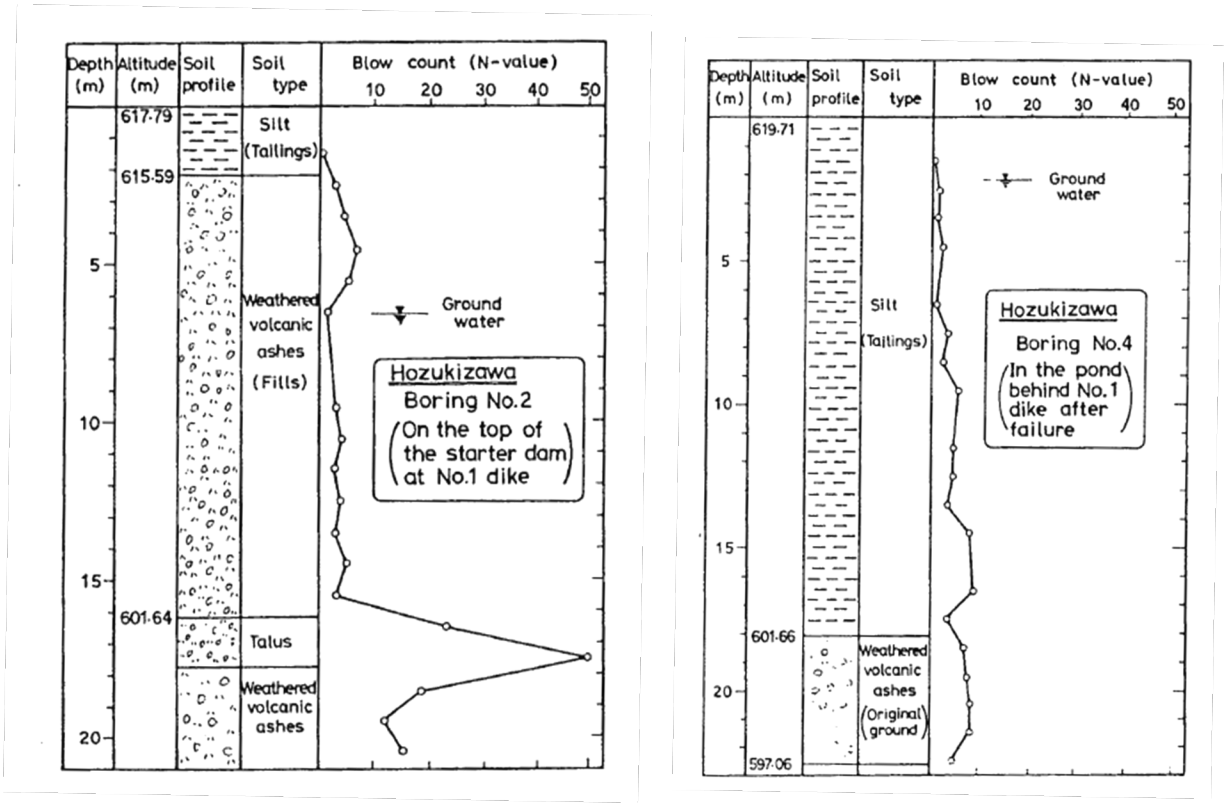

Figure B.11.6: Log of Borings No. 2 and 4 (reproduced from Ishihara, 1984)

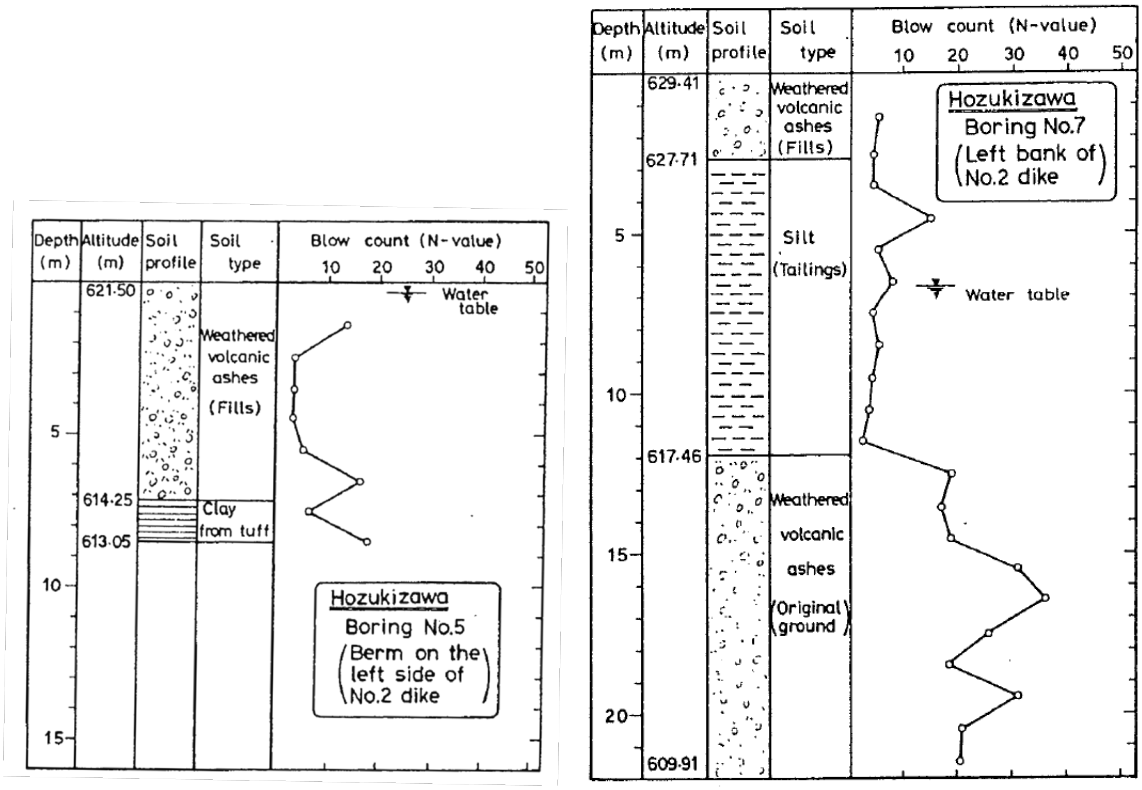

Figure B.11.7: Logs of Borings No. 5 and 7 (reproduced from Ishihara, 1984)

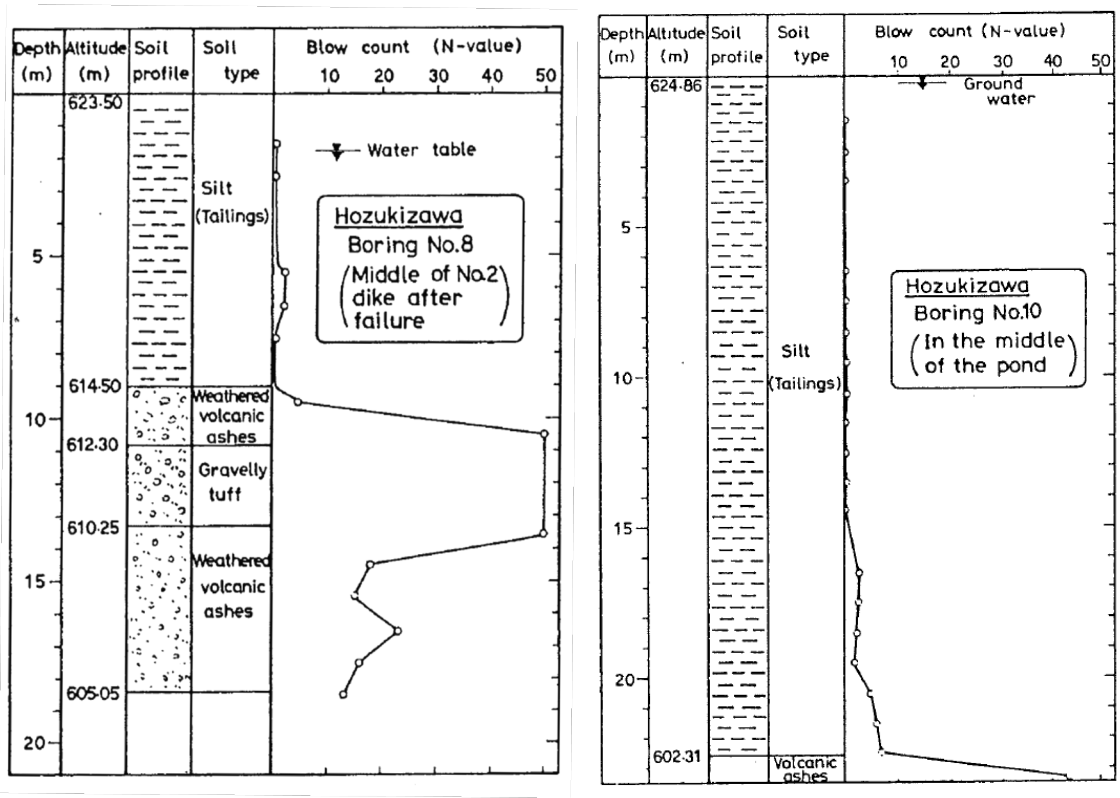

Figure B.11.8: Log of Borings No. 8 and 10 (reproduced from Ishihara, 1984)

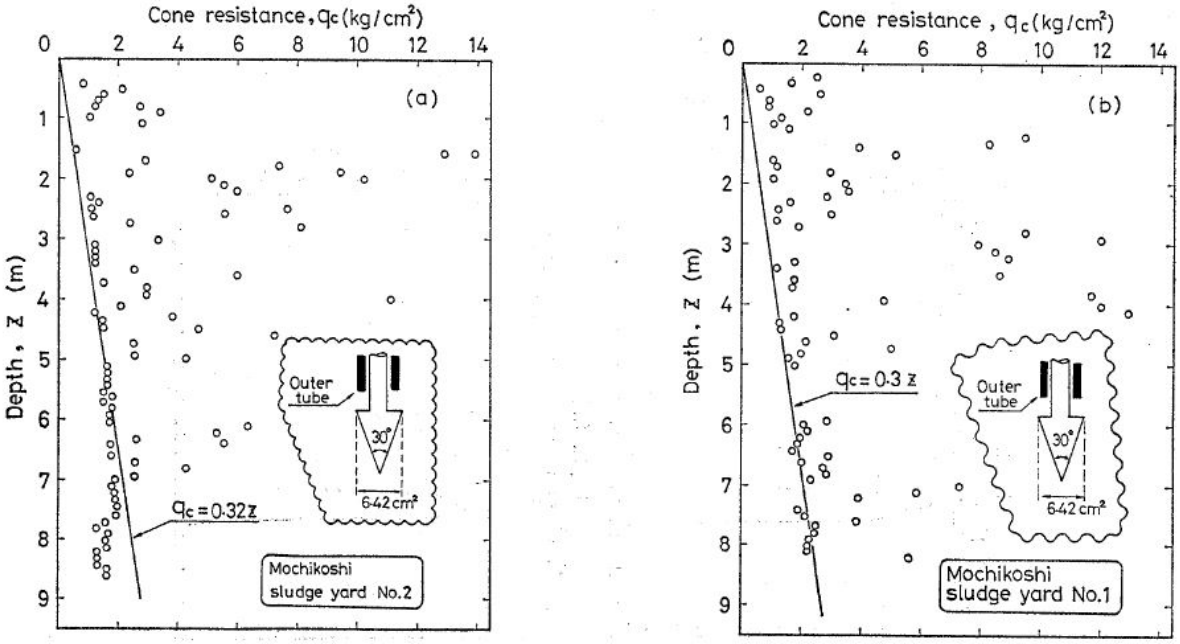

Fig. 4. Double-tube cone penetration test at Mochikoshi

Figure B.11.9: Results of two double-tube cone penetration test soundings performed after the failure (figure from Ishihara et al., 1990).

B.12 Nerlerk Embankment; Slides 1, 2, and 3 (Canada; 1983)

B.12.1 Brief Summary of Case History Characteristics

Name of Structure	Nerlerk Embankment; Slides 1, 2, and 3
Location of Structure	Beaufort Sea, Canada
Type of Structure	Hydraulic Fill Undersea Sand Berm
Dates of Failures	July 20, 25 and 28, 1983
Nature of Failure	Static, During Placement of Fill
Approx. Maximum Slope Height	Slide 1 = 67.5 ft, Slide 2 = 61.4 ft, Slide 3 = 67.8 ft

B.12.2 Introduction and Description of Failures

The Nerlerk undersea sand berm was an engineered, hydraulically placed sand mound created to provided a platform for hydrocarbon exploration in the Canadian Beaufort Sea. Figure B.12.1 shows the location of the berm, and the locations of seven additional berms.

Six undersea slope failures occurred during construction of the berm in 1982 and 1983. The first of these occurred in 1982, and was not reported in the open literature. The other five slope failures occurred between July 20 and August 4, 1983. Figure B.12.2 shows a plan view of the berm and the locations of these five failures. These five failures were well studied (e.g. Mitchell, 1984; Sladen et al., 1985 & 1987; Been at al., 1987; Sladen and Hewitt, 1989; Rogers et al., 1990; Konrad, 1991; and Lade, 1993). All five failures were liquefaction-induced flow failures, and all five exhibited very large runout ratios.

A number of similar sand berm platforms had previously been constructed for the same purpose (e.g. Figure B.12.2), and the designers did not anticipate the problems that occurred at the Nerlerk platform.

Placement of sand commenced in 1982. Borrow materials were obtained from a site near Ukalerk, and were transported to the berm site and deposited by hopper dredges. Later in 1982, and into 1983, borrow materials were obtained from a site nearer to Nerlerk, and were deposited at the still undersea berm by point source discharge. This point discharge appeared to produce an even looser fill, and side slopes of the point discharged fill were typically on the order of 10:1, rather than the 5:1 slopes specified in the design. Construction was temporarily halted to make changes in the point discharge equipment.

Fill placement re-commenced in July of 1983. On July 20, 1983, bathymetric surveys indicated that a large slope failure had occurred on the north face of the still submerged berm, as shown in Figure B.12.2. Four additional slides then occurred in fairly rapid succession on July 25, July 28, August 4 and August 8, 1983. The locations of these additional slides are also shown in Figure B.12.2. Figure B.12.2 is taken from Sladen et al. (1985), and Rogers et al. (1990) disagreed with some of the locations and extents of the slides as depicted.

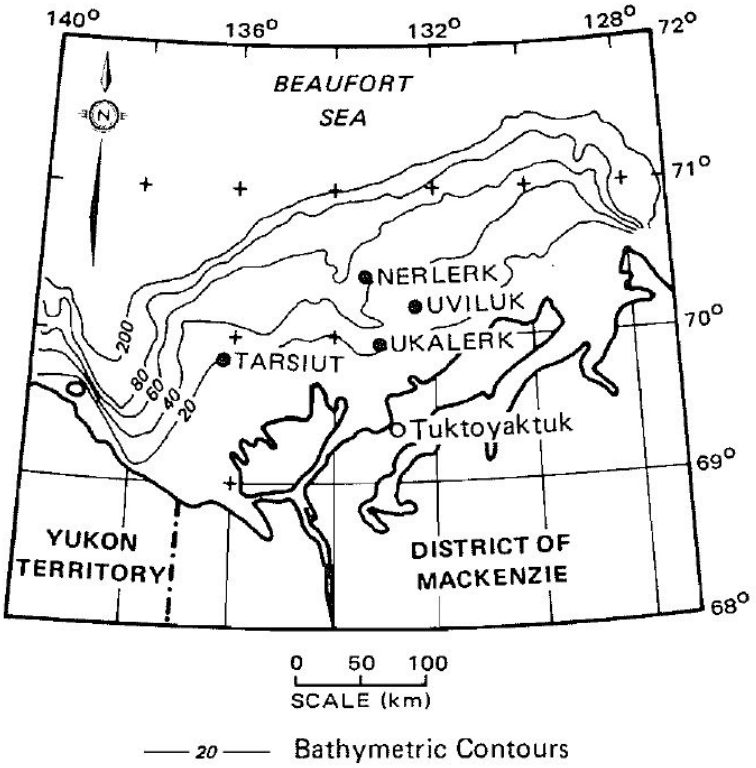

Figure B.12.1: Map of the of the region offshore of the Mackenzie and Yukon Districts of Canada, showing the locations of the Nerlerk Berm and three additional berm platforms, along with offshore bathymetric contours (Figure from Sladen et al., 1985).

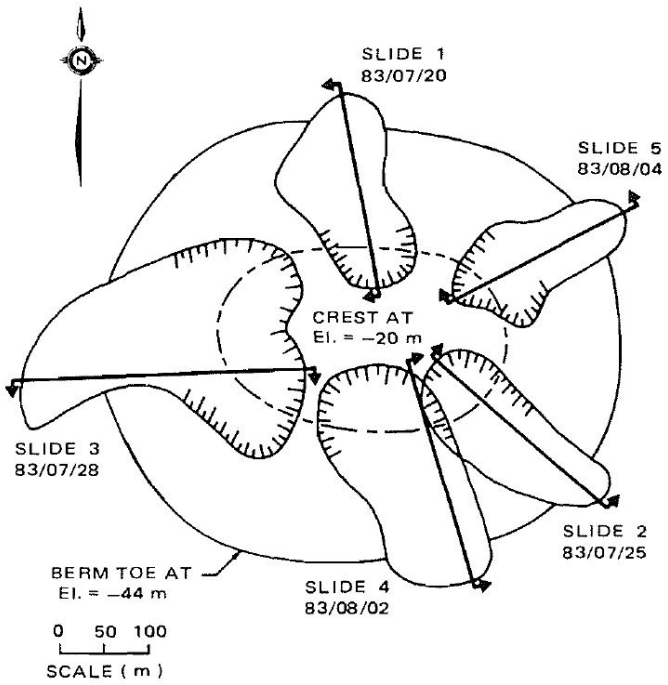

Figure B.12.2: Plan view of the Nerlerk Berm showing the five slope failures that occurred between July 20 and August 8, 1983 (Figure from Sladen et al., 1985).

Figure B.12.3 shows approximate pre-failure and post-failure cross-sections for the five slope failures from Figure B.12.2. Slides 1, 2 and 3 were judged to have sufficiently well-defined pre-failure and post-failure geometries as to warrant back-analyses, and these are the three failures that were back-analyzed in these current studies. The cross-sections of Figure B.12.3 are based on bathymetric surveys, as all of the slides occurred underwater during fill placement. Figure B.12.4 shows the interpreted bathymetric morphology of Slide 4, illustrating the complicated and three-dimensional nature of these flow slides.

B.12.3 Geology and Site Conditions

Figure B.12.5 shows the approximate gradations of the Nerlerk and Ukalerk sands placed to construct the berm. Figure B.12.6 shows a cross-section through the partially completed berm at the end of the 1982 season, showing the face slopes and the distribution of the Nerlerk and Ukalerk sands at that time. The Nerlerk sands had a slightly higher silty fines content of on the order of 2% to 12%, while the Ukalerk Sands had a lower fines content of approximately 0 to 3% (Sladen et al., 1985).

It is generally assumed that the failures occurred primarily within the upper, very loose Nerlerk sand fill materials. Twenty six CPT tests were performed to assess the conditions of these two materials, and the results are presented and discussed in Section B.12.7.

The underyling foundation materials upon which the berm was placed consisted of approximately 1 to 2 meters of high plasticity clay, underlain by poorly graded sands with some traces of silt.

B.12.4 Initial Yield Stress Analyses

Figure B.12.7 shows the cross-section used for back-analyses of the post-liquefaction initial yield strength $S_{r,yield}$ that would be required within the foundation and embankment materials of the typical section of Slide 1 to produce a calculated Factor of Safety equal to 1.0. This is not the actual post-liquefaction strength, but it proves to be useful in developing estimates of post-liquefaction strength (S_r) for this case history.

There were two general sets of potential failure mechanisms that could potentially explain the observed features: (1) the failures may have been incrementally retrogressive, initiating with a small "slice" near to the front of the feature, and then retrogressing on a slice by slice basis back towards the eventual back heel, or (2) the entire slide may have initiated monolithically (all at once). Both sets of possibilities were analyzed, and multiple potential "initial" failure surfaces were analyzed for the incrementally retrogressive scenario. In all cases, failure was modeled as occurring within the Nerlerk sands with failure surface allowed to go only deep enough as to slide tangent to the Ukalerk sands.

Unit weights of the Nerlerk sands were modeled with a unit weight of $\gamma_s \approx 120$ lbs/ft^3, and this was then varied over a range of 115 to 125 lbs/ft^3 for parameter sensitivity studies.

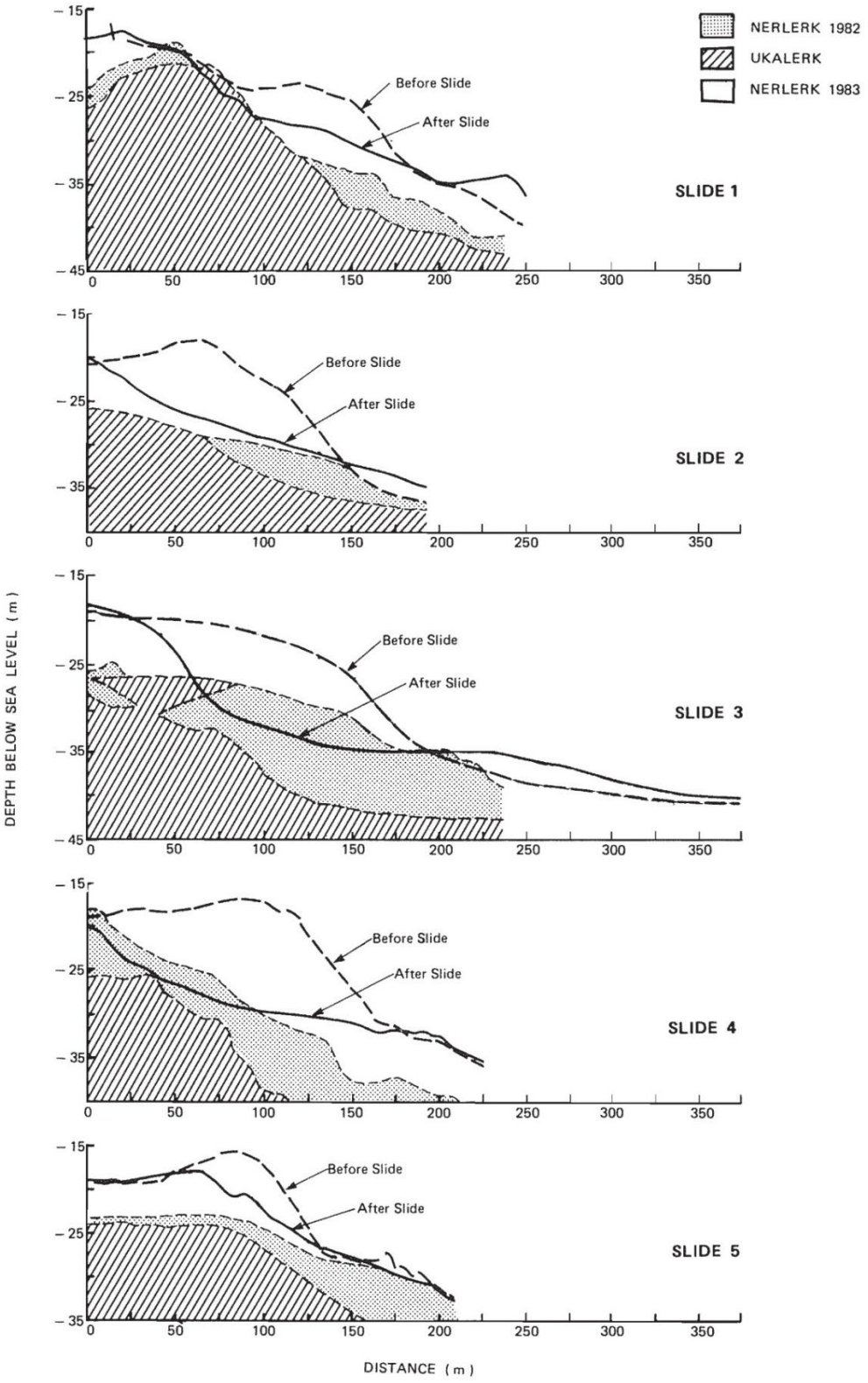

Figure B.12.3: Pre-failure and post-failure cross-sections of Slides 1 through 5 (from Sladen at al., 1985.

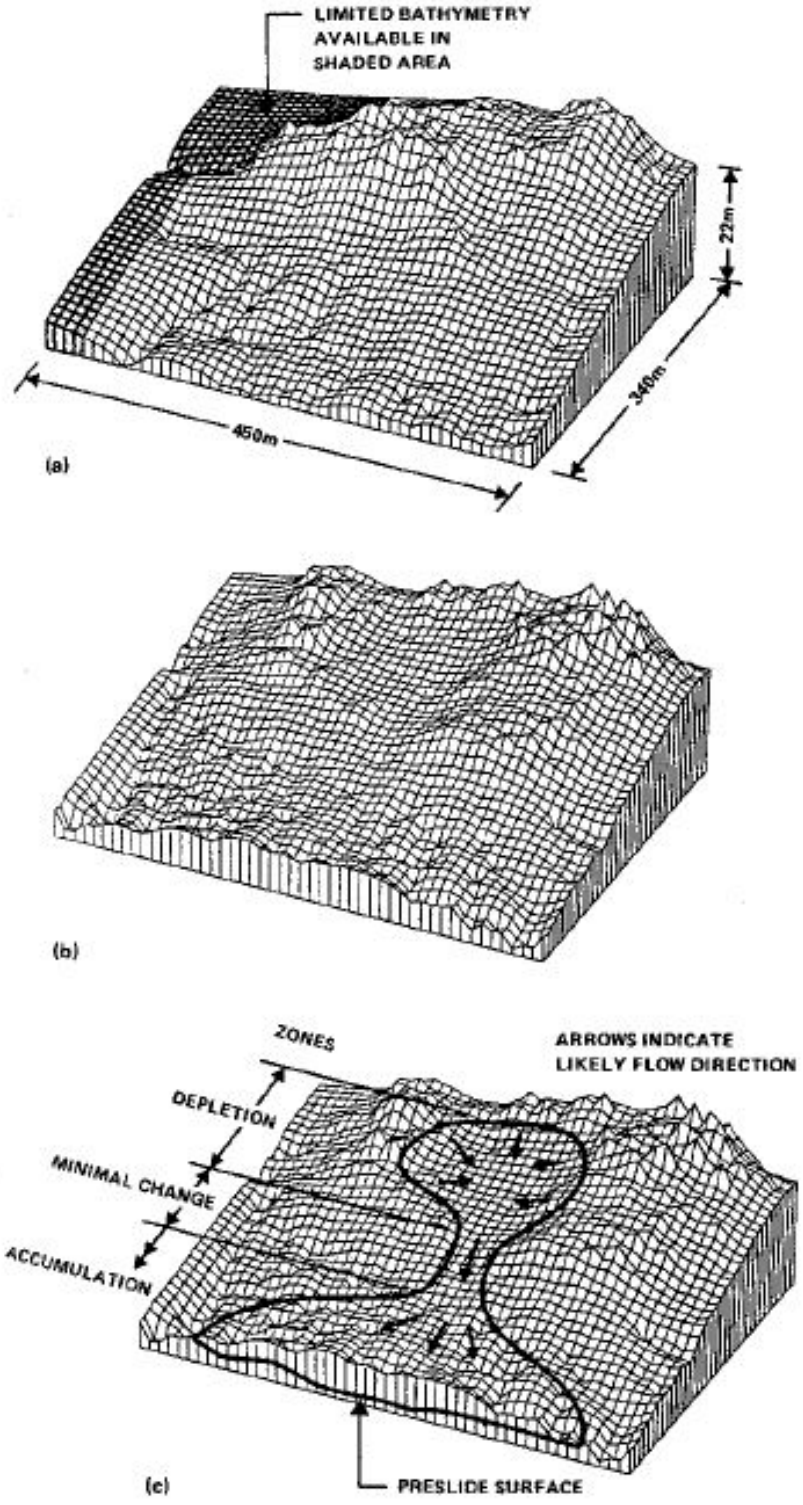

Figure B.12.4: Three-dimensional morphologies of Slide 4 based on detailed bathymetry; (a) pre -slide, (b) post-slide, and (c) interpretation of geomorphology based on (a) and (b). (Figure from Sladen et al., 1987).

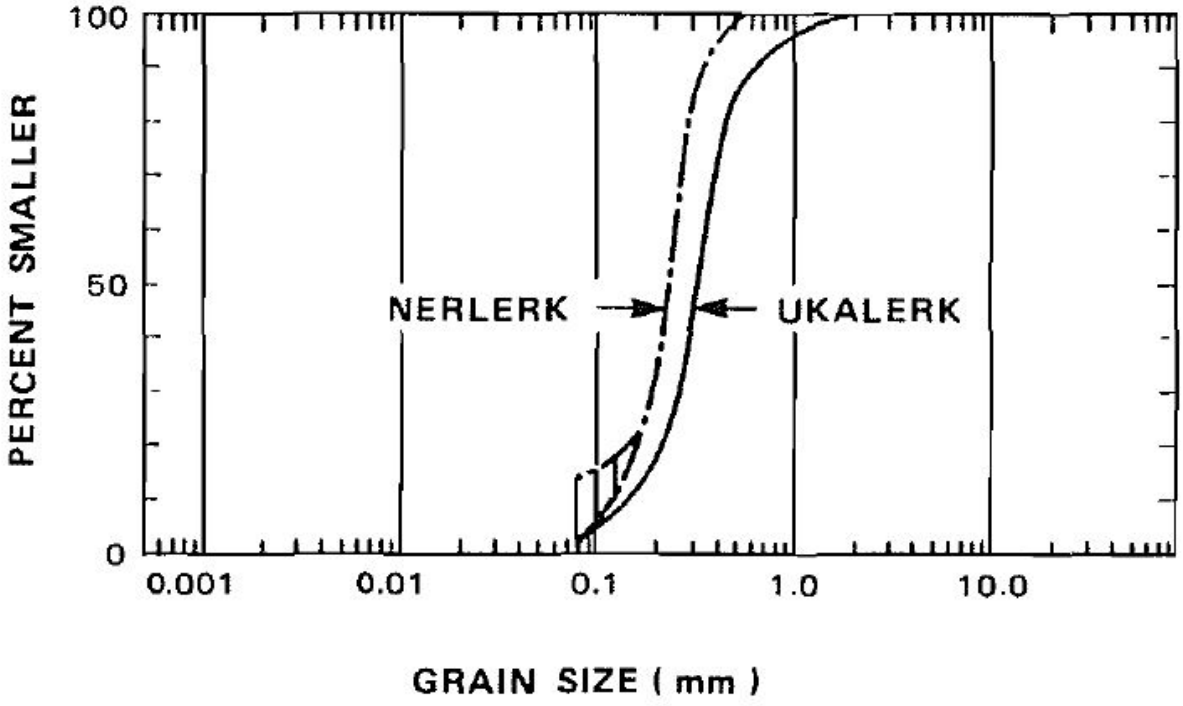

Figure B.12.5: Typical grain size distributions of the Ukalerk and Nerlerk sands (Sladen et al., 1985)

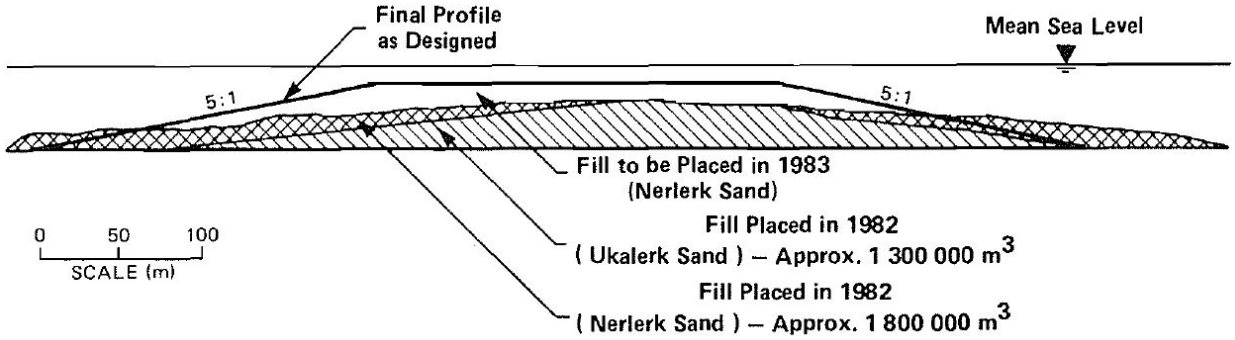

Figure B.12.6: Section through the Nerlerk berm showing distributions of materials types at the end of the 1982 construction season (Figure from Sladen et al., 1985)

Potential initial failure surfaces were modeled as either (1) wedge-like semi-translational features, or (2) semi-rotational/translational features, or (3) conforming essentially to the final observed overall failure scarp (the monolithically initiated scenario).

For the special case of the monolithically initiated scenario, involving initial failure on the eventual (final) observed overall failure scarp, the best estimate value of $S_{r,yield}$ was found to be $S_{r,yield} = 156$ lbs/ft^2, with a range of $S_{r,yield} \approx 115$ to 198 lbs/ft^2.

A significant number of smaller "initial" potential (first slice) failure surfaces were also analyzed, corresponding to a scenario in which the overall failure may have been retrogressive in nature. Figure B.12.7(a) shows a semi-rotational initial failure surface that was the most critical potential initiating failure surface found (lowest post-liquefaction Factor of Safety) but additional potential failure surfaces were also analyzed. The resulting best estimate value of $S_{r,yield}$ for smaller initial yield slices was found to be $S_{r,yield} = 67$ lbs/ft^2, with a likely range of $S_{r,yield} \approx 48$ to 88 lbs/ft^2.

In keeping with the tenets and protocols of these current studies, the values of $S_{r,yield}$ calculated for these potential "initial" slices were then averaged directly with the $S_{r,yield}$ values calculated for the monolithically initiated (eventual overall) failure surface as described above, and these averages values were taken as "representative" $S_{r,yield}$ values for incrementally retrogressive initiation scenarios. Both scenarios were taken as equally as likely and therefore the results were averaged with equal weighting. Based on the range of variations in properties and parameters, and a range of potential failure mechanisms and feasible failure surfaces, the resulting best estimate of "representative" overall $S_{r,yield}$ for Slide 1 was found to be $S_{r,yield} = 112$ lbs/ft^2, with a range of $S_{r,yield} \approx 82$ to 143 lbs/ft^2.

Additional analyses were performed in a similar manner to determine $S_{r,yield}$ for Slides 2 and 3. For Slide 2, example initial failure surfaces are shown on Figure B.12.8(a). The results from analyses assuming a monolithic mechanism produced a best estimate of $S_{r,yield} = 144$ lbs/ft^2, with a likely range of $S_{r,yield} \approx 105$ to 186 lbs/ft^2. A smaller "initial" failure surface assumption resulted in a best estimate of $S_{r,yield} = 201$ lbs/ft^2, with a likely range of $S_{r,yield} \approx 153$ to 253 lbs/ft^2. Equally weighting each mechanism, the resulting best estimate of "representative" overall $S_{r,yield}$ for Slide 2 was found to be $S_{r,yield} = 173$ lbs/ft^2, with a range of $S_{r,yield} \approx 129$ to 220 lbs/ft^2.

For Slide 3, example initial failure surfaces are shown on Figure B.12.9(a). The results from analyses assuming a monolithic mechanism produced a best estimate of $S_{r,yield} = 109$ lbs/ft^2, with a likely range of $S_{r,yield} \approx 86$ to 133 lbs/ft^2. A smaller "initial" failure surface assumption resulted in a best estimate of $S_{r,yield} = 236$ lbs/ft^2, with a likely range of $S_{r,yield} \approx 169$ to 295 lbs/ft^2. Equally weighting each mechanism, the resulting best estimate of "representative" overall $S_{r,yield}$ for Slide 2 was found to be $S_{r,yield} = 173$ lbs/ft^2, with a range of $S_{r,yield} \approx 128$ to 214 lbs/ft^2.

The results of all three slides were then averaged, as only a single set of indices will be used for the overall Nerlerk case history. This is because (1) the three slides are very similar, and so are the initial geometries and materials, and (2) it was desirable not to over-weight the contribution of this (three slide) case history to the eventual regressions that would subsequently be performed. Averaging the results of all three slides, it was judged that the overall best estimate of $S_{r,yield}$ for this case history is be $S_{r,yield} = 153$ lbs/ft^2, with a range of $S_{r,yield} \approx 113$ to 192 lbs/ft^2.

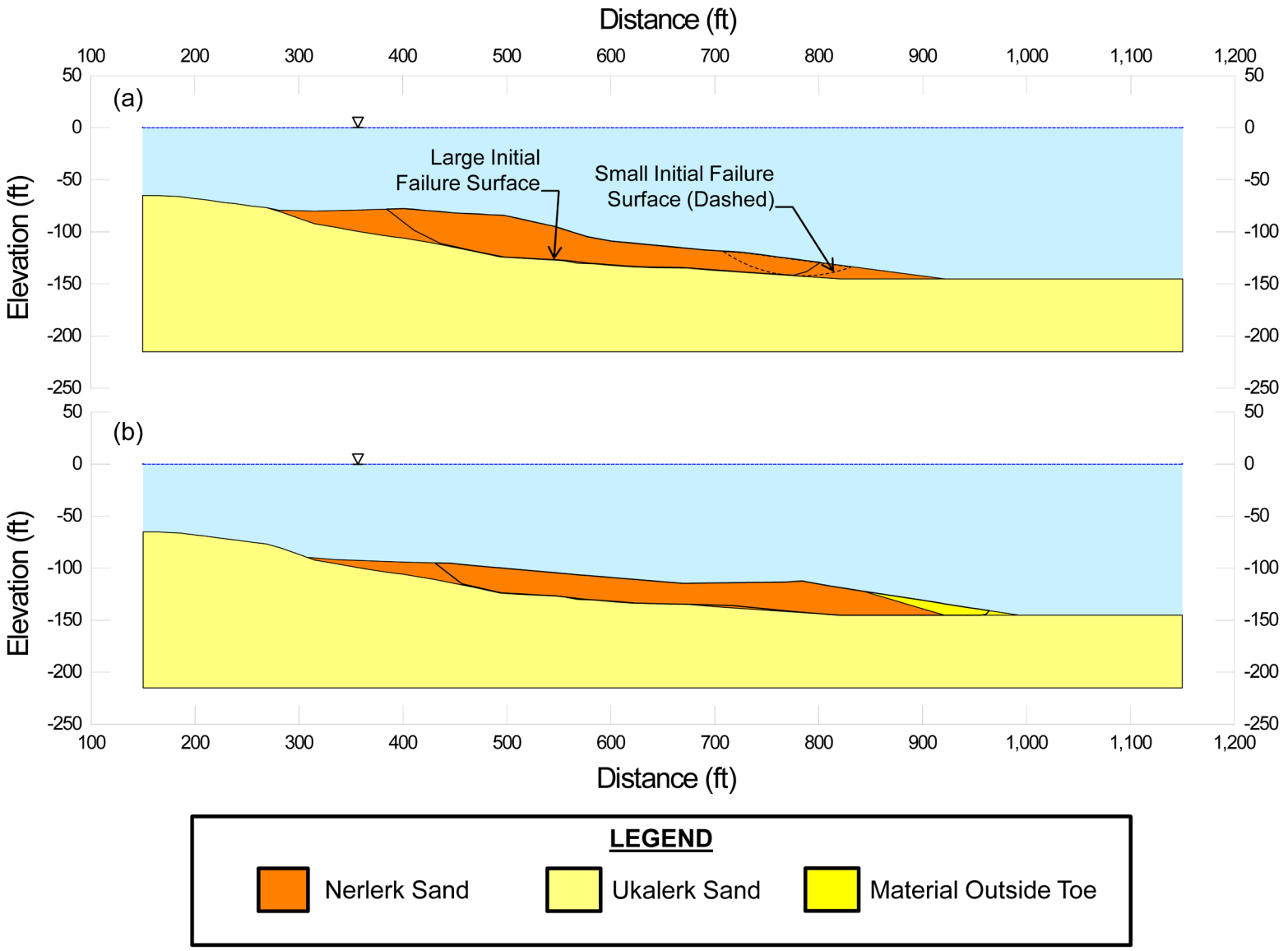

Figure B.12.7: Pre-failure and post-failure cross-sections used for back-analyses of Slide 1 of the Nerlerk Berm

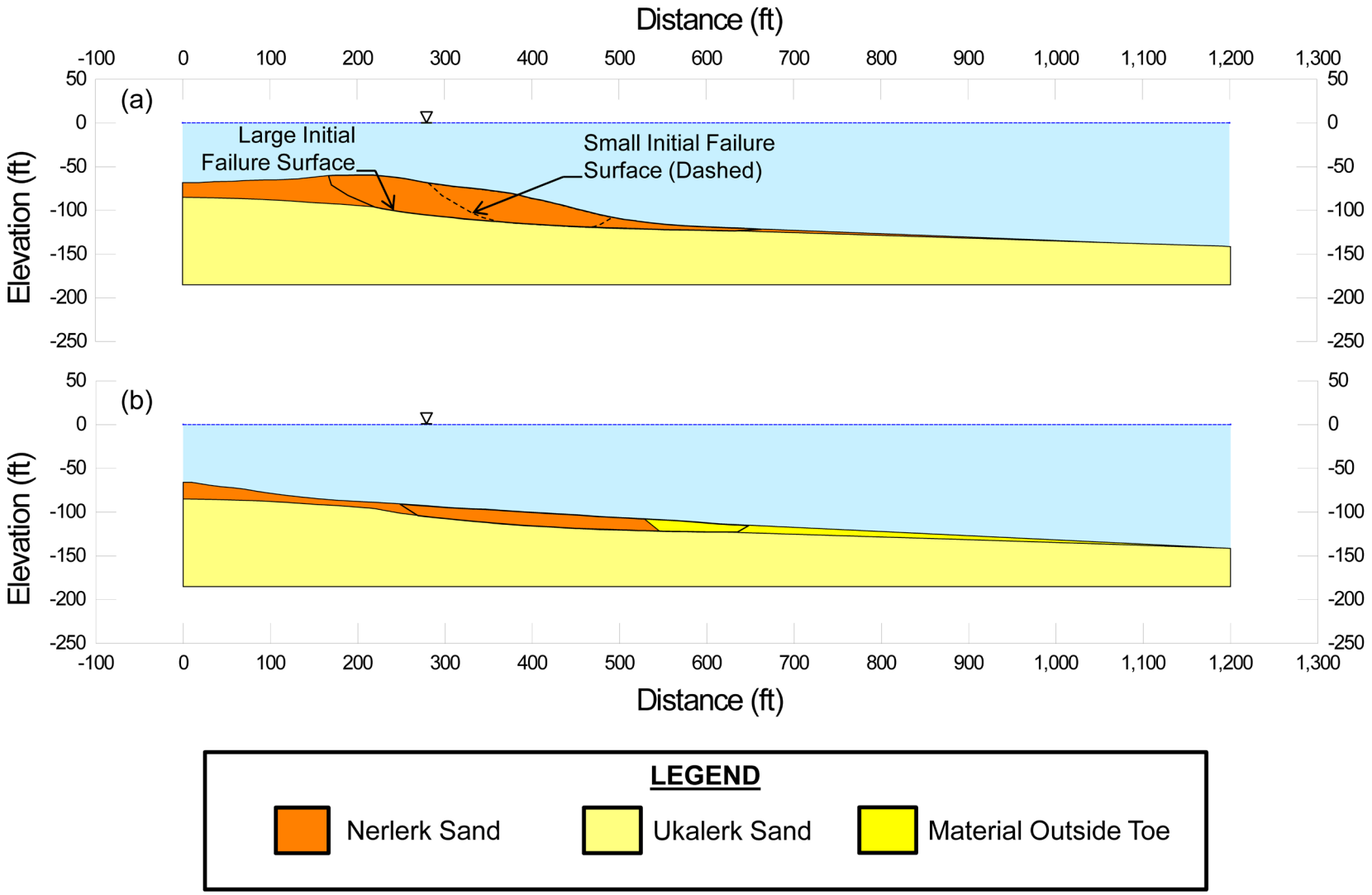

Figure B.12.8: Pre-failure and post-failure cross-sections used for back-analyses of Slide 2 of the Nerlerk Berm

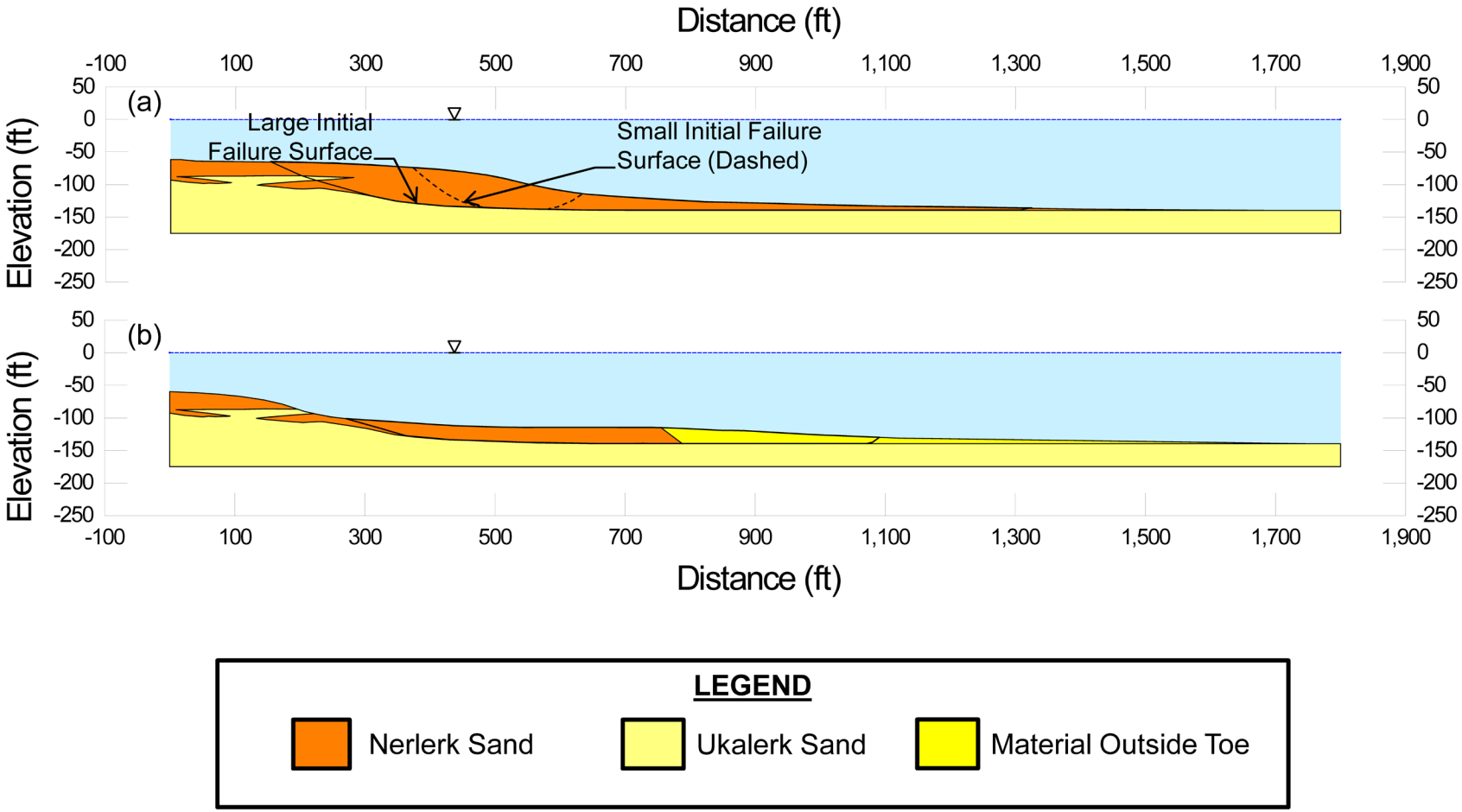

Figure B.12.9: Pre-failure and post-failure cross-sections used for back-analyses of Slide 3 of the Nerlerk Berm

Olson (2001) also performed back-analyses to evaluate $S_{r,yield}$ for each of the three Nerlerk slides considered in this study. He analyzed only wedge-type toe failures surfaces within the Nerlerk sand fill material. His resulting best estimate values of $S_{r,yield}$ for Slides 1, 2 and 3 are

Slide 1: $S_{r,yield}$ = 2.7 kPa (56 lbs/ft^2) with a range of 2.7 kPa (56 lbs/ft^2) to 4.0 kPa (84 lbs/ft^2)

Slide 2: $S_{r,yield}$ = 4.2 kPa (88 lbs/ft^2) with a range of 4.0 kPa (84 lbs/ft^2) to 4.8 kPa (100 lbs/ft^2)

Slide 3: $S_{r,yield}$ = 4.8 kPa (100 lbs/ft^2) with a range of 4.2 kPa (88 lbs/ft^2) to 5.7 kPa (84 lbs/ft^2)

Average = 3.9 kPa (81 lbs/ft^2)

These values are somewhat lower than the values calculated in these current studies because of the differences between the smaller toe wedges analyzed by Olson and the slightly larger rotational and rotational/translational toe failures analyzed in these current studies.

B.12.5 Residual Strength Analyses Based on Residual Geometry

The calculation of the "apparent" post-liquefaction strength ($S_{r,resid/geom}$) required to produce a calculated static Factor of Safety equal to 1.0 based on residual geometry for Slide 1 is illustrated in Figure B.12.7(b). This value of $S_{r,resid/geom}$ is not the post-liquefaction strength (S_r), as it neglects momentum effects and so underestimates S_r. It is, however, useful in evaluation of S_r.

Most modeling parameters and details are as described in the preceding section.

Occurring under the Beaufort Sea, these slides likely experienced some degree of the combined effects of (1) potential hydroplaning, and (2) potential sliding atop weaker seabed sediments as the toe of the slide mass traveled down slope outboard of the berm toe. These two effects were jointly modeled with an assumption that the best estimate of strength at the base of the portion of the slide mass sliding outside the original toe was equal to 50% of the post-liquefaction strength (S_r) of the liquefied Nerlerk sands. Parameter sensitivity studies were then performed, varying this over the range of 25% to 75% of S_r.

Based on the Slide 1 cross-sections shown in Figure B.12.7(b), and the properties and parameters described above, the best-estimate value of $S_{r,resid/geom}$ was $S_{r,resid/geom}$ = 86 lbs/ft^2. Parameters were next varied, as described previously, including analyses of alternate potential failure surfaces slightly above and below the failure surface shown in Figure B.12.7(b). Based on these analyses, it was judged that a reasonable range was $S_{r,resid/geom} \approx$ 66 to 108 lbs/ft^2.

Additional analyses were performed in a similar manner to evaluate $S_{r,resid/geom}$ for Slides 2 and 3, using the cross-sections of Figures B.12.8(b) and B.12.9(b), respectively. For Slide 2, an example residual failure surface is shown on Figure B.12.8(b). The results from these analyses produced a best estimate of $S_{r,resid/geom} \approx$ 41 lbs/ft^2, with a likely range of $S_{r,resid/geom} \approx$ 26 to 58 lbs/ft^2.

For Slide 3, an example residual failure surface is shown on Figure B.12.9(b). The results from the analyses of Slide 3 produced a best estimate of $S_{r,resid/geom}$ = 32 lbs/ft^2, with a likely range of $S_{r,resid/geom} \approx$ 23 to 44 lbs/ft^2.

The results of all three slides were then averaged, as only a single set of indices will be used for the overall Nerlerk case history. This is because (1) the three slides are very similar, and so are the initial geometries and materials, and (2) it was desirable not to over-weight the contribution of this (three slide) case history to the eventual regressions that would subsequently be performed. Averaging the results of all three slides, it was judged that the overall best estimate of $S_{r,resid/geom}$ = 53 lbs/ft^2, with a range of $S_{r,resid/geom} \approx$ 38 to 70 lbs/ft^2.

Olson (2001) also performed back-analyses to evaluate $S_{r,resid/geom}$ for each of the three Nerlerk slides considered in this study. He projected an estimate of runout geometry beyond the toe of the embankments, but does not then go on to show or clearly explain the failure surfaces he considered. His best estimate values of $S_{r,,resid/geom}$ for Slides 1, 2 and 3 are

Slide 1: $S_{r,resid/geom}$ = 2.5 kPa (52 lbs/ft^2) with no range given.

Slide 2: $S_{r,resid/geom}$ = 1.7 kPa (36 lbs/ft^2) with range ≈ 1.0 kPa (21 lbs/ft^2) to 2.4 kPa (84 lbs/ft^2)

Slide 3: $S_{r,resid/geom}$ = 1.5 kPa (31 lbs/ft^2) with range ≈ 1.2 kPa (25 lbs/ft^2) to 1.7 kPa (36 lbs/ft^2)

Average = 1.9 kPa (40 lbs/ft^2)

These values are only a bit lower than the values calculated in these current studies.

B.12.6 Overall Estimates of S_r

Overall estimates of S_r for this Class B case history were made based on the pre-failure geometry, the partial post-failure geometry, the approximate runout features and characteristics, and the values of $S_{r,yield}$ and $S_{r,resid/geom}$ as calculated and/or estimated in the preceding sections.

An average runout distance of the center of masses of the overall failures for Slides 1, 2 and 3 was approximately D = 240 feet, and the average initial failure slope height for the three slides was H = 65.6 feet. This produces a runout ratio (defined as runout distance traveled by the center of gravity of the overall failure mass divided by the initial slope height from toe to back heel of the failure) of D/H = 3.66. This allows Equation 4-4, and Figures 4.7 and 4.11, to serve as one basis for estimation of post-liquefaction strength S_r. Using the ranges of $S_{r,yield}$ and $S_{r,resid/geom}$ from Sections B.12.4 and B.12.5, and assuming that $\xi \approx 0.4$ to 0.65 for this long runout case, with 0.525 as the best estimate, provided a best estimate value of $S_r \approx$ 54 lbs/ft^2 and an estimated range of $S_r \approx$ 30 to 85 lbs/ft^2. A second basis for estimation of S_r was the use of the relationship of Figure 4.9, and the range of values of $S_{r,yield}$ from Section B.5.4. Based on the large runout distance, values of initial (pre-failure displacement) Factor of Safety were taken as approximately 0.35 to 0.55, and this produced a best estimate value of $S_r \approx$ 69 lbs/ft^2 and an estimated range of $S_r \approx$ 40 to

106 lbs/ft^2. No similar use was made of Figure 4.9 in conjunction with the ranges of $S_{r,resid/geom}$ estimated in Section B.12.5 because these estimates of $S_{r,resid/geom}$ were considered to be very approximate.

The estimates by each of the two methods above were then averaged together, and this produced a best estimate value of $S_r \approx 62$ lbs/ft^2 and an estimated range of $S_r \approx 30$ to 106 lbs/ft^2. These estimates of variance are non-symmetric about the best estimated mean value, and the range was judged to represent approximately +/- 2 standard deviations, so further adjustments were then necessary.

Overall, based on an assumed normal distribution, it was judged that the (mean and median) best estimate of post-liquefaction strength for this case history is

$$\overline{S_r} = 68 \text{ lbs/ft}^2$$

and that the best estimate of standard deviation of mean overall post-liquefaction strength is

$$\sigma_{\overline{S}} = 19 \text{ lbs/ft}^2$$

Olson (2001) and Olson and Stark (2002) did not apply their "kinetics" method to this case, and so they did not independently develop an estimate of S_r that incorporated momentum effects. Instead they simply used their value of $S_{r,resid/geom}$ as presented above in Section B.12.5 as a conservative approximation of S_r for this less well-defined case. Because these values are based on residual post-failure geometry with an assumed Factor of Safety equal to 1.0, they do not include momentum effects and so they will be too low.

A better estimate of S_r that approximately incorporates momentum effects, and a better basis for comparison with these current studies, can be obtained by employing Olson's best estimate averaged values of $S_{r,yield} = 81$ lbs/ft^2 and $S_{r,resid/geom} = 40$ lbs/ft^2, and an assumed average value of $\xi \approx 0.8$ in Equation 4-4 as

$$S_r \approx 0.5 \text{ x } [81 \text{ lbs/ft}^2 + 40 \text{ lbs/ft}^2] \text{ x } 0.8 = 48 \text{ lbs/ft}^2$$

This value ($S_r \approx 48$ lbs/ft^2) agrees reasonably well with the best estimate value of $S_r \approx 68$ lbs/ft^2 developed in these current studies, especially considering the uncertainties and the very different approaches taken by the two investigation teams.

Wang (2003) and Wang and Kramer (2008) did not employ their zero inertial force (ZIF) method to incorporate inertial effects in back-analyses of this failure. Instead they selected their value of S_r based on examination of back-analyses of several previous investigators, and in the end selected $\overline{S_r} = 178.5$ lbs/ft^2, and a standard deviation of $\sigma_{\overline{S}} = 32.1$ lbs/ft^2. Their best estimate appears to be unreasonably high, based on comparison with the values developed (1) by Olson (2001) and (2) these current studies. This appears to be the result of inadvertent double-counting of the high value of S_r proposed by Jeffries et al. (1990) in their averaging of four previous values, as described in Section 2.3.8.1(b)-(ii). The value of Jeffries et al. ($S_r = 308$ lbs/ft^2) was then adopted by Stark and Mesri (1992) who rounded it to 400 lbs/ft^2. That was not a second "independent" assessment.

Wang averaged both 408 lbs/ft^2 and 400 lbs/ft^2 as two of the four values from previous investigations to develop his resulting averaged value for this case.

Sladen et al. (1985) also performed back-analyses to develop estimates of S_r for this case, and averaging his values for Slides 1, 2 and 3 his resulting value would be S_r = 42 lbs/ft^2, in reasonable agreement with both Olson (2001) and these current studies.

B.12.7 Evaluation of Initial Effective Vertical Stress

Average initial (pre-failure) effective vertical stress was assessed for each of the three large final failure surfaces for Slides 1, 2 and 3 shown in Figures B.12.7(a) through B.12.9(a). Parameters and sensitivity analyses were as described previously in Section B.12.4. Additional analyses were then performed for alternate potential failure surfaces, including failure surfaces representing the end result of retrogressive incremental failures extending back to the apparent back heel of the final failure. Depths of failure surfaces were varied, and both rotational and translational (wedge-like) failure surfaces were considered. This produced a moderately large, but finite, range of estimated values of average pre-failure effective stress within the liquefied materials controlling the failure.

For failure Slide 1, the resulting best estimate of average pre-failure effective stress within the liquefied materials controlling the failure was then $\sigma_{vo}' \approx$ 1,066 lbs/ft^2, with a reasonable range of $\sigma_{vo}' \approx$ 813 to 1,326 lbs/ft^2.

For failure Slide 2, the resulting best estimate of average pre-failure effective stress within the liquefied materials controlling the failure was then $\sigma_{vo}' \approx$ 1,281 lbs/ft^2, with a reasonable range of $\sigma_{vo}' \approx$ 1,026 to 1,550 lbs/ft^2.

For failure Slide 3, the resulting best estimate of average pre-failure effective stress within the liquefied materials controlling the failure was then $\sigma_{vo}' \approx$ 1,148 lbs/ft^2, with a reasonable range of $\sigma_{vo}' \approx$ 899 to 1,411 lbs/ft^2.

Averaging the Results from Slides 1, 2 and 3, the resulting best estimate of average pre-failure effective stress within the liquefied materials controlling the failure was then $\sigma_{vo}' \approx$ 1,165 lbs/ft^2, with a reasonable range of $\sigma_{vo}' \approx$ 913 to 1,429 lbs/ft^2. This range is slightly non-symmetric about the median value, and this range was judged by the engineering team to represent approximately ± 2 standard deviations. Overall, the best characterization of initial (pre-failure) average effective vertical stress was then taken to be represented by a mean value of

$$\overline{\sigma'_{vo}} \approx 1{,}171 \text{ lbs/ft}^2$$

and with a standard deviation of

$$\sigma_{\bar{\sigma}} \approx 129 \text{ lbs/ft}^2$$

Estimates of σ_{VO}' were also back-calculated by Olson and Stark (2001, 2002). Averaging their best estimate values for Slides 1, 2 and 3 produces a resulting overall average value of $\sigma_{vo}' \approx 35.0$ kPa (731 lbs/ft^2), which is somewhat lower than the value developed in these current studies. Average initial vertical effective stresses were not directly reported by Wang (2003) and Kramer (2008), but they were published more recently in the publication by Kramer and Wang (2015). As discussed in Section 2.3.8.1(b)-(iii), Wang (2003) did not perform any independent analyses to assess σ_{vo}' for his 22 "secondary" cases, and this is one of those cases. Instead, he compiled values of S_r from multiple previous investigators, and averaged these for a best estimate. He also compiled multiple values of S_r/σ_{vo}' from previous investigators, and averaged these for a best estimate. He then used these two best-estimate values of S_r and S_r/σ_{vo}' to infer a resulting representative value of σ_{vo}'. As described in Section 2.3.8.1(b)-(iii), the resulting averaged values of S_r and S_r/σ_{vo}' were incompatible with each other for a number of Wang's "secondary" case histories, and this process produced unreasonable values for a number of case histories. Wang's value of $\sigma_{vo}' = 1{,}440$ lbs/ft^2 for this case is somewhat higher than the values developed by Olson (2001) and by these current studies.

B.12.8 Evaluation of $N_{1,60,CS}$

Sladen et al. (1985) report that results from soil borings indicate that the fines content of the Nerlerk sands had a fines content of about 10%, while Rogers et al.(1990) reported an average of 3%. It is not reported if any SPTs were performed as a part of those investigations.

Sladen et al. (1985) reported that 26 CPTs were performed at the site in the both the pipeline-placed Nerlerk and hopper-placed Ukalerk sands. Figure B.10.10 presents separate summaries of the tip resistances for the Nerlerk and Ukalerk sands. These serve to confirm that the hopper-placed Ukalerk sands have a higher penetration resistance, confirming the more critical state of the Nerlerk sands.

Olson (2001) reports representative penetration resistances from the Nerlerk sands from 2 CPTs that are reported to be near to Slides 1 and 2. Olson assumed the penetration resistance from the CPT near Slide 2 was also representative of Slide 3. He determined a representative penetration resistance and range for Slide 1 to be $q_{c1} = 4.5$ MPa, with a range from 2.6 to 7.8 MPa. The assigned representative penetration resistance and range for Slides 2 and 3 to be $q_{c1} = 3.8$ MPa, with a range from 1.9 to 8.0 MPa. While the individual CPT soundings used to produce those estimates were not reported by Olson, the values appear to be consistent with the average CPT values in Nerlerk sands shown in Figure B.12.11. He also reported a range of fines contents from 2 to 12% for the Nerlerk sands.

For this study, it was determined that a representative q_{c1} value for the Nerlerk sands of $q_{c1} \approx 3.8$, with a range of 3 to 4.5 MPa is appropriate. The ratio of $(q_c/Pa)/N_{60}$ was assumed to be approximately of 4 to 6. Based on the ranges of fines content reported form other studies, a fines content correction ranging from no correction to a slight correction was adopted. After applying the necessary corrections and conversions, the resulting best estimate mean value of $N_{1,60,CS}$ for the iron tailings was judged to be $\overline{N_{1,60,CS}} \approx 7.5$ blows/ft. Variance of $\overline{N_{1,60,CS}}$ was estimated

primarily based on the range of results assumed in this and other studies. Considering these, the representation of uncertainty in the representative median value of $\overline{N_{1,60,CS}}$ was taken as $\sigma_{\overline{N}} \approx 2.5$ blows/ft.

Olson (2001) developed the following estimates of penetration resistances for Slides 1, 2 and 3:

Slide 1: $N_{1,60}$ = 8.7 bpf, with a range of 5 to 15 bpf

Slide 2: $N_{1,60}$ = 7.2 bpf, with a range of 3.5 to 15.3 bpf

Slide 3: $N_{1,60}$ = 7.2 bpf, with a range of 3.5 to 15.3 bpf

These are in very good agreement with these current studies. Fines adjustments are essentially null for the Nerlerk sands.

Wang (2003) developed a significantly higher value of $N_{1,60,CS}$ = 11.4 bpf for this case. It is not clear what caused this value to be so much higher than the values of (1) Olson (2001) and (2) these current studies.

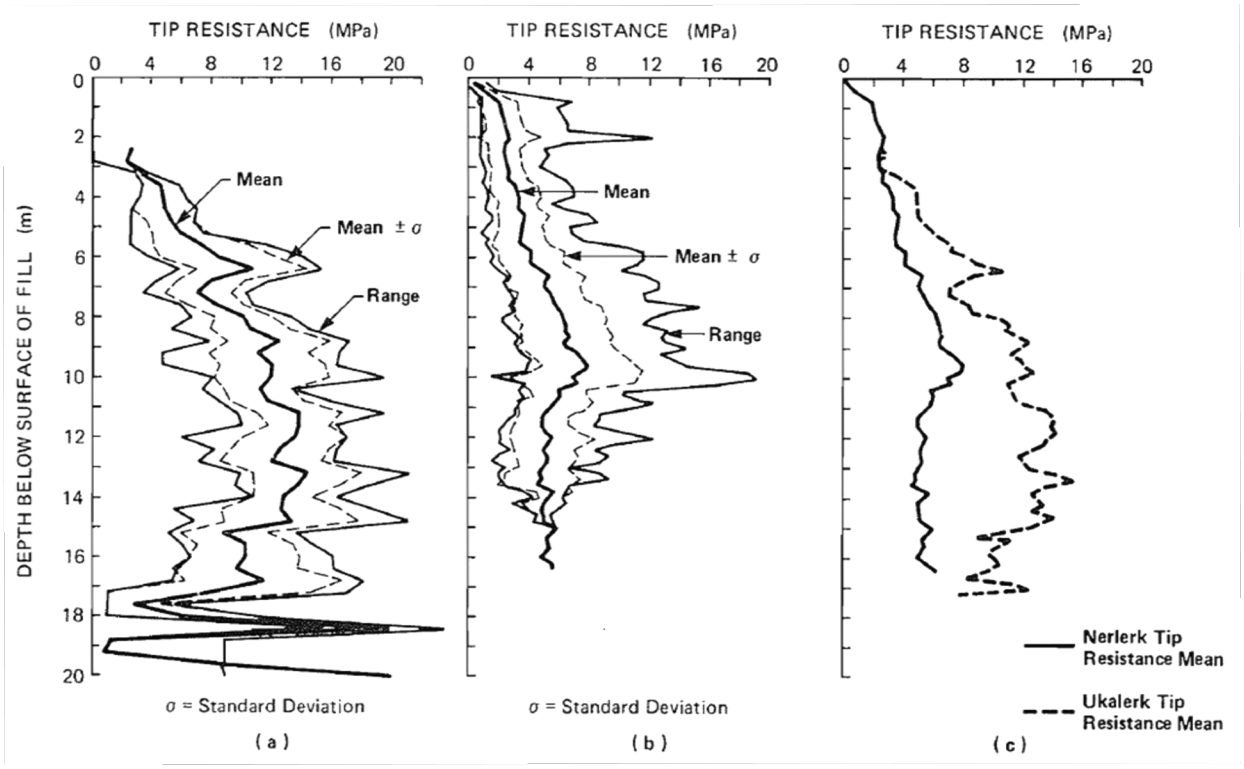

Figure B.12.10: Mean CPT tip resistances, and ranges, separated by material type (a) Ukalerk sand, (b) Nerlerk sand, (c) means of Ukalerk and Nerlerk sands (Figure from Sladen et al., 1985)

B.13 Asele Road Embankment (Sweden; 1983)

B.13.1 Brief Summary of Case History Characteristics

Name of Structure	Asele Road Embankment
Location of Structure	Sweden
Type of Structure	Earthen Embankment
Date of Failure	October 4, 1983
Nature of Failure	Cyclic, Road Pavement Repairs
Approx. Maximum Slope Height	29.2 ft.

B.13.2 Introduction and Description of Failure

Road No. 351 near Asele was constructed on a raised earthen embankment along the edges of two existing lakes, and the embankment would eventually be partially submerged due to the impoundment of a reservoir for a nearby hydropower facility. Figure B.13.1 shows a plan view site map. The embankment was constructed as prescribed using the "wet-fill" method, however it was constructed during the winter months, contrary to implied recommendations, allowing to embankment to potentially freeze during construction.

The Asele Road Embankment was completed and opened to traffic in August of 1978. Filling of the reservoir began five years later in August of 1983. When the water had risen to about 3 meters above the toe on September 18, 1983 longitudinal cracks along the embankment were noticed. By the time the water reached within about 2 meters of the road level, extensive damage had occurred, requiring the embankment road to be resurfaced. It was during this resurfacing effort, and specifically during the compaction of the subgrade by the use of a 3.6 ton vibratory roller drawn by a tractor on October 4, 1983, that a pair of liquefaction-induced slides of the embankment occurred. The tractor and vibratory roller were carried out by the larger of the two slide and travelled approximately 60 m laterally out into the reservoir (Ekstrom and Olofsson, 1985), and the operator perished. The failure occurred during the first pass of the large vibratory roller.

Figure B.13.1 presents a photograph (from Ekstrom and Olofsson, 1985) showing the scarp after the failure, and Figure B.13.2 shows a cross-section through the failed road embankment section (from Konrad and Watts, 1995, based on Ekstrom and Olofsson, 1985).

The failure was attributed by Ekstrom and Olofsson (1985) to cyclically initiated liquefaction of the loose embankment fill due to the shaking applied by the vibratory roller. Ekstrom and Olofsson attributed the loose nature of the fill material to the use of a "wet fill" method during winter months which reportedly left the fill susceptible to freezing, which in turn defeated efforts at compaction of the fill when the embankment was under construction.

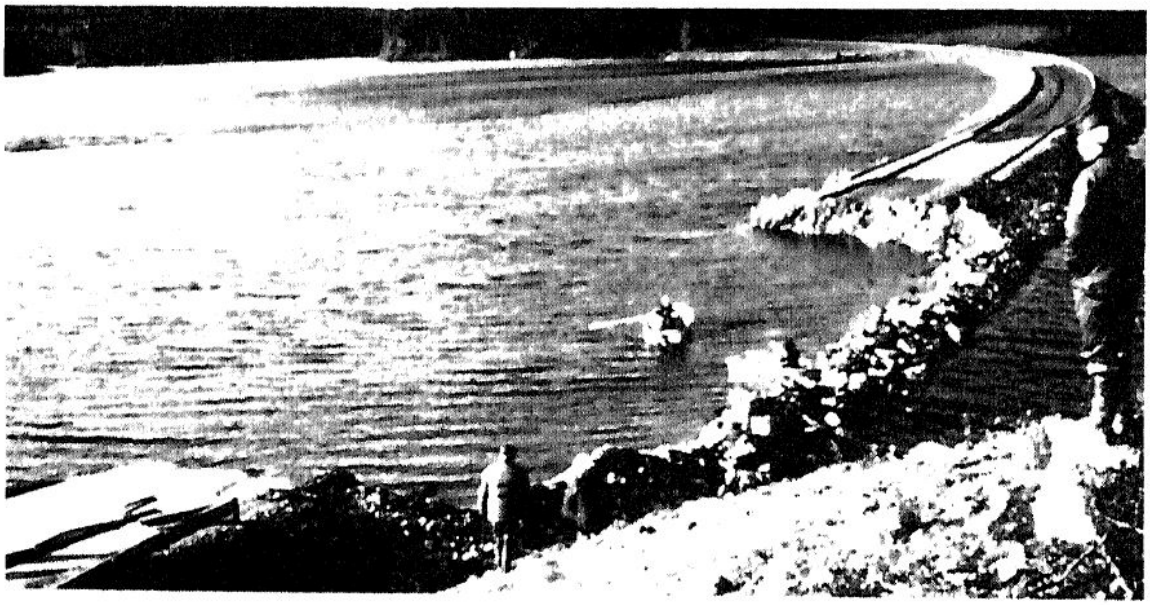

Fig. 1 View of the failure, October 4th 1983.

Figure B.13.1: Photograph of the Asele Road Embankment failure scarp and the remaining embankment on October 4, 1983 (Ekstrom and Olofsson, 1985).

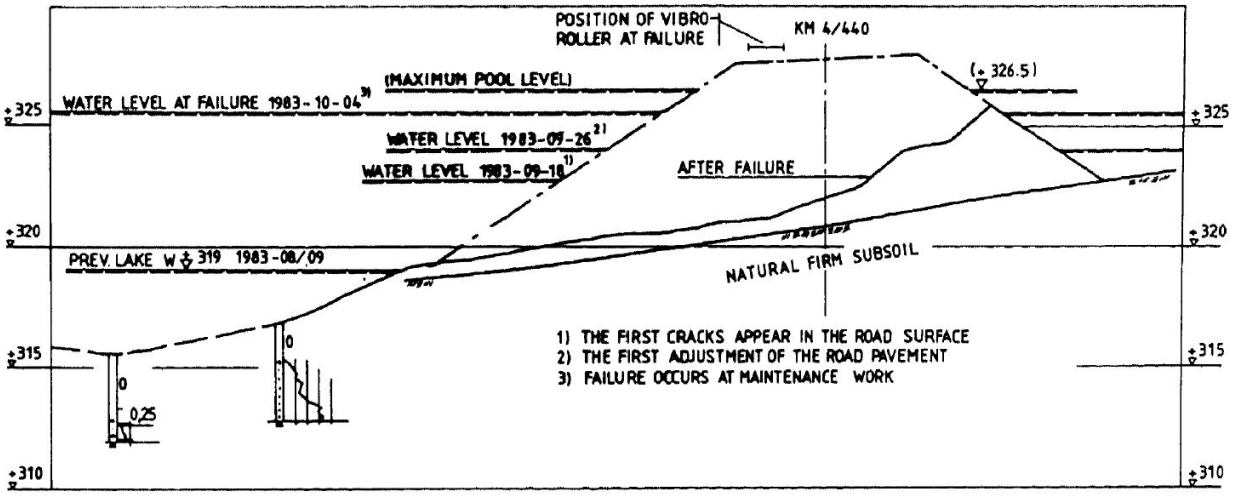

Figure B.13.2: Pre-failure and post-failure cross-sections of the Asele Road Embankment (Ekstrom and Olofsson, 1985).

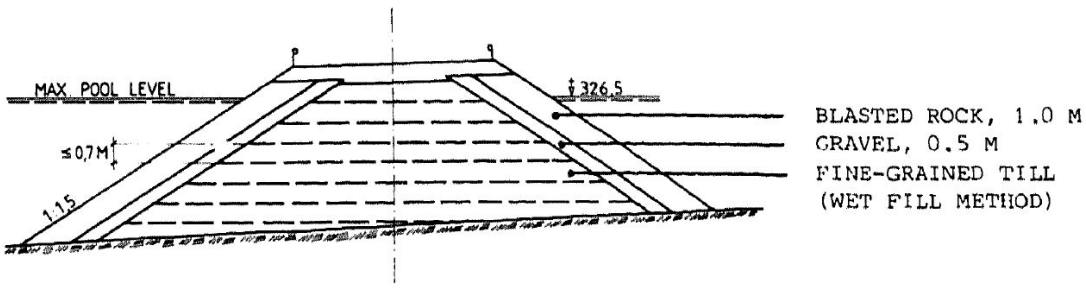

Fig. 4 Principal section for the construction of the embankment.

Figure B.13.3: Design cross-section for the Asele Road Embankment (Ekstrom and Olofsson, 1985).

B.13.3 Geology and Site Conditions

Figure B.13.3 shows the design cross-section for the Asele Road Embankment. The embankment was constructed with fine sandy till, with facings consisting of a layer of gravel overlain by coarser blasted rock. The foundation material consisted of what Ekstrom and Olofsson describe as natural firm (glacial) till. As shown in Figure B.13.2, the failure occurred within the loose, fine sandy till embankment. The water level at the time of the failure is reported in Ekstrom and Olofsson (1985) as being El +325.5 m., and this is also shown in Figure B.13.2.

The "fine-grained" till materials used for the main embankment fill were broadly well graded glacial till materials with maximum particle sizes of approximately ¾ inches, and fines contents of approximately 22% to 40% (Ekstrom and Olofsson, 1985). "Fine-grained" was a relative term here; distinguishing between the materials used to construct the main body of the embankment, and the coarser materials of the facings which were sized as slope face protection against wave erosion. The fines were silt dominated, and these soils are all generally of a potentially liquefiable nature.

There were no published penetration test data for this failure case history, but Konrad and Watts (1995) reported a personal communication from Prof. Rainer Masarch, who conducted a post-failure investigation of the Asele Road Embankment. Prof. Masarch reported an average $N_{1,60}$ value of approximately 6 to 8 blows/ft., but the details of SPT equipment and procedures, and the corrections and adjustments made to produce these $N_{1,60}$ values, are not known.

B.13.4 Initial Yield Stress Analyses

Figure B.13.4 shows the cross-section used for back-analyses of the post-liquefaction initial yield strength $S_{r,yield}$ that would be required within the foundation and embankment materials of the north dike section to produce a calculated Factor of Safety equal to 1.0. This is not the

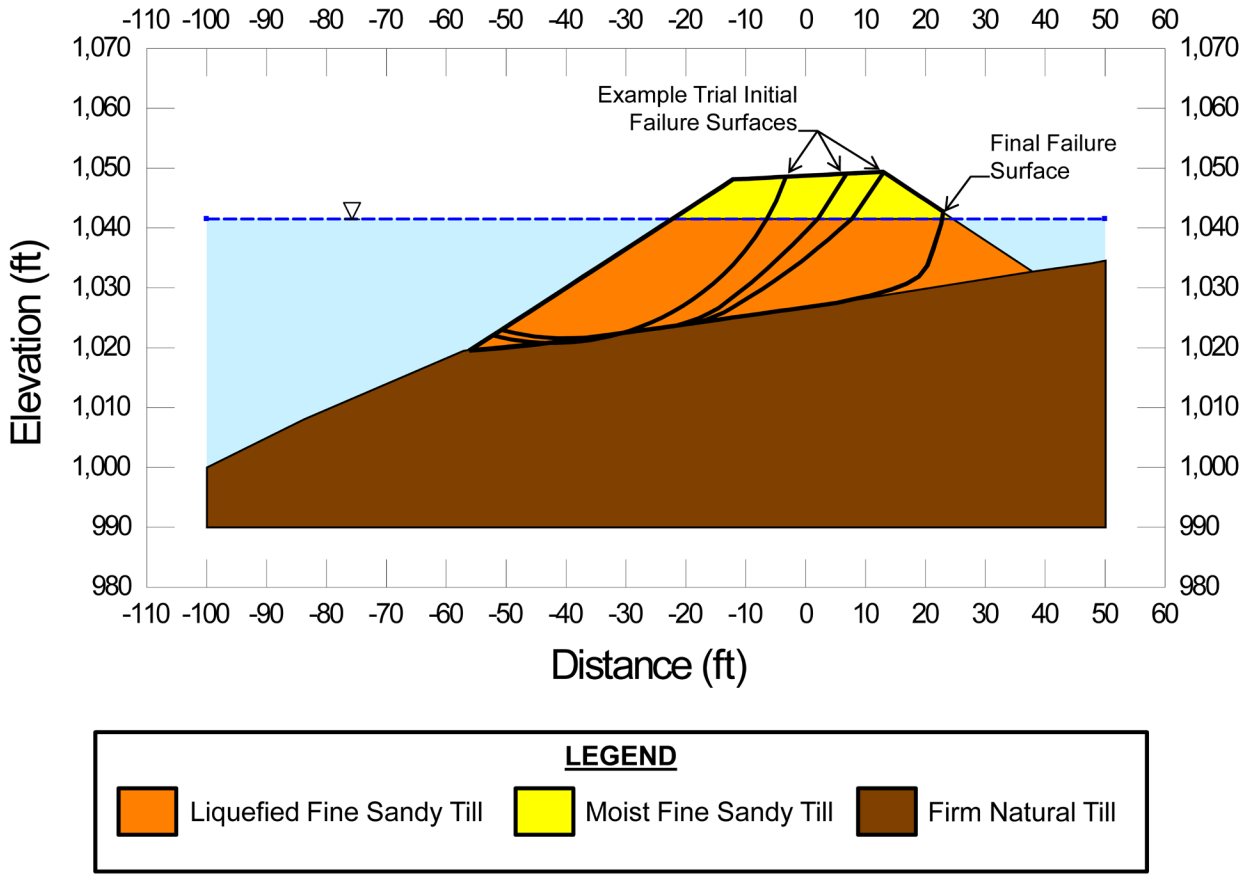

Figure B.13.4: Cross-section showing the pre-failure geometry and conditions for back-analyses of the initial yield strength ($S_{r,yield}$) for the failure section of the north dike of the Asele Road Embankment, showing examples of trial failure surfaces analyzed.

actual post-liquefaction strength, but it proves to be useful in developing estimates of post-liquefaction strength (S_r) for this case history.

The solid line in Figure B.13.4 shows the final back heel scarp of the slide. The dashed lines show a suite of potential initial failure surfaces analyzed for evaluation of $S_{r,yield}$. These are not a comprehensive representation, and additional potential failure surfaces were also analyzed here.

There were two general sets of potential failure mechanisms that could potentially explain the observed features: (1) the failure may have been incrementally retrogressive, initiating with a "slice" near to the front of the feature, and then retrogressing on a slice by slice basis towards the eventual back heel, or (2) the entire slide may have initiated monolithically (all at once). Both sets of possibilities were analyzed, and multiple potential "initial" failure surfaces were analyzed for the incrementally retrogressive scenario. In all cases, failure was modeled as occurring within the embankment fill. The phreatic surface was taken as the level of the lake at the time of the failure, and this was well-defined (as shown previously in Figure B.13.2.

Unit weights of the non-saturated sands and silty sands of the embankment fill above the phreatic surface were modeled with a unit weight of $\gamma_m \approx 115$ lbs/ft^3, and this was then varied over a range of 112 to 118 lbs/ft^3 for parameter sensitivity studies. Unit weights of the saturated sands and silty sands below the phreatic surface were modeled with a unit weight of $\gamma_s \approx 120$ lbs/ft^3, and this was then varied over a range of 117 to 123 lbs/ft^3 for parameter sensitivity studies. The friction angle of the embankment fill materials above the phreatic surface was modeled with $Ø' \approx 30°$, and a range of $Ø' \approx 28°$ to 32°.

As shown in Figure B.13.4, potential initial failure surfaces were modeled as either (1) wedge-like semi-translational features, or (2) semi-rotational/translational features, or (3) conforming essentially to the final observed overall failure scarp (the monolithically initiated scenario).

For the special case of the monolithically initiated scenario, involving initial failure on the eventual (final) observed overall failure scarp, the best estimate value of $S_{r,yield}$ was found to be $S_{r,yield} = 193$ lbs/ft^2, with a range of $S_{r,yield} \approx 154$ to 233 lbs/ft^2.

It was, however, the opinion of this current engineering team that the failure may have been at least somewhat incrementally retrogressive. Accordingly, a significant number of smaller "initial" potential (first slice) failure surfaces were also analyzed. The resulting best estimate value of $S_{r,yield}$ for smaller initial yield slices was found to be $S_{r,yield} = 344$ lbs/ft^2, with a range of $S_{r,yield} \approx 263$ to 426 lbs/ft^2.

In keeping with the tenets and protocols of these current studies, the values of $S_{r,yield}$ calculated for these potential "initial" slices were then averaged directly with the $S_{r,yield}$ values calculated for the monolithically initiated (eventual overall) failure surface as described above, and these averages values were taken as "representative" $S_{r,yield}$ values for incrementally retrogressive initiation scenarios. The averaging here was weighted averaging, based on judgment of the analysis team, using 2:1 weighting as

$$S_{r,yield} = [\ 2 \times S_{r,yield}\ (\text{smaller initial yield surface}) + S_{r,yield}\ (\text{final overall failure scarp})] / 3$$

Based on the range of variations in properties and parameters, and a range of potential failure mechanisms and associated feasible failure surfaces, the resulting best estimate overall of "representative" $S_{r,yield}$ was found to be $S_{r,yield} = 294$ lbs/ft^2, with a range of $S_{r,yield} \approx 227$ to 362 lbs/ft^2.

Olson (2001) also performed back-analyses to estimate $S_{r,yield}$. He analyzed a suite of two-wedge potential failure surfaces representing assumption of an overall retrogressive failure. The "initial" failure surfaces that he analyzed encompassed approximately 50% to 70% of the eventual overall failure, and he did not then average the resulting values of $S_{r,yield}$ with those associated with the eventual (final) overall failure scarp. Olson's best estimate of $S_{r,yield}$ was 16.8 kPa (351 lbs/ft^2), with a range of 13.9 to 18.9 kPa (290 to 395 lbs/ft^2), in reasonably good agreement with these current studies.

B.13.5 Residual Strength Analyses Based on Residual Geometry

It was not possible to perform rigorous and reliable back-analyses to determine the value of $S_{r,resid/geom}$ required to produce a calculated Factor of Safety equal to 1.0 based on residual geometry. This case is one of six cases (out of the 29 cases back-analyzed as part of these current studies) where the slide mass "went over a lip" and then traveled down a steeper slope, and the ensuing displacements either (1) could not be reliably tracked, or (2) could not be reliably back-analyzed. Both situations apply in this current case because the post-failure geometry of the failure mass runout is largely undefined. This is a significant source of uncertainty for this case history.

The large vibratory compactor had been rolling along at the forward edge of the level roadbed, just behind the lip of the pre-failure embankment. After the failure it was reported to have travelled laterally approximately 60 meters, in which case it would have ended up approximately 45 meters left of the pre-failure embankment toe shown in Figure B.13.4.

Konrad and Watts (1995) assumed that 60 meters at least approximately represented the distance of flow, and used the flow failure runout analysis method of Lucia (1981) to back-estimate an approximate value of $S_{r,resid/geom.} \approx$ 5 to 7.5 kPa (105 to 155 lbs/ft^2). Olson (2001) states that this back-calculation by the Lucia (1981) method produces shear strengths similar to those back-calculated by the simplified method, and so Olson adopts these values back-calculated by Konrad and Watts. The "simplified method" referred to by Olson is an infinite slope analysis of a stratum of uniform thickness, and is applied to post-liquefaction residual (final) geometry. The details of Olson's analyses using this approach are not presented.

The 60 meters of assumed slope displacement are not closely constrained by the available information. It is not clear that the heavy compactor would have experienced movements representative of those of the slope failure mass. The failure mass may have failed to transport the compactor the full distance, or the compactor may have traveled farther either by tumbling or due to its own momentum. These are, however, interesting points of comparison.

In these current studies, it was assumed that $S_{r,resid/geom}$ would have at least been higher than zero. Values of $S_{r,resid/geom}$ back-calculated from the reasonably well-documented Class A case histories were next examined, and for the range of effective overburden stress and $N_{1,60,CS}$ values for this current case an approximate range of $S_{r,resid/geom} \approx$ 101 to 162 lbs/ft^2 was conservatively assumed, based on analyses of other Class A and B case histories. This range of values was selected to be slightly conservatively biased (a conservative bias of approximately 10% reduction of best estimates of $S_{r,resid/geom}$ was targeted here), so that any resulting error in evaluation of overall S_r would also be slightly conservative (nominally by approximately 5% or so).

It is interesting to note that this range of $S_{r,resid/geom} \approx$ 101 to 162 lbs/ft^2 agrees fairly well with the ranges back-calculated by Konrad and Watts (1985) and also with the values apparently developed by Olson (2001), based on alternate approaches, as described above.

B.13.6 Overall Estimates of S_r

Overall estimates of S_r for this Class B case history were made based on the pre-failure geometry and the approximate runout features and characteristics, and the values of $S_{r,yield}$ and $S_{r,resid/geom}$ as calculated and/or estimated in the preceding sections.

Runout characteristics for this case cannot be accurately assessed due to the approximate nature of the post-failure cross section as reported. Runout distance, and runout ratio, appear to be "large", but the failure mass travelled out over a "lip" at the toe of the slide scarp, and then down what may have been a steeper slope.

Runout ratio (defined as runout distance traveled by the center of gravity of the overall failure mass divided by the initial slope height from toe to back heel of the failure) was taken to be at least medium to large. This allowed Equation 4-4, and Figures 4.7 and 4.11 to serve as one basis for estimation of post-liquefaction strength S_r. Using the ranges of $S_{r,yield}$ and $S_{r,resid/geom}$ from Sections B.13.4 and B.13.5, and assuming that $\xi \approx 0.35$ to 0.70 for this large runout case, with 0.525 as the best estimate, provided a best estimate value of $S_r \approx 112$ lbs/ft^2 and an estimated range of $S_r \approx 57$ to 178 lbs/ft^2. A second basis for estimation of S_r was the use of the relationship of Figure 4.9, and the range of values of $S_{r,yield}$ from Section B.5.4. Based on the large runout distance, values of initial (pre-failure displacement) Factor of Safety were taken as approximately 0.35 to 0.6, and this produced a best estimate value of $S_r \approx 140$ lbs/ft^2 and an estimated range of $S_r \approx 79$ to 217 lbs/ft^2. No similar use was made of Figure 4.9 in conjunction with the ranges of $S_{r,resid/geom}$ estimated in Section B.4.5 because these estimates of $S_{r,resid/geom}$ were considered to be very approximate.

The estimates by each of the two methods above were then averaged together, and this produced a best estimate value of $S_r \approx 126$ lbs/ft^2 and an estimated range of $S_r \approx 57$ to 217 lbs/ft^2. These estimates of variance are non-symmetric about the best estimated mean value, and the range was judged to represent approximately +/- 3 standard deviations.

Overall, based on an assumed normal distribution, it was judged that the (mean and median) best estimate of post-liquefaction strength for this case history is

$$\overline{S_r} = 137 \text{ lbs/ft}^2$$

and that the best estimate of standard deviation of mean overall post-liquefaction strength is

$$\sigma_{\overline{S}} = 27 \text{ lbs/ft}^2$$

Olson (2001) and Olson and Stark (2002) did not apply their "kinetics" method to this case, and so they did not independently develop an estimate of S_r that incorporated momentum effects. Instead they simply used their value of $S_{r,resid/geom}$ as a conservative approximation of S_r for this less well-defined case, and used $S_r = 5$ to 7.5 kPa (105 to 155 lbs/ft^2). in developing their predictive relationship. As described previously in Section B.13.5, this was actually the value of S_r back-calculated by Konrad and Watts (1995) based on back-calculation by the method of Lucia (1981), which was adopted by Olson (2001). Similarly, Wang (2003) and Wang and Kramer (2008) did

not employ their zero inertial force (ZIF) method to incorporate inertial effects in back-analyses of this failure. Instead they selected their value of S_r based on examination of back-analyses of several previous investigators, and in the end selected $\overline{S_r}$ = 163.6 lbs/ft^2, and a standard deviation of $\sigma_{\overline{S}}$ = 54.6 lbs/ft^2. Despite these differing approaches taken to evaluation and/or selection of S_r, agreement between the values used in these two previous studies, and the values developed and employed in these current studies, is good for this case history.

B.13.7 Evaluation of Initial Effective Vertical Stress

Average initial (pre-failure) effective vertical stress was assessed for the liquefied portion of the overall (final scarp) failure surface in Figure B.13.4. Parameters and sensitivity analyses were as described previously in Section B.13.4. Additional analyses were then performed for alternate potential failure surfaces, including failure surfaces initial (smaller) slices of a retrogressive incremental failure eventually extending back to the apparent back heel of the final failure. Depths of failure surfaces were varied, and both rotational and translational (wedge-like) failure surfaces were considered. When an initial (smaller) slice of a retrogressive failure was analyzed, the resulting average value of σ_{vo}' was then averaged with the value of the overall (Final slide scarp), and this averaged value of the two failure surfaces was taken as "representative" here. This produced a moderately large, but finite, range of estimated values of average pre-failure effective stress within the liquefied materials controlling the failure.

The resulting best estimate of average pre-failure effective stress within the liquefied materials controlling the failure was then $\sigma_{vo}' \approx$ 1,037 lbs/ft^2, with a reasonable range of $\sigma_{vo}' \approx$ 884 to 1,192 lbs/ft^2. This range is symmetric about the median value, and this range was judged by the engineering team to represent approximately ± 2 standard deviations. Overall, the best characterization of initial (pre-failure) average effective vertical stress was then taken to be represented by a mean value of

$$\overline{\sigma'_{vo}} \approx 1{,}037 \text{ lbs/ft}^2$$

and with a standard deviation of

$$\sigma_{\overline{\sigma}} \approx 77 \text{ lbs/ft}^2$$

An estimate of σ_{vo}' was also calculated by Olson and Stark (2001, 2002). They reported a weighted average mean value of $\sigma_{vo}' \approx$ 59.9 kPa (1,251 lbs/ft^2), in relatively good agreement with these current studies. Average initial vertical effective stresses were not directly reported by Wang (2003) and Kramer (2008), but they were published more recently in the publication by Kramer and Wang (2015). As discussed in Section 2.3.8.1(b)-(iii), Wang (2003) did not perform any independent analyses to assess σ_{vo}' for his 22 "secondary" cases, and this is one of those cases. Instead, he compiled values of S_r from multiple previous investigators, and averaged these for a best estimate. He also compiled multiple values of S_r/σ_{vo}' from previous investigators, and averaged these for a best estimate. He then used these two best-estimate values of S_r and S_r/σ_{vo}' to infer a resulting representative value of σ_{vo}'. As described in Section 2.3.8.1(b)-(iii), the

resulting averaged values of S_r and S_r/σ_{vo}' were incompatible with each other for a number of Wang's "secondary" case histories, and this process produced unreasonable, and in some cases physically infeasible, values of σ_{vo}' for a number of case histories. Wang's value of $\sigma_{vo}' = 1{,}573$ lbs/ft^2 appears physically infeasible, and so it is not considered a useful check here.

B.13.8 Evaluation of $N_{1,60,CS}$

As explained previously in Section B.13.3, there were no published penetration test data for this failure case history, but Konrad and Watts (1995) reported a personal communication from Prof. Rainer Masarch, who conducted a post-failure investigation of the Asele Road Embankment. Prof. Masarch reported an average $N_{1,60}$ value of approximately 6 to 8 blows/ft, but the details of SPT equipment and procedures, and the corrections and adjustments made to produce these $N_{1,60}$ values, are not known. There was also no information presented as to how potential interference of gravel sized particles was dealt with in this glacial till fill material with a maximum screened particle size of approximately ¾ inches. As a result, there is potentially significant uncertainty with regard to selection of representative $N_{1,60,CS}$ values for this case history.

Olson (2001) and Olson and Stark (2002) took the middle of the reported range, and selected a "representative" $N_{1,60}$ value of 7 blows/ft., with no range given. This was an $N_{1,60}$ value, and reflected no fines adjustment. Given the relatively high reported silty fines content of the fill, fines adjustment to produce $N_{1,60,CS}$ values would be expected to increase this value.

Wang (2003) and Kramer (2008) selected a somewhat higher fines adjusted value of $\overline{N_{1,60,CS}} \approx 11.0$ blows/ft, and a very high standard deviation of $\sigma_{\overline{N}} \approx 10.7$ blows/ft. This very high standard deviation produces a value of $N_{1,60,CS}$ equal to zero at just the mean minus 1.03 standard deviations level, and at a mean plus two standard deviations the value would be approximately 32.4 blows/ft, which appears to be unreasonably high for the materials as described (and as they performed). This very high standard deviation in mean $N_{1,60,CS}$ is an artifact of the rigorously defined approach taken to evaluation of $N_{1,60,CS}$ in Wang's work, and it should be noted that neither the negative $N_{1,60,CS}$ values at mean minus more than 0.71 standard deviations, nor the very high values at mean plus more than about 2 standard deviations, likely had significant impact on their overall predictive correlations. Their uncertainty or variance was exceptionally high with regard to $N_{1,60,CS}$, and the impact of this case history on the regressions that produced their predictive relationships was then even further reduced by assigning a very low "Weighting Factor" of WF = 0.20 for this case.

In these current studies, the values reported by Konrad and Watts (1995) attributed to Prof. Masarch were taken as the best available data, but with consideration of the associated uncertainties and variance. In these current studies, a best estimate value of $\overline{N_{1,60,CS}} \approx 9.5$ blows/ft was selected, with a standard deviation of $\sigma_{\overline{N}} \approx 2.0$ blows/ft.

Overall agreement with regard to characterization of $N_{1,60,CS}$ among these two previous studies, and the current study, is considered generally good for this case with the exception of characterization of variance (or standard deviation) of the mean value of $N_{1,60,CS}$.

B.14 Nalband Railway Embankment (Armenia; 1988)

B.14.1 Brief Summary of Case History Characteristics

Name of Structure	Nalband Railway Embankment
Location of Structure	Armenia
Type of Structure	Earthen Embankment
Date of Failure	December 7, 1988
Nature of Failure	Seismic, During 1988 Armenia Earthquake (M_S = 6.8)
Approx. Maximum Slope Height	20.5 ft.

B.14.2 Introduction and Description of Failure

The Nalband Railway Embankment experienced a liquefaction-induced ground and slope failure as a result of the Armenia earthquake of December 7, 1988 (M_S = 6.8) in the Northwest region of Armenia. A total more than 1,000 multistory buildings collapsed or were damaged beyond repair, and more than 40,000 casualties were attributed to the event. Areas where liquefaction was observed were investigated by researchers funded by the U.S. National Science Foundation. Liquefaction in the area was largely attributed to loose to medium dense gravelly sands (Yegian et al., 1994).

Figure B.14.1 presents a photo reproduced from Yegian et al. (1994) showing the damage attributed to liquefaction of the foundation soils at the Nalband Railway Embankment. Maximum observed displacements, as reported in Yegian et al. (1994), were approximately 3 meters vertically 2 meters horizontally.

The peak ground acceleration recorded at a strong motion station approximately 25 km away from the Nalband site was 0.2g. Peak ground accelerations between 0.5 to 1.0g were estimated closer to the Nalband site, based on damage observed in the area. Figure B.14.2 presents a plan view of the region, showing the location of the Nalband site, the location of the strong motion station, and the rupturing fault trace (Yegian et al., 1994).

B.14.3 Geology and Site Conditions

Figure B.14.3 shows a cross section of the failure as reported in Yegian et al. 1994.

Two borings (NB-1 and NB-2) were drilled following the event in the locations presented on the cross section presented in Figure B.14.3. Boring NB-1 was drilled through what appears to be the toe of the failure, and boring NB-2 was drilled adjacent to the heel of the failure outside of the apparent failure mass. Logs of these exploratory SPT borings as presented in Yegian et al. (1994) are reproduced as Figure B.14.5. Yegian et al. report that the phreatic surface was

unusually high in the area of the failure due to the shape of the natural terrain, and found evidence of a

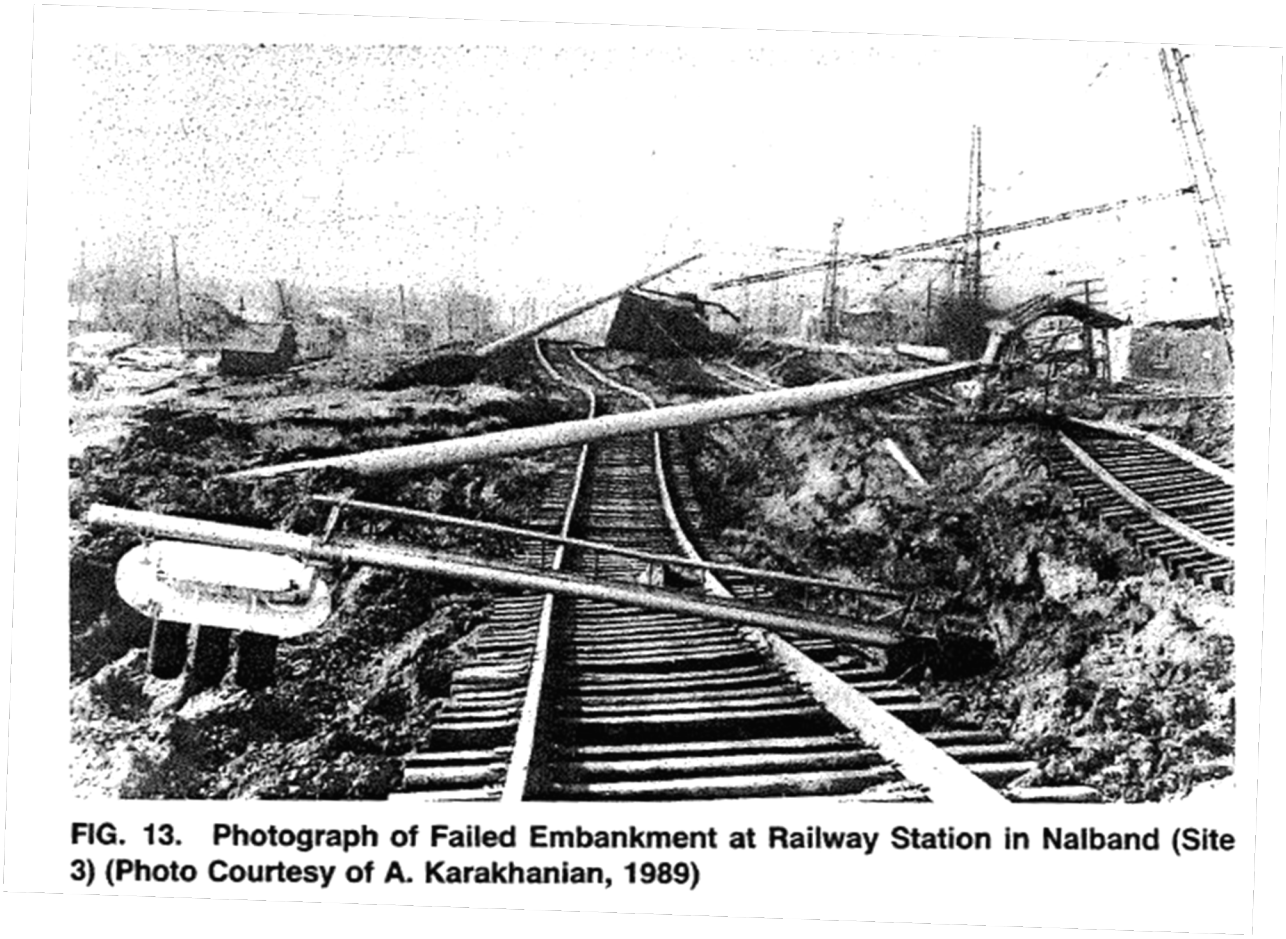

FIG. 13. Photograph of Failed Embankment at Railway Station in Nalband (Site 3) (Photo Courtesy of A. Karakhanian, 1989)

Figure B.14.1: Photo of the failure of the railway embankment near Nalband (from Yegian et al., 1994)

high phreatic surface in the area adjacent to the failed embankment. The embankment in this area was constructed of compacted sand fill over loosely dumped gravelly sand material, which was in turn underlain by naturally sloping volcanic tuff (Yegian et al., 1994).

B.14.4 Initial Yield Stress Analyses

Figure B.14.4 shows the cross-section used for back-analyses of the post-liquefaction initial yield strength $S_{r,yield}$ that would be required within the foundation and embankment materials of the north dike section to produce a calculated Factor of Safety equal to 1.0. This is not the actual post-liquefaction strength, but it proves to be useful in developing estimates of post-liquefaction strength (S_r) for this case history.

There were two general sets of potential failure mechanisms that could potentially explain the observed features: (1) the failure may have been incrementally retrogressive, initiating with a

"slice" near to the front of the feature, and then retrogressing on a slice by slice basis back towards the eventual back heel, or (2) the entire slide may have initiated monolithically (all at once). Both

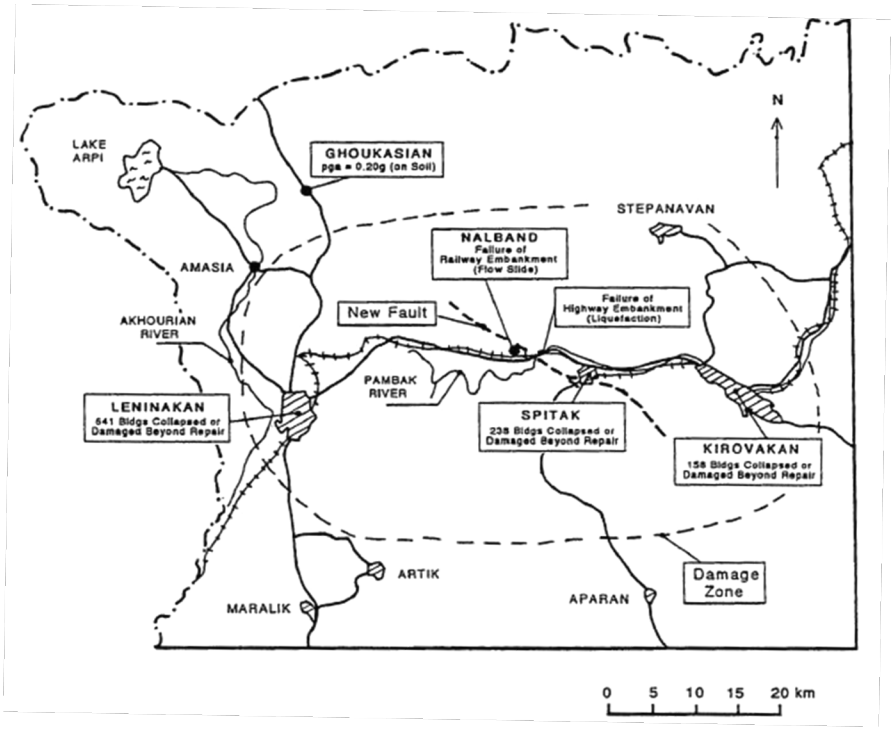

Figure B.14.2: Plan view of the failure of the region surrounding the Nalband Railway Embankment failure (from Yegian et al., 1994).

sets of possibilities were analyzed, and multiple potential "initial" failure surfaces were analyzed for the incrementally retrogressive scenario. In all cases, failure was modeled as occurring within the loose, saturated gravelly sand with silt immediately underlying the embankment fill.

Unit weights of the non-saturated compacted silty sand embankment fill above the phreatic surface were modeled with a unit weight of $\gamma_m \approx 128$ lbs/ft^3, and this was then varied over a range of $\gamma_m \approx 123$ to 133 lbs/ft^3 for parameter sensitivity studies. Unit weights of the saturated compacted silty sand below the phreatic surface were modeled with a unit weight of $\gamma_s \approx 133$ lbs/ft^3, and this was then varied over a range of 128 to 138 lbs/ft^3 for parameter sensitivity studies. The saturated foundation gravelly sand with silt below the phreatic surface were modeled with a unit weight of $\gamma_s \approx 125$ lbs/ft^3, and this was then varied over a range of 120 to 130 lbs/ft^3 for parameter sensitivity studies. The friction angle of the embankment fill materials above the phreatic surface was modeled with $Ø' \approx 33°$, and a range of $Ø' \approx 30°$ to 35°.

Potential initial failure surfaces were modeled as either (1) wedge-like semi-translational features, or (2) semi-rotational/translational features, or (3) conforming essentially to the final observed overall failure scarp (the monolithically initiated scenario).

For the special case of the monolithically initiated scenario, involving initial failure on the eventual (final) observed overall failure scarp, the best estimate value of $S_{r,yield}$ was found to be $S_{r,yield}$ = 172 lbs/ft^2, with a range of $S_{r,yield}$ ≈ 157 to 187 lbs/ft^2.

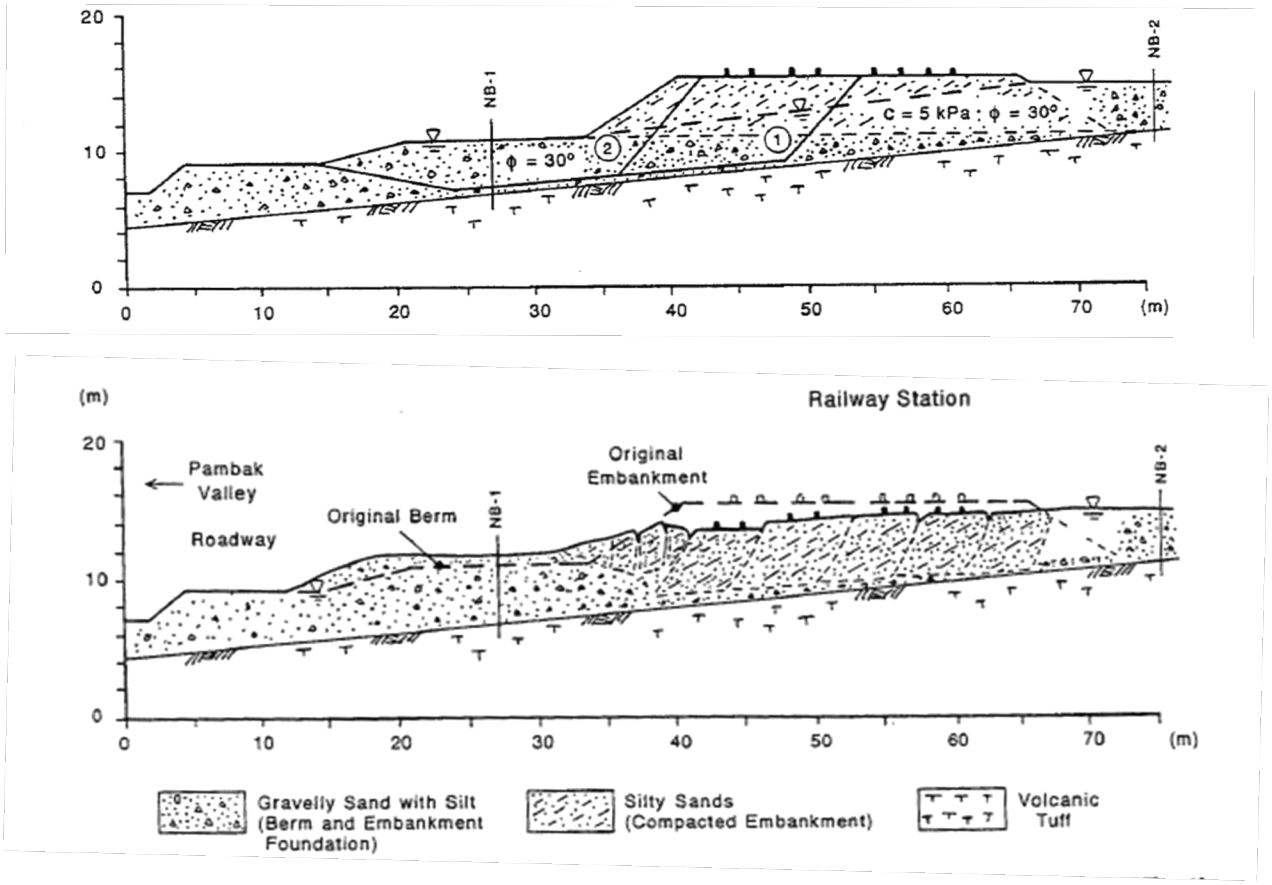

Figure B.14.3: Pre- and post-failure cross sections of the railway embankment failure near Nalband (from Yegian et al., 1994)

A significant number of smaller "initial" potential (first slice) failure surfaces were also analyzed, corresponding to a scenario in which the overall failure may have been retrogressive in nature. Figure B.14.4(a) shows a semi-rotational initial failure surface that was the most critical potential initiating failure surface found (lowest post-liquefaction Factor of Safety), but additional potential failure surfaces were also analyzed, including failure surfaces with their rear scarps set back further into the tailings impoundment. The resulting best estimate value of $S_{r,yield}$ for smaller initial yield slices was found to be $S_{r,yield}$ = 249 lbs/ft^2, with a likely range of $S_{r,yield}$ ≈ 231 to 268 lbs/ft^2.

In keeping with the tenets and protocols of these current studies, the values of $S_{r,yield}$ calculated for these potential "initial" slices were then averaged directly with the $S_{r,yield}$ values calculated for the monolithically initiated (eventual overall) failure surface as described above, and these averages values were taken as "representative" $S_{r,yield}$ values for incrementally retrogressive initiation scenarios. Both scenarios were taken as equally as likely and therefore the results were averaged with equal weighting.

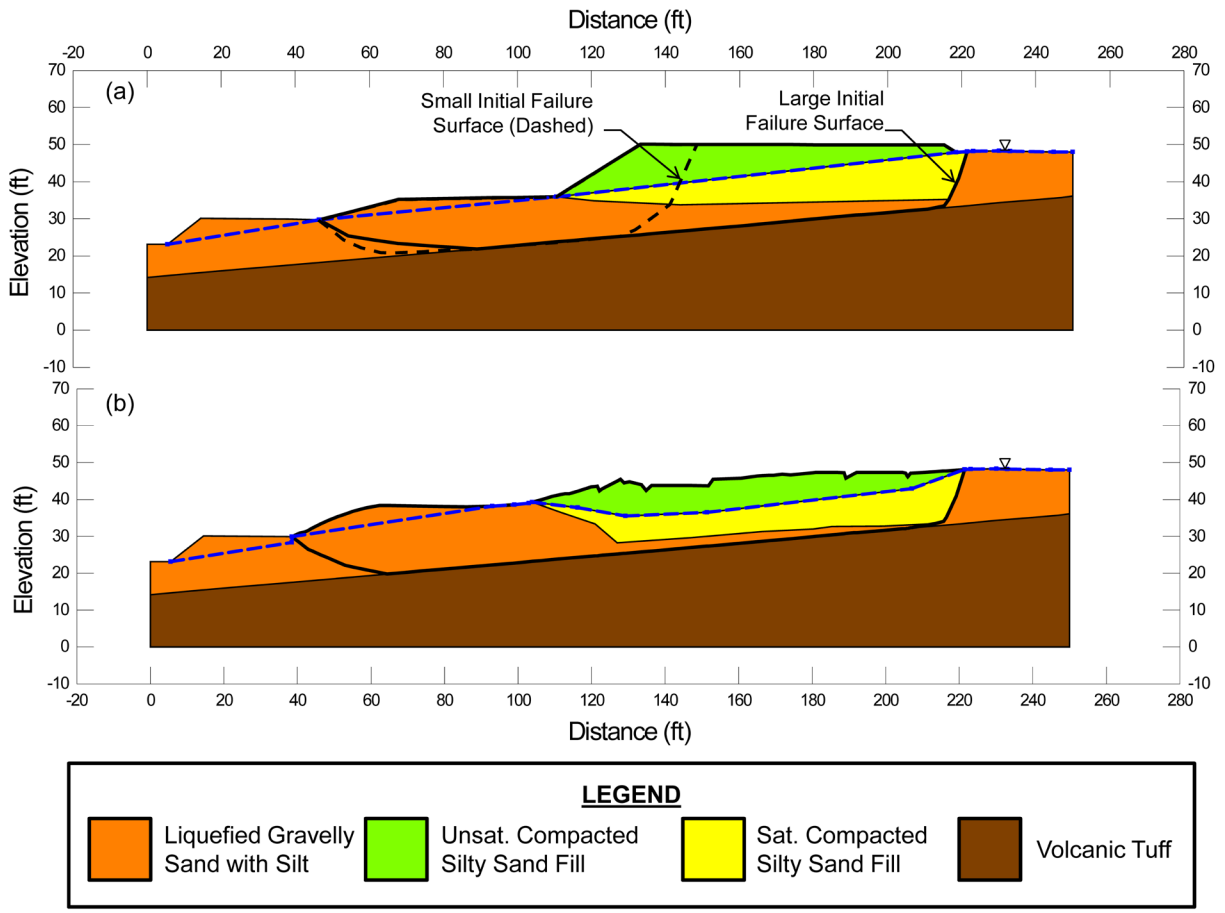

Figure B.14.4: Pre- and post-failure cross-sections of the Nalband Railway Embankment used for back-analyses of $S_{r,yield}$ and $S_{r,resid\ geom}$.

Based on the range of variations in properties and parameters, and a range of potential failure mechanisms and feasible failure surfaces, the resulting best estimate of "representative" overall $S_{r,yield}$ was found to be $S_{r,yield}$ = 211 lbs/ft^2, with a range of $S_{r,yield} \approx$ 194 to 228 lbs/ft^2.

Olson (2001) also performed back-analyses to evaluate $S_{r,yield}$. He analyzed only block surfaces within the fill material that were tangent to the volcanic tuff foundation, similar to initial surfaces utilized in this study as presented in Figure B.14.4(a). His best estimate value was $S_{r,yield}$ = 8.9 kPa (186 lbs/ft^2), with a range of $S_{r,yield} \approx$ 8.6 to 9.6 kPa (180 to 200 lbs/ft^2).

B.14.5 Residual Strength Analyses Based on Residual Geometry

The calculation of the "apparent" post-liquefaction strength ($S_{r,resid/geom}$) required to produce a calculated Factor of Safety equal to 1.0 based on residual geometry is illustrated in Figure B.14.3(b). Modeling parameters and details are as described in the preceding section.

Based on the cross-sections shown in Figure B.14.3(b), and the properties and parameters described above, the best-estimate value of $S_{r,resid/geom}$ was $S_{r,resid/geom}$ = 138 lbs/ft^2. Parameters

were next varied, as described previously, including analyses of alternate potential failure surfaces slightly above and below the failure surface shown in Figure B.5.4(b). Based on these analyses, it was judged that a reasonable range was $S_{r,resid/geom} \approx 128$ to 149 lbs/ft^2.

Olson (2001) also back-calculated values of $S_{r,resid/geom}$. His best estimate failure surface was a block failure tangent to the volcanic tuff foundation, similar to final surface assumed in this study presented in Figure B.14.3(b). He again assumed, however, that the fill materials largely controlled the failure. Olson's back-calculated best estimate of $S_{r,resid/geom}$ was 5.7 kPa (119 lbs/ft^2), with a range of 5.3 to 6.2 kPa (111 to 129 lbs/ft^2).

B.14.6 Overall Estimates of S_r

Overall estimates of S_r for this Class B case history were made based on the pre-failure geometry, the partial post-failure geometry, the approximate runout features and characteristics, and the values of $S_{r,yield}$ and $S_{r,resid/geom}$ as calculated and/or estimated in the preceding sections.

Runout distance of the center of mass of the overall failure was approximately D = 7 feet, and the initial failure slope height was H = 20.5 feet. This produces a runout ratio (defined as runout distance traveled by the center of gravity of the overall failure mass divided by the initial slope height from toe to back heel of the failure) of D/H = 0.34. This allows Equation 4-4, and Figures 4.7 and 4.11, to serve as one basis for estimation of post-liquefaction strength S_r. Using the ranges of $S_{r,yield}$ and $S_{r,resid/geom}$ from Sections B.13.4 and B.13.5, and assuming that $\xi \approx 0.8$ to 0.99 for this short runout case, with 0.9 as the best estimate, provided a best estimate value of $S_r \approx 158$ lbs/ft^2 and an estimated range of $S_r \approx 129$ to 187 lbs/ft^2. A second basis for estimation of S_r was the use of the relationship of Figure 4.9, and the range of values of $S_{r,yield}$ from Section B.5.4. Based on the large runout distance, values of initial (pre-failure displacement) Factor of Safety were taken as approximately 0.7 to 0.9, and this produced a best estimate value of $S_r \approx 169$ lbs/ft^2 and an estimated range of $S_r \approx 136$ to 205 lbs/ft^2. No similar use was made of Figure 4.9 in conjunction with the ranges of $S_{r,resid/geom}$ estimated in Section B.4.5 because these estimates of $S_{r,resid/geom}$ were considered to be very approximate.

The estimates by each of the two methods above were then averaged together, and this produced a best estimate value of $S_r \approx 163$ lbs/ft^2 and an estimated range of $S_r \approx 129$ to 205 lbs/ft^2. These estimates of variance are non-symmetric about the best estimated mean value, and the range was judged to represent approximately +/- 2.5 standard deviations, so further adjustments were then necessary.

Overall, based on an assumed normal distribution, it was judged that the (mean and median) best estimate of post-liquefaction strength for this case history is

$$\overline{S_r} = 167 \text{ lbs/ft}^2$$

and that the best estimate of standard deviation of mean overall post-liquefaction strength is

$$\sigma_{\overline{S}} = 15 \text{ lbs/ft}^2$$

Olson (2001) and Olson and Stark (2002) did not apply their "kinetics" method to this case, and so they did not independently develop an estimate of S_r that incorporated momentum effects. Instead they simply used their value of $S_{r,resid/geom}$ as a conservative approximation of S_r for this less well-defined case, and used S_r = 5.7 kPa (119 lbs/ft^2), with a range of 5.3 to 6.2 kPa (111 to 129 lbs/ft^2) in developing their predictive relationship. Because these values are based on residual post-failure geometry with an assumed Factor of Safety equal to 1.0, they do not include momentum effects and so they will be too low.

A better estimate of S_r that approximately incorporates momentum effects, and a better basis for comparison with these current studies, can be obtained by employing Olson's best estimate values of $S_{r,yield}$ = 186 lbs/ft^2 and $S_{r,resid/geom}$ = 119 lbs/ft^2, and an assumed average value of $\xi \approx 0.8$ in Equation 4-4 as

$$S_r \approx 0.5 \text{ x } [186 \text{ lbs/ft}^2 + 119 \text{ lbs/ft}^2] \text{ x } 0.8 = 122 \text{ lbs/ft}^2$$

This value ($S_r \approx$ 122 lbs/ft^2) agrees fairly well with the best estimate value of $S_r \approx$ 92 lbs/ft^2 developed in these current studies.

Similarly, Wang (2003) and Wang and Kramer (2008) did not employ their zero inertial force (ZIF) method to incorporate inertial effects in back-analyses of this failure. Instead they selected their value of S_r based on examination of back-analyses of several previous investigators, and in the end selected $\overline{S_r}$ = 140 lbs/ft^2, and a standard deviation of $\sigma_{\overline{S}}$ = 40.2lbs/ft^2. The best estimate was judged to be in fairly good agreement with the values developed in these current studies, but their standard deviation was significantly larger.

B.14.7 Evaluation of Initial Effective Vertical Stress

Average initial (pre-failure) effective vertical stress was assessed for the liquefied portion of the large final failure surface in Figure B.4.4. Parameters and sensitivity analyses were as described previously in Section B.14.4. Additional analyses were then performed for alternate potential failure surfaces, including failure surfaces representing the end result of retrogressive incremental failures extending back to the apparent back heel of the final failure. Depths of failure surfaces were varied, and both rotational and translational (wedge-like) failure surfaces were considered. This produced a moderately large, but finite, range of estimated values of average pre-failure effective stress within the liquefied materials controlling the failure.

The resulting best estimate of average pre-failure effective stress within the liquefied materials controlling the failure was then $\sigma_{vo}' \approx$ 1,201 lbs/ft^2, with a reasonable range of $\sigma_{vo}' \approx$ 1,021 to 1,397 lbs/ft^2. This range is slightly non-symmetric about the median value, and this range was judged by the engineering team to represent approximately ± 2 standard deviations. Overall, the best characterization of initial (pre-failure) average effective vertical stress was then taken to be represented by a mean value of

$$\overline{\sigma'_{vo}} \approx 1{,}209 \text{ lbs/ft}^2$$

and with a standard deviation of

$$\sigma_{\bar{\sigma}} \approx 94 \text{ lbs/ft}^2$$

An estimate of σ_{vo}' was also calculated by Olson and Stark (2001, 2002). They reported a weighted average mean value of $\sigma_{vo}' \approx 48.9$ kPa (1,021 lbs/ft^2), in good agreement with these current studies. Average initial vertical effective stresses were not directly reported by Wang (2003) and Kramer (2008), but they were published more recently in the publication by Kramer and Wang (2015). As discussed in Section 2.3.8.1(b)-(iii), Wang (2003) did not perform any independent analyses to assess σ_{vo}' for his 22 "secondary" cases, and this is one of those cases. Instead, he compiled values of S_r from multiple previous investigators, and averaged these for a best estimate. He also compiled multiple values of S_r/σ_{vo}' from previous investigators, and averaged these for a best estimate. He then used these two best-estimate values of S_r and S_r/σ_{vo}' to infer a resulting representative value of σ_{vo}'. As described in Section 2.3.8.1(b)-(iii), the resulting averaged values of S_r and S_r/σ_{vo}' were incompatible with each other for a number of Wang's "secondary" case histories, and this process produced unreasonable values for a number of case histories. Wang's value of $\sigma_{vo}' = 1{,}283$ lbs/ft^2 for this case, however, is in very good agreement with the value developed in these current studies. Overall, agreement between the values of (1) Olson (2001), (2) Wang (2003) and (3) these current studies is considered to be very good here.

B.14.8 Evaluation of $N_{1,60,CS}$

As discussed previously in Section B.14.3, there were two borings performed following the failure. The location of the borings and the logs of the borings can be seen in Figures B.14.3 and B.14.5, respectively. Only one of the explorations, boring NB-1 to approximately a depth of 9 ft (3 m), was performed in the failed mass. There were two recorded blowcounts, with N values of 4 and 14 blows/ft, in the saturated gravelly sand with silt (Yegian et al., 1994).

In this current study, it is judged that the loose material in the upper part of the layer (N = 4 blows/ft) is likely more representative of the material that controlled the failure. The higher blowcount (N = 14 blows/ft) found near the lower part of the unit was judged to have likely been influenced by the gravels reported to be present in the material, and may also have been by the underlying very dense gravel and fractured tuff material. The precise drilling procedure, equipment and conditions are unknown. Assuming no energy correction (ER = 60%), after applying corrections the approximate representative value of $N_{1,60} \approx 6$ blows/ft is assumed. The effects of fines content of the silty gravelly sand were also considered. Incorporating all corrections and considering the sparseness and large degree of uncertainty of the data for this case history, characterization of penetration resistance for these current studies was then taken as $\overline{N_{1,60,CS}} \approx 7.5$ blows/ft, with a standard deviation of $\sigma_{\overline{N}} \approx 2.5$ blows/ft.

Olson (2001), in his assessment of the data from Yegian et al. (1994), also assumed an energy ratio of about 60%. However, Olson elected to incorporate a gravel content correction suggested by Terzaghi et al. (1996) for the average 20% gravel content in the material. He did not

state what blowcount values were considered in his assessment. In the end, his selected representative penetration resistance was $N_{1,60} \approx 9.2$ blows/ft, with a range of 3.6 to 12.4 blows/ft.

Wang (2003) and Kramer (2008) also focused on the test (4 blows/ft) in the upper part of the unit for the assessment of the representative penetration resistance, however, it appears that either no corrections were applied or the corrections were counteracting as the representative value of $N_{1,60} \approx 4$ blows/ft was reported. A similar fines content correction was applied to produce an adjusted value of $\overline{N_{1,60,CS}} \approx 6.3$ blows/ft, and a high standard deviation of $\sigma_{\overline{N}} \approx 5.6$ blows/ft was selected.

Overall agreement with regard to characterization of $N_{1,60,CS}$ among these two previous studies, and the current study, is generally good for this case with the exception of characterization of variance (or standard deviation) of the mean value of $N_{1,60,CS}$.

B.15 Sullivan Mine Tailings Dam (British Columbia, Canada; 1991)

B.15.1 Brief Summary of Case History Characteristics

Name of Structure	Sullivan Mine Tailings Dam
Location of Structure	Southeastern British Columbia, Canada
Type of Structure	Tailings Dam
Date of Failure	August 23, 1991
Nature of Failure	Static liquefaction flow failure during dyke raising
Approx. Maximum Slope Height	37.6 ft.

B.15.2 Introduction and Description of Failure

The Sullivan Mine is a base metal mine that was established in 1905 near Kimberly in southeastern British Colombia, Canada. Impoundments have been produced over the years to contain the mine tailings. Not much is known about the either the design or construction methods implemented before the early 1970's. There was, however, an embankment failure in 1948 leading to a release of about 1 million tons of iron tailings. Beginning in the early 1970's, each impoundment raise was engineered independently, using increasingly modern approaches (Jefferies and Been, 2006).

On August 23, 1991, a static liquefaction failure occurred during a 2.4 m raising of an impoundment dyke. The failure encompassed about 300 m of crest, and the toe of the failure moved laterally up to 45 m in the downstream direction. About 75,000 m^3 (100,000 yd^3) of tailings were involved in the failure. Before the failure, the dyke had reached a maximum height of 21 m (approx. 70 ft.). Slopes of the post-failure mass reportedly ranged from 1:10 (V:H) to 1:5. The failure is reported to have occurred quickly, and sand boils were observed immediately after the event and continued for hours, leading to the conclusion that the failure was due to static liquefaction (Jefferies and Been, 2006).

Construction of the dyke had been performed by the upstream placement method. During the raising of the dyke, engineers were concerned about pore pressures and were monitoring piezometers at the site. Pore pressures are reported to have been in general within a few feet of the ground surface and above the dyke toe. The last recordings before the failure were taken in mid-July. At that time, some piezometers were showing a declining trend in pore pressures. It was not reported as to how the timing of the recordings correlated to timing of the construction of lifts of the dyke (Jefferies and Been, 2006).

A picture of the failed mass is presented in Figure B.15.1, and pre- and post-failure cross sections reported by Jefferies and Been are shown in Figure B.15.2.

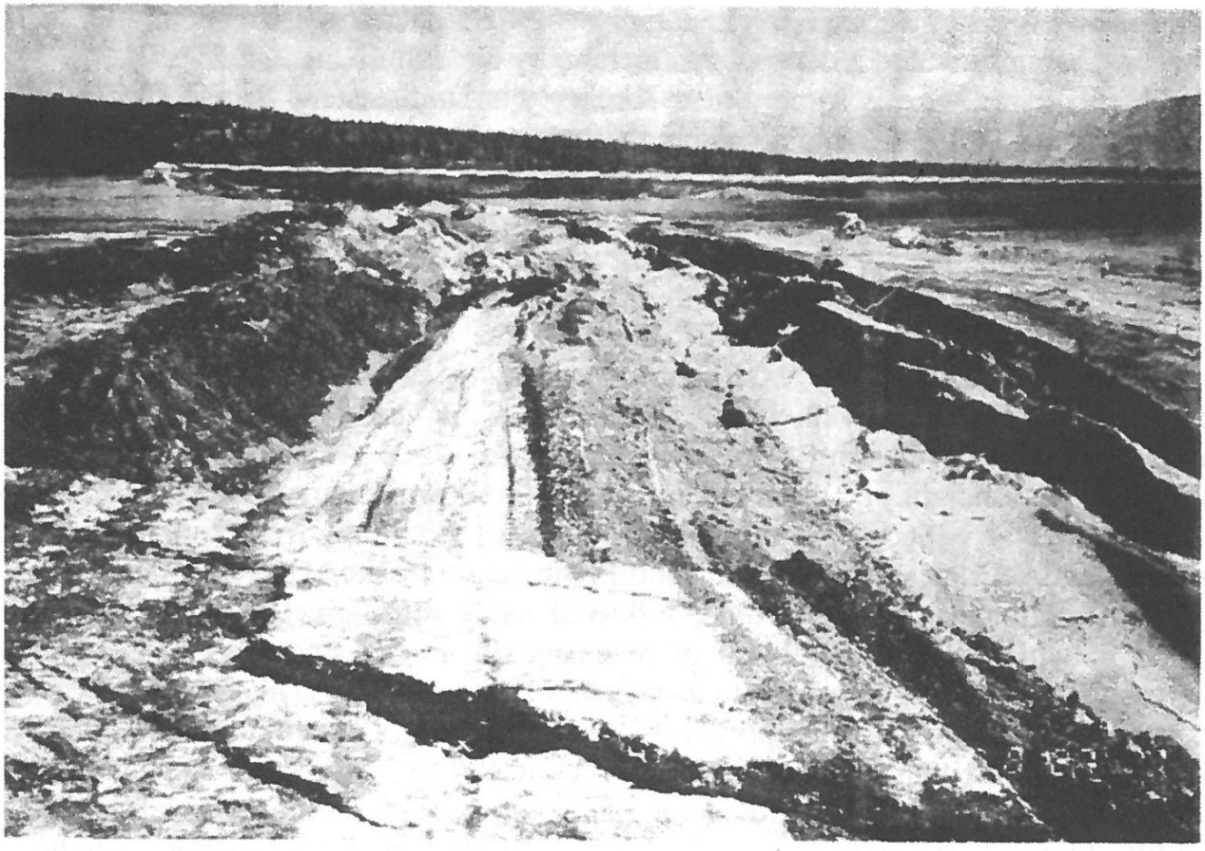

Figure B.15.1: Photograph showing the Sullivan Mine tailings dyke failure (from Jefferies and Been, 2006; originally from Davies, Dawson and Chin, 1998).

B.15.3 Geology and Site Conditions

Following the failure, 42 CPTs were advanced at the mine site. Of those 42 CPTs, 12 were advanced in the area of the failed mass. A sub-set of those explorations were reported by Jefferies and Been and are reproduced in figure B.15.4. The soils encountered in the explorations showed a wide range of materials. Dense sandy material was encountered in the areas of the containment dykes. Loose sandy silts were encountered in the area under the dykes and at the toe of the failure. The loose silts were underlain by dense till. (Jefferies and Been, 2006)

Jefferies and Been (2006) reported estimated bulk unit weights of the compacted fill and iron silt tailings as being 22.4 and 24.0 kN/m^3 (approximately 143 to 153 lbs/ft^3), respectively. The sandy silt iron tailings were also reported by Jefferies and Been to have a fines content of 50 percent or more (passing #200 sieve), and the silts were non-plastic.

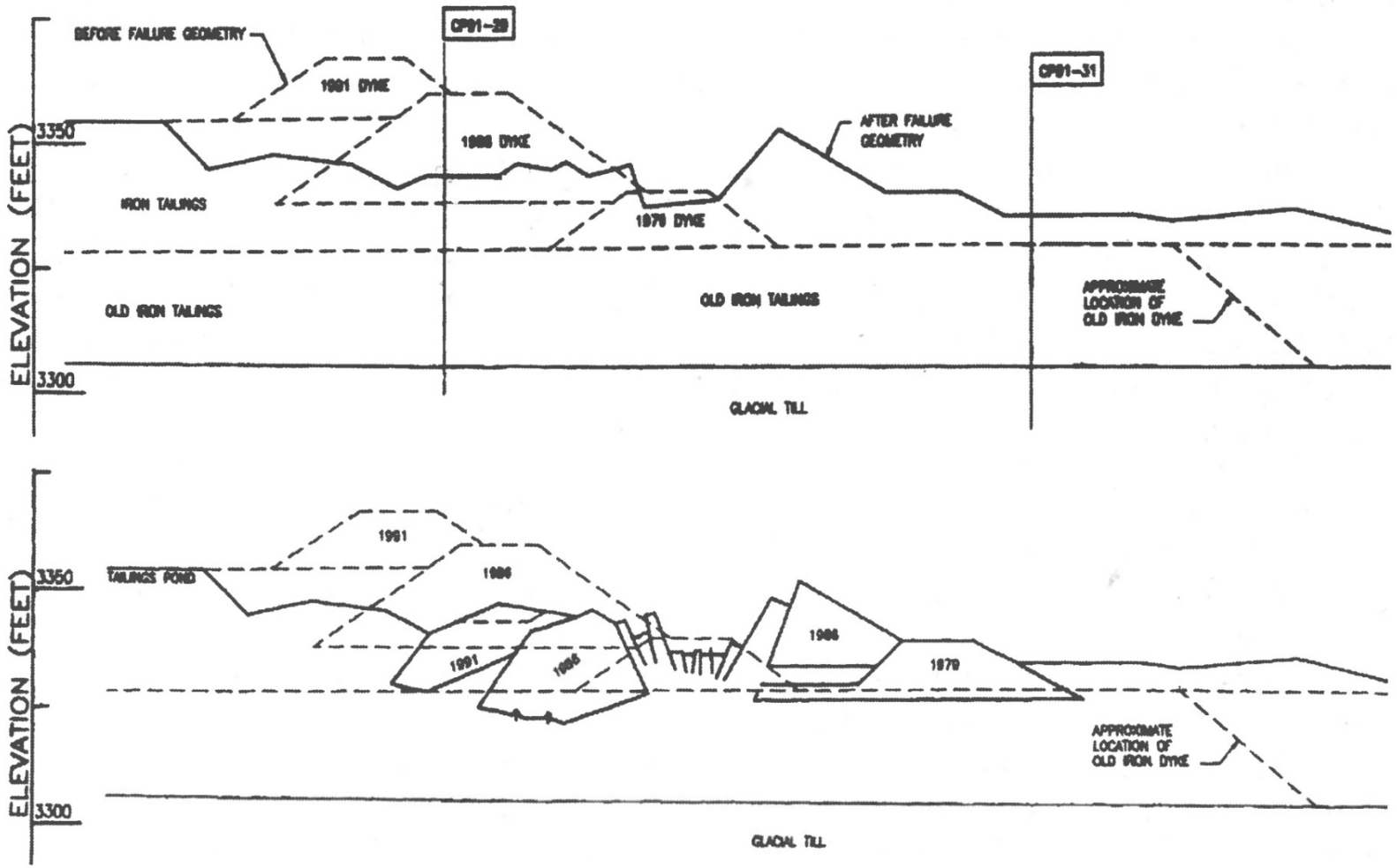

Figure B.15.2: Pre- and post-failure cross sections of the Sullivan Mine tailings dyke failure. Also shown is the location of CPTs CP91-29 and CP91-31 (from Jefferies and Been, 2006; originally from Davies, Dawson and Chin, 1998).

B.15.4 Initial Yield Stress Analyses

Figure B.15.3 shows the cross-section used for back-analyses of the post-liquefaction initial yield strength $S_{r,yield}$ that would be required within the tailings materials of the typical section of the Sullivan Mine tailings to produce a calculated Factor of Safety equal to 1.0 for static, pre-failure conditions. This is not the actual post-liquefaction strength, but it proves to be useful in developing estimates of post-liquefaction strength (S_r) for this case history.

Unit weights of the non-saturated compacted sand dyke fill above the phreatic surface were modeled with a unit weight of $\gamma_m \approx 130$ lbs/ft^3, and this was then varied over a range of $\gamma_m \approx 125$ to 135 lbs/ft^3 for parameter sensitivity studies. Unit weights of the saturated compacted sand dyke fill below the phreatic surface were modeled with a unit weight of $\gamma_s \approx 135$ lbs/ft^3, and this was then varied over a range of 130 to 140 lbs/ft^3 for parameter sensitivity studies. Unit weights of the moist iron tailings above the phreatic surface were modeled with a unit weight of $\gamma_m \approx 140$ lbs/ft^3, and this was then varied over a range of $\gamma_m \approx 135$ to 145 lbs/ft^3 for parameter sensitivity studies. Unit weights of the saturated iron tailings below the phreatic surface were modeled with a unit weight of $\gamma_s \approx 145$ lbs/ft^3, and this was then varied over a range of 140 to 145 lbs/ft^3 for parameter sensitivity studies. The friction angle of the compacted sand dyke fill materials above the phreatic surface was modeled with $Ø' \approx 35°$, and a range of $Ø' \approx 32°$ to 38°. The friction angle of the iron sandy silt tailings above the phreatic surface was modeled with $Ø' \approx 32°$, and a range of $Ø' \approx 29°$ to 35°.

Jefferies and Been (2006) interpreted the failure as starting with the translational movement of the embankment toe comprising the 1979 dyke and part of the 1986 dyke followed by movement of the remaining dyke sections. This description would lead to an initial failure surface that shears the 1986 dyke and exits past the toe of the 1979 dyke. Another interpretation of the failure would include the initiating movements encompassing the entire mass at once, with the 1979 dyke and part of the 1986 dyke separating and translating further downstream as the failure progressed. Given the post failure geometry, both interpretations appear to be potentially valid. Potential initial failure surfaces were modeled as either (1) wedge-like semi-translational features, or (2) semi-rotational/translational features, or (3) conforming essentially to the final observed overall failure scarp (the monolithically initiated scenario).

For the special case of the monolithically initiated scenario, involving initial failure on the eventual (final) observed overall failure scarp, the best estimate value of $S_{r,yield}$ was found to be $S_{r,yield} = 611$ lbs/ft^2, with a range of $S_{r,yield} \approx 565$ to 680 lbs/ft^2.

A significant number of smaller "initial" potential (first slice) failure surfaces were also analyzed, corresponding to a scenario in which the overall failure may have been retrogressive in nature. Figure B.15.3.3(a) shows an initial failure surface that was the most critical potential initiating failure surface found (lowest post-liquefaction, pre-displacement Factor of Safety) but additional potential failure surfaces were also analyzed, including failure surfaces with more translational features. The resulting best estimate value of $S_{r,yield}$ for smaller initial yield slices was found to be $S_{r,yield} = 643$ lbs/ft^2, with a likely range of $S_{r,yield} \approx 601$ to 715 lbs/ft^2.

The results of the various trial slip surfaces, shown in Figure B.15.3, and utilizing the best estimate parameters reported above, resulted in only moderate variations in $S_{r,yield}$ values. As modeled, the more critical toe failures were more rotational in nature and were unlikely to produce the translational nature of the failure at the toe. The large failure surfaces encompassing the entire embankment tended to produce failure surfaces more similar to that which could produce the movements observed. In keeping with the tenets and protocols of these current studies, the values of $S_{r,yield}$ calculated for these potential "initial" slices were then averaged directly with the $S_{r,yield}$ values calculated for the monolithically initiated (eventual overall) failure surface as described above, and these averages values were taken as "representative" $S_{r,yield}$ values for incrementally retrogressive initiation scenarios. Both scenarios were taken as equally as likely and therefore the results were averaged with equal weighting.

Based on the range of variations in properties and parameters, and a range of potential failure mechanisms and feasible failure surfaces, the resulting best estimate of "representative" overall $S_{r,yield}$ was found to be $S_{r,yield} = 627$ lbs/ft^2, with a range of $S_{r,yield} \approx 583$ to 698 lbs/ft^2.

Olson (2001) did not include this case history in his failure database and therefore did not perform back-analyses to evaluate $S_{r,yield}$.

B.15.5 Residual Strength Analyses Based on Residual Geometry

Back-analyses were also performed to evaluate the "apparent" post-liquefaction strength ($S_{r,resid/geom}$) required to produce a calculated static Factor of Safety equal to 1.0 based on residual geometry. This is not a direct measure of post-liquefaction strength (S_r), as it neglects momentum effects and would underestimate S_r, but it is useful for overall evaluation of S_r for this case history.

Figure B.15.3 (b) shows the post-failure cross-section geometry and example assumed range of slip surfaces utilized in the residual geometry analyses.

Based on the post-failure cross-section, with a failure surface corresponding to a location mid-way between the two potential failure surfaces shown in Figure B.15.4(b), and the properties and parameters described above, the best-estimate value of $S_{r,resid/geom}$ was $S_{r,resid/geom} = 124$ lbs/ft^2. Parameters were next varied, as described previously, and this included analyses of alternate potential failure surfaces. Based on these analyses, it was judged that a reasonable range was $S_{r,resid/geom} \approx 105$ to 146 lbs/ft^2.

There was no value of $S_{r,resid/geom}$ from Olson (2001) for this case history.

B.15.6 Overall Estimates of S_r

Overall estimates of S_r for this Class B case history were made based on the pre-failure geometry, the partial post-failure geometry, the approximate runout features and characteristics, and the values of $S_{r,yield}$ and $S_{r,resid/geom}$ as calculated and/or estimated in the preceding sections.

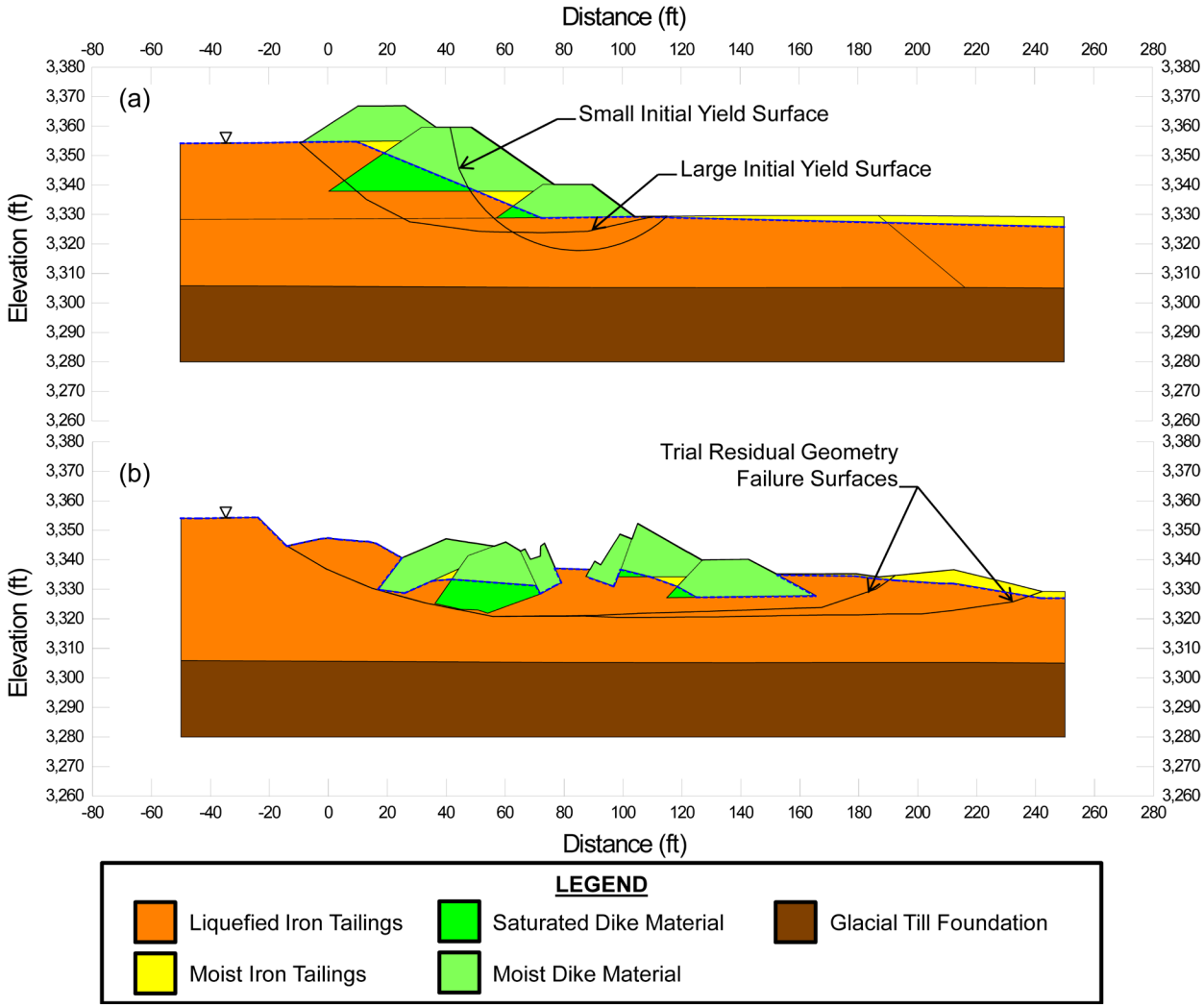

Figure B.15.3: Sullivan Mine Tailings Dyke: (a) pre-failure geometry and trail failure surfaces for initial yield stress analyses, and (b) post-failure geometry and failure surface for post-failure residual geometry analyses.

Runout distance of the center of mass of the overall failure was approximately D = 67 feet, and the initial failure slope height was H = 37.6 feet. This produces a runout ratio (defined as runout distance traveled by the center of gravity of the overall failure mass divided by the initial slope height from toe to back heel of the failure) of D/H = 1.78. This allows Equation 4-4, and Figures 4.7 and 4.11 to serve as one basis for estimation of post-liquefaction strength S_r. Using the ranges of $S_{r,yield}$ and $S_{r,resid/geom}$ from Sections B.15.4 and B.15.5, and assuming that $\xi \approx 0.60$ to 0.80 for this runout ratio, with 0.7 as the best estimate, provided a best estimate value of $S_r \approx 263$ lbs/ft^2 and an estimated range of $S_r \approx 206$ to 383 lbs/ft^2. A second basis for estimation of S_r was the use of the relationship of Figure 4.9, and the range of values of $S_{r,yield}$ from Section B.5.4. Based on the runout ratio, values of initial (pre-failure displacement) Factor of Safety were taken as approximately 0.3 to 0.5, and this produced a best estimate value of $S_r \approx 266$ lbs/ft^2 and an estimated range of $S_r \approx 204$ to 349 lbs/ft^2. No similar use was made of Figure 4.9 in conjunction with the ranges of $S_{r,resid/geom}$ estimated in Section B.4.5.

The estimates by each of the two methods above were then averaged together, and this produced a best estimate value of $S_r \approx 265$ lbs/ft^2 and an estimated range of $S_r \approx 204$ to 349 lbs/ft^2. These estimates of variance are non-symmetric about the best estimated mean value, and the range was judged to represent approximately +/- 3 standard deviations, so further adjustments were then necessary.

Overall, taking into consideration the largely asymmetric range of the results from assumed $S_{r,yield}$ slip surfaces, it was judged that the (median) best estimate of post-liquefaction strength for this case history is

$$\overline{S_r} = 277 \text{ lbs/ft}^2$$

and that the best estimate of standard deviation of mean overall post-liquefaction strength is

$$\sigma_{\overline{S}} = 24 \text{ lbs/ft}^2$$

Olson (2001) and Olson and Stark (2002), and Wang (2003) and Kramer (2008), did not consider this case history, therefore no comparison can be made to those studies. However, Jefferies and Been (2006) did estimate the residual strength as S_r = 10 kpa (approximately 200 lbs/ft^2) and a corresponding range of strength ratios of 0.07 to 0.13. Jefferies and Been report having estimated approximately the same residual strength from both a toe failure mechanism and also a retrogressive failure mechanism. It is unclear how momentum effects were taken into consideration, or if the effects were incorporated at all. Robertson (2010) presents a best estimate strength ratio of $S_r/P = 0.10$ for this case history. As a comparison, the best estimate of strength ratio for this current study is

$$S_r/P = 277 \text{ lbs/ft}^2 / 2{,}422 \text{ lbs/ft}^2 = 0.11$$

which is in good agreement with the value back-calculated by Robertson (2010), and which at least falls near the range of Jefferies and Been (2006). Overall, agreement between the back-analysis results of (1) Jeffries and Been (2006), (2) Robertson (2010) and (3) these current studies is very good.

B.15.7 Evaluation of Initial Effective Vertical Stress

Average initial (pre-failure) effective vertical stress was assessed for the liquefied portions of the failure surfaces for both rotational and wedge-like failures similar to the large failure surface shown in Figure B.15.3(a). Failure surfaces, parameters and sensitivity analyses were as described previously in Section B.15.4. Depths of failure surfaces were varied, and both rotational and translational (wedge-like) failure surfaces were considered.

The resulting best estimate of average pre-failure effective stress within the liquefied materials controlling the failure was then $\sigma_{vo}' \approx 2{,}413$ lbs/ft^2, with a reasonable range of $\sigma_{vo}' \approx 2{,}138$ to 2,706 lbs/ft^2. This range is slightly non-symmetric about the median value, and this range was judged by the engineering team to represent approximately ± 2 standard deviations.

Overall, the best characterization of initial (pre-failure) average effective vertical stress was then taken to be represented by a mean value of

$$\overline{\sigma'_{vo}} \approx 2{,}422 \text{ lbs/ft}^2$$

and with a standard deviation of

$$\sigma_{\bar{\sigma}} \approx 142 \text{ lbs/ft}^2$$

Olson (2001) and Olson and Stark (2002) in addition to Wang (2003) and Kramer (2008) did not consider this case history, therefore no comparison can be made to those studies. Jefferies and Been (2006) reported average initial vertical stresses of $\sigma'_{vo} \approx 80$ kpa (1,671 lbs/ft^2) for the initial toe failure and $\sigma'_{vo} \approx 140$ kpa (2,924 lbs/ft^2) for the final failure surface. The locations of these failure surfaces were not reported, however from the description of the failures they are assumed to be fairly similar to the initial failure surfaces used in this study. The stress corresponding to the final failure surface, which is the one most comparable to the surface used as representative of the initial vertical effective stress for this study, is about 500 lbs/ft^2 (27 percent) higher than the value back-calculated in these current studies.

B.15.8 Evaluation of $N_{1,60,CS}$

A total of 42 CPTs, 12 of which were in the vicinity of the failure, were performed on the Sullivan Mine following the failure. Six of the 12 CPTs in the vicinity of the failure were reported by Jefferies and Been (2006). Those six CPTs (three were pushed form the crest and three were pushed at the toe) were reported in Figure 15.4 (b). Figure 15.4 (a), shows CPT CP91-29, which was pushed through the failed mass. The processed data from CPT CP-91-29, as reported by Jefferies and Been, is reproduced as Figure 15.5. The fines content of the iron sandy silt tailings is reported as 50 percent or greater by Jefferies and Been. Figure 15.5 shows the interbedded nature of the iron tailings material, which is predicted to have a soil behavior type similar to that of both sand to silty sand and silty sand to silt. Similarly, Robertson (2010) reports an I_c of 2.6, which corresponds to the boundary between sand and silt mixtures.

Figure B.15.2 shows the locations of CPT's CP91-29 and CP91-31 performed to investigate the failures. Based on the available data, Jefferies and Been (2006) reported a normalized penetration resistance Q_k = 10 to 14 and a fines content of 50 percent or greater. Robertson (2010), in his evaluation of residual strength case histories, also considered this case history. Robertson reported a representative of normalized tip resistance of Q_{tn} = 15, a clean sand corrected normalized tip resistance of $Q_{tn,cs}$ = 50, and a representative fines content of approximately 50 percent.

Based on the available data for the crest and toe CPTs reproduced in Figure B.15.2, the representative q_c value for the tailings material encountered in the crest and toe CPTs range from about 2 to 4 MPa and 1 to 3 MPa, respectively. The ratio of $(q_c/Pa)/N_{60}$ for the tailings material was assumed to be in the range of 2 to 4. After applying the necessary corrections and conversions, resulting best estimate mean value of $N_{1,60,CS}$ for the iron tailings was judged to be $\overline{N_{1,60,CS}} \approx 9.5$ blows/ft. Variance of $\overline{N_{1,60,CS}}$ was estimated primarily on the range of results

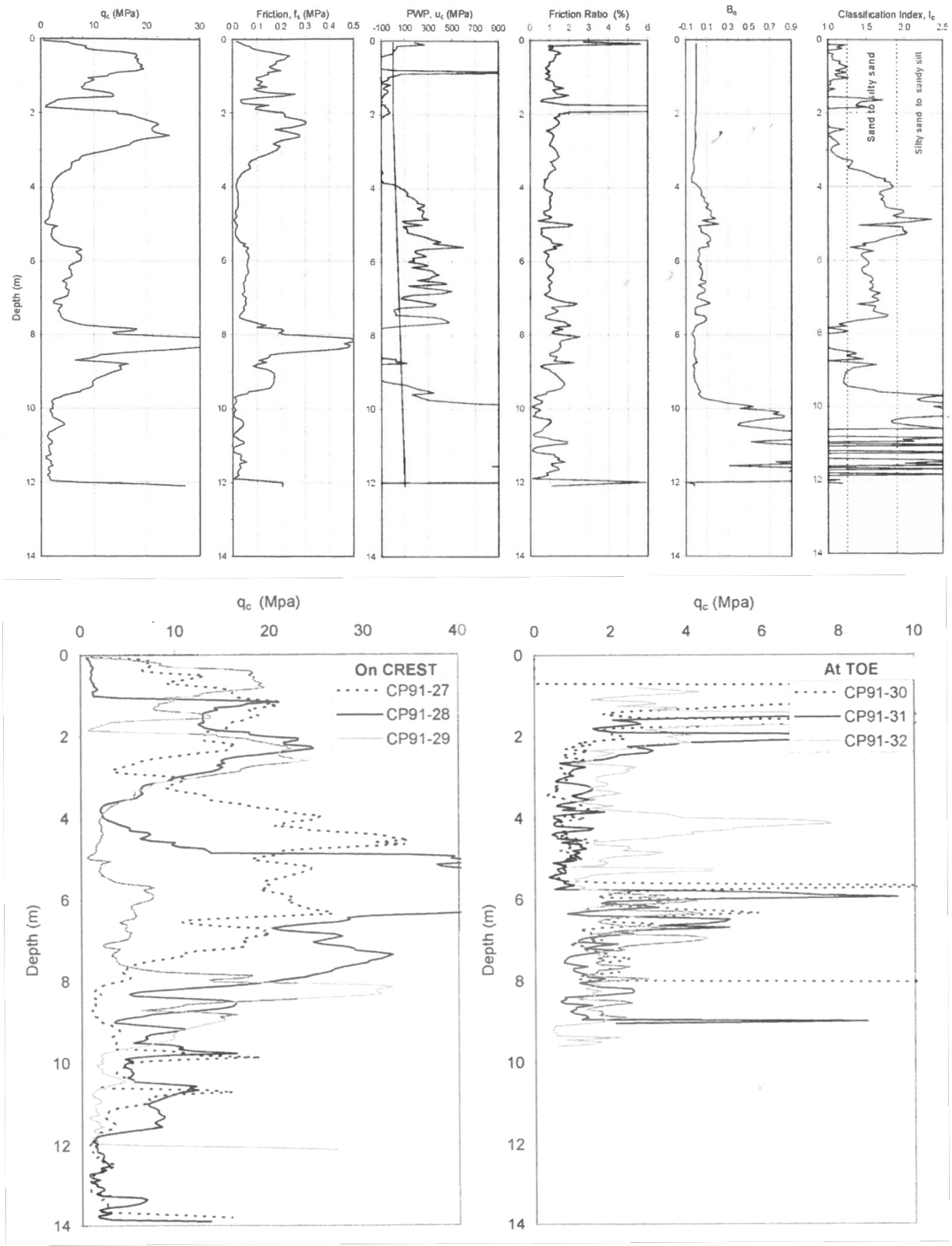

Figure B.15.4: Summary of (a) CPT CP91-29 and a (b) comparison of 6 CPTs, three from the crest and three from the toe (from Jefferies and Been, 2006).

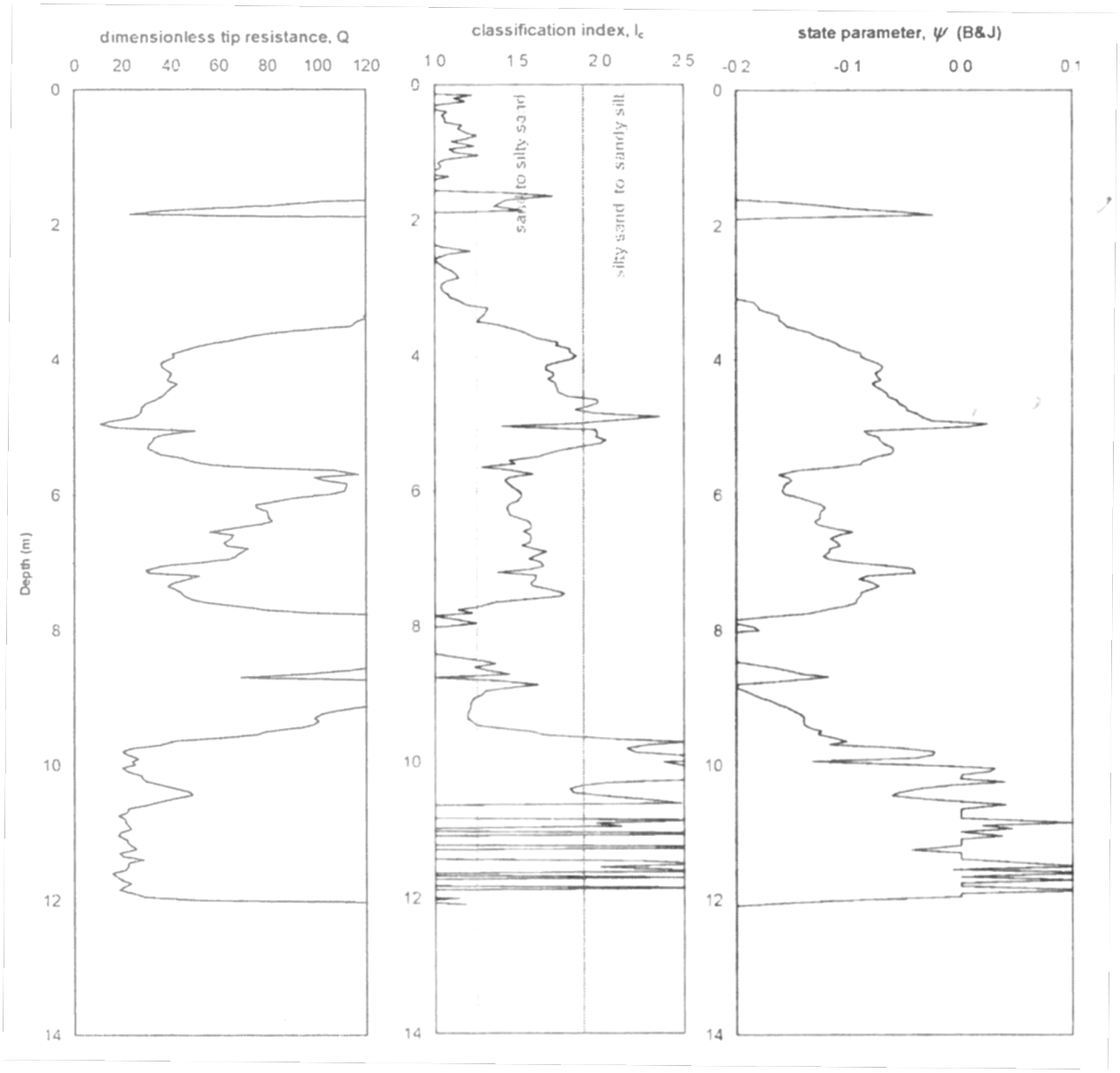

Figure B.15.5: Summary of the processed data from CPT CP91-29 as reported in Jefferies and Been (2006)

reported from the 6 CPTs. Considering these, the representation of uncertainty in the representative median value of $\overline{N_{1,60,CS}}$ was taken as $\sigma_{\overline{N}} \approx 2.5$ blows/ft.

Olson (2001) and Olson and Stark (2002) in addition to Wang (2003) and Kramer (2008) did not consider this case history, therefore no comparison can be made to those studies.

B.16 Jamuna Bridge (Bangladesh; 1994 to 1998)

B.16.1 Brief Summary of Case History Characteristics

Name of Structure	Jamuna Bridge, West Guide Bund
Location of Structure	Bangladesh
Type of Structure	Guide bund
Date of Failure	Between 1994 and 1998
Nature of Failure	More than 30 static liquefaction flow failures occurred during construction
Approx. Maximum Slope Height	64.5 ft.

B.16.2 Introduction and Description of Failure

The West Guide Bund of the Jamuna Bridge, located in Bangladesh along the Jamuna River, experienced more than 30 submarine static liquefaction flow slides during construction. The Jamuna River, the fifth longest river in the world, is a braided river that typically shifts significantly during the flood seasons. Two constraining guide bunds were constructed between 1994 and 1996 on each side of the river to train the river to travel under the 4.8 km bridge corridor (Yoshimine et al., 1999; Jefferies and Been, 2006).

Figure B.16.1 shows a plan view of the western Jamuna guide bund, and Figure B.16.2 shows a typical cross section of a failure experienced in the western guide bund.

B.16.3 Geology and Site Conditions

The construction of the Guide Bund slopes occurred in very young sediments, less than 200 years of age, deposited by the Jamuna River. The flow slides occurred in normally consolidated fine to medium-grained micaceous sand, which were tested to have approximately 15 to 30% mica content by weight. The mean gran size of this material was tested to be approximately 0.1 - 0.2 mm, with 2% to 10% passing by weight the 0.06 mm sieve (Yoshimine et al., 1999).

The slopes of the Guide Bund were placed at slopes ranging from 1:3.5 (V:H) to 1.5. Flow slides of the West Guide Bund cane to rest at slopes ranging from about 1:8 to 1:20 (Yoshimine et al., 1999).

B.16.4 Initial Yield Stress Analyses

Figure B.16.3 shows the cross-section used for back-analyses of the post-liquefaction initial yield strength $S_{r,yield}$ that would be required within the foundation and embankment materials of the typical section of the West Guide Bund to produce a calculated Factor of Safety equal to

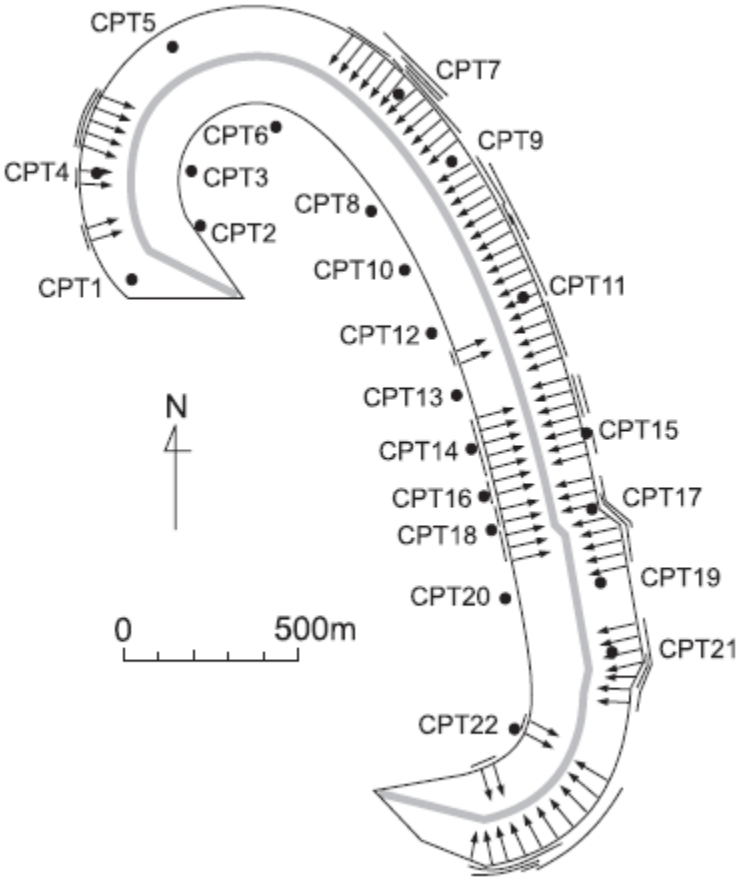

Figure B.16.1: Plan view of the West Guide Bind of the Jamuna Bridge, with arrows showing locations of failures and points noting locations of CPT's (from Yoshimine et al., 2001).

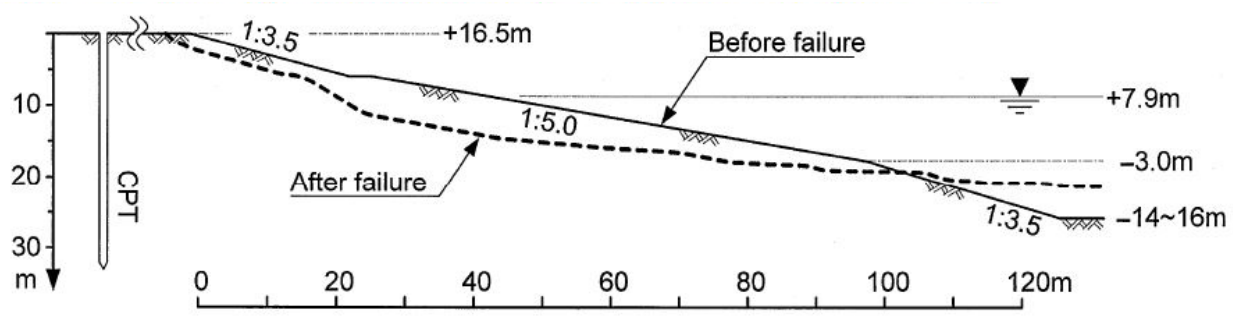

Figure B.16.2: Typical cross section of the West Guide Bind of the Jamuna Bridge with pre- and post-failure geometries depicted (from Yoshimine et al., 1999).

1.0. This is not the actual post-liquefaction strength, but it proves to be useful in developing estimates of post-liquefaction strength (S_r) for this case history.

There were two general sets of potential failure mechanisms that could potentially explain the observed features: (1) the failures may have been incrementally retrogressive, initiating with a "slice" near to the front of the feature, and then retrogressing on a slice by slice basis back towards the eventual back heel, or (2) the entire slide may have initiated monolithically (all at once). Both sets of possibilities were analyzed, and multiple potential "initial" failure surfaces were analyzed for the incrementally retrogressive scenario. In all cases, failure was modeled as occurring within the loose, saturated micaceous sands immediately underlying the Guide Bund fill.

Unit weights of the non-saturated compacted micaceous sand embankment fill above the phreatic surface were modeled with a unit weight of $\gamma_m \approx 115$ lbs/ft^3, and this was then varied over a range of $\gamma_m \approx 110$ to 120 lbs/ft^3 for parameter sensitivity studies. Unit weights of the saturated compacted sand below the phreatic surface were modeled with a unit weight of $\gamma_s \approx 120$ lbs/ft^3, and this was then varied over a range of 115 to 125 lbs/ft^3 for parameter sensitivity studies. The friction angle of the embankment micaceous sand materials above the phreatic surface was modeled with $Ø' \approx 28°$, and a range of $Ø' \approx 26°$ to 30°.

Potential initial failure surfaces were modeled as either (1) wedge-like semi-translational features, or (2) semi-rotational/translational features, or (3) conforming essentially to the final observed overall failure scarp (the monolithically initiated scenario).

The results of the various trial slip surfaces, (examples are shown in Figure B.16.3), and utilizing the best estimate parameters reported above, resulted in only moderate variations in $S_{r,yield}$ values. Based on a range of potential failure surfaces encompassing these possibilities, and the parameters (and parameter variations) described above, it was judged that the resulting best estimate value was $S_{r,yield} \approx 350$ lbs/ft^2, with a range of $S_{r,yield} \approx 321$ to 409 lbs/ft^2.

Olson (2001) did not include this case history in his failure database and therefore did not perform back-analyses to evaluate $S_{r,yield}$.

B.16.5 Residual Strength Analyses Based on Residual Geometry

Back-analysis were also performed to evaluate the "apparent" post-liquefaction strength ($S_{r,resid/geom}$) required to produce a calculated Factor of Safety equal to 1.0 based on residual geometry. This is not a direct measure of post-liquefaction strength (S_r), as it neglects momentum effects and would underestimate S_r, but it is useful for overall evaluation of Sr for this case history.

Figure B.16.3 (b) shows the post-failure cross-section geometry and example assumed slip surface utilized in the residual geometry analyses.

Based on the post-failure cross-section with the example assumed slip surface shown in Figure B.5.4(b), and the properties and parameters described above, the best-estimate value of $S_{r,resid/geom}$ was $S_{r,resid/geom} = 90$ lbs/ft^2. Parameters were next varied, as described previously, and

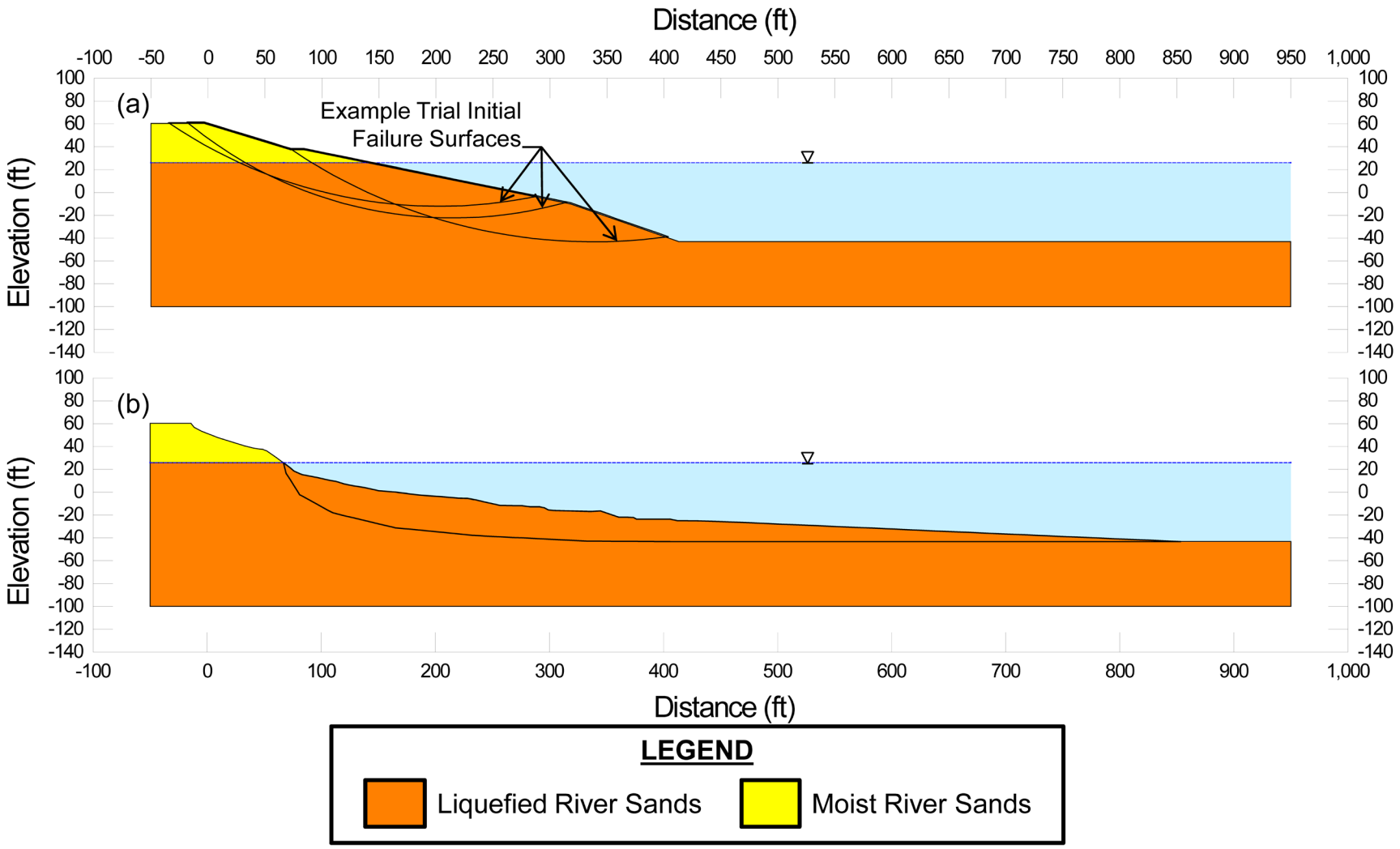

Figure B.16.3: Jamuna Bridge West Guide Bund: (a) pre-failure geometry and trail failure surfaces for initial yield stress analyses, and (b) post-failure geometry and Scenario A failure surface for post-failure residual geometry analyses.

this included analyses of alternate potential failure surfaces slightly above and below the failure surface shown in Figure B.5.4(b). Based on these analyses, it was judged that a reasonable range was $S_{r,resid/geom} \approx 76$ to 106 lbs/ft^2.

There was no value of $S_{r,resid/geom}$ from Olson (2001) for this case history.

B.16.6 Overall Estimates of S_r

Overall estimates of S_r for this Class B case history were made based on the pre-failure geometry, the partial post-failure geometry, and the approximate runout features and characteristics, and the values of $S_{r,yield}$ and $S_{r,resid/geom}$ as calculated and/or estimated in the preceding sections.

Runout distance of the center of mass of the overall failure was approximately D = 109 feet, and the initial failure slope height was H = 64.5 feet. This produces a runout ratio (defined as runout distance traveled by the center of gravity of the overall failure mass divided by the initial slope height from toe to back heel of the failure) of D/H = 1.69. This allows Equation 4-4, and Figures 4.7 and 4.11 to serve as one basis for estimation of post-liquefaction strength S_r. Using the ranges of $S_{r,yield}$ and $S_{r,resid/geom}$ from Sections B.13.4 and B.13.5, and assuming that $\xi \approx 0.58$ to 0.82 for this large runout case, with 0.7 as the best estimate, provided a best estimate value of $S_r \approx 154$ lbs/ft^2 and an estimated range of $S_r \approx 128$ to 180 lbs/ft^2. A second basis for estimation of S_r was the use of the relationship of Figure 4.9, and the range of values of $S_{r,yield}$ from Section B.5.4. Based on the large runout distance, values of initial (pre-failure displacement) Factor of Safety were taken as approximately 0.4 to 0.55, and this produced a best estimate value of $S_r \approx 168$ lbs/ft^2 and an estimated range of $S_r \approx 140$ to 193 lbs/ft^2. No similar use was made of Figure 4.9 in conjunction with the ranges of $S_{r,resid/geom}$ estimated in Section B.4.5 because these estimates of $S_{r,resid/geom}$ were considered to be very approximate.

The estimates by each of the two methods above were then averaged together, and this produced a best estimate value of $S_r \approx 160$ lbs/ft^2 and an estimated range of $S_r \approx 115$ to 225 lbs/ft^2. These estimates of variance are non-symmetric about the best estimated mean value, and the range was judged to represent approximately +/- 2.5 standard deviations, so further adjustments were then necessary.

Overall, taking into consideration the largely asymmetric range of the results from assumed $S_{r,yield}$ slip surfaces, it was judged that the (median) best estimate of post-liquefaction strength for this case history is

$$\overline{S_r} = 175 \text{ lbs/ft}^2$$

and that the best estimate of standard deviation of mean overall post-liquefaction strength is

$$\sigma_{\overline{S}} = 22 \text{ lbs/ft}^2$$

Olson (2001) and Olson and Stark (2002), and Wang (2003) and Kramer (2008), did not consider this case history, therefore no comparison can be made to those studies. However, Yoshimine et al. (1999) did estimate the range of strength ratio for this case to be between 0.11 and 0.26. Robertson (2010) presents a best estimate strength ratio of 0.15 for this case history. As a comparison, the best estimate of strength ratio for this current study is

$$S_r/P = 175 \text{ lbs/ft}^2 / 1{,}404 \text{ lbs/ft}^2 = 0.12$$

which is in fairly good agreement with the value back-calculated by Robertson (2010), and which at least falls within the range of Yoshimine et al. (1999).

B.16.7 Evaluation of Initial Effective Vertical Stress

Average initial (pre-failure) effective vertical stress was assessed for the liquefied portions of the failure surfaces for both rotational and wedge-like failures similar to the one shown in Figure B.16.3. Failure surfaces, parameters and sensitivity analyses were as described previously in Section B.16.4. Depths of failure surfaces were varied, and both rotational and translational (wedge-like) failure surfaces were considered.

The resulting best estimate of average pre-failure effective stress within the liquefied materials controlling the failure was then $\sigma_{vo}' \approx 1{,}392$ lbs/ft^2, with a reasonable range of $\sigma_{vo}' \approx 984$ to 1,824 lbs/ft^2. This range is slightly non-symmetric about the median value, and this range was judged by the engineering team to represent approximately ± 2 standard deviations. Overall, the best characterization of initial (pre-failure) average effective vertical stress was then taken to be represented by a mean value of

$$\overline{\sigma'_{vo}} \approx 1{,}404 \text{ lbs/ft}^2$$

and with a standard deviation of

$$\sigma_{\bar{\sigma}} \approx 210 \text{ lbs/ft}^2$$

Olson (2001) and Olson and Stark (2002) in addition to Wang (2003) and Kramer (2008) did not consider this case history, therefore no comparison can be made to those studies. Also no estimate of representative initial vertical effective stress was directly reported in Yoshimine et al. (1999).

B.16.8 Evaluation of $N_{1,60,CS}$

A total of 22 CPTs were performed on the shoulder of the West Guide Bund. The apparent representative fines content of the material was about 15% (Yoshimine et al., 1999).

Figure B.16.1 shows the locations of CPT tests performed to investigate the failures. A summary of these explorations can be seen in Figure B.16.4. Based on the available data and information, a representative range of normalized and fines corrected $(q_{c1N})_{CS}$, corrected using the

procedure recommended by Robertson and Wride (1998), as reported in Yoshimine et al. (1999), is approximately 50 to 65. Yoshimine suggested that the mean minus one sigma values would lie in a range of 40 to 65. The ratio of $(q_c/Pa)/N_{60}$ was assumed to be approximately of 5 to 6. The resulting best estimate mean value of $N_{1,60,CS}$ for the micaceous silty sands was thus found to be $\overline{N_{1,60,CS}} \approx 10.5$ blows/ft. Variance of $\overline{N_{1,60,CS}}$ was estimated primarily on the range of results reported from the 22 CPTs. Considering these, the representation of uncertainty in the representative median value of $\overline{N_{1,60,CS}}$ was taken as $\sigma_{\overline{N}} \approx 2.5$ blows/ft.

Olson (2001) and Olson and Stark (2002) in addition to Wang (2003) and Kramer (2008) did not consider this case history, therefore no comparison can be made to those studies. Representative $(q_{c1N})_{CS}$ was reported in Yoshimine et al. (1999) is 40 to 55, however that range appears to be intended to represent mean minus one sigma values. Robertson (2010) presents a representative normalized value of $Q_{tn,cs} = 57$ for this case history.

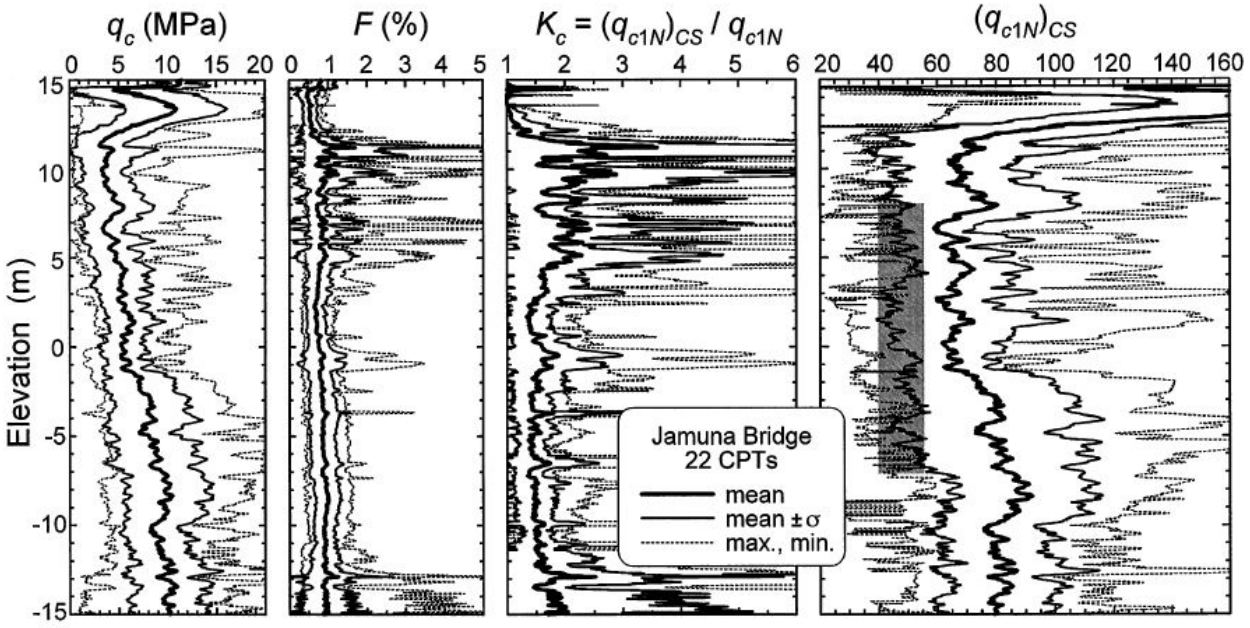

Figure B.16.4: Summary of 22 CPTs preformed at the West Guide Bund of the Jamuna Bridge as reported by Yoshimine et al. (1999).

Appendix C:

Processing and Interpretation of In-Situ Penetration Test Data and Development of Representative SPT $N_{1,60,CS}$ Values

Appendix C: Processing and Interpretation of In-Situ Penetration Test Data

These current studies evaluated the "representative" corrected Standard Penetration Test (SPT) penetration resistance ($N_{1,60,CS}$), with procedural, equipment, overburden, and fines content corrections applied, for each back-analyzed case history in conformance with Cetin et al. (2018a,b). The evaluation procedures and processes used are summarized in Section 4.2.4 of the main text of this report and are described in further detail in this Appendix. The procedures used are discussed herein not only to document the processes and procedures followed in the back-analyses of these current studies, but also to provide guidance for the evaluation of "representative" SPT $N_{1,60,CS}$ for forward engineering analyses using the empirically-based correlations for engineering assessment of post-liquefaction residual strength (S_r) presented in Chapter 5 of the main text.

C.1 Evaluation of Representative SPT $N_{1,60,CS}$ Values

The availability of penetration resistance data for the suites of field performance case histories back-analyzed in these studies required the evaluation of a number of different data sources and types, including both (1) modern, well-documented, SPT data and (2) the evaluation of non-standard and/or "older" testing and/or other types of data from which equivalent corrected SPT $N_{1,60,CS}$ values were inferred. For cases in which modern and well-documented SPT data were available, the processing of raw SPT N-values to produce procedurally corrected, effective overburden corrected, energy corrected, and fines corrected $N_{1,60,CS}$ values was as described below.

C.1.1 Corrections for Modern SPT Penetration Resistance Data

For cases where modern, and properly well-documented, SPT data were available, correction of field SPT N-values to generate procedural, equipment, and overburden corrected $N_{1,60}$ values were determined using the following equation:

$$N_{1,60} = N \cdot C_N \cdot C_R \cdot C_S \cdot C_B \cdot C_E \qquad \text{[Eq. C-1]}$$

where

$N_{1,60}$ = SPT blowcount value corrected for energy, equipment, and procedure factors
N = field measured SPT penetration resistance (blows/ft)
C_N = overburden correction factor
C_R = SPT correction for the rod length
C_S = SPT correction for potential non-standard sampler configuration
C_B = SPT correction for borehole diameter
C_E = SPT correction for hammer energy ratio

The SPT correction factors applied in these studies are correspond with those proposed by Cetin et al. (2018a,b), except that (1) a slightly reduced adjustment was made for short rod effects at shallow depths as per Deger (2014), and (2) normalization of N_{60}-values for effective overburden stress effects was performed using the relationships recommended by Deger (2014).

These two minor variations did not significantly affect the resulting $N_{1,60,CS}$ values, and the procedures set forth in Cetin et al. (2018a,b) will produce essentially the same engineering results.

C.1.2 Application and Impact of the Deger (2014) C_R and C_N Correction Factors

Deger (2014) evaluated field data from twenty four SPT borings instrumented for the purposes of impact calibration of automatic mechanical trip hammers, and developed a new rod length correction factor (C_R) relationship. His recommended short rod correction factor relationship is presented in Figure C.1. Figure C.2 presents a comparison of the Deger (2014) C_R relationship compared to those from Morgano and Liang (1992), Youd et al. (2001), and Valiquette et al. (2010). The slightly reduced short rod correction had an essentially negligible effect in these current studies, as few SPT data were used from the very shallow depths at which this might have produced a noticeable difference.

Deger (2014) also assessed the overburden correction factor (C_N) by evaluating large-scale calibration chamber data with clean sands and field SPT tests performed in 30 dam foundation units. The common form of the C_N equation is given as

$$C_N = \left(\frac{P_a}{\sigma'_v}\right)^m \qquad \text{[Eq. C-2]}$$

where the reference stress, P_a, and vertical effective stress, σ'_v, are in the same units. Cetin et al. (2018a,b), consistent with recommendations from Youd et al. (2001), adopt the Liao and Whitman (1986) recommendation of a constant 0.5 value for the exponent m. Deger (2014), similar to Idriss and Boulanger (2008), evaluated a non-linear relationship for the exponent m. The resulting effective overburden stress normalization relationships of Deger (2014) provide normalization curves somewhat intermediate between those of Cetin et al. (2018a,b) and of Idriss and Boulanger (2008). The composite relationship of the exponent m for both clean and silty sands from Deger (2014), presented in Figure C.3, was utilized in these studies.

Considering the ranges of representative SPT penetration resistance and pre-failure vertical effective stresses in the liquefied layers of the field performance case history database analyzed in these current studies, the application of the non-linear exponent m of Deger (2014) for the determination of C_N in these current studies is judged to have only a relatively minor impact, and the treatment of "m" in the relationship of Cetin et al. (2018a,b) is judged to be in largely suitable conformance with these current studies.

Given minor differences among the above applied relationships, for all practical purposes, the SPT correction procedures of Cetin et al. (2018a,b) are closely compatible with the corrections employed in these current studies, and they are the recommended basis for forward analyses of additional cases and/or applications to engineering project evaluations. In addition, the procedural and equipment corrections made herein were largely similar to those of Seed et al. (1984, 1985), and of Idriss and Boulanger (2008), and they would also produce largely compatible results for most of the field liquefaction failure (and S_r) case histories.

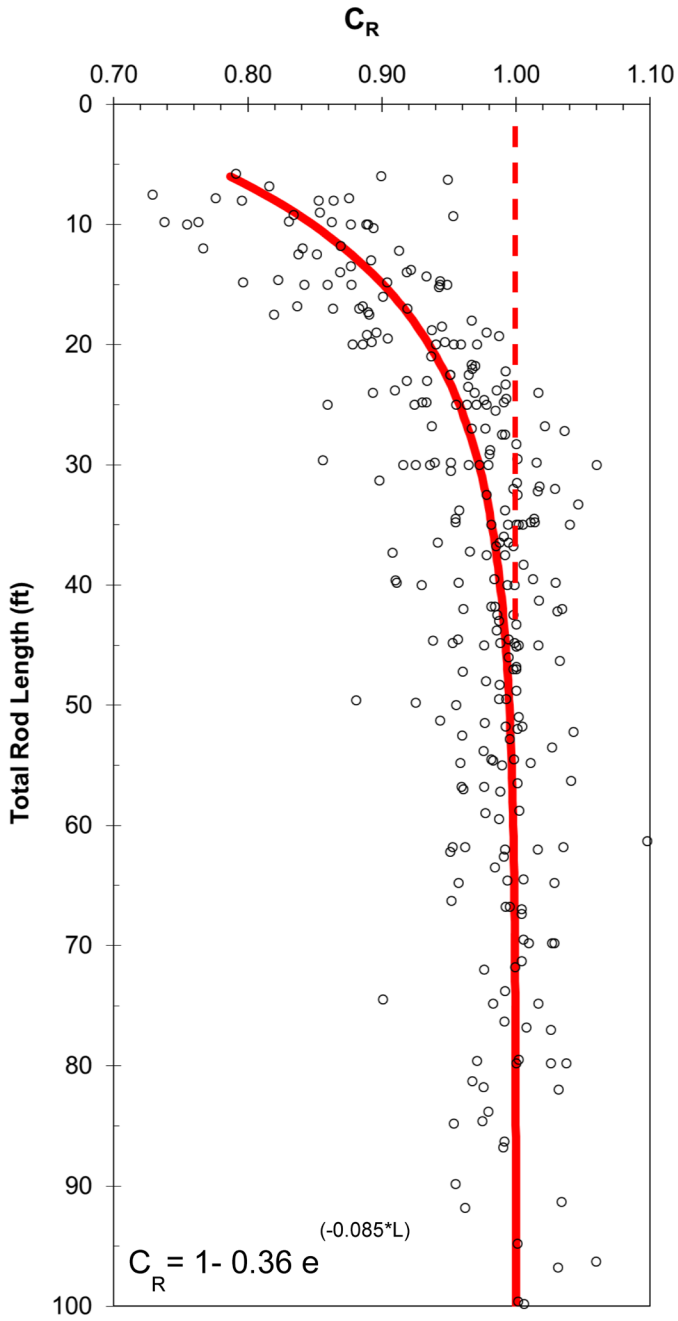

Figure C.1: Recommended rod length correction factor (C_R) relationship of Deger (2014), (from Deger, 2014)

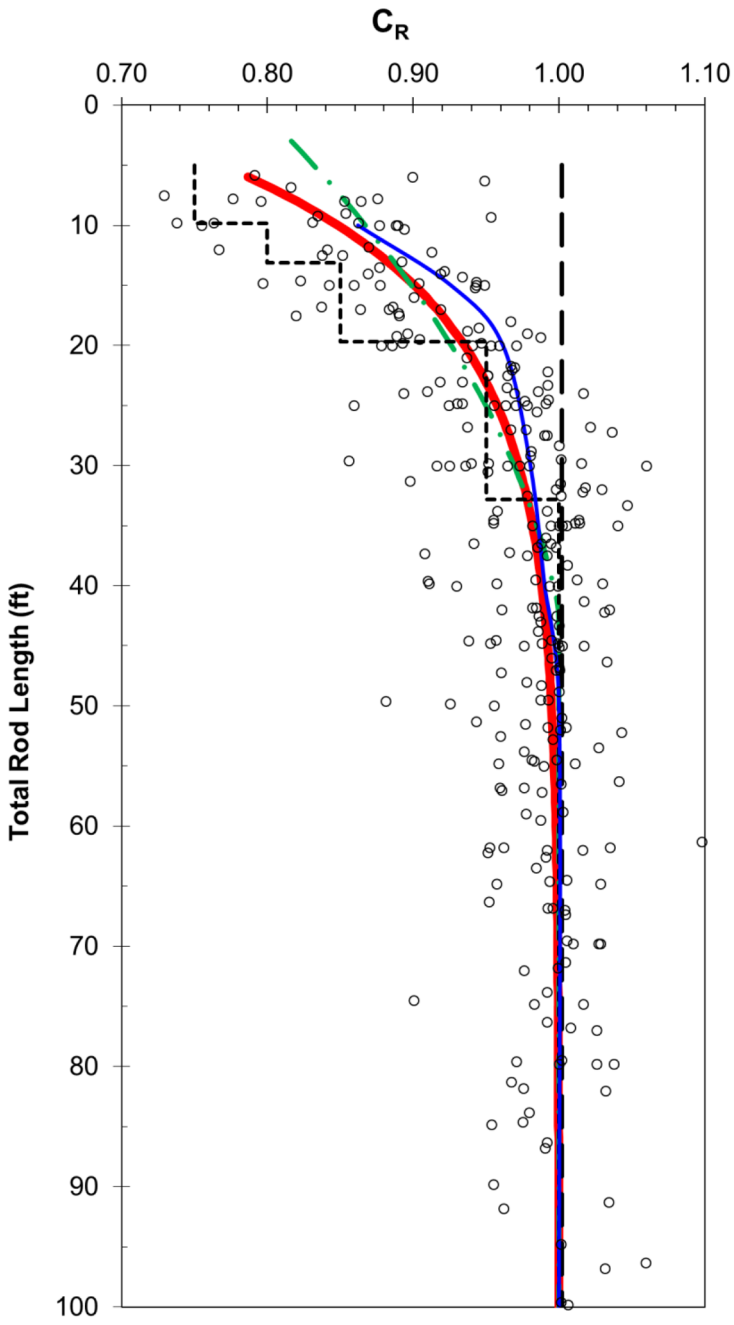

Figure C.2: Comparison of rod length correction factor (C_R) relationships of Deger (2014) [red solid line], Valiquette et al. (2010) [green dash-dot line], Morgano and Liang (1992) [thin blue line], and Youd et al. (2001) [stair-stepped black dashed line], (from Deger, 2014)

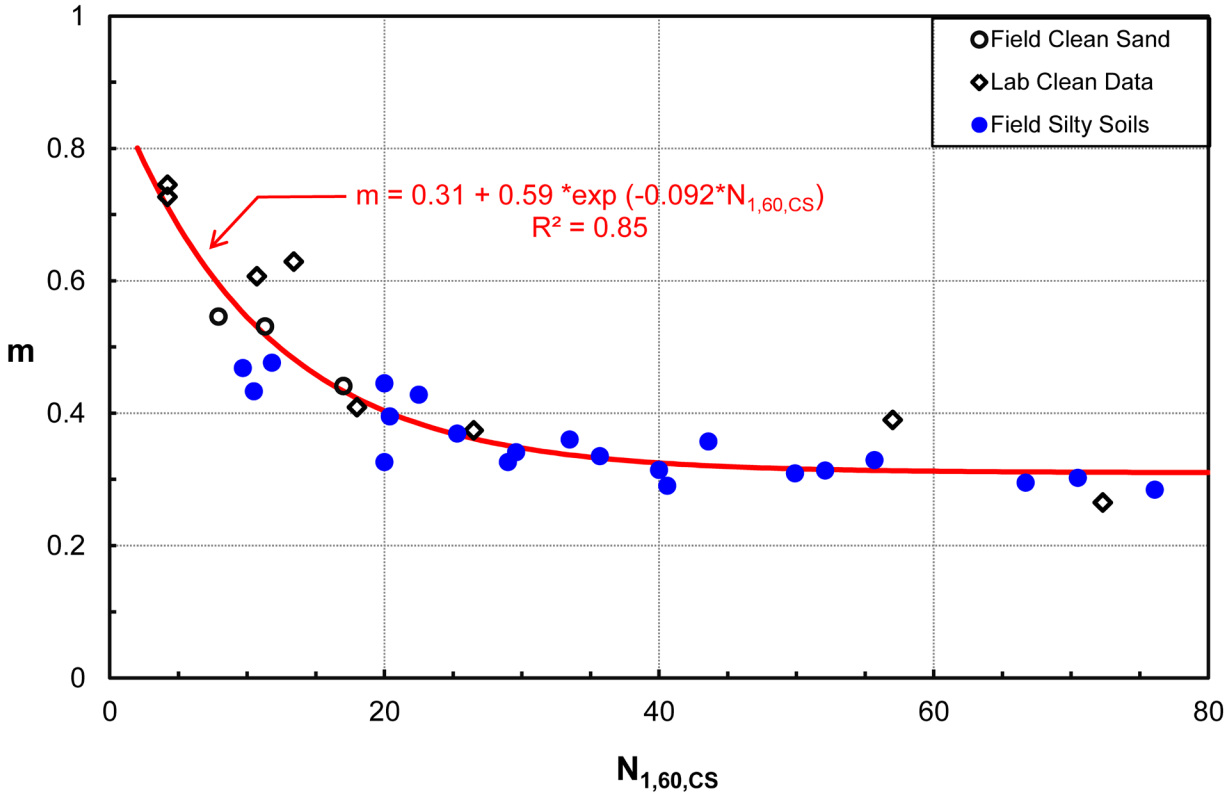

Figure C.3: Overall Deger (2014) composite relationship of C_N power exponent (m) for both clean and silty sands as a function of $N_{1,60,CS}$. (from Deger, 2014)

C.1.3 SPT Penetration Resistance Correction for Fines Content

Fines corrections for this study were made using the fines corrections recommended by Cetin et al. (2018a,b). This is an area where some minor differences occur between various investigation teams working on studies of post-liquefaction S_r. The fines adjustment of Cetin et al. (2018a,b) is somewhat intermediate between the fines adjustments of Seed et al. (1984, 1985) and the fines adjustment that Seed (1987) suggested specifically for S_r purposes. In the end, the fines corrections of these current studies, and (1) those employed by Seed (1987) and (2) those recommended by Idriss and Boulanger (2008) do not produce major differences, but they do vary slightly relative to each other. Olson and Stark (2001, 2002) elected not to employ any fines corrections, so that they used $N_{1,60}$-values rather than $N_{1,60,CS}$-values, and that causes a number of their characterizations of SPT penetration resistance to vary somewhat from the other studies for soils with higher fines contents.

The recommended basis for making adjustments for equipment, energy, procedural, fines and effective overburden corrections to develop $N_{1,60,CS}$ values for use of the post-liquefaction residual strength relationships developed in these current studies is the set of corrections set forth in Cetin et al. (2018a,b), which are judged to be suitably compatible with the values used in these current studies.

C.1.4 Evaluation of Representative SPT Penetration Resistance for Cases with Non-Standard SPT Data

Some of the case histories back-analyzed in these current studies had no well-documented modern SPT data, and so characterization of the critical potentially liquefiable soil strata required the evaluation of the alternate available data as a basis for development of estimated representative SPT penetration resistances. Sometimes equivalent $N_{1,60,CS}$ values were inferred from CPT data. And for some case histories, characterization of representative $N_{1,60,CS}$ values involved making use of non-standard and/or "older" types of penetration testing data and/or other types of data from which equivalent corrected SPT $N_{1,60,CS}$ values were inferred. When either CPT data, or non-standard penetration data, or lesser quality information regarding field emplacement conditions and history, etc. were used to develop estimates of equivalent SPT $N_{1,60,CS}$ values, the details of ascertaining and/or estimating both mean $N_{1,60,CS}$ values and standard deviations of the overall mean $N_{1,60,CS}$ values are presented on a case by case basis in Appendices A and B. The following is a list of case histories that required, at least in part, use of non-standard procedures for evaluation of penetration resistance as $N_{1,60,CS}$ values: A.3 Uestu Line Railway Embankment (1964), A.11 Soviet Tajik May 1 Slope Failure (1989), A.12 Shibecha-Cho Embankment (1993), B.1 Zeeland-Vlieteploder (1889), B.2 Sheffield Dam (1925), B.3 Helsinki Harbor (1936), B.4 Solfatara Canal Dike (1940), B.5 Lake Merced Bank (1957), B.6 El Cobre Tailings Dam (1965), B.7 Metoki Road Embankment (1968), B.8 Hokkaido Tailings Dam (1968), B.10 Tar Island Dyke (1974), B.12 Nerlerk Embankment, Slides 1, 2 and 3 (1983), B.13 Asele Roadway Embankment (9183), B.15 Sullivan Tailings (1991), B.16 Jammuna Bridge (1994). Please refer to those individual appendix sections for explanations as to how the representative $N_{1,60,CS}$ values were determined.

For two of the case histories (Wachusset Dam and Fort Peck Dam) additional corrections were required for ageing effects, as multiple decades elapsed between the occurrences of these two failures and the eventual performance of modern SPT investigations. The details of the corrections made for ageing effects in these two cases were case specific, and those details are presented in Appendix A, Sections A.1 and A.2, respectively.